The dynamic action of gusty winds on long-span bridges

Larose, Guy

Publication date:
1997

Document Version
Publisher's PDF, also known as Version of record

BYG•DTU

DANMARKS
TEKNISKE
UNIVERSITET

Guy L. Larose

The dynamic action of gusty winds on long-span bridges

Rapport
BYG•DTU R-029
2002
ISSN 1601-2917
ISBN 87-7877-088-2

The dynamic action of gusty winds on long-span bridges

Guy L. Larose

Department of Civil Engineering
DTU-bygning 118
2800 Kgs. Lyngby
http://www.byg.dtu.dk

2002

.

The dynamic action of gusty winds on long-span bridges

Submitted on April 24, 1997 in partial fulfillment of the requirements for the degree of Doctor of Philosophy at the Technical University of Denmark.

.

Abstract

The wind loads induced by the buffeting action of the turbulence on long-span bridges are the object of this thesis. The study focused on the description of the spatial distribution of the aerodynamic forces for closed-box girder bridge decks with cross-sections that have been designed with emphasis put on aerodynamics and have, therefore, the appellation "streamlined".

Central to this research is a series of wind-tunnel experiments that provided an instantaneous image of the wind loading across the span of a two-dimensional motionless bridge deck in a turbulent flow field. The experiments were organised in a parametric study that aimed at defining the influence of the width of the deck in relation to the scales of the turbulence on the dynamic loading.

The experiments illustrated the importance of the three-dimensionality of the lift and overturning forces. The current buffeting theory based on the strip assumption did not suffice to represent the measured wind loading. A three-dimensional analytical model of the gust loading on a thin airfoil that departs from the strip assumption explained the observed larger span-wise coherence of the forces when compared to the span-wise coherence of the incident velocity fluctuations.

Based on the parametric study, an empirical model of the gust loading on closed-box girder bridge decks was proposed. The empirical formulations included expressions for the aerodynamic admittance as a function of the ratio of the scale of the turbulence to the deck width. The span-wise coherence of the forces was also found to be a function of the ratio of the turbulence scale to the deck width and a function of the slenderness of the deck.

.

Preface

The research presented here was carried out in the framework of my Ph.D. programme at the Department of Structural Engineering and Materials (BKM) of the Technical University of Denmark from September 1994 to April 1997. The programme was initiated under the hospice of the Danish Research Academy in collaboration with the Danish Maritime Institute (DMI). The fabrication of the models, the experiments and the data reduction were carried out at DMI while the analysis was made at BKM.

This thesis is presented as a collection of papers written during the course of my research on wind-structure interactions. It focuses on the description of the gust loading on motionless bridge decks. Other aspects of wind engineering kept my attention during my Ph.D. studies, namely the effects of wind on bridges during construction and the unique field measurements of the wind-induced response of a 254 m high free-standing pylon for the Storebælt East Bridge. The results of the research on both topics were reported through two conference papers but are not included here.

It was also a pleasure and an inspiration for me to review, in collaboration with Niels Franck, the works of Danish wind engineering pioneers. I learned that the first worldwide wind-tunnel measurements of surface pressure were carried out in Copenhagen almost exactly 100 years ago. We wrote a paper on that topic and presented it at the 9^{th} International Conference on Wind Engineering in New-Delhi, India.

My supervision committee was composed of Prof. Niels J. Gimsing, Dr. Claës Dyrbye and Prof. Hiroshi Tanaka. Their knowledgeable guidance is most sincerely acknowledged as well as their clairvoyance in encouraging me to learn about wind on a sailboat across the Atlantic Ocean.

I would like also to express my grateful thanks to the COWIfoundation for the financial support that made possible the experimental part of this research. Acknowledgements are extended to DMI's management, in particular Aage Damsgaard, who encouraged and made room for this study, and to my colleagues at DMI and BKM who kindly coped with me. The invaluable discussions and contributions of my friends and co-authors Jakob Mann from Risø and Flora M. Livesey from DMI are warmly acknowledged.

This is the second edition of my Ph.D. thesis. It includes the revisions suggested by the members of my examining committee composed of Professors Erik Hjorth-

Hansen and Steen Krenk, and Dr Allan Larsen. Their comments and suggestions are greatly acknowledged. The first edition was submitted on April 24, 1997 in partial fullfillment of the requirements for the degree of Doctor of Philosophy at the Technical University of Denmark.

Enfin, mille mercis à Simone et Emil pour leur patience légendaire et leurs multiples encouragements ainsi qu'à Flora sans qui la vie ne serait pas la même.

Cette thèse est dédiée à ma famille qui m'est très chère et qui ne cesse de grandir.

GLL, Lyngby, Oct. 25, 1999

Contents

Nomenclature

$\|A(f^*)\|$	aerodynamic admittance function or AAF
A^*_{1-4}	dimensionless aerodynamic derivatives associated with the torsional degree of freedom of a bridge deck
B	deck width
$B_{x,z,\theta}$	subscript, background or quasi-steady component of the dynamic response in the given degree of freedom
c, c_1, c_2, c_3	exponential decay constants for span-wise co-coherence of the wind fluctuations and aerodynamic forces
$cocoh_{w,L}$	span-wise co-coherence (or normalized co-spectrum) of the w component of the wind or the vertical aerodynamic forces L
$coh^{1/2}_{w,L}$	span-wise root coherence of the w component of the wind velocity or the vertical aerodynamic forces
C_m	steady moment coefficient in the torsional direction, torsion about the bridge axis, based on B^2
C_x	steady body-force coefficient in the horizontal direction, based on B
C_z	steady body-force coefficient in the vertical direction, based on B
$C'_{m,x,z}$	$= dC_{m,x,z}/d\alpha$: rate of change (slope) of the respective steady force coefficients with angle of wind incidence α in radians
C_p	pressure coefficient
Co_{12}	co-spectrum, i.e. real (in-phase) component of the cross spectrum between points 1 and 2
D	depth of bridge deck
$F_{m,x,z}$	aerodynamic force per unit length in the given degrees of freedom
f	frequency
$f_{x,z,\theta}$	frequency of first symmetric mode of vibration respectively in the lateral, vertical and torsional degrees of freedom, in still air
f_j	natural frequency of mode j in still air
f^*	$= fB/V$, reduced frequency
f^*_j	reduced frequency based on the natural frequency of mode j
f_m	frequency associated with the Fichtl-McVehil spectrum
$G_{x,z,\theta}$	damping coefficient in the lateral, vertical and torsional direction
G^*_j	generalized damping coefficient for mode j
G_{crit}	critical damping
g	gravitational acceleration or statistical peak factor
H^*_{1-4}	dimensionless aerodynamic derivatives associated with the vertical degree of freedom of a bridge deck
$I_{u,v,w}$	longitudinal, transversal and vertical turbulence intensity, respectively

I_θ	mass moment of inertia per unit length of a bridge deck
$J(f^*)$	joint acceptance function or JAF
J_0, J_1	Bessel functions
K_j^*	generalized stiffness of the deck in mode j
$K_{1/6,5/6}$	modified Bessel functions of the second kind
k_1	$= 2\pi f/\bar{V}$, wave number
$\tilde{k}_1$	$k_1 B/2$
L	length scale associated with the von Kármán spectrum
$L_{u,v,w}^{x,y,z}$	horizontal, transversal and vertical integral length scales of turbulence in the x, y, z direction
l	span length
$\mathcal{L}$	length scale of turbulence corresponding to the inverse of the wave number at which the wind spectrum has its maximum
M_j^*	generalized mass of mode j
m	mass of the deck per unit length
$p(\alpha)$	probability distribution of angle α
Qu_{12}	quadrature spectrum i.e. imaginary (out-of-phase) component of the cross spectrum between points 1 and 2
R_{12}	cross-correlation coefficient between points 1 and 2
$R_{x,z,\theta}$	subscript, resonant component of the dynamic response in the given degree of freedom
r	peakness parameter of the Fichtl-McVehil spectrum
$\bar{r}$	mean response
$\tilde{r}$	root-mean-square response
$\hat{r}$	expected peak response
$\tilde{r}_{R_j}$	resonant root-mean-square modal response
$S_{u,v,w}$	spectra of the fluctuations of the wind velocity components, longitudinal, transversal and vertical
S_{F_z}	spectrum of the vertical wind load on a bridge span
S_L	spectrum of the lift force on a chord-wise strip of the deck
$S_{L_1L_2}$	cross-spectrum of the lift forces between point 1 and 2
t	time
u	longitudinal component of the wind velocity
V	wind velocity in the along-wind direction
$\bar{V}$	mean wind velocity
V_r	apparent velocity of the wind
V^*	$= V/fB$, reduced velocity
v	transversal component of wind velocity
w	vertical component of wind velocity or angular velocity

x	horizontal direction, perpendicular to the bridge axis
$\dot{x}$	first derivative of horizontal motion with respect to time (velocity)
y	span-wise or transversal direction
z	vertical direction
$\dot{z}$	first derivative of vertical motion with respect to time (velocity)
α	instantaneous angle of wind incidence
$\Delta\bar{x}$	mean horizontal amplitude of the deck motion
Δy	span-wise separation between points y_1 and y_2
η	modified von Kármán parameter
$\eta_{a;\theta}$	normalized aerodynamic stiffness in torsion
Γ	Gamma function
γ	von Kármán parameter
μ_j	mode shape of a given mode j
ν	cycling rate
ω_j	angular frequency of vibration of a given mode j
$\phi^2(f^*)$	theoretical aerodynamic admittance function
ρ	air density
σ_B, σ_{R_j}	root-mean-square background and resonant response
$\sigma_{u,v,w}$	root-mean-square of wind velocity fluctuations
θ	designates torsional degree of freedom or rotation of the deck about the bridge axis
ζ_{a_j}	aerodynamic damping as a fraction of critical for mode j
ζ_{s_j}	structural damping as a fraction of critical for mode j

.

General introduction

Objective and impetus for research

The knowledge of the spatial distribution of the forces induced by the gustiness of the wind is at the heart of the predictions of the buffeting response of long-span bridges. The objective of this work is to describe the spatial distribution of these forces on a motionless closed-box girder bridge deck.

The impetus for the research came from an analysis of the error margin of the current prediction methods of bridge buffeting. In the early phase of this study, a review of the comparisons found in the literature between analytical predictions of the buffeting response and measured response in full scale or model scale was carried out. It revealed that in some instances the error margin of the analytical predictions was found to be small while in other cases, the analytical predictions greatly overestimated or underestimated the measured response.

This apparent inconsistency suggested that a more in-depth study of each case be conducted to arrive at a reliable assessment of the error margin since many parameters could influence the comparisons. For example, the description of the incident wind field in full-scale is an important source of uncertainty, let alone its modelling in a wind tunnel. Also, the evaluation of the structural damping and its variability with amplitude of motion is another major parameter that influences the comparisons.

Often, however, the background information is not sufficient to conduct such in-depth studies, leaving room for interpretation and doubts. This brought the author to perform a review of the shortcomings of the analytical methods of predicitons of the buffeting of long-span bridges which is presented in Part I of this thesis. The review indicated that the modelling of the action of the turbulence on closed-box girder bridge decks was not clear. This is especially true when the bridge deck has a characteristic length (e.g. width) similar to the length scales of the incident gusts. This is the case for the majority of modern closed-box girder bridge decks with deck width ranging from 20 to 40 m immersed in atmospheric boundary layer winds with $\approx$200 m long gusts but with vertical and lateral length scales not larger than $\approx$30 to 50 m.

The analytical calculations of bridge buffeting, either in the frequency domain or in the time domain, are generaly based on the strip assumption despite the fact that this assumption is valid only when the incident gusts have much larger scales than the characteristic length of the bridge deck. Based on the strip assumption, the span-wise coherence of the aerodynamic forces can be represented by the span-wise coherence of the incident wind velocity fluctuations. The experiments carried out in the present research programme and reported in full in Part II-A of this thesis aimed at defining the error margin of the calculations of the vertical and torsional gust

loading on a motionless bridge deck based on the strip assumption. The influence of the ratio between the size of the gusts and the deck width was also studied by systematically changing both quantities in turn.

The distinction "motionless" is made in an attempt to dissociate the aerodynamic forces due uniquely to the incident wind turbulence from the motion-induced forces often associated with the wake of the bridge deck. It has been observed that the spatial distribution of the wind loading can differ importantly if the two-dimensional body is in motion or not and if this motion is organised or not. Here the emphasis is made on the forces induced by the wind gustiness only and any distortion and reorganisation of the turbulence that could occur if the bridge deck would undergo relatively important oscillations in term of amplitudes is not considered.

This research is a logical progression of the work carried out by the author in the framework of a M. Eng. Sc. thesis at The Boundary Layer Wind Tunnel Laboratory of The University of Western Ontario, Canada. During that earlier work, the evaluation of the span-wise distribution of the lift and torsional forces on a closed-box girder bridge deck based on the strip assumption led to an underestimation of the forces when compared to direct measurements in a wind tunnel. The lift cross-sectional admittance was found, however, to be lower than predicted by the linear theory for a thin airfoil in a fully correlated gust. The cross-section studied was the deck of the Storebælt East Bridge.

In the present research, a parametric study of the influence of the width of the deck and of the turbulence scales on the dynamic wind loading was made by keeping constant the deck depth and the edge configuration but varying the deck width of the experimental model. The edge configuration selected is similar to the configuration of the Storebælt East Bridge.

A secondary objective of this research was to quantify the relationships between the scales of turbulence, the slenderness of the deck, and the gust loading. This analysis was performed to define a model of the loading that departs from the strip assumption and reduces the error margin of the buffeting predictions.

Synopsis

This thesis is divided into three parts that followed closely the pattern adopted during this research: **Part 1: Background** exposes the theoretical background for the research and presents the impetus for the research. **Part 2: Experiments and analysis** presents a detailed account of the experimental work carried out in the framework of this research. It also presents the analytical treatment of the data followed by the definition of a model of the buffeting wind loading. **Part 3: Applications** presents some applications of the proposed model. Each part was subdivided into two smaller parts which are presented in the form of stand-alone papers with their own introduction, development and conclusions.

Initially a review of the current methods of prediction of the buffeting response of bridge decks was made, with emphasis on the limitations and shortcomings of the spectral approach. A summary of this review is given in Part I-A, with some suggestions for improvements of the analytical predictions. In Part I-B, a detailed state-of-the-art description of the spatial distribution of the aerodynamic forces on closed-box girder bridge decks is given. This part was presented at an international colloquium on bluff-body aerodynamics during the course of the study and was published in the proceedings.

Part I-B sets the stage for the planning and execution of the experiments described in Part II-A. The main findings of the parametric study are also given in Part II-A. Part II-B focused on the analysis of the results and the building-up of empirical models of the cross-sectional admittances and span-wise coherence of the aerodynamic forces for the family of closed-box girder bridge decks of this study. The empirical formulations are based on a three-dimensional (3-D) analytical model of the gust loading on a thin airfoil that departs from the strip assumption.

This 3-D analytical model of the gust loading is presented in Part II-B along with examples of calculations for isotropic turbulence. Part II-B brings forward a physical and analytical explanation for previously reported observations regarding the variations of the cross-sectional admittance of the lift forces and its span-wise distribution as a function of reduced frequency and length scales of turbulence. The contents of both Part II-A and Part II-B were published in summarised form in two refereed journal papers.

In Part III, some applications of the models of Part II-B are reported. A method of evaluation of the admittance of bridge decks of any cross-section is described in Part III-A. The quantity measured has a 3-D character and was termed aerodynamic admittance of a segment (segmental admittance) as opposed to cross-sectional admittance since it includes in its definition a portion of the span-wise coherence of the aerodynamic forces. The validation of the method was made possible through the empirical model presented in Part II-B.

Predictions of the buffeting response for various closed-box girder bridge decks are given in Part III-B and are compared to buffeting predictions for a flat plate. The analytical calculations are based on the theory presented in Part I-A with the improvements suggested by Part II-B and the experimental technique presented in Part III-A for the determination of the aerodynamic admittance. Part III-A and Part III-B were published in refereed journals.

.

Part I
Background

Part I-A
Prediction of the buffeting response

GUY L. LAROSE[a,b]

[a] *Department of Structural Engineering and Materials, Technical University of Denmark, 2800 Lyngby, Denmark*
[b] *Danish Maritime Institute, Hjortekærsvej 99, 2800 Lyngby, Denmark*

Abstract

A review of the methods of prediction of the buffeting response of long-span bridges and other line-like structures is presented. Analytical and experimental approaches are discussed, with emphasis on the spectral approach. Limitations, shortcomings and suggestions for improvements of the buffeting theory are summarized.

1 Introduction

Long-span bridges must be designed to withstand the static drag forces induced by the time-averaged wind pressure. If not properly designed, the drag load and the self-excited aerodynamic moment on the deck section can cause static buckling (lateral buckling and torsional divergence). In addition, bridges may respond dynamically to the effects of the wind flow over the deck section. This wind-induced dynamic response is generally classified into three major categories, depending on the mechanisms involved:

- random response due to buffeting by turbulence;
- vortex-induced response; and
- aerodynamic instability.

For the prototype structure, not only more than one of these types of response occur at the same time, but also the different modes of oscillation of the structure may be susceptible to different excitation. Wind tunnel tests carried out in smooth and turbulent flow on two-dimensional section models in dynamic systems with adjustable frequency and damping or on three-dimensional aeroelastic models allow the study of these three categories of response.

Here, only the response due to buffeting by turbulent wind will be described, with emphasis on the prediction of the full scale behaviour based on the results of the section model tests combined with the spectral approach.

2 Theoretical background

2.1 Definition

Buffeting is the random response of the bridge due to wind forces associated with the pressure fluctuations on the bridge deck caused by gustiness of the wind flow over the section. Since this gustiness has vertical as well as horizontal variations in velocity, the analysis must include the effects of a random variation in the angle of attack. Buffeting normally increases monotonically with the mean velocity and is thus more important at maximum winds. It is also a function of the turbulence intensity of the oncoming flow and of the structural damping of the bridge.

2.2 Linearised equation of motion

The prediction of the buffeting response to turbulent wind is generally secondary to the question of aerodynamic stability. However, when the bridge is shown to be stable, the question of the response to gusts is important for the design of the superstructure and the assessment of the user comfort by predicting the acceleration level. The theoretical approach developed by Davenport in 1961 [1, 1] is the result of the first thorough analytical investigation of the problem and is the most widely used method of prediction of the effects of gusts on civil engineering structures. Sections 3.1 and 3.2 give a summary of this approach.

The derivation of the theoretical expressions for the prediction of the response of a bridge deck to turbulent wind, assuming quasi-steady aerodynamics, has been described in detail elsewhere [5]. Only the main expressions are reproduced here, focusing on the vertical degree of freedom.

Assuming quasi-steady aerodynamics: and referring to Fig. 1, the vector of the velocity of the wind relative to the deck in motion (or the apparent velocity) can be expressed by:

$$V_r = \sqrt{(w - \dot{z})^2 + (\bar{V} + u - \dot{x})^2} \tag{1}$$

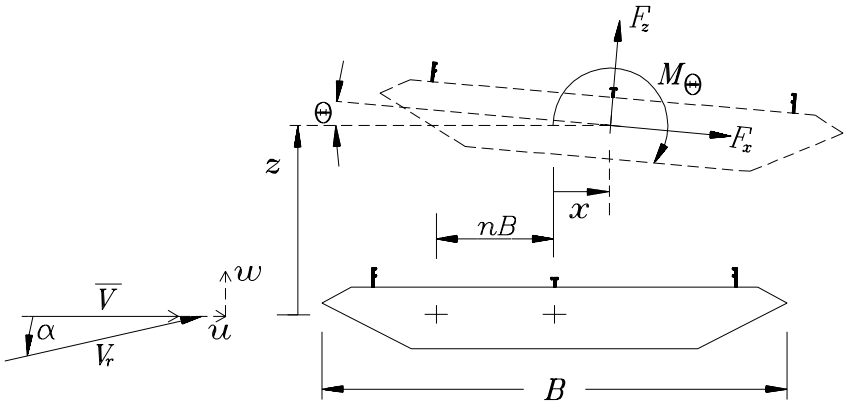

Figure 1: Notation for deck motion

$$V_r^2 = w^2 - 2w\dot{z} + \dot{z}^2 + \bar{V}^2 + \bar{V}u \tag{2}$$

$$-\bar{V}\dot{x} + u\bar{V} + u^2 - u\dot{x} - \dot{x}\bar{V} - \dot{x}u + \dot{x}^2. \tag{3}$$

where u and w are respectively the longitudinal and the vertical components of the wind fluctuations, $\bar{V}$ is the mean wind speed, x and z and their time derivative $\dot{x}$ and $\dot{z}$ denote in turns displacement and velocity of the deck in the lateral and vertical degrees of freedom.

For small displacements and small velocity fluctuations, the terms involving the products of $w, u, \dot{x}, \dot{z}$ can be neglected and the above expression can be reduced to:

$$V_r^2 = \bar{V}^2 + 2\bar{V}u - 2\bar{V}\dot{x}. \tag{4}$$

The apparent instantaneous angle of attack is given by:

$$\alpha = \theta + \frac{w - \dot{z} - nB\dot{\theta}}{\bar{V} + u - \dot{x}} \tag{5}$$

where n is a factor representing the position of the point of application of the vertical aerodynamic forces that produce a torsional motion. For a thin airfoil at low reduced frequency, $n \approx 0.25$, i.e. the equivalent point of application of the lift forces is a quarter of the chord, B, upstream of the torsional centre. For bridge decks the quasi-steady values of n is often taken as ≈ 0.25 but in practice it varies with reduced frequency. The term $nB\dot{\theta}$ was in fact originally introduced for bridge decks by Irwin [8] where n was kept as a floating paramter, to express quasi-statically the contribution of the torsional aerodynamic damping in the equation of motion.

Defining the lift coefficient C_z as a linear function of the angle of wind incidence α we have:

$$C_z(\alpha) = C_{z_0} + C'_z\alpha \tag{6}$$

where C_z' is the rate of change of the lift coefficient with angle of wind incidence in radians. Note that C_z is the lift or vertical force coefficient for a coordinate system fixed to the bridge deck, and C_{z_0} is the linearised lift coefficient at $\alpha = 0$. The lift force per unit length is defined by:

$$F_z = C_z(\alpha)(\frac{1}{2}\rho V_r^2)B \tag{7}$$

$$F_z = (C_{z_0} + C_z'\alpha)\left[\frac{1}{2}\rho B(\bar{V}^2 + 2\bar{V}u - 2\bar{V}\dot{x})\right] \tag{8}$$

$$= \left(C_{z_0} + C_z'\left(\theta + \frac{w - \dot{z} - nB\dot{\theta}}{\bar{V} + u - \dot{x}}\right)\right)\left[\frac{1}{2}\rho B\bar{V}^2 + \rho B\bar{V}u - \rho B\bar{V}\dot{x}\right]. \tag{9}$$

Neglecting the terms with the product of u, w and $\dot{z}$, $\dot{x}$, equation (9) becomes:

$$F_z = \frac{\rho B}{2}\Big(C_{z_0}\bar{V}^2 + 2C_{z_0}\bar{V}u + C_z'w\bar{V} - C_z'\dot{z}\bar{V} - 2C_{z_0}\bar{V}\dot{x} + C_z'\theta\bar{V}^2 - C_z'nB\dot{\theta}\bar{V}\Big). \tag{10}$$

The first term represents the mean wind load, the second and third terms represent the buffeting wind load due to, respectively, the along-wind gusts and the vertical gusts, the fourth term is a motion-induced wind load and represents an aerodynamic damping which reduces the dynamic loading if C_z' is positive, and the last terms represent the wind load due to coupling between along-wind, vertical and torsional motions. Similar formulations can be derived for the drag force and pitching moment.

The wind loads due to the buffeting action of the wind (subscript b) are expressed by:

$$F_{x,b} = \frac{\rho\bar{V}B}{2}\left[2C_x u + C_x' w\right] \tag{11}$$

$$F_{z,b} = \frac{\rho\bar{V}B}{2}\left[2C_z u + C_z' w\right] \tag{12}$$

$$M_{\theta,b} = \frac{\rho\bar{V}B^2}{2}\left[2C_m u + C_m' w\right]. \tag{13}$$

Combining the load fluctuations from the wind with the equations of motion of the deck, the quasi-steady equations for motion of a suspended deck in gusty wind can be expressed as follows for the three main degrees of freedom [5]:

$$M_x\ddot{x} + (G_x + \rho\bar{V}BC_x)\dot{x} + K_x x + \left[\frac{1}{2}\rho\bar{V}BC_x'\dot{z} - \frac{1}{2}\rho\bar{V}^2BC_x'\theta\right] = F_{x,b} \tag{14}$$

$$M_z\ddot{z} + (G_z + \frac{1}{2}\rho\bar{V}BC_z')\dot{z} + K_z z + \left[\rho\bar{V}BC_z\dot{x} - \frac{1}{2}\rho\bar{V}^2BC_z'\theta - \frac{1}{2}\rho\bar{V}nB\dot{\theta}\right] = F_{z,b} \tag{15}$$

$$I_\theta\ddot{\theta}+(G_\theta+\frac{1}{2}\rho B^3 C'_m n\bar{V})\dot{\theta}+(K_\theta-\frac{1}{2}\rho\bar{V}^2B^2C'_m)\theta+\left[\rho\bar{V}B^2C_m\dot{x}+\frac{1}{2}\rho\bar{V}B^2C'_m\dot{z}\right]=M_{\theta,b} \tag{16}$$

where $M_{x,z}$ and I_θ represent the effective inertias of the deck for the horizontal, vertical and torsional motions, $G_{x,z,\theta}$ represent the effective viscous damping and $K_{x,z,\theta}$ the effective stiffness. The terms in [ ] are coupling terms, and all products of a force coefficient and a position or velocity represent motion-induced forces (or self-excited forces).

The importance of the steady aerodynamic force coefficients can be depicted from this set of equations:

- C_x and C'_z contribute to the damping in drag and lift respectively by an amount proportional to the mean wind velocity;
- since C_x is always positive for small angles of wind incidence, its contribution to the horizontal damping will always be positive;
- the vertical aerodynamic damping is proportional to C'_z. If this slope is negative, the overall vertical damping will be negative for a certain wind speed and galloping instability will develop;
- the pitching moment coefficient C'_m contributes to the torsional stiffness of the system. If it is positive, the torsional stiffness will decrease in proportion to V^2. The torsional frequency will thus decrease and at some wind velocity it will approach the vertical frequency creating grounds for development of classical flutter. At some other velocity the effective torsional stiffness will become negative and this time divergent instability will arise.

  A steep pitching moment slope C'_m would mean a fast reduction of the effective torsional stiffness and would likely induce larger torsional forces due to vertical gusts;
- aerodynamic coupling terms are present for the three degrees of freedom. The terms in C_m and C'_x will be negligible for a streamlined bridge deck since these aerodynamic terms evaluated at zero incidence are generally small. This means practically no coupling in the horizontal motion. Coupling will occur only if two or three modes of vibration in different degrees of freedom have a similar frequency and mode shape;
- the gust forces depend on the longitudinal and vertical component of the fluctuating velocity, u and w. The contribution of the longitudinal component is a function of the aerodynamic coefficients at zero incidence which are in most cases relatively small except for the horizontal direction where the slope C'_x is even smaller;

- a steep slope for C_z' would provide strong vertical aerodynamic damping but would also induce larger vertical forces due to the vertical gusts w.

This set of equations does not include unsteady aerodynamic coefficients that represent the out-of-phase components of the aerodynamic forces and contribute to the aerodynamic damping and stiffness of the system. The unsteady coefficients can be introduced when measurements of motional aerodynamic derivatives have been performed.

The equations above can represent aerodynamically coupled motions. However, the coupling terms are often small and therefore neglected. Also the contribution of the aerodynamic stiffness is often considered negligible in comparison to the stiffness of the bridge itself. This leaves the aerodynamic damping as the most significant aerodynamic force induced by motion. If it is negative and greater than the structural damping, large motion will result. The response of each uncoupled mode of vibration to the turbulent wind can be studied separately and superimposed at the end; usually, only the lowest modes are significant.

3 The spectral approach

A review of what is known as Davenport's spectral approach for the prediction of the buffeting response of a bridge deck is presented in this section. It is a statistical approach, based on work by Liepmann [2], which defines the wind loading as a stochastic process of the stationary random type.

Power spectra can thus be used to describe the stochastic loading as well as the statistical properties of the turbulence. The mathematical formulation is therefore simple since it can be presented as a product of linear functions of frequency or reduced frequency f^*.

It relies heavily on the aerodynamic properties of the deck cross-section obtained from wind tunnel tests on section models in turbulent flow. The more aerodynamic information about the cross-section studied, the better the predictions. However, the advantages of the frequency domain formulation are numerous, since, for example, all the unsteady characteristics of the deck are better described in the frequency domain and are extracted frequency by frequency from experiments. It is also well suited for predictions of extreme responses.

3.1 Assumptions and limitations

The assumptions and limitations of the original formulation are summarized as follows:

- wind loading due to gusts is a stochastic process of the stationary random type;

- quasi-steady assumption: the instantaneous forces on the deck are taken to be equal to the steady forces induced by a steady wind having the same relative velocity and direction as the instantaneous wind. The steady force coefficients of the deck cross-section and their variations with angle of attack are thus considered sufficient to solve the equations of motion of the deck in turbulent wind as described in the previous section;

- strip assumption: the aerodynamic forces on one strip are only due to the incident wind fluctuations on that strip. The spatial description of the wind fluctuations can then be taken as representative of the spatial distribution of the buffeting loading;

- the natural frequencies of the mode of vibrations of the structure are well separated so that coupling can be neglected. The analysis can thus be done mode by mode and the response can be determined by a superposition of a series of single degree-of-freedom systems;

- The turbulent fluctuations are assumed small enough compared to the mean velocity so that gust loads can be expressed as linear functions of the gust velocities. Also, the variation of the static coefficients around 0° is taken as being linear;

- the worst wind direction is assumed to be wind normal to the bridge axis and the mean angle of wind incidence is taken as 0°;

- cross-spectra between the u and w components of the wind are negligible;

- aerodynamic damping varies linearly with wind speed and is independent of amplitude. The contribution of the aerodynamic stiffness is neglected;

- and, the parent distribution of the extreme response is assumed to be Gaussian.

This approach is most valid for small reduced frequency $f^* = fB/V$ (or large reduced velocity) where the time taken for the flow to traverse the bridge deck is very short compared to the oscillation time or, in other words, the effects of the motion of the deck are communicated rapidly to the flow region surrounding it. In another sense, it is valid when disturbances in the flow have appreciably larger dimensions than the deck itself.

The limitations of the quasi-steady aerodynamic assumption can be lifted using the notion of aerodynamic admittance as first proposed by Sears and used by Liepmann [2] (a thorough discussion of this aspect as well as the use of the strip assumption is presented in Part II-B). Davenport suggested applying the aerodynamic admittance [1] to represent: i) the loss of lift for the higher frequency components of the turbulence (the small gusts); and, ii) the spatial variations in the flow since

the forces are not necessarily due to the wind fluctuations at one point but on a region surrounding a chord-wise strip.

Davenport also suggested in [5] the use of unsteady aerodynamic coefficients determined from the in-phase and out-of-phase components of the aerodynamic forces to evaluate the aerodynamic damping forces. This was introduced in the buffeting formulation at a later stage by Irwin [8] and Scanlan [6].

3.2 Buffeting analysis: lift

Assuming that the buffeting loading is a stationary random process, equation (12) can be transformed to the frequency domain:

$$S_L(f^*) = \left(\frac{\rho \bar{V} B}{2}\right)^2 \left(4C_z^2\, S_u(f^*)\, |A_{u,z}(f^*)|^2 \;+\; C_z'^{\,2}\, S_w(f^*)\, |A_{w,z}(f^*)|^2\right) \qquad (17)$$

where $S_L(f^*)$ is the spectrum of the lift force per unit length on a cross-sectional strip of the deck (also referred to as point-like load), f^* is the reduced frequency $= fB/\bar{V}$, $|A_{u,w;z}(f^*)|^2$ are the lift aerodynamic admittances due to the u or w components of the wind turbulence, and $S_{u,w}(f^*)$ are the spectral densities of the u and w components of the wind.

The aerodynamic admittances can either be measured, evaluated or approximated using analytical expressions derived for a thin airfoil (as described in Part II-B). Liepmann's approximation to the Sears' function is the most commonly used form for the lift aerodynamic admittance for a thin airfoil [2]:

$$|\, \phi_z(f^*)\, |^2 = \frac{1}{1 + 2\pi^2 f^*}. \qquad (18)$$

This approximation is within 10% of the more evolved Sears' function and is preferred to the latter due to its simplicity and since it has shown in some occasions to represent qualitatively direct measurements on bridge decks.

For drag, Irwin has derived an analytical expression for the admittance of the u component which varies as a function of the ratio between the scales of the turbulence and the size of the bridge deck [8].

In practice it is difficult to distinguish between the effects of u and w so the admittances are generally lumped and (17) becomes:

$$S_L(f^*) = \left(\frac{\rho \bar{V} B}{2}\right)^2 \; |A_z(f^*)|^2 \left(4C_z^2 S_u(f^*) + C_z'^{\,2} S_w(f^*)\right). \qquad (19)$$

From point-like to line-like: The transition from point-like load to load on a span l or line-like load is made via the joint acceptance function $J_z(f_j^*)$:

$$S_{F_z}(f_j^*) = S_L(f^*) \;\; |\, J_z(f_j^*)\, |^2 \qquad (20)$$

where

$$|J_z(f_j^*)|^2 = \int_0^l \int_0^l \frac{S_{L_1L_2}(\Delta y, f^*)}{S_L(f^*)} \ \mu_j(y_1)\ \mu_j(y_2)\ \mathrm{d}y_1 \mathrm{d}y_2, \tag{21}$$

μ_j is the j^{th} mode shape and $S_{L_1L_2}$ is the cross-spectrum of the lift force between strips 1 and 2 separated by Δy.

The natural wind is composed of gusts that can be visualized as *cigars*, e.g. 200 m long and 30-40 m in diameter, being transported and streched by the mean flow field. These gusts will pass by the structure and generate buffeting forces. Given a 1000 m bridge span for example, it is unlikely that a series of large gusts will pass by the entire span at the same time. The buffeting forces are thus not fully correlated span-wise. Also, the gust loading pattern will affect the structure in a different way for each different mode of vibration. The joint acceptance function takes these effects into account. It measures the correlation between the spatial distribution of the forces across the span and the mode. There is one joint acceptance function per mode of vibration of the deck.

The evaluation of the cross-spectrum of the lift forces is difficult, but under the basis of the strip assumption:

$$\frac{S_{L_1L_2}(\Delta y, f^*)}{S_L(f^*)} \approx \frac{S_{w_1w_2}(\Delta y, f^*)}{S_w(f^*)} = coh_w^{1/2}(\Delta y, f^*). \tag{22}$$

It has been reported that (22) might not be valid for closed-box girder bridge decks since their width is often of the same dimension as the scales of the w component of the turbulence. The evaluation of the span-wise root coherence of the aerodynamic forces $coh_L^{1/2}(\Delta y, f^*)$ is thus at the heart of the definition of the wind loading on a span. Part II-A and Part II-B of this thesis deals with its experimental and analytical evaluation.

Spectrum of the buffeting response: The spectrum of the response of a given mode to the buffeting forcing described above can be calculated using;

$$S_{r_z}(f_j^*) = S_{F_z}(f_j^*)\ \ |H(f_j^*)|^2 \tag{23}$$

where $H(f_j^*)$ is the single degree-of-freedom mechanical admittance function of mode j. $H(f_j^*)$ is a function of reduced frequency and damping, both being influenced by the aerodynamic forcing. This influence is represented by adding the contribution of the aerodynamic damping ζ_a to the structural damping ζ_s and also by correcting the frequency term to take into account the aerodynamic stiffness. The latter correction often has negligible influence on the buffeting response and is thus omitted in the following. $H(f_j^*)$ can be expressed by:

$$|\ H(f_j^*)\ |^2 = \frac{1}{\left(1 - (\frac{f^*}{f_j^*})^2\right)^2 + \left(2(\zeta_{s,j} + \zeta_{a,j})\frac{f^*}{f_j^*}\right)^2}. \tag{24}$$

The mean square vertical response of mode j is:

$$\sigma_{r_j}^2 = \int_0^\infty S_{F_z}(f_j^*) \ |H(f_j^*)|^2 \mathrm{d}f^*, \tag{25}$$

and the mean square response for all modes at span-wise position y is:

$$\sigma_r^2(y) = \sum_{j=1}^{n} \sigma_{r_j}^2 \ \mu_j^2(y). \tag{26}$$

Background and resonant components: The dynamic response can be divided in its background and resonant components:

$$\sigma_{Background}^2 = \int_0^\infty f^* S_L(f^*) \ \mid J_z(f^*) \mid^2 \ \mathrm{d}\ln f^* \tag{27}$$

$$\sigma_{Resonant_j}^2 \approx f_j^* S_L(f_j^*) \ \mid J_z(f_j^*) \mid^2 \ \frac{(\pi/4)}{\left(\zeta_{s_j} + \zeta_a(f_j^*)\right)} \tag{28}$$

where the last two terms of equation (28) are an approximation (error of less than $+10\%$) of the area under the resonant peak of the product of $S_{F_z}(f_j^*)$ and $|H(f_j^*)|^2$.

The background response is the part of the dynamic response that is acting quasi-statically due to slow variations of wind speeds. It covers a broad frequency band below the lowest natural frequency. The resonant response is concentrated in a peak at the natural frequency, the height of which is controlled by the damping. For flexible long-span structure, the resonant component dominates the response, especially in lift and torsion. For more rigid structure such as guyed-mast towers, the background component generally dominates.

The contributions of the w component of the turbulence to the expressions for σ_B^2 and $\sigma_{R_j}^2$ can be written as follows for the vertical forces:

$$\sigma_{B_z}^2 = \left(\frac{\rho \bar{V}^2 B C'_z}{2}\right)^2 \left(\frac{\sigma_w}{\bar{V}}\right)^2 \int_0^\infty \frac{f^* S_w(f^*)}{\sigma_w^2} \ \mid A_z(f^*) \mid^2 \mid J_z(f^*) \mid^2 \ \mathrm{d}\ln f^* \tag{29}$$

$$\sigma_{R_{z_j}}^2 \approx \left(\frac{\rho \bar{V}^2 B C'_z}{2}\right)^2 \left(\frac{\sigma_w}{\bar{V}}\right)^2 \frac{f^* S_w(f^*)}{\sigma_w^2} \ \mid A_z(f^*) \mid^2 \mid J_z(f_j^*) \mid^2 \ \frac{(\pi/4)}{\left(\zeta_{s_j} + \zeta_a(f_j^*)\right)}. \tag{30}$$

Similar expressions for the torsion can be written with θ and m replacing z and introducing an additional deck width B. For the lateral direction $2C_x$ replaces C'_z and u replaces w.

If the left hand terms are normalized by the $(\rho \bar{V}^2 B C'_z)^2$ term, the response is a function primarily of the reduced frequency f^* and the intensity of turbulence

$(\sigma_w/\bar{V})$, two homologous quantities which link the full-scale bridge behaviour with any dynamically scaled model. Otherwise, the turbulence controlled response is bound up in the functional form of the turbulence spectrum, S_w, the aerodynamic admittance, A_z, the joint acceptance function, J_z, and the aerodynamic damping ζ_a.

Peak response: The peak response, $\hat{r}$, solution of the equations of motion, is composed of the following:

$$\hat{r} = \bar{r} + g\sqrt{\sigma_B^2 + \sum \sigma_{R_j}^2} \tag{31}$$

where $\bar{r}$ is the mean response, g is a statistical peak factor, σ_B^2 is the mean square background response, and $\sigma_{R_j}^2$ is the mean square modal response at or near the j^{th} resonant frequency.

The peak factor g is based on the definition of the largest instantaneous value of a stationary random variable with a Gaussian distribution:

$$g(\nu T) = \sqrt{2\ln(\nu T)} + \frac{0.577}{\sqrt{2\ln(\nu T)}} \tag{32}$$

where ν is the cycling rate of the process and T is the sampling period. The longer the sampling period, the smaller the variations of g. The cycling rate is defined by:

$$\nu^2 = \frac{\int_0^\infty f^2 S_R(f)\mathrm{d}f}{\int_0^\infty S_R(f)\mathrm{d}f}. \tag{33}$$

Typical values of g for the buffeting response range from 3 to 4.

Quasi-steady aerodynamic damping: Linking damping with the velocity term of equation (10), the vertical aerodynamic damping force can be expressed by:

$$F_{z,damping} \approx \frac{\rho B}{2}(C_z'\bar{V}\dot{z}). \tag{34}$$

Damping as a fraction of critical is defined as the ratio of the work done by one cycle against the lift to the total energy stored in the system:

$$\zeta_{aero}(f_j^*) = \frac{\Delta E}{4\pi E} = \frac{G_j^*}{G_{crit}} = \frac{\frac{\rho B}{2}(C_z'\bar{V})\ \int_0^l \mu_j^2(y)\mathrm{d}y}{2w_j M_j^*} \approx \frac{\frac{\rho B}{2}(C_z'\bar{V})}{4\pi f_j m} \tag{35}$$

where G_j^* and M_j^* are respectively the generalized damping and mass of mode j, and m is the mass per unit length of the deck (assumed here and in the following as being constant along the span so that $M_j^* = m\int_0^l \mu_j^2(y)\mathrm{d}y$).

The expressions for the quasi-steady aerodynamic damping as a fraction of critical $\zeta_{a;x,z,\theta}$, and the aerodynamic stiffness, $\eta_{a;\theta}$, reduce to:

$$\zeta_{a;x} = \frac{C_x}{4\pi}\frac{V}{f_x B}\frac{\rho B^2}{m}; \qquad \zeta_{a;z} = \frac{C'_z}{8\pi}\frac{V}{f_z B}\frac{\rho B^2}{m} \tag{36}$$

$$\zeta_{a;\theta} = \frac{nC'_m}{8\pi}\frac{V}{f_\theta B}\frac{\rho B^4}{I_\theta}; \qquad \eta_{a;\theta} = -\frac{C'_m}{8\pi^2}\left(\frac{V}{f_\theta B}\right)^2\frac{\rho B^4}{I_\theta} \tag{37}$$

Aerodynamic damping from aerodynamic derivatives: The aerodynamic damping of a given cross-section can also be obtained from wind tunnel experiments on section models or three-dimensional aeroelastic models, in smooth or turbulent flow.

The estimation of the aerodynamic damping can be done in the time domain simply by correlating the increase or reduction of the total damping of a mechanical system with an increase in wind speed [8]; or in the frequency domain by identifying the aerodynamic forces 90° out-of-phase with the motion for various wind speeds [6].

These experiments are generally linked with the determination of the aerodynamic derivatives that describe in detail the motion-induced forces. The ideal case is to carry out a series of experiments that will make possible the system identification in turbulent flow on the transient response as described by Bogunovic-Jakobsen [10] or Zasso [9]. The identification in smooth flow is however much simpler and reliable if motions are kept at small amplitudes [10].

The motional aerodynamic derivatives can easily be converted to equivalent viscous damping and used directly in the calculation of the mechanical admittance function of the system or in equation (30). The conversion of the aerodynamic derivative terms H_1^* and A_2^* in Scanlan notation [6] can be made using the following expressions [6]:

$$\zeta_{a;z}(f_j^*) = -H_1^*(f_j^*)\frac{\rho B^2}{2m} \tag{38}$$

$$\zeta_{a;\theta}(f_j^*) = -A_2^*(f_j^*)\frac{\rho B^4}{2I_\theta}. \tag{39}$$

3.3 Simplified expression, resonant modal response

Defining the resonant root-mean-square modal response $\tilde{r}_{R_j}$ by:

$$\tilde{r}_{R_j} = \frac{\sqrt{\sigma_{R_j}^2}}{K_j^*} \quad \text{where} \quad K_j^* = \omega_j^2 \int_0^l m\mu_j^2(y)\,\mathrm{d}y, \tag{40}$$

and K_j^* and ω_j^2 are respectively the generalized stiffness and angular velocity of oscillation of mode j. Rearranging equation (30), a general expression for the normalized vertical resonant rms modal response (acceleration) can be obtained:

$$\frac{\tilde{r_j}}{I_w B \omega_j^2} = \frac{C_z'}{8\pi^2}\left[\frac{\bar{V}}{f_j B}\right]^2 \frac{\rho B^2}{m}\sqrt{\frac{f^* S_w(f^*)}{\sigma_w^2}}|A_z(f^*)||J_z(f_j^*)|\sqrt{\frac{\frac{\pi}{4}}{\zeta_s + \zeta_a(f^*)}}. \qquad (41)$$

Equation (41) is a product of dimensionless parameters that can all be evaluated with a relatively high confidence level through section model tests and full scale measurements at the site. It is valid for all modes where the deck dominates the aerodynamic forces and can be easily transformed to express the lateral and torsional responses. Note that if the structural damping is considered dominant in equation (41), thus neglecting the aerodynamic damping term, the resonant rms response will tend to be proportional to the reduced velocity at a power in the vincinity of 2 since $A_z(f^*)$ and $J_z(f_j^*)$ are proportional to the reduced velocity [11]. On the other hand, if the aerodynamic damping is dominant, the exponent will have a value approaching 2 given the variation of ζ_a with the reduced velocity in the denominator of equation (41).

3.4 Shortcomings

The frequency domain approach described in this section has been shown to be a relatively simple and reliable method to calculate the wind loads on a bridge deck due to the buffeting action of the wind. Its error margin is directly related to the extent of the knowledge of the aerodynamic properties (steady and unsteady) of the bridge deck considered. This is probably its main shortcoming.

If only the static coefficients are known, error margins of the order of 150-200% overestimation of the rms response compared to measured response in full scale or model scale can be expected [6]. If the unsteady properties are known, e.g. aerodynamic derivatives, aerodynamic admittance and span-wise coherence of the forces, this error margin can be considerably reduced to a more acceptable level, $\approx +20 - 30\%$.

Its main limitations are assumptions of linearity, the disregarding of coupling effects and the use of the strip assumption to define the span-wise coherence of the wind loading. The latter is investigated in detail in Part II. It is reported in Part II-A that the error margin associated with the strip assumption only, varied from an overestimation of more than 200% to an underestimation of the wind loading of 50%, depending on the reduced frequency when compared to direct measurements on section models.

Coupling: Coupling between modes is disregarded in the spectral approach described here. The error margin associated with this simplification is hard to evaluate in a general manner.

Experience has shown that for service limit state calculations, where the wind speeds of interest are far from the range of aerodynamic instability, coupling effects are small and are most often beneficial. Coupling between modes will disorganize the motion and transfer energy from one mode to an other which will appear as damping.

In the early phases of the design, the structural engineer will aim at avoiding structural coupling between the fundamental modes. In some instances however, a certain level of coupling is unavoidable, for example between a torsional mode and a lateral mode of an arch shape structure.

Linearity: The buffeting theory is valid for bridge decks with static coefficients that vary linearly with angle of wind incidence between say -3° and +3°. Here also the designer will aim at choosing a cross-sectional shape that satisfies this assumption. For more bluff sections or due to the presence of appendages such as wind breaks or crash barriers, this might not be possible.

For non-linear variations of the static coefficients, the error margin of the spectral approach could be important and another method of evaluation is advisable, either experimentally with an aeroelastic simulation or in the time domain where the non-linear variations of the coefficients can be modelled easily.

For what concerns non-linear variations of damping or stiffness of the structure with amplitude of motions, the spectral approach by itself is not adequate. Damping for example has to be evaluated a priori for an assumed amplitude. This is often made for conditions in the neighbourhood of the design wind speed. The combination of time domain buffeting simulations and non-linear finite element analysis programmes can better deal with such eventualities, especially when ultimate limit state conditions have to be studied [12]. A review of the developments of the time domain buffeting analysis is presented in the Section 4.

Aerodynamic damping: For the vertical and the lateral degrees of freedom, quasi-steady aerodynamics can in general predict the level of aerodynamic damping of a deck cross-section within an acceptable error margin [6].

However, for the torsional degree of freedom, quasi-steady aerodynamics is often not adequate to predict the aerodynamic damping. In many occasions, quasi-steady aerodynamics using $n = 0.25$ predicted positive damping while in reality, negative damping (which adds energy to the motion) was present [8]. Experiments on section models to evaluate the torsional aerodynamic damping or the $A_2^*(f_j^*)$ aerodynamic derivatives are strongly recommended.

3.5 Improvements

Part II-A and Part II-B of this thesis deal with improvement of the current buffeting analysis methods where it is believed that a substantial reduction of the error

margin of the predictions can be achieved. It concerns the application of the strip assumption and presents a model that departs from this assumption to calculate the aerodynamic admittance and the span-wise coherence of the forces.

For non-streamlined bridge decks, an experimental method to evaluate the aerodynamic admittance is proposed in Part III-A. The method links cross-section admittance to the span-wise coherence of the forces on a span. The measured quantity can be used directly in the current spectral approach to predict wind loading and buffeting response. Other areas of improvement are discussed in the following.

Variations of the angle of wind incidence: To reduce the statistical uncertainties related to the linearisation of the static coefficients used in the buffeting analysis, Irwin and Xie [13] have proposed an equivalent linearisation method.

It consists of calculating the weighted average values of the static coefficients using a Gaussian probability density distribution for the instantaneous angle of attack α:

$$\bar{C}_z(I_w) = \int_{-\infty}^{\infty} C_z(\alpha)\, p(\alpha, I_w)\, \mathrm{d}\alpha; \quad \bar{C}'_z(I_w) = \int_{-\infty}^{\infty} \frac{\mathrm{d}C_z(\alpha)}{\mathrm{d}\alpha}\, p(\alpha, I_w)\, \mathrm{d}\alpha \tag{42}$$

where

$$p(\alpha, I_w) = \frac{1}{\sqrt{2\pi} I_w} \exp\left[-\frac{1}{2}\frac{\alpha^2}{I_w^2}\right] \tag{43}$$

is a Gaussian distribution and I_w is the vertical turbulence intensity.

This weighted average method is a clever way to deal with the problem of the non-linearity of the static coefficients and can be introduced easily in the current buffeting theory. An example of the application of this method is given in Fig. 2 for static coefficients measured in turbulent flow on a section model of a closed-box girder bridge deck.

Calculation of the joint acceptance function: Under the strip assumption the root coherence of the forces can be represented by the root coherence of the wind velocity. In turn, the root coherence of the wind velocity is often expressed by an exponential function:

$$coh_L^{1/2}(\Delta y, f^*) \approx coh_w^{1/2}(\Delta y, f^*) \approx \exp\left[-c\frac{f\Delta y}{\bar{V}}\right] \tag{44}$$

where c represents the width of the correlation and varies from 4 to 14 depending on the site (8 is most often used) [1].

Equation (44) is an empirical expression and was found to be most valid for separation Δy somewhat smaller than the scale of turbulence. Collapse of the root coherence curves is expected for the smaller separation when plotted against reduced

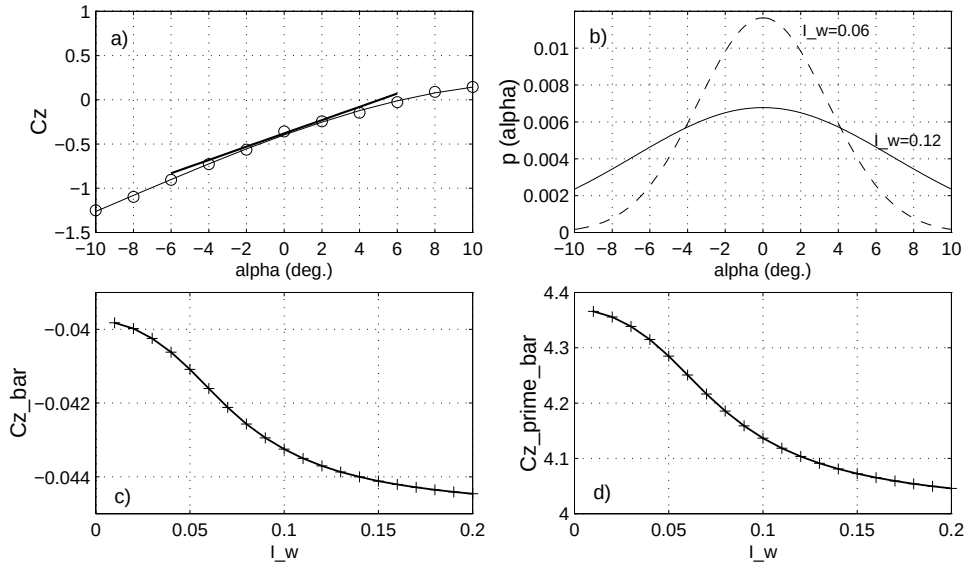

Figure 2: Application of the weighted average method for a closed-box girder bridge deck. **a)** shows a linearization ($-0.38+4.3\alpha$, thick line) of the measured coefficients; **b)** shows the Gaussian probability of α for two levels of I_w; **c)** and **d)** give respectively the variations of $\bar{C}_z$ and $\bar{C}'_z$ as a function of I_w using (42).

frequency $f\Delta y/\bar{V}$, which is the ratio of the separation to the wave length of the fluctuations. For the case where the separation is of the order of or larger than the turbulence scales, (44) is not adequate, the root coherence curves decaying like *a series of diminishing humps* [1].

Irwin [8] has shown that the use of this simple exponential expression could introduce an important overestimation of the response at low frequencies since it represents turbulence with infinite length scales. In reality, the turbulence length scales are finite and the root coherence for low frequencies and large separations drops considerably below 1.0 where equation (44) will put it. This was confirmed on several occasions by other researchers, in model scale [6, 10] and in full-scale [19].

Among others, Irwin suggested the use of an expression derived from the isotropic turbulence model based on the von Kármán spectrum. Part II-A of this thesis describes in detail the use of such a model to fit the root coherence data. It suggests a correction for low frequencies and large separations of the parameter $f\Delta y/B$ normally used in the buffeting analysis. The correction is based on turbulence

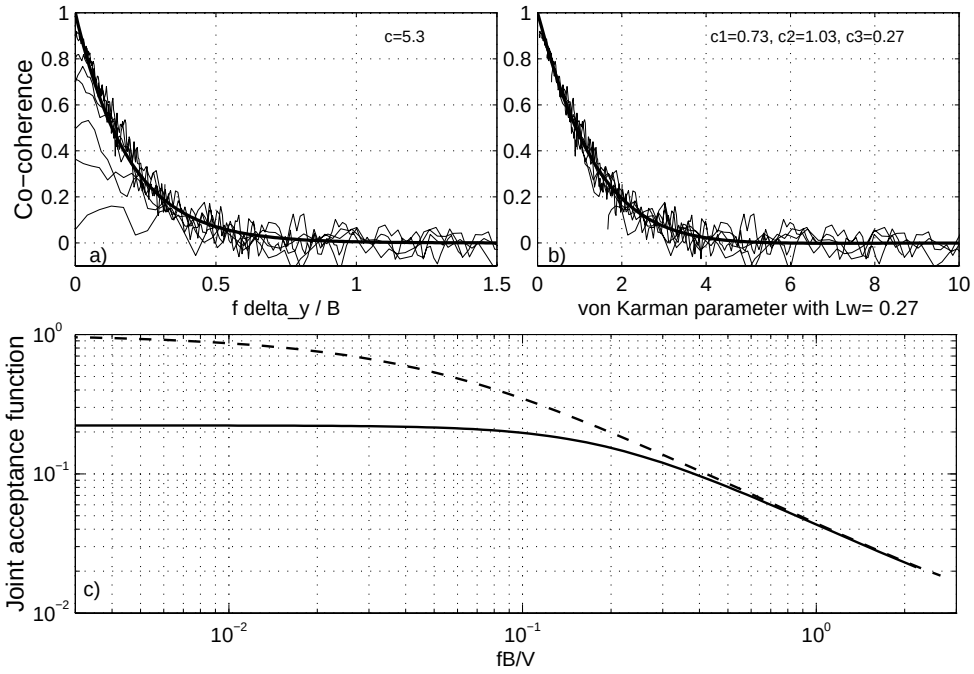

Figure 3: Variations of the joint acceptance function with reduced velocity for a uniform mode shape $\mu(y) = 1$ for two representations of the wind co-coherence: a) solid line: $cocoh_w(\Delta y, f) = \exp[-cf\Delta y/B]$; b) solid line: $cocoh_w(\Delta y, f) = \exp[-c_1\gamma^{c_2}]\cos(c_3\gamma)$. On c) $\mid J_z(f_j^*) \mid^2$ was calculated using the fits based on $f\Delta y/B$ (dashed line) and based on the von Kármán parameter (solid line).

length scales and is of the form:

$$\gamma = k_1 \Delta y \sqrt{1 + \frac{1}{k_1^2 L^2}} \tag{45}$$

where $k_1 = 2\pi f/\bar{V}$, L is a length scale and γ is called the von Kármán collapsing parameter [4].

Fig. 3 compares curves of span-wise co-coherence of the wind velocity as a function of $f\Delta y/V$ and γ, and illustrates the effect of the two expressions on the calculation of the joint acceptance function. Co-coherence (or normalized co-spectrum) is the real part of the cross-spectrum normalized by the one-point spectrum and it is equivalent to the root coherence for isotropic turbulence. The error margin (overestimation) of the joint acceptance function associated with the simple exponential expression at low frequencies is considerable and could be easily avoided.

Directionality: The problems associated with directionality of the incident wind have been dealt in detail in a *modified buffeting theory for yawed wind* by Kimura and Tanaka [16]. Directionality effects are often more important for bridges during construction than in service conditions and should certainly be combined with the annual probability distribution of wind direction for a given site.

4 Predictions in the time domain: a review

A great deal of work on the formulation of the unsteady aerodynamic forces on a thin airfoil in sinusoidal gusts and later in random gusts has been published since the 1930's [17]. The original formulations proposed by the pioneers such as Sears, Wagner and Kussner have been further developed, especially in the 1970's and 1980's to a high degree of sophistication and are commonly used today in the aerospace industry.

At first, the formulations were developed in the time domain, then linearized, and the problems were solved in the frequency domain [2]. It appears that this practice is still true when it comes to general buffeting problems of aircraft flying in turbulence or bridges buffeting in natural wind [17]. However, the development of computer aided flying and the active flutter control of wings has pushed the need to express the unsteady aerodynamic forces in a time variant manner. Very efficient algorithms were developed in the time domain to perform the servo-control of flaps and are based on aerodynamic data obtained experimentally in the frequency domain.

In the bridge aerodynamics field, the frequency domain approach is also predominantly applied to solve the problem of wind effects, even if the original formulations were done in the time domain [1]. It was in the early 1970's that Scanlan, Beliveau and Budlong first worked on solving the problem entirely in the time domain, introducing the indicial functions put forward earlier in the aeronautical field. It is, however, only recently that much effort has been invested in developing efficient time domain formulations of the unsteady aerodynamic forces that could be combined with a finite element model of the structure and could include all the non-linearities that have been omitted in the past [18]. This development has been justified with the planning of very long bridges such as the bridge over the Stretto di Messina and the Akashi Kaikyo Bridge.

The following are brief remarks concerning what can be found in the recent literature on this topic. It should be noted first that no less than five papers out of twenty on bridge aerodynamics were concerned with time domain predictions of the response at the last International Conference on Wind Engineering in January, 1995. These papers give a good account of the state-of-the-art in the formulation of the unsteady aerodynamic forces on bridge decks.

The problem of the formulation of the time varying wind load in the time domain can be summarized as follows:

1. The bridge deck is excited by the turbulence of the wind at a certain time t but also by what happened between the eddies in the flow and the deck at time t-z. That is to say that the wind loading has a memory or that there exists a phase lag and time lag between the source of the excitations and the loading or aerodynamic forces themselves. In the frequency domain this memory effect is expressed by an aerodynamic admittance function. The memory effect is a sole function of the cross-sectional geometry of the deck.

2. The motion of a deck in a moving fluid induces forces that interact with the initial forcing and creates new oscillations. These forces are called motion-induced forces or self-excited forces and can be concentrated in one or several degrees of freedom (coupling of modes). They are normally best described in the frequency domain and their conversion to the time domain is problematic.

3. The aerodynamic forces are far from being fully correlated along the span of the bridge. The span-wise correlation of the approaching wind fluctuations, combined with the mode shapes of the deck govern the span-wise distribution of the aerodynamic forcing. Also, the span-wise coherence of the aerodynamic forces is not necessarily identical to the span-wise coherence of the approaching flow, as stated by the strip assumption. None of the papers reviewed here have dealt with this aspect.

4. The simulation of the approaching wind has also its share of difficulties. An adequate simulation should model all the one-point and two-point statistics of the wind fluctuations. Locally it should respect the first and second moments for each wind component as well as auto spectrum and cross spectrum between the components and span-wise. It should also model the cross spectra of the respective components, u, v and w. A discussion of this aspect is given in [19] and no comments will be made here concerning the approaches found in the literature in connection with the wind loading formulation. Needless to say, this aspect is of prime importance because, no matter how good the wind loading algorithm is, if the input is not adequate, the output will suffer.

   In some instances it was found that the wind simulation was "trimmed" or "filtered" to account for some of the problems described above (e.g. aerodynamic admittance).

The approaches found in the literature can be classified in five categories: i) quasi-steady aerodynamics; ii) corrected quasi-steady aerodynamics; iii) indicial functions (Fourier Transform); iv) rational function approximations (Laplace Transform); v) equivalent oscillator (neural network and black box).

4.1 Quasi-steady aerodynamics

Miyata et al. [20] clearly present the advantages of the time domain predictions of the action of wind on long span bridges when combined with a finite element model of the structure. The formulation used here is fairly simple and very much along the same lines as the original formulation by Davenport. Quasi-steady aerodynamics is assumed as well as the strip assumption. Kovacs et al. [12] has a similar approach except that the finite element model of the structure includes structural non-linearities for large deflection in order to evaluate the ultimate state conditions.

Even though the limitations of these quasi-steady aerodynamics approaches are numerous, Miyata et al. [20] obtained surprisingly good agreement between simulation and wind tunnel tests for a very large suspension bridge (Akashi Kaikyo). The limitations are: non-inclusion of the motion-induced forces (besides quasi-steady aerodynamic damping) in the wind load model; memory function expressed as an aerodynamic admittance filtering the wind field simulation; inadequate representation of the span-wise coherence of the forces; and, the assumption that the center of the aerodynamic forces is fixed at a distance 1/4 of the deck width from the deck centerline. This assumption allows the inclusion of the torsional motion in the definition of the apparent angle of attack or in the relative wind velocity. The position of the center of the aerodynamic forces is known to vary with reduced velocity.

4.2 Corrected quasi-steady aerodynamics

The work by Diana et al. [21, 22] in relation to the studies for the proposed bridge over Stretto di Messina has taken a similar approach with the exception that some of the above limitations have been lifted by the development of a "corrected" quasi-steady theory. Here, the motion-induced forces are fully included in the formulation of the aerodynamic forces via the experimentally determined motional aerodynamic derivatives. The location of the center of the aerodynamic forces is also determined from the aerodynamic derivatives.

To include the motion-induced forces, Diana [21] proposed an equivalent linearisation, for each reduced velocity, of the type:

$$C_L^*(\alpha) = C_{L_s}(\alpha_0) + \int_{\alpha_0}^{\alpha} K_L^* \, d\alpha_z \tag{46}$$

where:

$C_L^*(\alpha)$ = corrected aerodynamic coefficient;
$C_{L_s}(\alpha_0)$ = static coefficient at angle of attack α_0 of the equilibrium position;
K_L^* = aerodynamic derivatives (e.g. lift slope varying with reduced velocity).

Here α is defined as the apparent angle of attack based on the relationship:

$$\alpha = \theta - \frac{\dot{z}}{\bar{V}} - b_{1z}\frac{B\dot{\theta}}{\bar{V}} + \frac{w}{\bar{V}} \tag{47}$$

where z and θ represent respectively a vertical displacement and rotation of the deck, and b_{1z} is the position of the point of applications of the vertical aerodynamic forces and is a function of reduced velocity.

This formulation has been shown to be adequate in many ways [22] except when it deals with the response of the higher modes. The limitations attributed to the memory effects and the span-wise coherence of the forces are also not dealt with by Diana.

4.3 Indicial functions

In a series of papers spanning several years, Scanlan, Beliveau and Budlong [23, 24, 25] described the use of indicial functions for the inclusion of the motion-induced forces in the time domain formulation of the aerodynamic forces. The formulation of the self-excited lift forces L_{se} can be read as follows:

$$L_{se} = \frac{1}{2}\rho V^2 B \frac{\mathrm{d}C_L}{\mathrm{d}\alpha} \int_0^s [\Phi_L(s-\tau)\alpha'(\tau) + \Psi_L(s-\tau)\frac{z''(\tau)}{B}]d\tau \tag{48}$$

where $s = Vt/B$, $()' = \mathrm{d}/\mathrm{d}s$ and,

$\Phi_L(s)$ = indicial response function due to a step change in angle of attack;
$\Psi_L(s)$ = indicial response function due to a step change in vertical velocity.

$\Phi_L(s)$ and $\Psi_L(s)$ could be of the form

$$\Phi_L(s) = c_0 + c_1 e^{c_2 s} + c_3 e^{c_4 s} \tag{49}$$

where the coefficients c_i of the indicial functions are extracted by non-linear least square fitting of the aerodynamic derivative curves. Even though this approach appears to be efficient, very few examples of its application can be found in the literature.

Recently, Lin et al. [26] proposed another model for the self-excited forces on a bridge deck based on the indicial function idea. The self-excited loads are expressed in terms of convolution integrals of response functions due to a unit impulse displacement (vertical or angular). These impulse response functions are obtained from inverse Fourier transformations of the frequency response functions of the form (for moments due to the change of angle of attack α):

$$F_{M_\alpha}(\omega) = \rho B^2 V^2 \left[c_1 + \frac{B}{V} i\omega c_2 + \frac{c_3 i\omega}{c_5 V/B + i\omega} + \frac{c_4 i\omega}{c_6 V/B + i\omega}\right] \tag{50}$$

$$F_{M_\alpha}(\omega) = \rho B^2 V^4 \omega^2 (A_3^* + iA_2^*) \tag{51}$$

where the coefficients c_1 to c_6 are obtained from non-linear fitting of the aerodynamic derivative curves (A_i^* and H_i^*) and K is a reduced frequency.

Li et al. [27] have presented a method to determine experimentally the coefficients c_1 to c_6 and therefore the impulse response functions. A complete example of the use of this formulation is given by Xiang et al. [28] for the motion-induced forces. Comparisons are made between time domain predictions and wind tunnel test results for the Shanton Bay Bridge. The agreement is remarkable, even though here also the buffeting forces are calculated using quasi-steady aerodynamics.

4.4 Rational function approximations

Fujino et al. [29], in dealing with the problem of active control of flutter for bridges, have formulated a method to express the motion-induced forces in the time domain. This method is directly inspired from work in the aerospace industry. Rational function approximations are used to express the equation of motion of the deck in a linear time invariant state-space form where the unsteady aerodynamic forces do not depend explicitly on reduced velocity [30, 31].

The aerodynamic derivatives obtained from experiments are stored in tabular form in the reduced frequency domain and are approximated in the Laplace domain by rational functions and a series of coefficients. The rational functions are then inverse Laplace transformed to the time domain to solve the space-state equation of motion (see Tiffany and Adams 1988 [32]). The level of accuracy is a function of the number of "aerodynamic states" used for the approximation, but once the numerical problems are solved this method appears to be effective [29] and is currently used in aerospace applications [33].

Li and He [34] present a formulation of the unsteady forces that includes rational function approximations for the motion-induced forces and the buffeting forces are expressed by convolution integrals of impulse aerodynamic transfer functions determined experimentally from wind tunnel tests. An example of the calculations is given but no comparisons with measured aeroelastic responses on a physical model are made. This method appears to be the most complete of all the above-described approaches.

4.5 Equivalent oscillator

Diana et al. [35] have initiated research on new methods to express the aerodynamic forces in the time domain including buffeting, motion-induced forces and vortex-shedding forces using numerical models comprised of the bridge deck and an equivalent oscillator. The new methods include "black-box models", a neural network model and sophisticated parameter identification algorithms using an Extended Kalman Filter. Preliminary evaluations of the methods have shown satisfactory results, especially for non-linear phenomena such as vortex-shedding induced oscillations.

5 Experimental approaches

The study of wind effects on long span bridges is possible to some extent through theoretical predictions but is almost always dependent on aerodynamic information provided by wind tunnel tests [36]. For example, the somewhat straightforward prediction of the mean lateral deflection of a suspension bridge deck is dependent on the steady drag force coefficient obtained from wind tunnel tests on a section model.

Wind tunnel testing of bridges involves the interaction of a structure with an oncoming flow. It is then important to stress that not only must the structure be modelled properly but also the flow must be at the right scale in relation to the structure and, moreover, representative of the wind at the prototype bridge site.

5.1 Section model method

Section model tests on a representative span-wise portion of a bridge deck is the most employed technique to obtain first level aerodynamic information on the deck cross-section. Section models are used to detect signs of vortex-induced oscillations and instability, as well as a source of a panoply of aerodynamic properties ranging from static force coefficients to aerodynamic derivatives. They are limited by their two-dimensional character but are often used early in the bridge design process to help define the deck geometry.

The theoretical basis for *extended* section model testing in turbulent flow stipulates that for the section model and full bridge responses to be similar the following restrictions must hold [37]:

- the motion-induced aerodynamic forces at all locations across the span must have the same linear function as the local motion of the deck (rigid model);
- the scale of turbulence at the resonant frequency is small in comparison with the length of the model (hence the term "extended" section model), but still in proportion with the geometrical scale of the model; and,
- the aerodynamic forces on the cables and towers must be small compared to those of the deck.

Early section model tests have shown satisfactory qualitative agreement with full bridge model tests and have adequately predicted unstable behaviour of full-scale bridges [38, 39]. However, significant deficiencies in the earlier approach were noted [37] and an alternative approach was proposed by Davenport [40]. This approach includes tests in turbulent flow as well as in smooth flow and utilizes the measured response of an *extended* section model with suitable corrections for discrepancies in the intensity and spectrum of turbulence, the damping and the mode shape. The responses are determined from estimates of the dynamic wind loads in the lowest

symmetric and asymmetric modes as well as the steady wind loads for the lateral, vertical and torsional degrees of freedom.

From these experiments it is possible to extract the aerodynamic input necessary for the application of the buffeting theory and predict analytically the response of the prototype bridge. However it is also possible to convert the section model results to full-scale equivalent static loads, as described below, and to apply this loading to the prototype structure to calculate the buffeting response.

5.2 Predictions of full-scale response

Static response: The static part of the response (or the mean response) can be predicted from the static force coefficients of the deck obtained from the section model tests. The lateral and vertical steady wind forces applied to the deck through the cables can be significant and should be included in many cases [41]. The effect of the mean lateral displacement of the top of the pylons should also be included in the predictions of the mean response.

The static coefficients, determined in turbulent flow and expressed in the deck local coordinate system, are converted to full-scale static wind forces as a function of the wind speed. The static response is obtained by dividing the static wind forces by the generalized stiffness of the fundamental mode studied.

For example, the mean lateral amplitude $\Delta\bar{x}$ of the deck can be estimated from the following expression if the mean drag coefficient C_x, evaluated at 0° of wind incidence, and the fundamental horizontal mode shape $\mu(y)$ (normalized to unit maximum amplitude) are known:

$$\frac{\Delta\bar{x}}{B} = \frac{\bar{F}_x}{BK_x^*} = \frac{\frac{1}{2}\rho\bar{V}^2 C_x l B}{B\omega_x^2 \int_0^l m(y)\mu(y)^2 \mathrm{d}y}. \tag{52}$$

The mean horizontal displacement at a given point y on the deck is then given by $\Delta\bar{x}\mu(y) = \bar{x}(y)$ so that :

$$\frac{\bar{x}(y)}{B} = \frac{\frac{1}{2}\rho\bar{V}^2 C_x l}{(2\pi f_x)^2 m \int_0^l \mu^2(y)\mathrm{d}y}\,\mu(y), \tag{53}$$

assuming a constant mass per unit length $m(y) = m$.

Dynamic response: The background and resonant components of the dynamic response are expressed respectively by equations (29) and (30). These expressions apply to both the full scale bridge and a section model in a turbulent wind tunnel flow. If the main characteristics of the full scale turbulence can be reproduced adequately in the wind tunnel with respect to the scale of the model, the results of the dynamic tests can be directly adapted to full scale with minimal corrections. Tests of extended section models (with 1:7 aspect ratio or the like) in a turbulent

flow generated behind large spires have shown that it is possible. Although the turbulence scale and intensity cannot be made to correspond exactly to full scale, the values can be made sufficiently close.

To adapt the results of the dynamic section model testing to full scale, corrections need to be applied as follows:

1. Corrections of the low frequency background response, σ_B^2, largely omitted from the section model due to the deficit in the vertical velocity spectrum generated by the spires. This can be estimated with reasonable accuracy from equation (29) using either theoretical or experimental data as outlined below.

2. Corrections of the terms in the resonant response σ_R^2 for the discrepancies in the turbulence intensity, vertical velocity spectrum, joint acceptance function and damping.

   The correction factors are found from the ratios of the quantities involved for model and full-scale. For example, the correction factor for the turbulence intensity is a constant (i.e. the ratio of target full scale to model values). Similarly, the correction factor for the vertical velocity spectrum is the ratio between the target full scale spectra and the model scale spectra at a given frequency. The joint acceptance function correction, converts the uniform mode shape values of the section model to the quasi-sinusoidal mode shapes of the prototype. The damping correction combines structural damping and aerodynamic damping to satisfy equation (41). Through the appropriate selection in the section model tests of turbulence characteristics, structural damping and geometrical scale, these corrections can be kept relatively small.

Comparisons: For an adequate wind simulation, the extended section model method is superior to the analytical spectral approach in many ways. None of the limiting assumptions of the buffeting theory are necessary and it can also simulate motion-induced forces in turbulent flow or with non-linear behaviour. It has the disadvantage that a new series of buffeting tests is required for each additional structural configuration, e.g. frequency ratio or generalized mass.

5.3 Three-dimensional physical models

Full-bridge aeroelastic model: Wind tunnel testing of full bridge aeroelastic models in adequately simulated atmospheric boundary layer flow is the best method of prediction of the response, besides testing the prototype bridge itself in natural wind. It allows the determination of the stability of the bridge in high winds, investigation of any vortex-induced oscillations and characterization of the buffeting response [42].

The main character of this technique is its three dimensionality. Three-dimensional wind gusts exciting 3-D pylons, cables and deck with 3-D vibration mode shapes is provides a wealth of information for bridge aerodynamicists. Non-linearity effects, mass and stiffness distribution effects, non-uniform deflected shape effects as well as aerodynamic coupling effects are included in the simulation.

This approach is most suited for the study of the behaviour of the structure in complex terrain, for yaw winds, in service and for some critical construction stages [43].

Complexity of the model design and construction, as well as higher costs limit this technique. Froude number similitude is generally respected (a must for suspension bridges where the geometrical stiffness of the main cables is the dominant stiffness), which suggests that the bigger the model the better if the aerodynamics of the structure at low wind speeds should be studied. However, limitations in the size of the experimental facilities for testing models of very long span bridges at large scale seems not to be a factor any longer with the construction of very large wind tunnels to accommodate such models.

Taut strip model approach: This approach offers most of the advantages of the full-bridge aeroelastic model study at a lower cost. The pylons, the cables and the side spans (if any) are not modelled but the 3-D character of the motion of the main span is respected. Froude number similitude can be relaxed which can be an important advantage when both vortex-shedding induced oscillations at low wind speeds and aerodynamic instability at high wind speed should be studied.

For this approach, the length scale and the time scale can be selected independently. It can be described as an extended section model test where many 3-D modes are studied at the same time. Coupling effects between the vertical and torsional modes are modelled, however, only for the first fundamental symmetric modes. A thorough description and analysis of this approach is given in [6].

Concluding remark: The treatment of the three dimensionality of the wind loading on line-like structures by the analytical prediction methods is the source of an important level of uncertainty. Therefore, the experimental methods representing the 3-D character of the wind-structure interactions continue to be superior to the theoretical approaches. Part I-B focuses on the description of the spatial distribution of the wind loading due to wind gusts.

References

[1] Davenport A.G., "Buffeting of a suspension bridge by storm winds", *J. Structural Eng.*, ASCE, **88**, (3), 1962, 233-268.

[2] Davenport A.G., "The response of slender, line-like structures to a gusty wind", *Proc. Institution of Civil Engineers*, **23**, 1962, 389-408.

[3] Davenport A.G., "The action of wind on suspension bridges", *Proc. Int. Symp. on Suspension Bridges*, LNEC Lisbon, Portugal, 1966, 79-100.

[4] Liepmann H.W., "On the application of statistical concepts to the buffeting problem", *J. Aero. Sc.*, **19** (12), 1952, 793-800.

[5] Irwin H.P.A.H., *Wind Tunnel and Analytical Investigations of the Response of Lions' Gate Bridge To Turbulent Wind*, National Research Council of Canada, NAE LTR-LA-210, June 1977, 62 p.

[6] Scanlan R.H. and Gade R.H. "Motion of suspended bridge spans under gusty winds", in *J. of Structural Division*, ASCE, **103**, no. ST 9, Sept. 1977, 1867-1883.

[7] Larose G.L., *The response of a suspension bridge deck to turbulent wind: the taut strip model approach*, M.E.Sc. Thesis, The University of Western Ontario London, Ontario, Canada, March 1992.

[8] Bogunovic Jakobsen J., *Fluctuating wind load and response of a line-like engineering structure with emphasis on motion-induced wind forces*, Ph.D. Thesis, The Norwegian Institute of Technology, Trondheim, Norway, 1995.

[9] Zasso A., Cigada A. and Negri S., "Flutter derivatives identification through full bridge aeroelastic model transfer function analysis", *J. Wind Eng. Ind. Aerodyn.*, **60** (1996), 17-33.

[10] Poulsen N.K., Damsgaard A. and Reinhold T.A., "Determination of flutter derivatives for the Great Belt Bridge", *J. Wind Eng. Ind. Aerodyn.*, **41-44** (1992), 153-164.

[11] Larose, G.L., Davenport A.G. and King, J.P.C., "Wind effects on long span bridges: consistency of wind tunnel results", *J. Wind Eng. Ind. Aerodyn.*, **41-44** (1992), 1191-1202.

[12] Kovacs I., "Analytical aerodynamic investigation of Cable-Stayed Helgelands Bridge", *J. Structural Eng.*, ASCE, **118**, No.1, Jan. 92, 147-168.

[13] Irwin H.P.A.H. and Xie J., "Wind tunnel testing for the Second Severn Bridge", in *Proc. of Third Asia-Pacific Symposium on Wind Eng.*, Dec. 13-15, 1993, 107-112.

[14] Mann J., Kristensen L. and Courtney M.S., *The Great Belt Coherence Experiment - A study of atmospheric turbulence over water*, Risø Report No. R-596, 1991, 51 p.

[15] Roberts J.B. and Surry D., "Coherence of grid generated turbulence", in *J. Engineering Mechanics*, ASCE, **99**, No. EM6, Dec. 1973, 1227-1245.

[16] Kimura K. and Tanaka H., "Bridge buffeting due to wind at yaw angles" *J. Wind Eng. Ind. Aerodyn.*, **41-44** (1992), 1309-1320.

[17] Scanlan R.H., "Problematics in formulation of wind-force models for bridge decks", *J. Engineering Mechanics*, ASCE, **119**, No. 7, 1993, 1353-1375.

[18] Falco M., Curami A. and Zasso A., "Nonlinear effects in sectional model aeroelastic parameters identification", *J. Wind Eng. Ind. Aerodyn.*, **41-44** (1992), 1321-1332.

[19] Mann J. and Krenk S., "Turbulent wind field simulation" accepted for publication in *J. Probabilistic Eng. Mechanics*, 1997.

[20] Miyata Y., Yamada H., Boonyapinyo V. and Santos J.C., "Analytical investigation on the response of a very long suspension bridge under gusty wind", in *Proc. of 9th Int'l Conf. on Wind Eng.*, New-Delhi, India, Jan. 1995, 1006-1017.

[21] Diana G., Cheli F., Zasso A., Collina A. and Brownjohn J., "Suspension bridge parameter identification in full-scale tests", *J. Wind Eng. Ind. Aerodyn.*, **41-44** (1992), 165-176.

[22] Diana G., Cheli F., Bruni S., Collina A. and Larose G.L., "Comparison between wind tunnel test on a full aeroelastic model of the proposed Messina Bridge and numerical results, Part II", in *Proc. of the 3rd Asia-Pacific Symposium on Wind Eng.*, Hong Kong, Dec. 1993, 137-142.

[23] Scanlan R.H., Beliveau, J.G. and Budlong, K.S., "Indicial aerodynamic functions for bridge decks", *J. Engineering Mechanics*, ASCE, **100**, No. EM4, August 1974, 657-672.

[24] Beliveau J.G.,"Self-excited aerodynamic instability", in *Proc. of 2nd U.S. National Conf. on Wind Eng. Research*, Fort Collins, U.S.A., 1975.

[25] Scanlan R.H., "Role of indicial functions in buffeting analysis of bridges", *J. Structural Eng.*, ASCE, **110**, No. 7, July 1984, 1433-1446.

[26] Lin Y.K., "New stochastic theory for bridge stability in turbulent flow" *J. Engineering Mechanics*, ASCE, **119**, 1993, 113-127.

[27] Li Q.C., "Measuring flutter derivatives for bridge sectional models in water channel", *J. Engineering Mechanics*, ASCE, **121**, No. 1, Jan. 1995, 90-101.

[28] Xiang H.F., Liu C.H. and Gu M., "Time domain analysis for coupled buffeting response of long-span bridges", in *Proc. of 9th Int'l Conf. on Wind Eng.*, New-Delhi, India, Jan. 1995, 881-892.

[29] Fujino Y., Wilde K., Masakawa J. and Bhartia B., "Rational function approximation of aerodynamic forces on bridge deck and its application to active control of flutter", in *Proc. of 9th Int'l Conf. on Wind Eng.*, New-Delhi, India, Jan. 1995, 994-1005.

[30] Roger K. L., "Airplane math modelling methods for active control design", AGARD-CP-228, 1977.

[31] Karpel M., "Design for active and passive flutter suppression and gust alleviation", NASA Contractor Report 3492, 1981.

[32] Tiffany S.H. and Adams W.M., "Non-linear programming extensions to rational function approximation methods for unsteady aerodynamic forces", NASA Technical Paper 2776, 1988.

[33] Tewari A. and Brink-Spulink J., "Mulitple pole rational-function approximations for unsteady aerodynamics", *J. Aircraft*, **30**, No. 3, 426-428.

[34] Li M.S. and He D.X., "Buffeting response of large bridges", in *Proc. of 9th Int'l Conf. on Wind Eng.*, New-Delhi, India, Jan. 1995, 893-904.

[35] Diana G., Cheli F. and Resta F., "Time domain aeroelastic force identification on bridge decks", in *Proc. of 9th Int'l Conf. on Wind Eng.*, New-Delhi, India, Jan. 1995, 938-949.

[36] Scanlan R.H., *State of the Art Methods for Calculating Flutter, Vortex-induced and Buffeting Response of Bridge Structures*, Federal Highway Administration, Office of Research and Development, Structures and Applied Division, Washington D.C., USA, 1981. 75 p.

[37] Davenport A.G., Isyumov N. and Miyata T., "The experimental determination of the response of suspension bridges to turbulent wind", in *Proc. 3rd Int. Conf. on Wind Effects on Buildings and Structures*, Tokyo, Japan, 1971, 1207-1219.

[38] Farquharson F.B. and Vincent G.S., *Aerodynamic stability of suspension bridges with special reference to the Tacoma Narrows Bridge* Bull. No. 116, Parts I-IV, Univ. Washington Eng. Station, USA, 1949-54.

[39] Frazer R.A. and Scruton C., *A summarized account of the Severn Bridge aerodynamic investigation* Report NPL/Aero/222, National Physical Laboratory, UK, 1954.

[40] Davenport A.G. and King J.P.C., *A study of wind effects for the Sunshine Skyway Bridge, Tampa, Florida - Concrete and steel alternates*, BLWTL Research Reports SS24/25-1982, University of Western Ontario, Canada.

[41] King J.P.C., Larose G.L. and Davenport A.G., *A study of wind effects for the New Bridge over Johnston's Bay, Sydney, Australia*, BLWTL Research Report SS11-1991, University of Western Ontario, Canada.

[42] Davenport A.G., Isyumov N., Fader D.J. and Bowen C.F.P., *A study of wind action on a suspension bridge during erection and completion*, University of Western Ontario, Canada, Research Report BLWT-3-1969, May 1969 and March 1970.

[43] Larose G.L. and Livesey F.M., "On cable-stayed bridge during construction: modelling and prediction of aerodynamic behaviour", in *Proc. of AFPC Conf. Cable-stayed and Suspension Bridges*, Vol.2, Deauville, France, Oct. 1994, 73-80.

Part I
Background

Part I-B
The span-wise coherence of wind forces

GUY L. LAROSE[a,b]

[a] *Department of Structural Engineering and Materials, Technical University of Denmark, 2800 Lyngby, Denmark*
[b] *Danish Maritime Institute, Hjortekærsvej 99, 2800 Lyngby, Denmark*

Abstract

Forces due to gusts acting on a streamlined bridge deck can be more correlated along the bridge span than the oncoming wind velocity fluctuations. This implies non-negligible secondary cross flows and brings some limitations to the strip assumption.

Based on a review of the effects of turbulence on the aerodynamics of a bluff body, a description of the flow mechanisms that could explain the observed larger correlation of the forces is proposed in this paper. A summary of the empirical expressions recently proposed to model the span-wise coherence of the forces on line-like structures in turbulent flow is also given.

1 Joint acceptance function and span-wise coherence

The joint acceptance function is defined in Part I-A (Section 3.2) as a measure of the correlation between the spatial distribution for the buffeting forces across a span and the mode shapes of that span. It allows the calculation of the wind load applied on a span given the wind load on a chord-wise strip.

The problematic part is to define the spatial distribution of the forces given an incident turbulent flow field. This question is at the heart of all prediction methods of the response of line-like structures to turbulent wind, either analytically in the time domain and the frequency domain or experimentally.

[1] Parts of this paper have been published in *Proceedings of the Third International Colloquium on Bluff Body Aerodynamics and Applications*, Blacksburg, Virginia, July 1996.

Given the forces F_1 and F_2 acting on a bridge deck at the span-wise positions y_1 and y_2 at time t and causing the excitation of the j^{th} mode shape μ_j, the mean square of the time varying wind force on the span with length l can be expressed by [1]:

$$\overline{F_j^2(t,\Delta y)} = \int_0^l \int_0^l \overline{F_1(t,y_1)F_2(t,y_2)}\,\mu_j(y_1)\,\mu_j(y_2)\,\mathrm{d}y_1\mathrm{d}y_2 \tag{1}$$

where the term $\overline{F_1(t,y_1)F_2(t,y_2)}$ represents the covariance of the buffeting wind loads between point y_1 and y_2 on the span.

In the frequency domain, the covariance is transformed into a cross-spectrum which can be normalized by the one-point spectrum of the forces on a strip, S_L, to obtain a normalized cross-spectrum of the load, $R_L(f,\Delta y)$. Equation (1) becomes:

$$S_F(f_j) = S_L(f)\int_0^l \int_0^l R_L(f,\Delta y)\,\mu_j(y_1)\mu_j(y_2)\mathrm{d}y_1\mathrm{d}y_2 \tag{2}$$

where the double integral is known as the joint acceptance function, $\mid J(f_j)\mid^2$.

The spatial distribution of the forces is represented by $R_L(f,\Delta y)$. As a starting point and for many cases it is reasonable to assume that the spatial distribution of the incident wind will be representative of $R_L(f,\Delta y)$.

On the basis of the strip assumption and for cases where the size of the structure is small in comparisons to the size of the gusts, Davenport proposed [1]:

$$R_F(f,\Delta y) \approx R_w(f,\Delta y) = coh_w^{1/2}(f,\Delta y) \tag{3}$$

where w is a component of the wind fluctuations and $coh_w^{1/2}$ is the span-wise root coherence of w.

The magnitude squared coherence function is defined as the ratio of the square of the real and imaginary parts of the cross-spectrum between two points, to the product of the auto-spectra at these points:

$$coh(f,\Delta y) \quad = \quad \frac{\mid Co_{12}(f) + Qu_{12}(f)\mid^2}{S_{L_1}(f)S_{L_2}(f)} \tag{4}$$

where: $Co_{12}(f)$ = Co-spectrum, i.e. real component of the cross-spectrum between points 1 and 2;

$Qu_{12}(f)$ = Quadrature spectrum, i.e. imaginary (out-of-phase) part of the cross-spectrum.

The root coherence is the square root of equation (4). For the buffeting problem, the contribution of the quadrature spectrum is nil even though $Qu_{12}(f)$ of the wind

can represent a non-negligible phase angle. The root coherence is thus replaced by the co-coherence or normalized co-spectrum which is defined as:

$$cocoh(f, \Delta y) = \frac{Co_{12}(f)}{\sqrt{S_{L_1}(f) S_{L_2}(f)}}. \tag{5}$$

There is evidence now that the limitation of the strip assumption is an important source of uncertainty, especially for structures such as closed-box girder bridge decks where it is simply not valid. The span-wise coherence of the aerodynamic forces on a bridge deck was found to be larger than the coherence of the oncoming flow fluctuations.

The main objective of this paper is to describe the flow behaviour when it is passing by a two-dimensional bluff body that has cross-sectional dimensions of similar size to the size of the gusts. A second objective is to give a summary of the empirical models recently proposed to express the span-wise coherence of the forces for bridge decks in order to introduce the experiments reported in Part II-A.

2 Flow over a bridge deck with sharp edges

To determine the cause of the observed larger span-wise coherence of the forces than the incident flow it is important to begin with the description of the main feature of the flow around a sharp-edged body. The dominating phenomenon is the generation of a shear layer at the leading edge (at a sharp corner). The shear layer might or might not reattach depending on the length and geometry of the after-body, the turbulence of the flow, etc. In the shear layer, a recirculating zone is formed defining a separation bubble.

Experience has shown that it is in the separation bubble that the largest peak pressures, thus forces, are formed on the body [2]. For closed-box girder bridge decks, separation bubbles on the top and bottom surfaces are formed and dominate the surface pressure distribution [6]. Referring to Fig. 1, the following is a summary of observations extracted from studies of the reattaching shear layer for sharp-edged bodies.

Smooth flow, chord-wise and span-wise:

- Rolled-up vortices are initiated at the separation point, a separation bubble is formed and in the bubble [4, 5, 6]:
  - smaller eddies are stretched to larger scales and contact with the surface at $x/x_R = 0.5$ (where x_R is the chord-wise location of the reattachment point);
  - in the center of the bubble, the large-scale coherent vortices are contaminated by smaller eddies;

– larger scale vortices are found at the surface and outer layers.

- Weak production of eddies in the bubble up to a certain amount inducing a growth of the bubble, followed by an explosion to shed a larger vortex, and then contraction of the bubble.
- Vortices are shed at the reattachment point at $\frac{fx_R}{V} = 0.6$.
- Flapping motion of the shear layer at $\frac{fx_R}{V} = 0.12$ is initiated.
- L_u^x is constant, $\approx 0.12x_R$, across the bubble due to contamination of small scale eddies.
- L_u^y is equal to 0.5 L_u^x at the center of the bubble, but L_u^y =2.6 L_u^x at the edge of the shear layer.
- Amalgamation of rolled-up vortices produces larger and larger vortices, this process is faster span-wise than chord-wise creating an increase of the span-wise correlation of velocity fluctuations and surface pressures.

Turbulence effect, chord-wise:

- Oncoming turbulence mixes up with rolled-up vortices, increases entrainment rate and reduces the bubble length [7, 8, 9]. For example, $x_R = 4.40D$ in smooth flow and $x_R = 2.45D$ in turbulent flow [2].

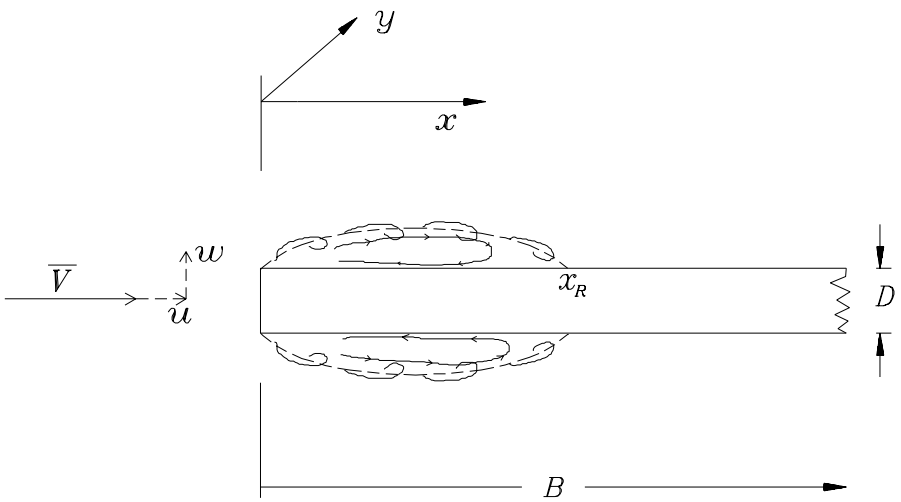

Figure 1: Notation for the description of the flow over a sharp-edged body. The dashed line marks the boundary of the separation bubble.

- When I_u increases, x_R decreases but the peak suction increases and maximum rms C_p moves upstream [2, 11].
- When L_u^x increases, $\overline{C_p}$ stays constant but rms C_p increases [11], for example, when L_u^x increases by 5:1, rms C_p increases 1.5:1 [2].

Turbulence effect, span-wise:

- When I_u increases, x_R reduces, the bubble is more 2-D and $R_{P_1P_2}$ increases (span-wise correlation of surface pressures) and then reaches a plateau.
- Out of the reattaching layer, L_u^x increases when I_u increases, and the diffusion of the shear layer vorticity is enhanced.
- When L_u^y/D increases, $R_{P_1P_2}$ increases and the bubble is elongated, therefore more 2-D [2, 8, 11].

Effect of chord-to-thickness ratio:

- When B/D increases, $R_{P_1P_2}$ increases, the bubble size reduces in length and height, and the rms C_p reduces which helps the bubble to become more 2-D [8].

3 Some effects of the deck on the turbulence

In light of the above, the following description of some effects of the deck on the oncoming turbulence are proposed to explain the larger span-wise correlation. The bridge deck:

- creates a distortion of the turbulence: i.e. stretching and rotating of the vortex line filaments as they are convected past the bodies. The distortion follows the mean velocity streamlines [12, 13].

  For the larger vortices, $L_w^x/B \approx 2$, and for larger B/D, the energy in w is transferred to u and v (splashing) as they are passing over the deck.

  For $L_u^x/D < 1$, u increases and v, w remain constant;
- breaks up some of the large vortices. The resulting smaller scale turbulence mixes up with the shear layer to increase the entrainment rate. The separation bubble reduces in length but becomes more elongated span-wise (more 2-D);
- sheds body-induced vortices. These vortices stretch more rapidly span-wise than chord-wise.

The combination of the distortion created by the deck on the approaching turbulence, the physical averaging by the deck of the wind fluctuations and the 2-D character of the separation bubbles can partly explain the observed larger correlation of the forces. It suggests also that the larger the chord-to-depth ratio, the larger the span-wise coherence of the wind forces.

4 Empirical models of span-wise coherence

In this section, a review of the empirical models of the span-wise coherence of the forces due to turbulence on a motionless bridge deck is given.

4.1 Models based on the strip assumption

If the strip assumption holds, the spatial distribution of the wind velocity fluctuations suffices to describe the span-wise coherence of the forces.

Davenport proposed one of the first empirical models of the spatial distribution of the u component of the wind based on field measurements in the atmospheric boundary layer [14]:

$$coh_u^{1/2}(f, \Delta y) \approx \exp[-c\frac{f\Delta y}{V}] \tag{6}$$

where c is a fitted constant defining the extent of the correlation and $f\Delta y/V$ is a reduced frequency also used as a collapsing parameter.

This expression has become almost a standard to solve the buffeting problem. Solari [15] has made an extensive review of all the different values of c found in the literature for various sites and atmospheric conditions. Equation (6) offers a simple solution to a complex problem but is associated with a certain level of uncertainty especially at low frequencies and large separations (see Part I-A, Section 3.5) and does not always fit particularly well the observed data.

To improve the fit of full-scale data for a sea exposure, Naito [16] has added an exponent to (6) so that:

$$coh_u^{1/2}(f, \Delta y) \approx \exp\left[\left(-c_1\frac{f\Delta y}{V}\right)^{c_2}\right] \tag{7}$$

where c_2 varies between 1.0 and 2.0 depending on the site.

Another approach is to fit the span-wise root coherence data with an analytical model of the cross-spectrum calculated from a model of the one-point spectrum. Typically, the isotropic turbulence model based on the von Kármán spectrum is used and it was found to fit the coherence data fairly well even for non-isotropic wind conditions.

As described in Part I-A (Section 3.5), Irwin [8] has used this approach, as well as Thompson [9] and Roberts and Surry [4]. It has the advantage of fitting well

the data for the low frequency and large separation range where (6) fails. A more complete model of the spatial distribution of an isotropic wind field based on the von Kármán spectrum was derived by Mann et al. [19] and is used in Part II-A of this thesis.

4.2 When the strip assumption is not valid

To the author's knowledge, Nettleton was the first to demonstrate the effect on the span-wise variations of the lift forces of having gusts passing by a thin airfoil with a larger chord than the vertical scale of the turbulence (reported in [4]). For this case, the strip assumption is not valid and he observed that the forces were more correlated than the incident wind.

The width of the correlation can be represented by the integral length scale as:

$$L^y = \int_0^\infty R_{12}(\Delta y)\ \mathrm{d}(\Delta y) \tag{8}$$

where R_{12} is the cross-correlation coefficient. It was found from Nettleton's data that the correlation width of the forces was 3.6 times larger than the correlation width of the incident wind (L^y_w=0.1 m and B=0.38 m):

$$L^y_L = 3.6\ L^y_w. \tag{9}$$

Melbourne [5] came to similar conclusions by comparing the span-wise coherence of the leading edge pressures on the West Gate Bridge to the coherence of the incident wind velocity. The experiments were first conducted in full scale on the prototype bridge and verified later in model scale in grid turbulence. It is the only full-scale investigation of the spatial distribution of the wind pressure ever published for a bridge deck.

Melbourne's results clearly indicated a larger span-wise coherence of the pressures. Obviously it was not possible to restrain the prototype deck from moving which might have increased the coherence of the pressure. However, the results are convincing, especially when compared to model scale.

Melbourne fitted the coherence [2] data with exponential functions. He obtained:

$$coh_{pressure} = \exp[-4\frac{f\Delta y}{V}] \tag{10}$$

for the full-scale and model-scale leading edge pressures (at 10% of B downstream of the leading edge) and,

$$coh_u = \exp[-16\frac{f\Delta y}{V}] \tag{11}$$

for the incident velocity fluctuations of the u component.

[2] Since reference [5] does not give a definition of the coherence function used in the paper, it has been interpreted as being the coherence as in (4) and not the root coherence.

Empirical model by Hjorth-Hansen et al.

Hjorth-Hansen et al. presented in [23] an empirical model of the root coherence of the aerodynamic forces based on the exponential decay function (6) to which a correction term was added. The correction term takes into account the lack of coherence of the forces at low frequency and large separations. It includes directly the integral length scale of the aerodynamic force, L_D^y, as a key parameter for the correction. Hjorth-Hansen et al. remarked that the integral length scale of the drag forces was found to be from 20% to 200% larger than the integral length scale of the u-component of the wind, L_u^y.

The coherence data was obtained from wind tunnel experiments on a bridge deck with a rectangular cross-section (larger depth than width) with constant width but with varying depth span-wise. The forces were obtained by integration of unsteady surface pressures simultaneously on three strips.

The root coherence data was fitted with an exponential function of the form:

$$coh^{1/2}(f,\Delta y) = \exp\left\{-\left[c_1(f\Delta y/V) + c_2\left(\frac{\Delta y}{L_D^y}\right)^2\right]\right\}. \tag{12}$$

The values of the constants $c_1 = 7$, $c_2 = 2-3$ and $L_D^y = 0.20$ m were observed as providing the best fit to the span-wise coherence of the drag force. The best fit for the u component was $c_1 = 10$ and $c_2 = 1$ and $L_u^y = 0.10$ m.

Hjorth-Hansen et al. also noted lower than anticipated drag forces on a strip when compared to quasi-steady buffeting theory and suggested that the observed larger coherence could be compensated for by a lower cross-sectional admittance [23].

Empirical model by Larose

A study of the spatial variations of the lift and pitching forces on a closed-box girder bridge deck in turbulent boundary layer flow was carried out by Larose and reported in [6, 7]. The section studied had a width-to-depth ratio of 7.5:1 and had the same fairing proportions as the decks studied in the present research.

The unsteady forces were obtained by integration of surface pressures on chord-wise strips of a fixed model. The span-wise correlation and root coherence of the forces were found to be considerably larger than the incident wind characteristics, even though the length scales of turbulence were adequately scaled in relation to the size of the model to represent full-scale conditions. The ratio of the length scale of the vertical gusts to the deck width was $\mathcal{L}_w/B = 1.2$. These experiments are unique since they were conducted in a properly simulated atmospheric boundary layer flow field (non-isotropic).

The variations of the cross-correlation coefficient R_{12} with $\Delta y/B$ obtained by Larose are reproduced in Fig. 2 for the vertical and torsional aerodynamic forces and

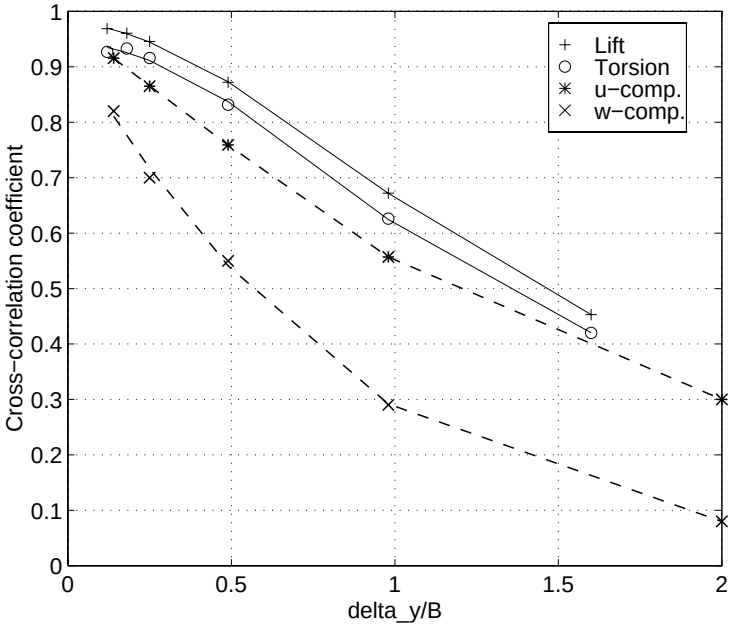

Figure 2: Correlation of the aerodynamic forces and wind fluctuations as a function of normalized separation, after Larose [3].

the longitudinal and vertical components of the boundary layer flow. By integration of these curves the correlation width can be calculated as follows:

$$L_L^y = 2.24\ L_w^y. \tag{13}$$

An attempt was made by Larose to collapse the forces root coherence curves with the von Kármán parameter that had modelled well the incident flow. The curves did not collapse but were however organized in a manner suggesting a $\Delta y/B$ dependence. Larose thus proposed adding a reduced frequency term fB/V to the von Kármán collapsing parameter so that:

$$\gamma' = k_1 \Delta y \sqrt{1 + \frac{1}{(1.34 k_1 \mathcal{L}_w)^2}} + \frac{fB}{V} \tag{14}$$

For very small B the added term is negligible and the root coherence of the forces is then represented by the root coherence of the wind. A good collapse of the root coherence of the bulk of the data was obtained with γ' and the resulting curve was fitted with an exponential function:

$$coh_L^{1/2}(k_1, \Delta y) \ = \ \exp\{-c_1(\gamma')^{c_3}\} \ = \ \exp\{-c_1 \left(\gamma + c_2 \frac{fB}{V}\right)^{c_3}\} \tag{15}$$

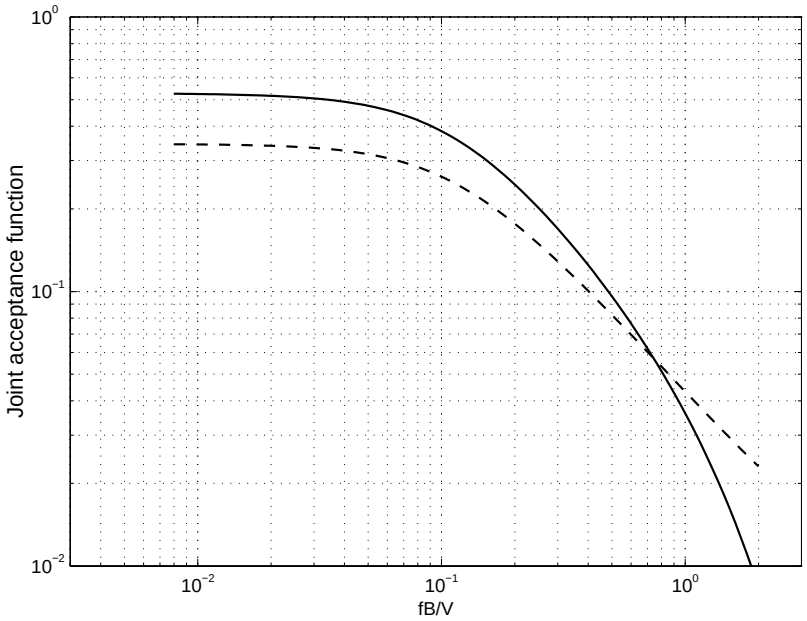

Figure 3: Joint acceptance functions for a uniform mode shape $\mu(y) = 1$, calculated using a fit of the wind velocity root coherence (dashed line) and using the measured root coherence of the lift forces (solid line), after Larose [3].

$$\begin{aligned} \text{where: } c_1 &= 0.73,\ c_2 = 0,\ c_3 = 1 \quad \text{for the vertical wind fluctuations;} \\ c_1 &= 0.18,\ c_2 = 1,\ c_3 = 2 \quad \text{for the vertical forces;} \\ c_1 &= 0.14,\ c_2 = 2,\ c_3 = 2 \quad \text{for the torsional forces.} \end{aligned}$$

Using (15) and the coefficients above, the joint acceptance function can be calculated using both the forces directly or the wind as representative of the spatial distribution of the forces. Larose reported the calculations in [6]. A similar comparisons is shown in Fig. 3 for a span length of 1 m.

Empirical model by Bogunovic Jakobsen

Similar experiments were carried out by Bogunovic Jakobsen [10, 26] on a 1:70 scale model of closed-box girder bridge deck with B/D= 4.5:1. The tests were conducted in grid turbulence with $L_w^y = 0.108$ m, on a motionless section model 2.64 m long and 0.286 m wide resulting in a ratio $\mathcal{L}_w^y/B = 0.56$ for these experiments.

The unsteady forces were calculated by integration of surface pressure measurements simultaneously on 4 chord-wise strips of the model. Bogunovic Jakobsen compared the measured forces to the incident wind and obtained for the correlation

width:

$$L_L^y = 3.0\ L_w^y. \tag{16}$$

With a least square algorithm, Bogunovic Jakobsen fitted the co-coherence data with the same exponential function for both the wind and the forces. The function has a built-in correction for the low frequency large separation range and is of the form:

$$coh_{L;w}^{1/2}(f, \Delta y) = \exp\left\{ - \left[\Delta y \sqrt{c_2^2 + (c_3 f/V)^2} \right]^{c_1} \right\} \tag{17}$$

where c_1, c_2 and c_3 are fitted to the observed co-coherence data.

The results of the fit are summarized in Table 1. Using (17) and the coefficients of Table 1, Bogunovic Jakobsen calculated the joint acceptance functions and obtained an important underestimation of $\mid J(f_j B/V) \mid^2$ when the strip assumption was assumed to be valid. The calculations are reproduced in Fig. 4 for a span length of 2.64 m.

Table 1: Least square fit of co-coherence data using (17), after Bugonovic Jakobsen.

	c_1	c_2 (m^{-1})	c_3
Wind, w component	1.00	4.21	5.47
Forces, Lift	1.40	2.11	2.24
Forces, Torsion	1.35	2.44	2.15

Empirical model by Kimura et al.

Kimura et al. have reported in [27, 9] experiments on flat cylinders in grid turbulence focusing on the description of the chord-wise and span-wise distribution of the forces. Their main conclusion is in agreement with the results described above, with the exception that for the drag forces, the spatial distribution of the incident wind described well the distribution of the forces [9].

Three cross-sections were studied: a flat hexagonal cylinder with B/D = 8.7:1 and two rectangular cylinders with B/D= 8.7:1 and 4:1. The width of the models was kept constant at 0.148 m. The forces were obtained by integration of surface pressures on chord-wise strips of the models. The effects of the scales of the gusts on the buffeting forces was studied using three different grids resulting in the following L_w^y/B ratios: 0.47, 0.30 and 0.20.

The analysis of the incident wind field was based on the work by Irwin [8] who derived analytically a root coherence function of the w component based on the von Kármán spectrum. This function fitted well the wind root coherence data. Kimura et al. attempted to fit the lift force root coherence data with the same

expression. The fit was not satisfactory and to improve the fit, modifications to the analytical expression were made. The measured turbulence length scale was increased by a factor of 4.5 and the frequency was raised to a power of 0.74. The modified von Kármán root coherence function proposed by Kimura et al. is of the form:

$$coh_L^{1/2}(f,\Delta y) = 0.994\left(\eta^{5/6}K_{5/6}(\eta) - \frac{\eta^{11/6}K_{1/6}(\eta)}{1+188.7\left[f^{\mathbf{0.74}}(\frac{\mathbf{4.5}L_w^y}{V})\right]^2}\right) \tag{18}$$

where

$$\eta = \frac{\Delta y}{\mathbf{4.5}L_w^y}\,0.747\sqrt{1+70.8\left[f^{\mathbf{0.74}}(\frac{\mathbf{4.5}L_w^y}{V})\right]^2}, \tag{19}$$

$K_{5/6,1/6}$ are modified Bessel functions of the second kind and L_w^y is a span-wise length scale of the w component of the wind. The numbers in bold face represent the modification made by Kimura et al.

This empirical expression fitted well the span-wise co-coherence curves of the lift forces for the three cross-sections studied. Kimura et al. also compared the measured lift spectrum on a strip to theoretical calculations based on the buffet-

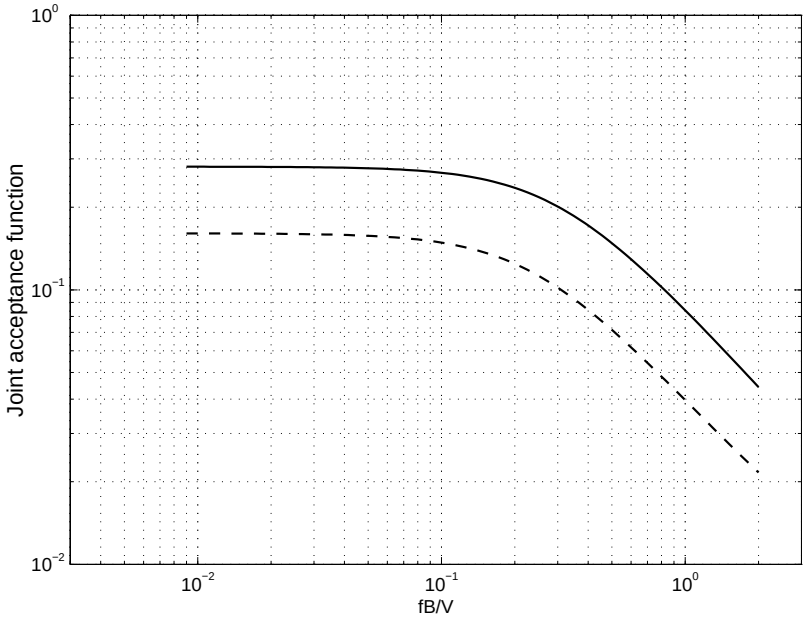

Figure 4: Joint acceptance functions for a uniform mode shape $\mu(y) = 1$, calculated using a fit of the wind velocity co-coherence (dashed line) and using the measured co-coherence of the lift forces (solid line), after Bogunovic Jakobsen [25].

ing theory. They observed a smaller cross-sectional lift force than anticipated, in agreement with results reported by Larose in [6].

Kimura et al. suggested that this discrepancy was due to three-dimensional effects (or secondary cross-flow) that reduces the force due to an incident gust chord-wise but increases its influence span-wise. They also remarked that the smaller the scale of turbulence the larger this effect.

5 Concluding remarks

The description of the behaviour of the vorticity in the reattaching shear layer presented in Section 2 can partly explain the observed span-wise redistribution of the wind pressure when gusts are passing by a closed-box girder bridge deck. However, the flow mechanisms described here happen at high frequencies corresponding to the frequency range of the body-induced turbulence. Experiments have shown that larger span-wise coherence was also observed in the low frequency range. Something other than that described here must happen to the larger incident gusts at low frequencies.

The span-wise coherence of the aerodynamic forces has been expressed by

$$coh_L^{1/2}(f, \Delta y) \approx coh_w^{1/2}(f, \Delta y) \approx \exp\{-c(\frac{f\Delta y}{V})\} \tag{20}$$

on the basis of the strip assumption. Several experimental studies have indicated that the above expression was not valid and was an important source of uncertainty for the calculation of the buffeting response.

Empirical models have been proposed to represent better the spatial distribution of the forces on line-like structures. The models based on the von Kármán spectral tensor are the most promising since they represent well the incident wind conditions and could be adapted to model the forces.

In general, the empirical models failed to describe the flow mechanisms involved. Intuitively, the root coherence of the forces should be a function of:

$$coh_L^{1/2} = \mathcal{F}\left(k_1, \Delta y, \frac{B}{L_w}, \frac{B}{D}\right). \tag{21}$$

The experiments reported in Part II-A of this thesis aim at defining the relationship between cross-sectional admittance, span-wise coherence and the influence of the size of the gusts compared with the size of the bridge deck on these quantities. Another objective is to study the influence of the deck aspect ratio B/D on the unsteady aerodynamic forces. It is believed that it could provide the missing information needed to build a more general model of the spatial distribution of the lift and pitching forces on closed-box girder bridge decks and similar bluff bodies.

References

[1] Davenport A.G., "The response of slender, line-like structures to a gusty wind", *Proc. Institution of Civil Engineers*, **23**, 1962, 389-408.

[2] Saathoff P.J. and Melbourne W.H., "The generation of peak pressures in separated/reattaching flow", *J. Wind Eng. Ind. Aerodyn.*, **32** (1989), 121-134.

[3] Larose G.L., *The response of a suspension bridge deck to turbulent wind: the taut strip model approach*, M. E. Sc. Thesis, The University of Western Ontario London, Ontario, Canada, March 1992.

[4] Kiya M. and Sasaki K. "Structure of a turbulent separation bubble", *J. Fluid Mech.* (1983), **137**, 83-113.

[5] Kiya M. and Sasaki K. "Structure of a large-scale vortices and unsteady reverse flow in the reattaching zone of a turbulent separation bubble", *J. Fluid Mech.* (1985), **154**, 463-491.

[6] Cherry N.J., Hillier R. and Latour M.E.M.P. "Unsteady measurements in a separated and reattaching flow", *J. Fluid Mech.* (1984), **144**, 13-46.

[7] Laneville A., Gartshore I.G. and Parkinson G.V., "An explanation of some effects of turbulence on bluff bodies" in *Proc. of 4th Int'l Conference on Buildings and Structures*, London, England, Sept. 1975, Cambridge Univ. Press, 333-342.

[8] Hillier R. and Cherry N.J., "The effect of stream turbulence on separation bubbles", *J. Wind Eng. Ind. Aerodyn.*, **8** (1981), 49-58.

[9] Kiya M. and Sasaki K. "Free-stream turbulence effects on a separation bubble", *J. Wind Eng. Ind. Aerodyn.*, **14** (1983), 375-386.

[10] Sankaran R. and Jancauskas E.D., "Measurements of cross-correlation in separated flows around bluff cylinders", *J. Wind Eng. Ind. Aerodyn.*, **49** (1993), 279-288.

[11] Li Q.S. and Melbourne W.H., "An experimental investigation of the effects of free-stream turbulence on streamwise surface pressures in separated and reattaching flows", *J. Wind Eng. Ind. Aerodyn.*, **54-55** (1995), 313-323.

[12] Bearman P.W., "An investigation of the forces on flat plates normal to a turbulent flow", *J. Fluid Mech.* (1971), **46**, 177-198.

[13] Bearman P.W., "Some measurements of the distortion of turbulence approaching a two-dimensional bluff body", *J. Fluid Mech.* (1972), **53**, 451-467.

[14] Davenport A.G., "The spectrum of horizontal gustiness near the ground in high winds", *J. Royal Meteorological Society*, **87**, 1961, 194-211.

[15] Solari G., "Turbulence modelling for gust loading", *J. Structural Engineering*, ASCE, **117**(7), 1987, 1550-1569.

[16] Naito G., "The spatial structure of surface wind over the ocean", *J. Wind Eng. Ind. Aerodyn.*, **13** (1983), 67-76.

[17] Irwin H.P.A.H., *Wind Tunnel and Analytical Investigations of the Response of Lions' Gate Bridge To Turbulent Wind*, National Research Council of Canada, NAE LTR-LA-210, June 1977, 62 p.

[18] Engineering Sciences Data Unit, *Characteristics of Atmospheric Turbulence Near The Ground, Part III: variations in space and time for strong winds*, Data Item 86010, October 1986.

[19] Roberts J.B. and Surry D., "Coherence of grid generated turbulence", *J. Engineering Mechanics*, ASCE, **99**, No. EM6, Dec. 1973, 1227-1245.

[20] Mann J., Kristensen L. and Courtney M.S., *The Great Belt Coherence Experiment - A study of atmospheric turbulence over water*, Risø Report No. R-596, 1991, 51 p.

[21] Ektin B, *Dynamics of Atmospheric Flight*, John Wiley and Sons, 1971, pp. 547-548.

[22] Melbourne W. H., "Comparison of model and full-scale tests of a bridge and chimney stack", in *Proc. of Int'l Workshop on Wind Tunnel Modelling*, Maryland, USA, 1982, 637-653.

[23] Hjorth-Hansen E., Jacobsen A. and Strømmen A., "Wind Buffeting of a Rectangular Box Girder Bridge", *J. Wind Eng. Ind. Aerodyn,* **41-44** (1992), 1215-1226.

[24] Larose G.L., Davenport A.G., and King J.P.C., "On the unsteady aerodynamics forces acting on a bridge deck in turbulent flow", in *Proc. of the 7th US National Conference on Wind Engineering*, UCLA, Los Angeles, USA, June 1993.

[25] Bogunovic Jakobsen J., *Fluctuating wind load and response of a line-like engineering structure with emphasis on motion-induced wind forces*, Ph.D. Thesis, The Norwegian Institute of Technology, Trondheim, Norway, 1995.

[26] Bogunovic Jakobsen J., "Span-wise structure of lift and overturning moment on a motionless bridge girder", in *Proc. of 3rd Int'l Colloquium on Bluff Body Aerodynamics and Applications*, Blacksburg, Virginia, USA, July 1996.

[27] Kimura K. and Fujino Y., "Turbulence scale effects on buffeting forces of a flat hexagonal section", in *Proc. of the 3rd Asia-Pacific Symposium on Wind Engineering*, Hong-Kong, Dec. 1993, pp. 637-642.

[28] Kimura K., Fujino Y., Nakato S. and Tamura H. "Characteristics of the buffeting forces on flat cylinders", in *Proc. of 3rd Int'l Colloquium on Bluff Body Aerodynamics and Applications*, Blacksburg, Virginia, USA, July 1996.

Part II
Experiments and Analysis

Part II-A
Direct measurements of buffeting wind forces on bridge decks

GUY L. LAROSE[a,b]

[a] *Danish Maritime Institute, Hjortekærsvej 99, 2800 Lyngby, Denmark*
[b] *Department of Structural Engineering and Materials, Technical University of Denmark, 2800 Lyngby, Denmark*

Abstract

Direct measurements of the forces induced by the buffeting action of wind on a motionless bridge deck have been carried out at the Danish Maritime Institute (DMI). The wind tunnel experiments aimed at defining the spatial distribution of the wind loading as a function of the deck width and the scales of the oncoming turbulence.

This paper presents the main findings of the experiments and illustrates the impetus behind this research which was to evaluate, for closed-box girder bridge decks, the error margin of the wind load predictions based on the strip assumption.

1 Introduction

A research project aimed at defining the error margin of the buffeting response prediction for line-like structures highlighted a number of shortcomings of the current theory. These included: the linearisation of the wind loading, the evaluation of the aerodynamic damping and cross-sectional admittance, and the theoretical

[1] A 10-page summary of Part II-A has been published in *J. of Wind Engineering and Industrial Aerodynamics* **74-76** (1998), 809-818, co-authored by Hiroshi Tanaka, Niels J. Gimsing and Claës Dyrbye.

modelling of the transition from point-like forces to dynamic loads on an entire span.

The relationship between incident wind velocity fluctuations and resulting wind loads is an important source of uncertainty in bridge aerodynamics. To study this aspect, a series of experiments were conducted with the objective of directly measuring the dynamic wind loading on motionless streamlined bridge decks in turbulent flow.

A second objective was to conduct a parametric study of the influence of the deck width, railings, turbulence intensity and scales of turbulence on the buffeting wind loads. The purpose of the parametric study was to develop a three-dimensional model of the wind forces induced by turbulence on bridge decks.

This paper presents the main findings of the experiments as well as a succinct description of the methodology employed. The background for the research is given in Part I-B.

2 Description of the experiments

2.1 Instantaneous force measurements

A 2.55 m long section model was rigidly mounted in DMI's Wind Tunnel II that has a 2.6 m wide $\times$ 1.8 m high $\times$ and 21 m long working section. Any wind-induced motions of the model were prevented using guy wires stretched between the model and the wind tunnel boundaries. The eigen frequency of the structural system was found to be above 80 Hz. The 0.7 m long centre portion of the model was made of acrylic and was instrumented to measure unsteady surface pressures. The rest of the model was made of a combination of wood and foam and was put in place only to ensure the 2-dimensionality of the flow and to avoid end effects. Photographs describing the experimental set-up are presented in Appendix.

The dynamic force measurements were based on simultaneous measurements of surface pressures around three chord-wise strips of the centre portion of the model. Each strip was fitted with at least 32 pressure taps and the span-wise separation of the strips was adjustable. Three electronic pressure scanners (PSI ESP-32HD) were mounted directly inside the model to keep the tubing length (150 mm) to a minimum ensuring a good frequency response up to at least 100 Hz.

The frequency response of the tubing system (hard vinyl tubes with 1 mm inside diameter) was verified in-situ by comparing the auto-spectra of the surface pressure measured on the windward face of a square plate placed normal to the oncoming turbulent flow for various tubing lengths. The smallest possible length of the vinyl tubing (15 mm) was used as a reference. Fig. 1 compares the frequency response of the reference length with the tubing length used in this study.

A similar verification of the frequency response of the tubing was done in the laboratory. For this case, the source of fluctuating pressures was a loudspeaker driven

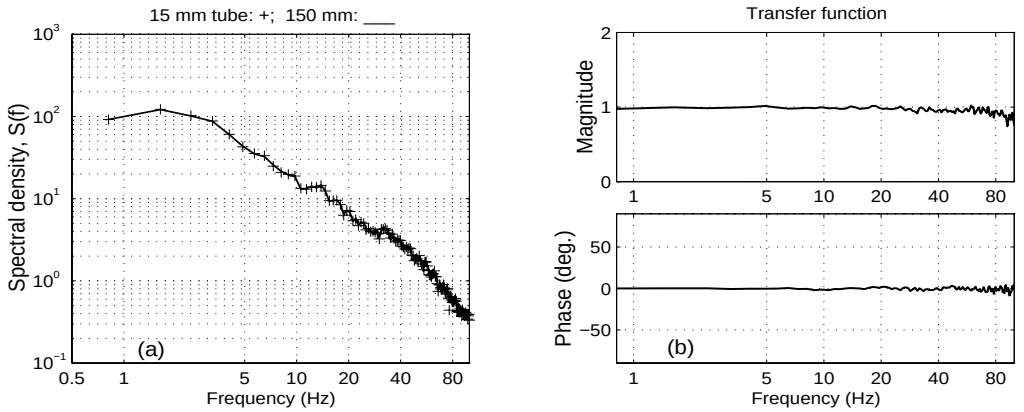

Figure 1: In-situ frequency response of a typical tube used in this study; **a)** comparisons of auto-spectra of surface pressures, **b)** variations of the magnitude and phase of the transfer function between the reference tube and a 150 mm tube.

by a white noise signal. Spectral comparisons up to 100 Hz between the reference 15 mm tube and tubes of various lengths showed good behaviour in magnitude and in phase for tubing lengths up to 250 mm, even though the fluctuating pressures from the loudspeaker had a resonant peak at 80 Hz as seen in Fig. 2.

The cross-section studied was typical of a closed-box girder bridge deck (Fig. 3). The model was made in modules so the width-to-depth ratio, B/D, of the cross-section could be changed from 5 to 10 and finally 12.67, the depth being kept constant at 30 mm (Fig. 4). The edge configuration (taken similar to the Storebæalt

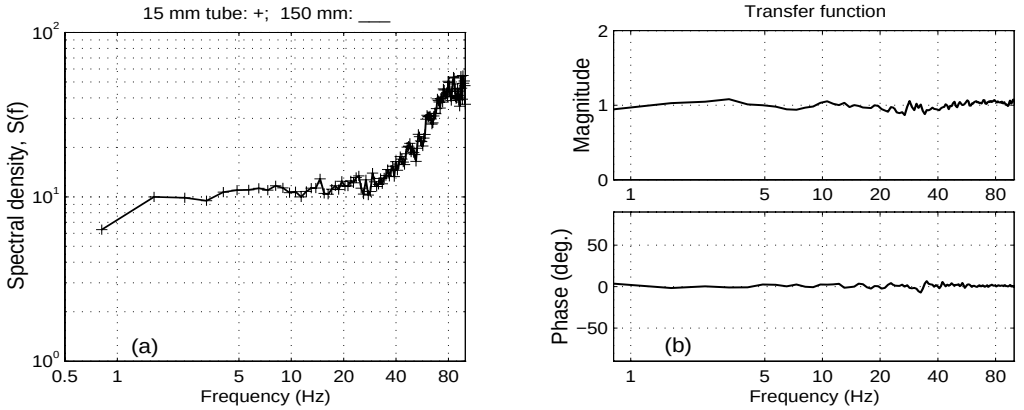

Figure 2: Tubing frequency response to fluctuating pressures produced by a loudspeaker: **a)** comparisons of auto-spectra; **b)** transfer function between the reference tube and a 150 mm tube.

East Bridge configuration) was kept constant. Note that the B/D ratio of 7.5 on Fig. 4 was studied on another occasion and the results are reported elsewhere [2,3]. Other parameters in the tests were the presence or lack of railings on the top surface of the deck and the angle of wind incidence (-2° to +2°).

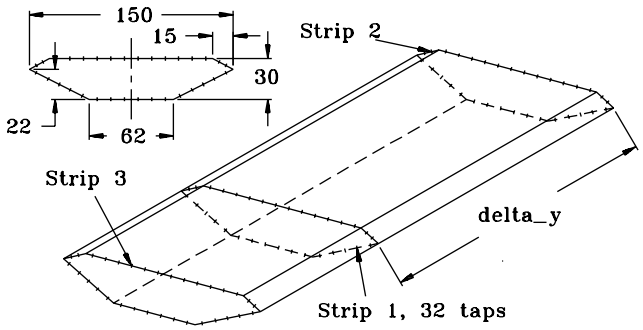

Figure 3: The centre portion of the section models (dimensions in mm).

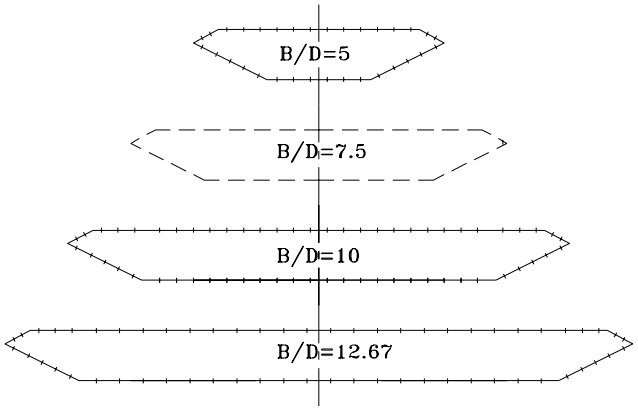

Figure 4: The various width-to-depth ratios investigated.

The pressure taps were positioned in an equidistant manner chord-wise so that the contributory area of each of the taps was equivalent. For the larger width-to-depth ratios, up to 64 pressure taps were fitted per strip. Two-to-one pneumatic manifolding of the surface pressures was thus performed for the models with B/D =10 and 12.67. A verification of the effect of the local pressure averaging was made by measuring the surface pressures for each of the 64 taps of a strip of the B/D= 10 model and comparing the results with two-to-one manifolded pressures. Mean, rms and power spectral densities of the integrated vertical and torsional forces were found to match within a 3% error margin.

The 96 pressure transducers were sampled at a frequency of 208 Hz for 2 periods of 60 seconds. Data reduction consisted of digital low-pass filtering, integration

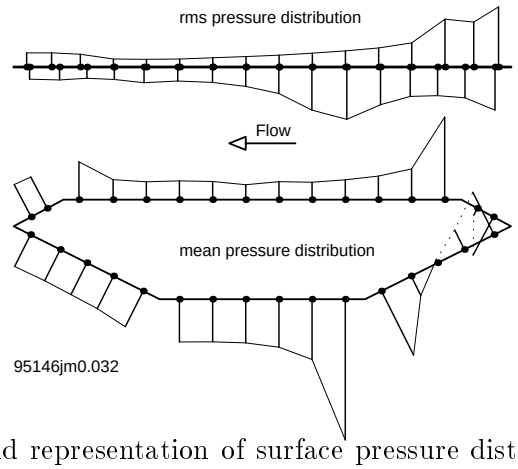

Figure 5: Vector field representation of surface pressure distribution on B/D= 5, medium spire exposure, with railings, 15 ms^{-1}. Scaling: depth of deck= mean C_p of 1 and rms C_p of 0.5. Polarity: negative away from the surface. The rms distribution is given for the projected tributary area.

of surface pressures to form time-varying force coefficients (vertical, torsional and along-wind) and spectral analysis. Cross-sectional admittances and span-wise coherence of wind forces were calculated for each case. Figs. 5 and 6 show examples of surface pressure distributions in turbulent flow.

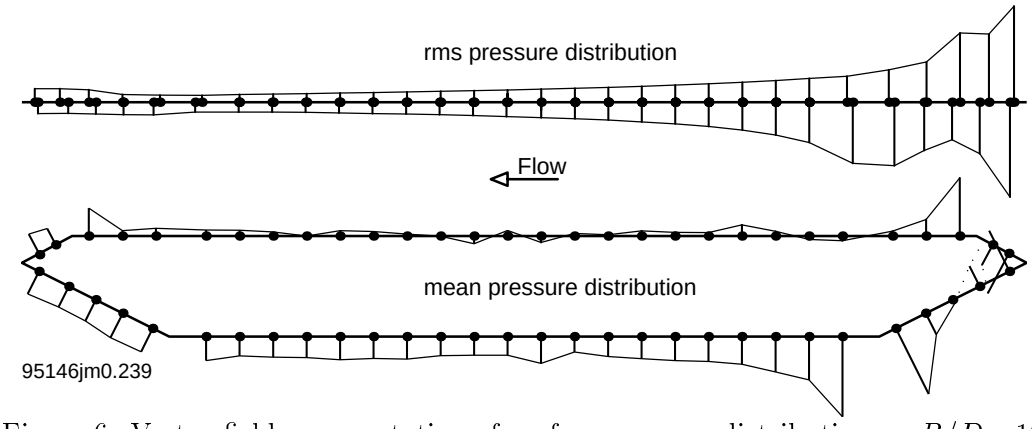

Figure 6: Vector field representation of surface pressure distribution on B/D= 10, large spire exposure, with railings, 15 ms^{-1}. Scaling: depth of deck= mean C_p of 1 and rms C_p of 0.5. Polarity: negative away from the surface.

2.2 Flow investigations

Three turbulent flow conditions were investigated, two generated by spires 15 m upstream of the model and one by a coarse grid placed 4.6 m upstream. The two spire sets gave similar length scales of turbulence but different turbulence intensities while the position of the grid was selected to match the turbulence intensity of one of the spire sets but giving much smaller length scales.

The grid had an isotropic mesh of 0.34 m with a bar size of 0.085 m. The medium spires, in a set of three placed 15 m upstream of the model, where 0.32 m wide at the base, 0.20 m at the top and 1.8 m high, while the large spires where 0.36 m at the base, 0.23 m at the top and 1.72 m high. The tests in the wind tunnel were typically conducted at a mean wind speed of 15 ms^{-1}.

The turbulent flow characteristics were defined using hot-wire anemometry (Dantec's StreamLine and StreamWare system). Typically, two sets of bi-dimensional probes (Dantec 55P61) were used to measure the u and w components of the wind fluctuations, and subsequently were rotated 90° to measure the v component. The tests were carried out at the section model position, without the model in place. A total of 8 span-wise separations of the probes were investigated to define the flow field in terms of one-point and two-point statistics. The separations ranged from 14 mm to 450 mm (i.e. 14 mm, 30 mm, 60 mm, 90 mm, 130 mm, 240 mm, 300 mm, 450 mm). The sampling frequency was set at 625 Hz for a sampling time of 180 seconds. A 6^{th}-order Butterworth low pass filter set at 300 Hz was applied to the signal before data acquisition.

3 Analysis of the flow conditions

3.1 Isotropic turbulence model and the von Kármán spectrum

In wind tunnels, the turbulence behind grids or large spires has an isotropic character [4]. This is especially true for locations away from the wind tunnel boundaries. It is thus appropriate to compare the flow conditions of this study with an isotropic turbulence model based on the von Kármán spectrum. A detailed discussion of the applicability of isotropic turbulence model in wind engineerring can be found in [4, 19].

Here, the isotropic tensor given by Mann in [18], based on the von Kármán energy spectrum, was fitted to the measured wind spectra for the u, v and w wind components. The one-point spectrum for the u component can be expressed by:

$$S_u(k_1) = \frac{9}{55}\alpha\epsilon^{\frac{2}{3}}\frac{1}{\left(L^{-2}+k_1^2\right)^{\frac{5}{6}}} \tag{1}$$

and for the v and w components:

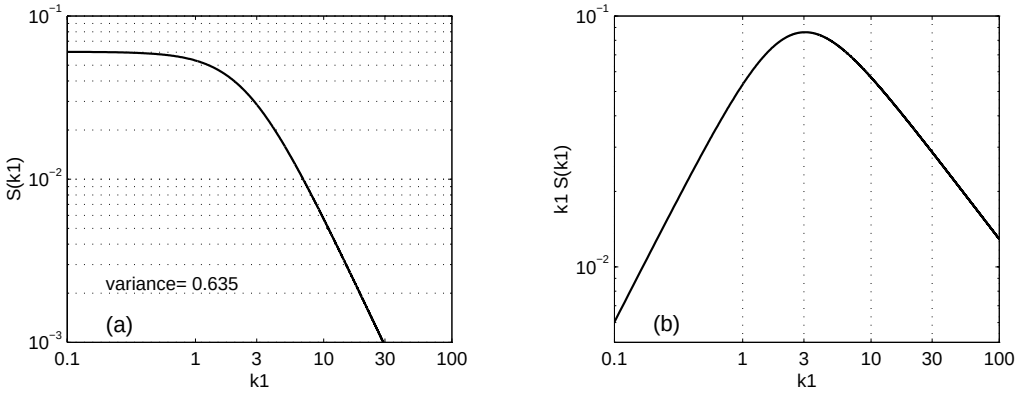

Figure 7: Graphical representation of L_u^x and $\mathcal{L}$ for the von Kármán spectrum of u, (1), with L= 0.4 and $\alpha\epsilon^{\frac{2}{3}}$= 1.7: **a)** $L_u^x = \pi S_u(0)/\sigma^2$= 0.3 m; **b)** $\mathcal{L}$ is the inverse of k_1 corresponding to the maximum of $k_1 S_u(k_1)$: $\mathcal{L}$= 0.33 m.

$$S_{v,w}(k_1) = \frac{3}{110}\alpha\epsilon^{\frac{2}{3}}\frac{3L^{-2}+8k_1^2}{\left(L^{-2}+k_1^2\right)^{\frac{11}{6}}} \tag{2}$$

Here, k_1 is a wave number ($2\pi f/V$), ϵ represents the rate of viscous dissipation of turbulent kinetic energy, α is the von Kármán constant and L is a length scale common to the three components of the spectral tensor.

Relationships exist between L and the integral length scales L_u^x, L_v^x and L_w^x for isotropic turbulence [19]:

$$L_u^x = L\frac{1}{\sqrt{\pi}}\frac{\Gamma(1/3)}{\Gamma(5/6)} \approx \frac{3}{4}L \tag{3}$$

$$= \frac{\pi}{\sigma_u^2}S_u(k_1=0) \tag{4}$$

$$L_{v,w}^x = \frac{1}{2}L_u^x \approx \frac{3}{8}L \tag{5}$$

Equation (4) expresses that the integral length scales (also defined as $L_u^x = \int_0^\infty R_{uu}(x)dx$ for example) are related to the wind spectrum at frequency zero. The physical meaning of L_u^x is not obvious and it is considered here, as in [18], that the wave length, denoted $\mathcal{L}$, associated with the peak of $k_1 S_u(k_1)$ or $f S_u(f)$ is a more appropriate characteristic length to describe a turbulent flow field.

$\mathcal{L}$ represents the length of the eddies that carry most of the energy of the turbulence and it will be used as a reference length later in this study. Fig. 7 defines graphically L_u^x and $\mathcal{L}$.

$\mathcal{L}$ is related to L for the von Kármán spectrum by:

$$\mathcal{L}_u = \left(\frac{2}{3}\right)^{\frac{1}{2}} L \approx 0.816L \tag{6}$$

$$\mathcal{L}_{v,w} = \frac{2}{(6+3\sqrt{5})^{\frac{1}{2}}} L \approx 0.561L \tag{7}$$

The variances for isotropic turbulence are all equal and can be expressed [18] by:

$$\sigma^2_{u,v,w} = \frac{9}{55}\frac{\Gamma\left(\frac{1}{3}\right)}{\Gamma\left(\frac{5}{6}\right)}\sqrt{\pi}\alpha\epsilon^{\frac{2}{3}}L^{\frac{2}{3}} \approx 0.688\alpha\epsilon^{\frac{2}{3}}L^{\frac{2}{3}} \tag{8}$$

3.2 Two-point statistics: the span-wise coherence

Analytical derivations of cross-spectra based on the von Kármán spectrum exist in various forms, notably due to Irwin [8] and Thompson [9]. This constitutes a clear advantage in using the isotropic turbulence model. Here the more complete derivations due to Mann et al. [19] is used to define the span-wise coherence of the oncoming flow fluctuations.

The coherence function between points 1 and 2 is expressed by the magnitude squared of the real and imaginary parts of the cross-spectrum divided by the product of the one-point spectra at 1 and 2. For isotropic turbulence, the imaginary part of the cross-spectrum, Qu, is zero, so that only the real part, Co, is necessary to describe the coherence as a function of k_1 and span-wise separation Δy:

$$coh_u(\Delta y, k_1) = \frac{Co^2(\Delta y, k_1)}{S_u^2(k_1)} \tag{9}$$

$$coh_u^{1/2}(\Delta y, k_1) = \frac{Co(\Delta y, k_1)}{S_u(k_1)} \tag{10}$$

Equation (10) is also referred to as the normalized co-spectrum [4] or co-coherence, *cocoh*. For any separation and length scale L, the co-coherences are expressed in [19] by:

$$cocoh_u(\Delta y, k_1) = \frac{2}{\Gamma\left(\frac{5}{6}\right)}\left(\frac{\gamma}{2}\right)^{\frac{5}{6}}\left[K_{5/6}(\gamma) - \frac{1}{2}\gamma K_{1/6}(\gamma)\right] \tag{11}$$

$$cocoh_v(\Delta y, k_1) = \frac{2}{\Gamma\left(\frac{5}{6}\right)}\left(\frac{\gamma}{2}\right)^{\frac{5}{6}}\left[K_{5/6}(\gamma) + \frac{3(\Delta y k_1)^2}{3\gamma^2 + 5(\Delta y k_1)^2}\gamma K_{1/6}(\gamma)\right] \tag{12}$$

$$cocoh_w(\Delta y, k_1) = \frac{2}{\Gamma\left(\frac{5}{6}\right)}\left(\frac{\gamma}{2}\right)^{\frac{5}{6}}\left[K_{5/6}(\gamma) - \frac{3\left(\frac{\Delta y}{L}\right)^2}{3\gamma^2 + 5(\Delta y k_1)^2}\gamma K_{1/6}(\gamma)\right] \tag{13}$$

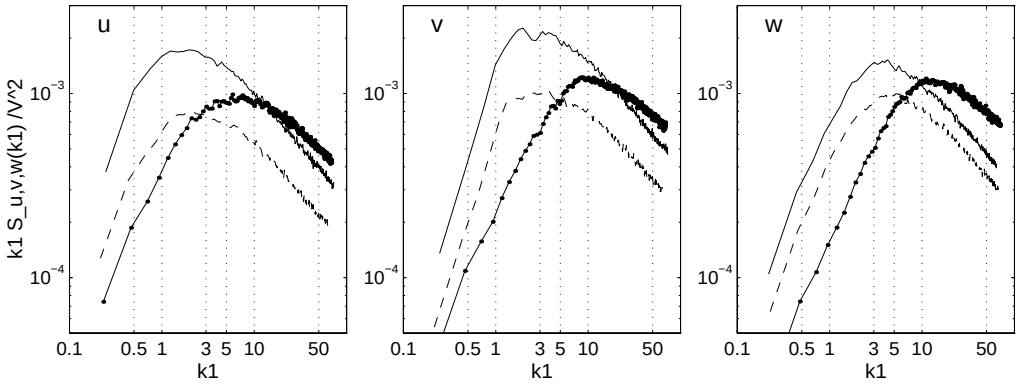

Figure 8: Averaged auto-spectra of the wind fluctuations normalized by the mean wind velocity squared for the exposures of this study. Solid lines: large spires; dashed lines: medium spires; dotted lines: grid.

where $K_{1/6,5/6}$ are modified Bessel functions of the second kind and,

$$\gamma = \left(\Delta y^2 k_1^2 + \frac{\Delta y^2}{L^2} \right)^{\frac{1}{2}} = k_1 \Delta y \sqrt{1 + \frac{1}{k_1^2 L^2}} \tag{14}$$

is the von Kármán collapsing parameter.

3.3 Least square fit of wind data

One-point spectra of the wind fluctuations in u, v and w were calculated for each of the three exposures. For each case, a total of 16 spectra measured at different span-wise loactions at the section model position were averaged to define a *universal* spectra for each exposure. Fig. 8 presents the averaged one-point spectra. The grid exposure has its maximum at wave numbers almost 4 times larger than the spire exposures, implying 4 times smaller scales of turbulence.

To characterise the flow conditions at the section model position, the averaged spectra were fitted with the von Kármán model, (1) and (2) leaving L and $\alpha\epsilon^{\frac{2}{3}}$ as floating parameters.

The least square fit was made with a Simplex search method [7], part of the Matlab analysis software. Figs. 9 compares the experimental data to the fitted von Kármán spectra, while Table 2 presents the results of the fits and summarises the characteristics of the turbulence for the three exposures.

The turbulence intensities $I_{u,v,w}$ were defined as the standard deviation of the velocity fluctuations of a given component divided by the mean of u, that is $\bar{V}$.

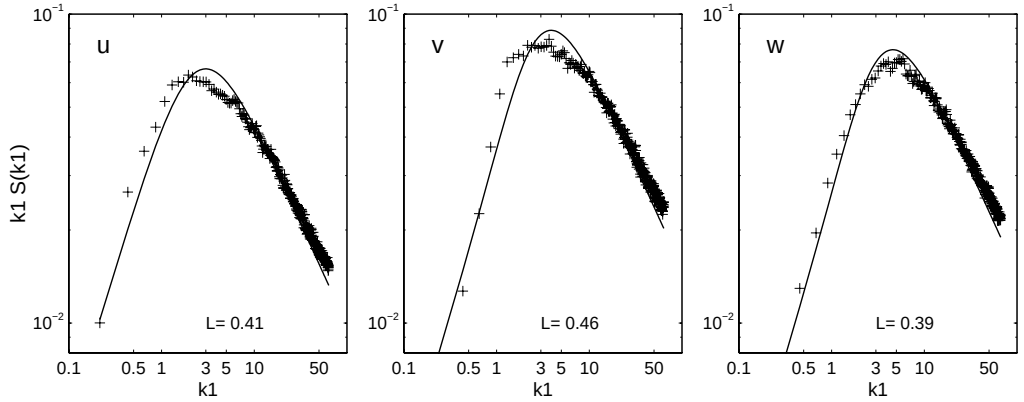

Figure 9: Least square fit of the von Kármán model, (1) and (2), for the averaged spectra for the medium spire exposure. The fitted parameters were L and $\alpha\epsilon^{\frac{2}{3}}$.

Table 2: Characteristics of flow conditions for the three exposures based on the least square fit of the von Kármán spectrum.

Expo-sures	u-component				v-component				w-component			
	I_u (%)	L (m)	$\alpha\epsilon^{\frac{2}{3}}$ ($\frac{\mathrm{m}^{\frac{4}{3}}}{\mathrm{s}^2}$)	$\mathcal{L}_u$ (m)	I_v (%)	L (m)	$\alpha\epsilon^{\frac{2}{3}}$ ($\frac{\mathrm{m}^{\frac{4}{3}}}{\mathrm{s}^2}$)	$\mathcal{L}_v$ (m)	I_w (%)	L (m)	$\alpha\epsilon^{\frac{2}{3}}$ ($\frac{\mathrm{m}^{\frac{4}{3}}}{\mathrm{s}^2}$)	$\mathcal{L}_w$ (m)
Large spires	9.1	0.53	1.75	0.43	10.3	0.54	2.07	0.30	8.8	0.43	2.09	0.24
Medium spires	6.8	0.41	1.26	0.34	7.9	0.46	1.48	0.26	7.2	0.39	1.47	0.22
Grid	7.4	0.16	2.60	0.13	8.0	0.16	3.05	0.09	7.6	0.15	3.00	0.09

The standard deviations were corrected to include the contribution of the higher frequencies ($\approx 10\%$) by extrapolating the wind spectra using a $k_1^{-2/3}$ turbulence decay relationship.

If the flow conditions were truly isotropic, the turbulence intensities as well as the length scales L would have been the same for the three wind components. This was not observed here for the spire exposures where the v component appeared to have larger characteristics. However, the grid exposure had quasi-isotropic characteristics.

Span-wise co-coherence: A similar least square fit analysis was performed for the co-coherence data, using the equations describing the two-point statistics for the istropic turbulence model presented in the earlier section. The co-coherence data were calculated by fast Fourier transforms (FFT) of the time series of the

wind fluctuations, sampled at 625 Hz for 180 seconds. Averaging the 220 blocks of 512-point FFT resulted in co-coherence spectral estimates with a coefficient of variation of 6.7%.

Each of the co-coherence sets of data for eight span-wise separations, from 14 mm to 450 mm, were fitted with equations (11) to (13). The median of the resulting eight von Kármán length scales L, one per separation, was calculated and selected as an adequate representation of L_{coh} [2] for a given wind component and exposure. For smaller separations, which is approaching isotropic turbulence conditions, the dispersion in the results of the fits of L_{coh} was very limited compared to the dispersion obtained for the larger separation. The median L_{coh} for each case is given in Table 3 and a comparison between analytical calculations of co-coherence and experiments are given on Figs. 10 and 11 for 4 separations, respectively for the medium spire exposure and the grid exposure.

The isotropic turbulence model fitted well the span-wise co-coherence measurements in most of the cases, even though the characteristics of the one-point spectrum showed that the flow conditions were not entirely isotropic. The results of the fit of the w component showed lower values than for u and v. It appeared that the anisotropy of the flow affected more the w component.

Table 3: Least square fit of the von Kármán length scale L_{coh} for the co-coherence data for the three exposures.

Exposures	u-component	v-component	w-component
	L_{coh} (m)	L_{coh} (m)	L_{coh} (m)
Large spires	0.43	0.44	0.33
Medium spires	0.44	0.40	0.27
Grid	0.20	0.18	0.12

Collapsing of the co-coherence data: To verify the use of γ as a collapsing parameter, the span-wise co-coherence data for the three exposures for all separations were plotted versus γ (14). Fig. 12 illustrates clearly that all data for the medium spires collapsed well on one line for u, v and w.

An empirical expression, orginally used in [6], was fitted to the collapsed data. This expression (15) is similar to a Weibull function and will be used later on for further analysis of the span-wise co-coherence. The results of the fit are given in Table 4.

$$cocoh(\gamma) = \exp\left[-c_1\gamma^{c_2}\right]\cos(c_3\gamma) \tag{15}$$

[2] The subscript coh was introduced to differentiate the length scale obtained from a fit of the co-coherence data, L_{coh}, with the length scale L obtained from a fit of the one-point spectrum. For isotropic conditions $L_{coh} = L$.

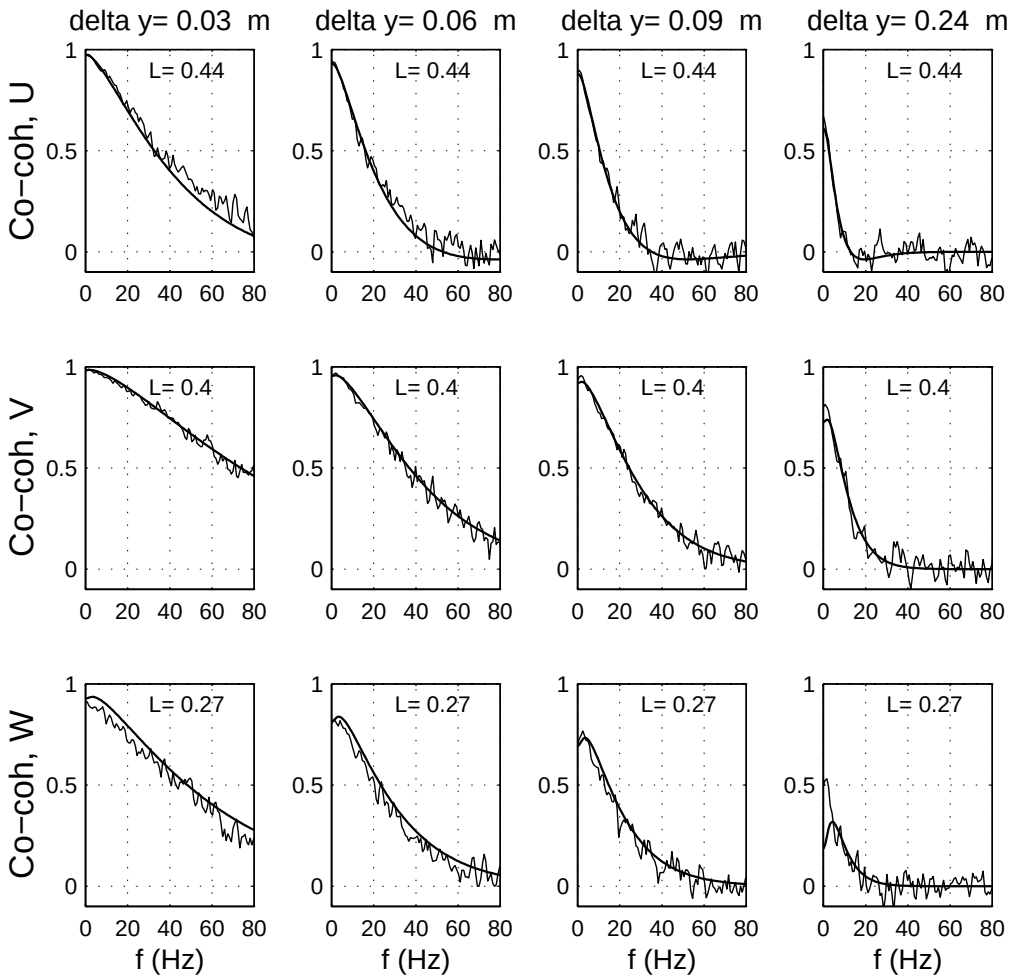

Figure 10: Variations of co-coherence as a function of frequency, separations and wind components for the medium spire exposure. The solid lines on the graphs are the results of the least square fit of the experimental data with (11) to (13) with L_{coh} as a floating parameter.

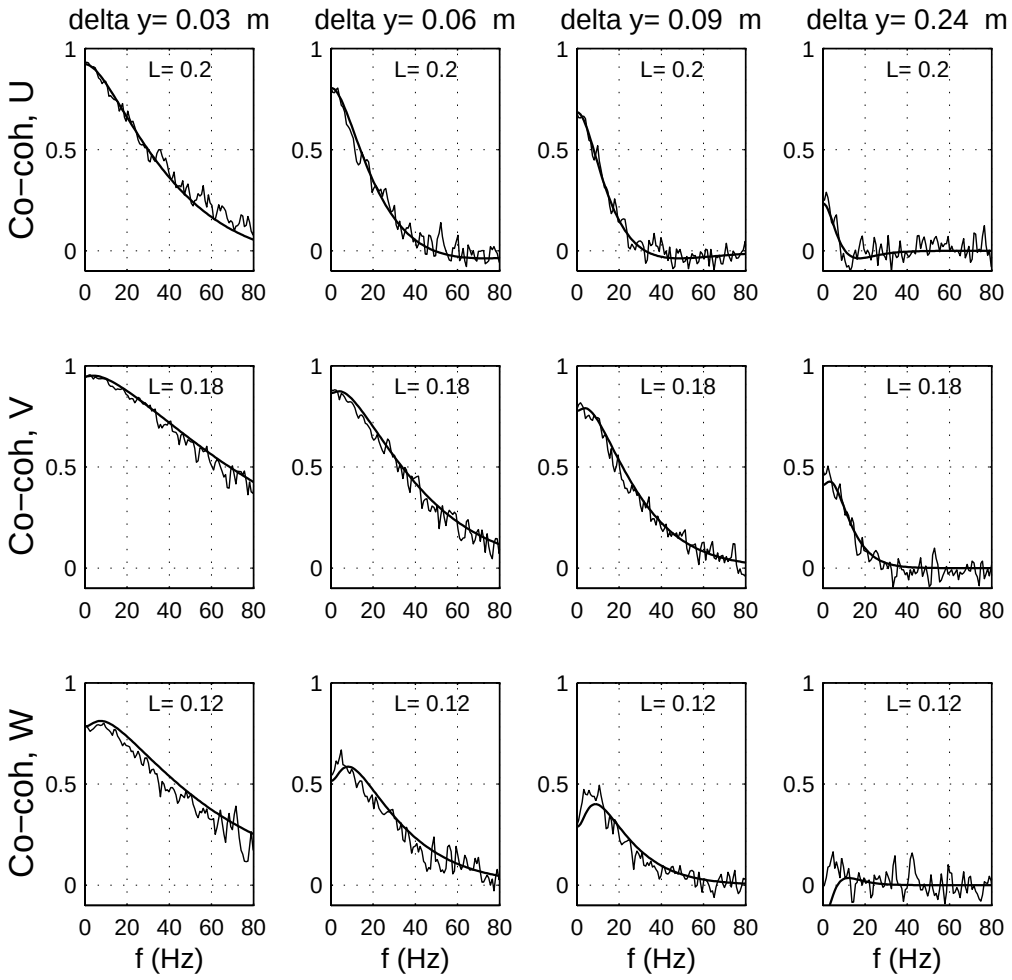

Figure 11: Variations of co-coherence as a function of frequency, separations and wind components for the grid exposure. The solid lines on the graphs are the results of the least square fit of the experimental data with (11) to (13) with L_{coh} as a floating parameter.

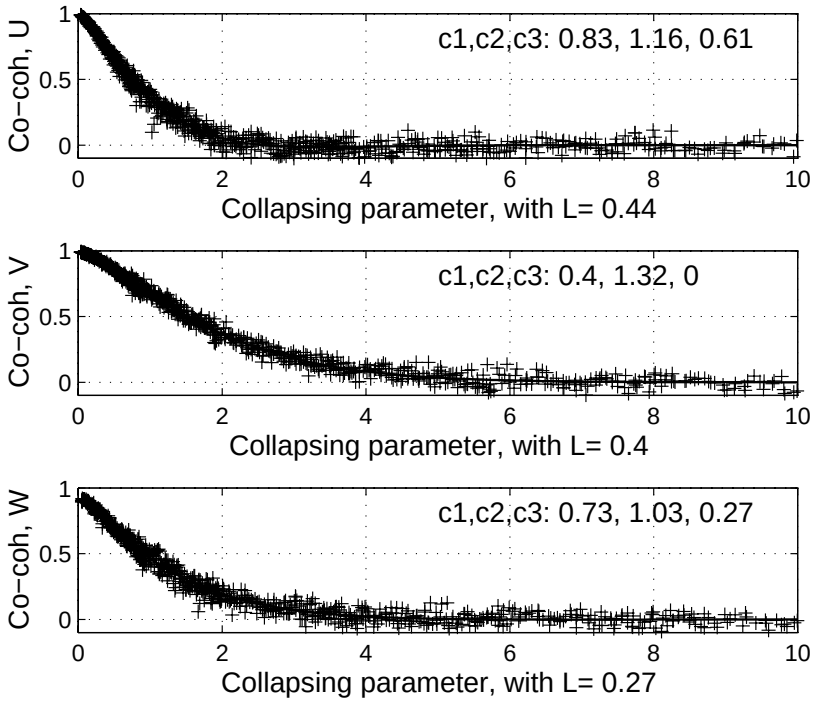

Figure 12: Variations of co-coherence as a function of the collapsing parameter (14) for the medium spire exposure.

Table 4: Least square fit of the collapsed co-coherence data for the three exposures for all separations. c_1, c_2 and c_3 are the fitted parameters.

Exposures	u-component			v-component			w-component		
	c_1	c_2	c_3	c_1	c_2	c_3	c_1	c_2	c_3
Large spires	0.83	1.16	0.63	0.38	1.32	0.12	0.71	1.03	0.29
Medium spires	0.83	1.16	0.61	0.40	1.32	0.00	0.73	1.03	0.27
Grid	0.85	1.13	0.62	0.43	1.26	0.00	0.81	1.04	0.24

3.4 The Fichtl-McVehil spectrum

It was observed in the earlier section that the one-point spectrum of the isotropic turbulence model did not fit adequately the experimental data for the three exposures. The shape of the measured spectra seemed less *peaky*, indicating some shear in the flow [18], and the fit seemed to be pulled towards the higher wave numbers.

To improve the fit of the spectra from the wind tunnel wind data, the Fichtl-McVehil spectrum [10] was chosen for its flexibility. This spectral shape has the advantage of having a floating parameter r that can be adjusted to match the peakiness of the spectrum, while the other floating parameter f_m is adjusted to match the position of the peak on the abscissa. In fact f_m corresponds to the frequency in Hz at which $fS_u(f)$ has a maximum. It is thus very helpful to determine $\mathcal{L}$.

The Fichtl-McVehil spectrum is of the form:

$$\frac{fS_{u,v,w}(f)}{\sigma^2_{u,v,w}} = \frac{a\left(\frac{f}{f_m}\right)}{\left(1+1.5\left(\frac{f}{f_m}\right)^r\right)^{\frac{5}{3r}}} \tag{16}$$

where

$$a = \frac{1.5^{\frac{1}{r}}\, r\, \Gamma\left(\frac{5}{3r}\right)}{\Gamma\left(\frac{2}{3r}\right)\Gamma\left(\frac{1}{r}\right)}. \tag{17}$$

Note that when $r = 2$, (16) is equivalent to the von Kármán spectrum of the u component and when $r = 1$, (16) has the Kaimal spectral shape [6].

The one-point spectra described in the previous section were fitted in a least squares manner with (16), keeping r and f_m as floating parameters. Examples of the fit for the medium spires and the grid exposures are given in Figs. 13 and 14. Table 5 gives a summary of the results.

The length scales, $\mathcal{L}$, corresponding to the peak of the spectrum appeared to be slightly higher using the Fichtl-McVehil spectral shape compared to the von Kármán model.

Table 5: Least square fit of the Fichtl-McVehil spectrum for the three exposures.

Exposures	u-component			v-component			w-component		
	r	f_m (Hz)	$\mathcal{L}_u$ (m)	r	f_m (Hz)	$\mathcal{L}_v$ (m)	r	f_m (Hz)	$\mathcal{L}_w$ (m)
Large spires	1.20	2.58	0.51	1.46	3.89	0.32	1.57	5.88	0.24
Medium spires	1.12	3.63	0.39	1.24	5.17	0.27	1.44	6.54	0.22
Grid	1.04	9.15	0.14	1.35	15.56	0.085	1.55	18.19	0.09

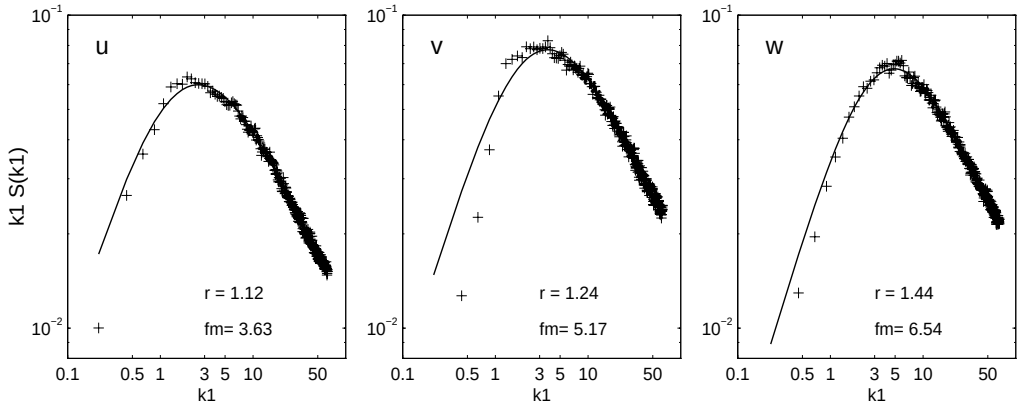

Figure 13: Least square fit of the Fichtl-McVehil spectrum (16) for the averaged spectra for the medium spire exposure. The fitted parameters were r and f_m.

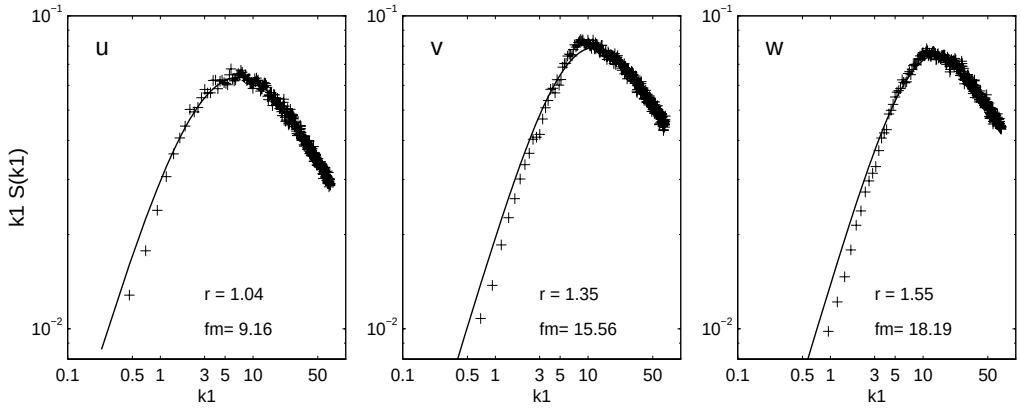

Figure 14: Least square fit of the Fichtl-McVehil spectrum (16) for the averaged spectra for the grid exposure.

4 Characteristics of the unsteady wind forces

4.1 Cross-sectional forces and aerodynamic admittance

The aerodynamic lift forces induced by gusty winds on a cross-sectional strip of a bridge deck can be described (see Part I-A) by:

$$F_{z,b}(t) \approx \frac{\rho \bar{V} B}{2} \left[2C_z u(t) + C'_z w(t) \right] \tag{18}$$

The buffeting lift forces are proportional to w and intuitively it can be deduced that the duration of only the larger gusts will be sufficiently long to generate variations of surface pressures and thus lift variations. Oncoming flow with larger length scales will then be more efficient in generating unsteady lift on a strip than flow with the same turbulence intensity but smaller length scales. This is illustrated in Fig. 15 where the spectral densities of the lift and torque coefficients, $C_{z,m}$, are compared for two exposures keeping all the other test parameters constant. The spectra showed a much larger magnitude for the medium spire exposure than for the grid exposure.

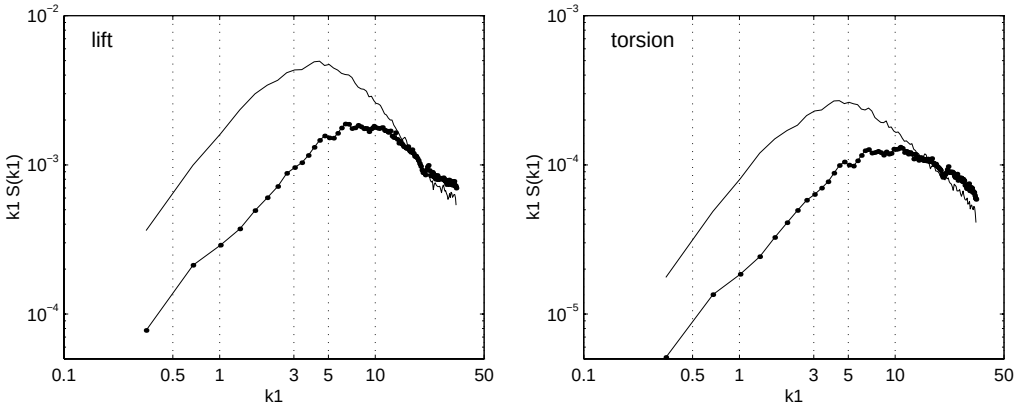

Figure 15: Power spectral density of $C_{z,m}$ versus k_1 for the medium spire exposure (solid line) and the grid exposure (dotted line); $B/D = 5$, $\bar{V}$ =15 ms^{-1} and I_w= 7.2 – 7.6 %.

This concept is expressed in the frequency domain by the aerodynamic admittance and was introduced for bridge decks by Davenport (see Part I). The ratio between the scales of turbulence and the deck width, $\mathcal{L}/B$, is thus an important parameter to characterise the aerodynamic admittance. Table 6 presents $\mathcal{L}/B$ for the test conditions of this study.

Table 6: Ratio of the turbulence length scales to the deck width, $\mathcal{L}/B$ for the three exposures and the three aspect ratios.

	Large spires			Medium spires			Grid		
	u	v	w	u	v	w	u	v	w
B/D=5	-	-	-	2.60	1.80	1.50	0.93	0.57	0.57
B/D=10	1.70	1.10	0.80	1.30	0.90	0.73	0.46	0.28	0.29
B/D=12.67	1.30	0.84	0.63	1.00	0.71	0.58	0.37	0.27	0.23

The aerodynamic admittance of the various deck configurations was calculated by dividing the spectrum of the force coefficients, $S_{C_{z,m}}$, on one chord-wise strip by the spectrum of the oncoming wind velocity fluctuations, $S_{u,w}$. For the case of the lift forces, the admittance can be expressed by:

$$|A_z(f)|^2 = \frac{\bar{V}^2 S_{C_z}(f)}{4 C_z^2 S_u(f) + C_z'^2 S_w(f)} \tag{19}$$

where C_z' is the derivative near 0° of the lift coefficient C_z with respect to the angle of wind incidence in radians. Table 7 illustrates typical variations of the static coefficients and their derivatives with increasing width-to-depth ratio.

Table 7: Time averaged aerodynamic force coefficients for the medium spire exposure, deck without railings (based on B).

	$C_z(0^\circ)$	$C_m(0^\circ)$	$C_z'(0^\circ)$	$C_m'(0^\circ)$
B/D=5	-0.154	0.026	4.04	1.03
B/D=10	-0.118	0.010	4.62	1.18
B/D=12.67	-0.128	-0.004	4.75	1.14

Fig. 16 presents results of the aerodynamic admittance measurements for four cases, two aspect ratios and two wind conditions. The vertical turbulence intensity was the same for each case, but the ratio $\mathcal{L}_w/B$ was varied from 1.5 to 0.29. It indicates that the larger the ratio between the size of the gusts and the deck width, the larger the admittance.

Fig. 16 **b)** compares the measured admittance for B/D= 5 and the medium spire exposure to the Liepmann's approximation to the Sears function analytically derived for a thin airfoil with a lift slope of 2π [7]. The ordinate is the product of $C_z'^2$ and $|A_z(f)|^2$. The measured admittance never produced more lift than the linear theory predicted for a thin airfoil and showed much less admittance at low reduced frequency. It can also be said that even though the deck cross-section studied was

a poorer lift generator, it could generate as much lift than a thin airfoil at higher reduced frequency. Body-induced turbulence might explain this behaviour.

For this case, the test conditions were representative of full scale conditions where a ratio $\mathcal{L}_w/B$ = 40 m /30 m is frequently seen. A thorough analysis of the aerodynamic admittance measurements is presented in Part II-B.

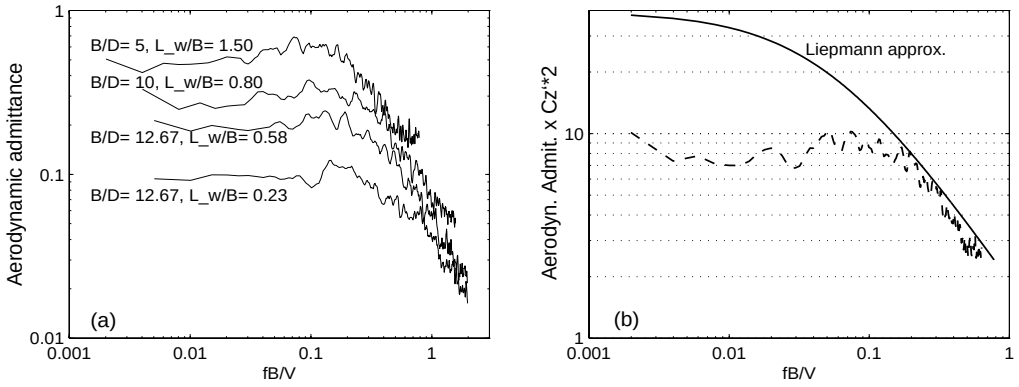

Figure 16: **a)** Variations of lift aerodynamic admittance with reduced frequency for four cases in turbulent flow. **b)** Comparisons of the product of the admittance and lift slope squared, for B/D= 5 with railings, medium spire, $\mathcal{L}_w/B$= 1.5 (dashed line), with theoretical predictions for a thin airfoil (solid line) [7].

4.2 Span-wise cross-correlation and co-coherence

The span-wise variations of the unsteady wind forces acting on the deck can be expressed by the co-coherence function (as defined in Section 3) between forces measured simultaneously on two distinct chord-wise strips. A total of six span-wise separations were analysed for each case, varying from 30 mm to 300 mm. Similar measurements to characterize the oncoming flow field were reported in the previous section (separations from 14 mm to 450 mm).

Figs. 17 and 18 illustrate the variations of the co-coherence of the forces with frequency for four span-wise separations and various test conditions. It was observed that for a given wind exposure, the larger the deck width, the larger the span-wise coherence; and that for a given deck width, the smaller the scales of turbulence the smaller the co-coherence. While the latter observation was not surprising, the former indicated that the application of the strip assumption could have some limitations for the bridge decks studied.

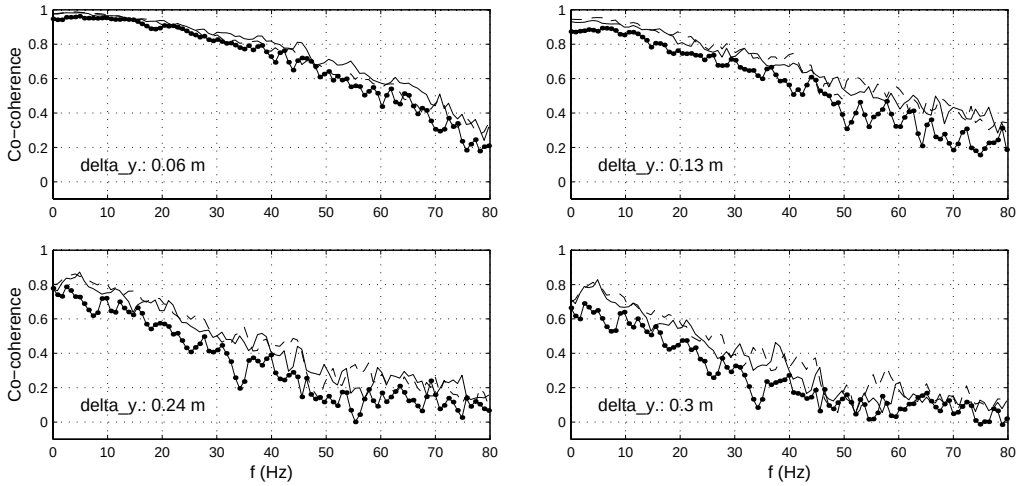

Figure 17: Variations of the co-coherence of the lift forces with frequency, span-wise separations and bridge deck aspect ratios for the medium spire exposure. Dotted line: $B/D = 5$; solid line: $B/D = 10$ and dashed line: $B/D = 12.67$.

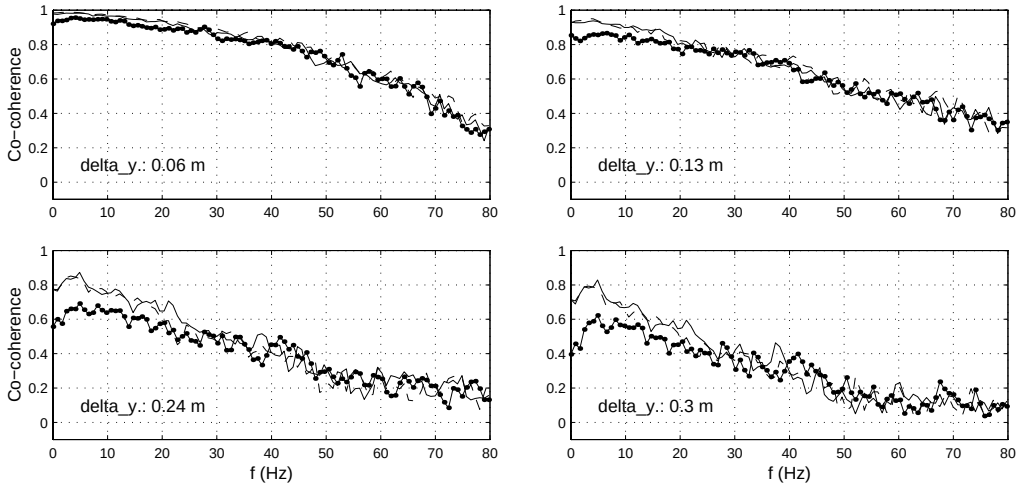

Figure 18: Variations of the co-coherence of the lift forces with frequency, span-wise separations and wind exposures for $B/D = 10$. Dotted line: grid exposure; solid line: medium spire exposure and dashed line: large spire exposure.

4.2.1 Cross-correlation coefficient

The purpose of the analysis that follows is to compare the two-point statistics of the input (the wind fluctuations) to the characteristics of the output (the aerodynamic forces). The first parameter to compare is the span-wise cross-correlation coefficient defined as:

$$R_{12}(\Delta y) = \frac{\sigma_{12}^2}{\sigma_1 \sigma_2} \tag{20}$$

where σ_{12}^2 is the co-variance between points 1 and 2 separated by Δy. R_{12} is an indicator of the correlation of the process for the entire frequency range (zero time-lag) and it is thus only a function of the separation.

The cross-correlation coefficients were calculated for the various tests conditions and a summary of the results is given in Figs. 19 to 21. For all cases, the cross-correlation of v was the largest of the three wind components, and the cross-correlation of the forces was always considerably larger than the oncoming wind (Fig. 19). Also, it was observed that the larger the deck width, the larger the cross-correlation, for all exposures.

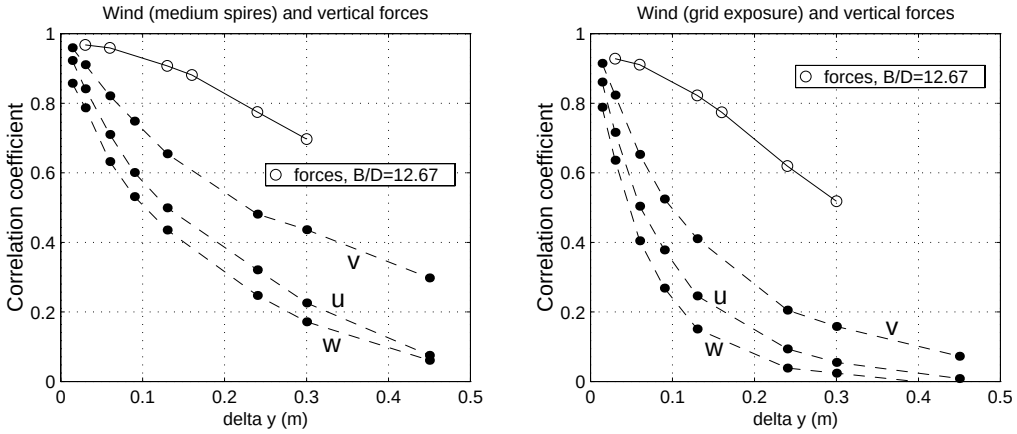

Figure 19: Variations of the span-wise cross-correlation coefficient of the vertical aerodynamic forces (solid line) for B/D=12.67 and the wind velocity fluctuations (dashed lines) for the medium spire exposure and the grid exposure.

Figs. 20 and 21 compare the correlation of the forces for different B/D ratios as a function of the normalized separation $\Delta y/B$. The curves tend to collapse on one line for the lower values of $\Delta y/B$ but for the higher values, the curve associated with the smaller deck width showed larger correlation. That is to say that the model with the smaller B/D ratio showed a larger correlation length in relation to its width than the other models. Since the narrower model has the larger L_{coh}/B ratio, this observation is consistent with earlier findings [6] that R_{FF} increases with an increase of L_{coh}/B (see Part I-B).

The larger cross-correlation of the forces than the velocity fluctuations was to be expected since the process to generate the forces implies that only the larger scale gusts will create lift. The structure does some *conditional sampling*, selecting only the more correlated part of the wind. However, this can only explain a small part of the difference between R_{ww} and R_{FF}. It also suggests the non-validity of the strip assumption.

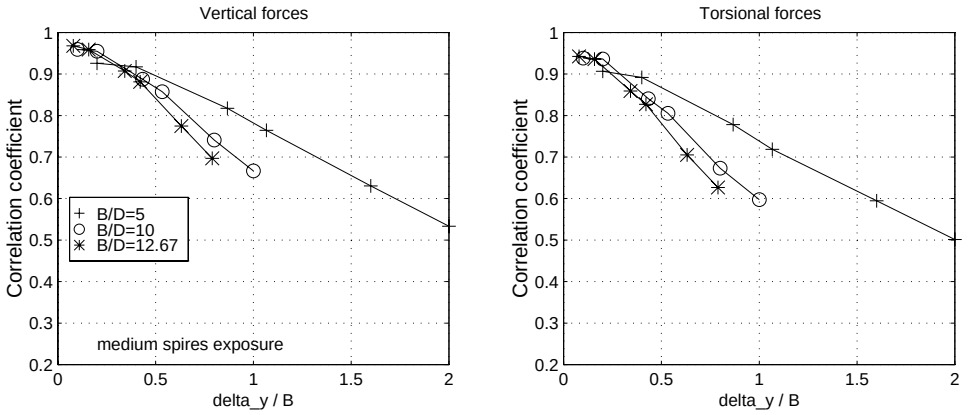

Figure 20: Variations of the span-wise cross-correlation coefficient of the aerodynamic forces as a function of normalized separations $\Delta y/B$ for the medium spire exposure.

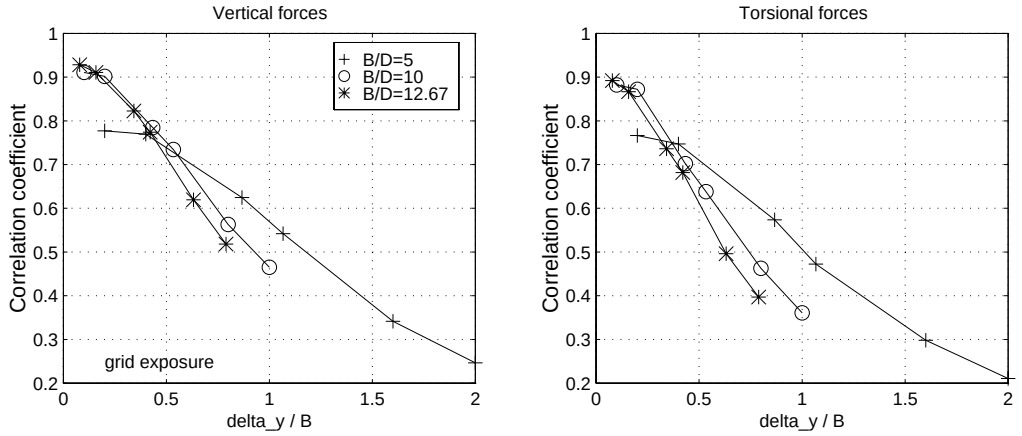

Figure 21: Variations of the span-wise cross-correlation coefficient of the aerodynamic forces for the grid exposure.

4.2.2 Co-coherence: wind velocity versus forces

A comparison of the co-coherence of the lift forces for two aspect ratios to the co-coherence of the velocity fluctuations in v and w is given in Fig. 22. The comparisons are made for two separations. The co-coherence of the forces is clearly larger than the co-coherence of w but is similar to the co-coherence of v. This similarity is possibly only coincidental.

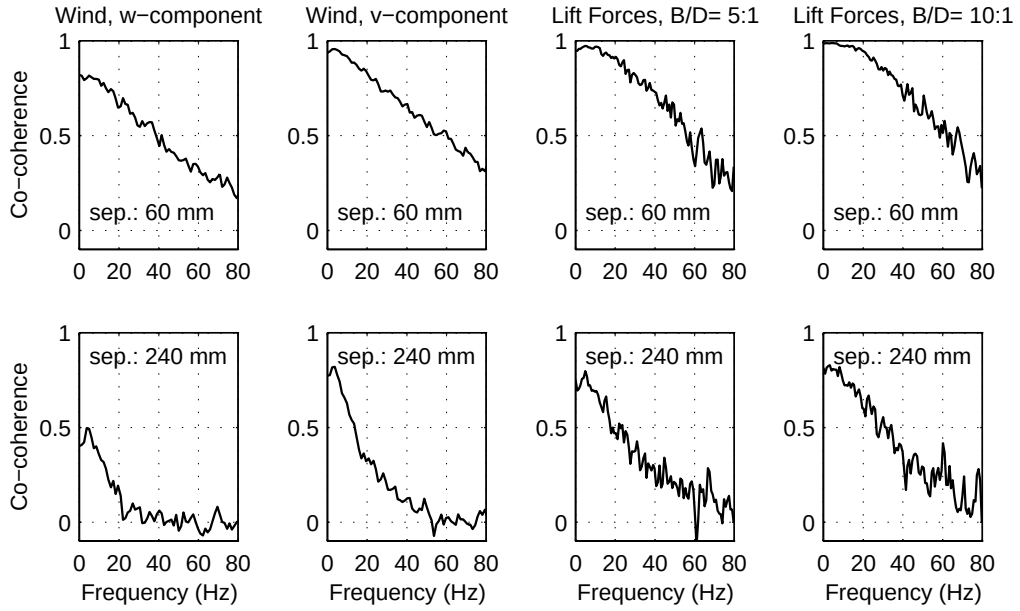

Figure 22: Variations of the span-wise co-coherence of the forces and of the velocity fluctuations for two separations as a function of frequency.

To verify this last aspect and to describe in details the relationships between the co-coherence of the wind and the resulting forces, curves showing the variations of these quantitites with the separation to the wave length ratio, $k_1\Delta y$, are given in Figs. 23 to 30. All the test cases are represented on these figures for the configuration without railings and a mean wind speed of 15 ms^{-1}. The co-coherence of the wind fluctuations is represented by the von Kármán model, equations (12) and (13), with L_{coh} obtained by a least square fit of the co-coherence data (see Section 3.3).

Fig. 23 shows results for the case where the L_{coh}/B was the largest for this study and is representative of full-scale conditions. For span-wise separations larger than 30% of $\mathcal{L}_w$, the co-coherence of the forces is much larger than the co-coherence of w and equivalent to the co-coherence of v for $k_1\Delta y$ smaller than 1.0. The strip assumption is thus clearly not valid for this case (and for all the subsequent cases). However, for the smaller span-wise separation where $\Delta y/\mathcal{L}_w = 15\%$, the co-coherence of w and the lift forces were found to be equivalent for the above-mentioned test case.

Fig. 29 presents the results for another test case representative of full-scale conditions. It is for the large spire exposure and the $B/D = 10$. Here also, the co-coherence of lift is much larger than the co-coherence of w and somewhat larger than the co-coherence of v. This figure shows that the observation made earlier associating co-coherence of v and lift force was coincidental except for small $k_1\Delta y$.

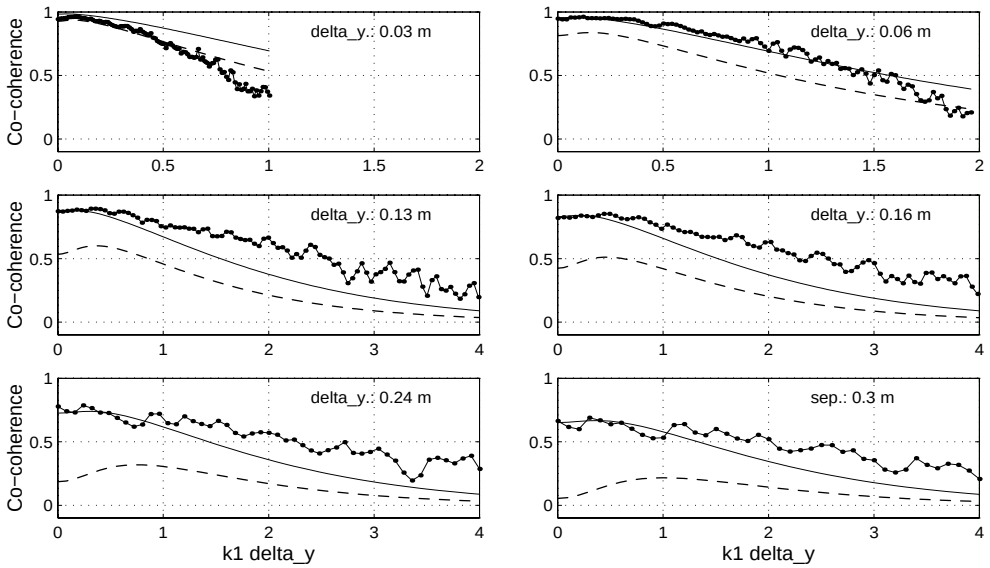

Figure 23: Co-coherence as a function of $k_1\Delta y$ for the lift forces (dotted line) for $B/D = \mathbf{5}$ and for the wind for the **medium spire exposure**. Solid line: v with L_{coh}= 0.40 and $\mathcal{L}$=0.27 m; dashed line: w with L_{coh}= 0.27 and $\mathcal{L}$=0.22 m.

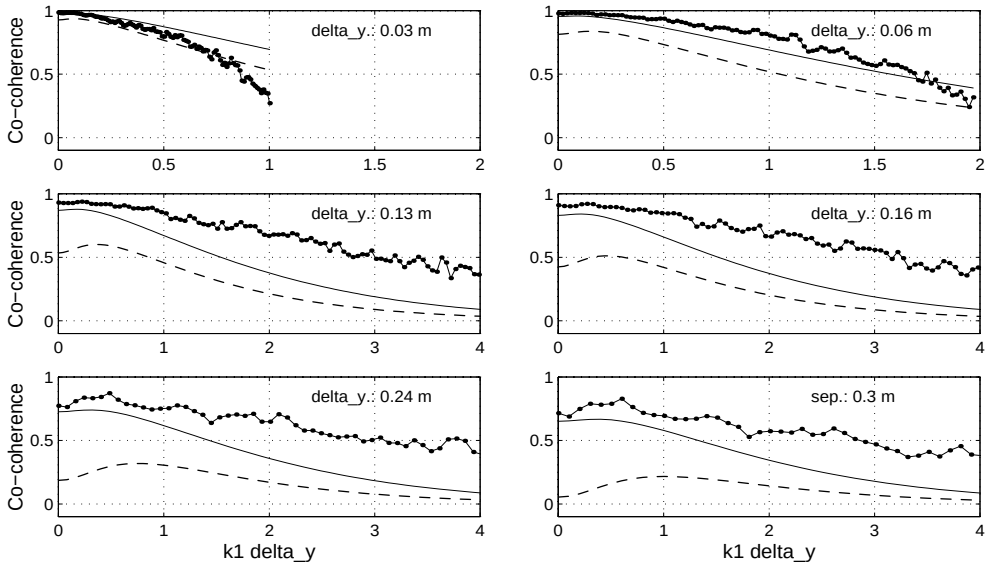

Figure 24: Co-coherence as a function of $k_1\Delta y$ for the lift forces (dotted line) for B/D **= 10** and for the wind for the **medium spire exposure**. Solid line: v with L_{coh}= 0.40 and $\mathcal{L}$=0.27 m; dashed line: w with L_{coh}= 0.27 and $\mathcal{L}$=0.22 m.

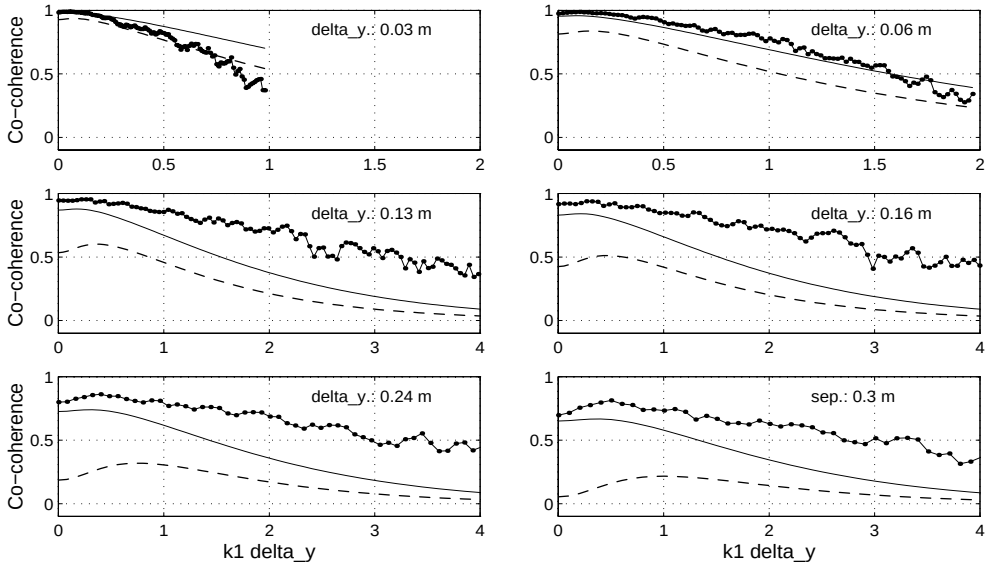

Figure 25: Co-coherence as a function of $k_1\Delta y$ for the lift forces (dotted line), B/D **= 12.67** and for the wind for the **medium spire exposure**. Solid line: v with L_{coh}= 0.40 and $\mathcal{L}$=0.27 m; dashed line: w with L_{coh}= 0.27 and $\mathcal{L}$=0.22 m.

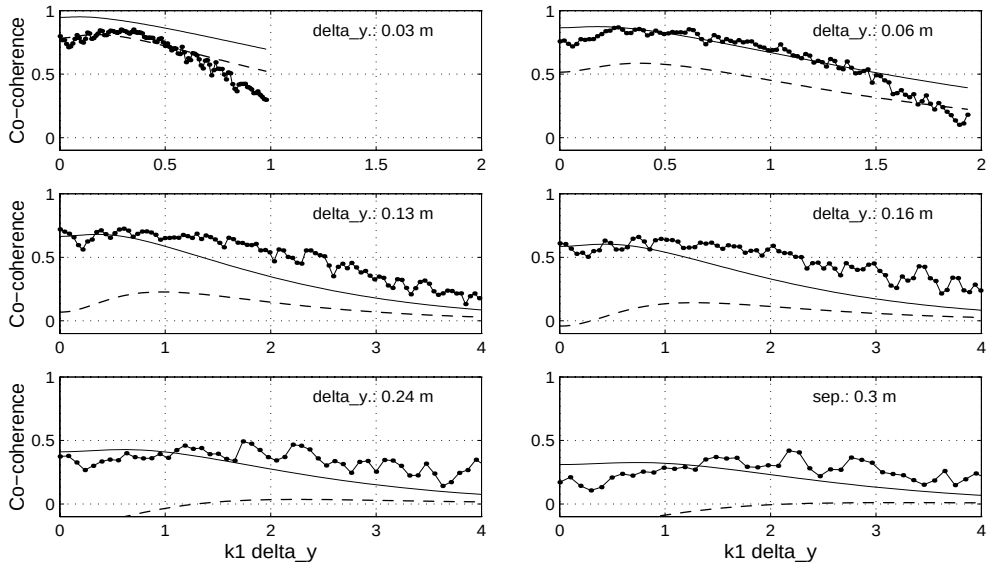

Figure 26: Co-coherence as a function of $k_1\Delta y$ for the lift forces (dotted line) for B/D **= 5** and for the wind for the **grid exposure**. Solid line: v with L_{coh}= 0.18 and $\mathcal{L}$=0.085 m; dashed line: w with L_{coh}= 0.12 and $\mathcal{L}$=0.09 m.

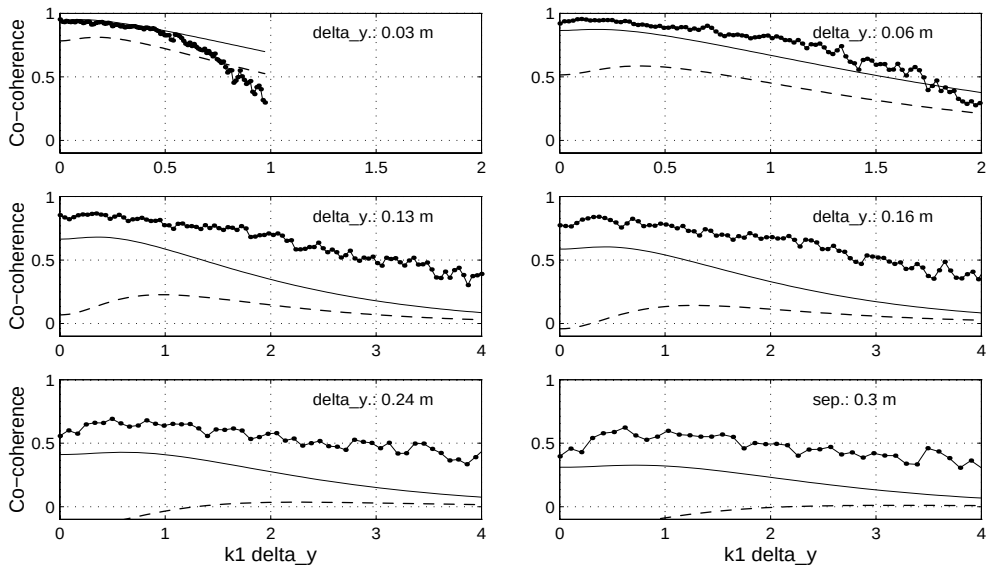

Figure 27: Co-coherence as a function of $k_1\Delta y$ for the lift forces (dotted line) for B/D **=10** and for the wind for the **grid exposure**. Solid line: v with L_{coh}= 0.18 and $\mathcal{L}$=0.085 m; dashed line: w with L_{coh}= 0.12 and $\mathcal{L}$=0.09 m.

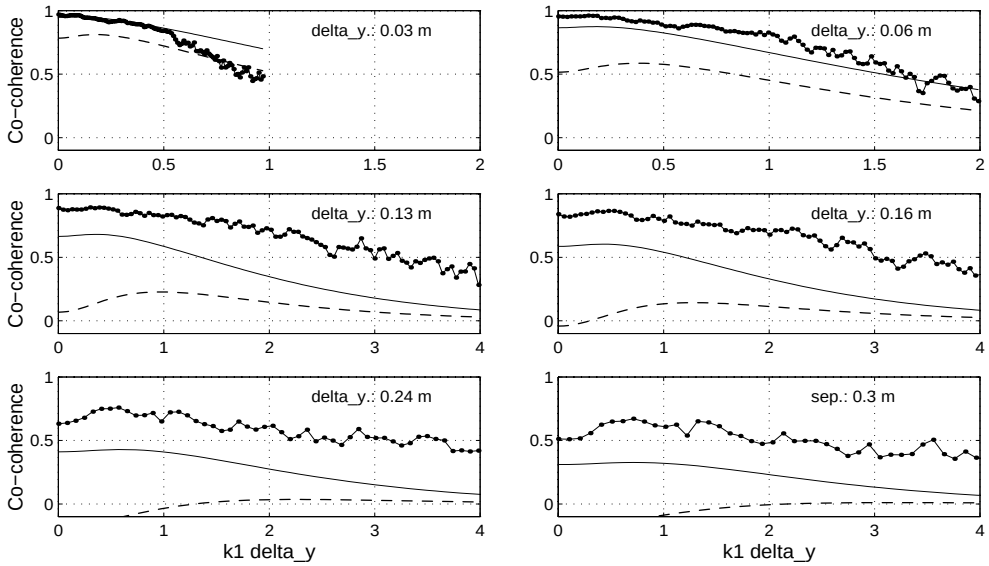

Figure 28: Co-coherence as a function of $k_1\Delta y$ for the lift forces (dotted line) for B/D **= 12.67** and for the wind for the **grid exposure**. Solid line: v with L_{coh}= 0.18 and $\mathcal{L}$=0.085 m; dashed line: w with L_{coh}= 0.12 and $\mathcal{L}$=0.09 m.

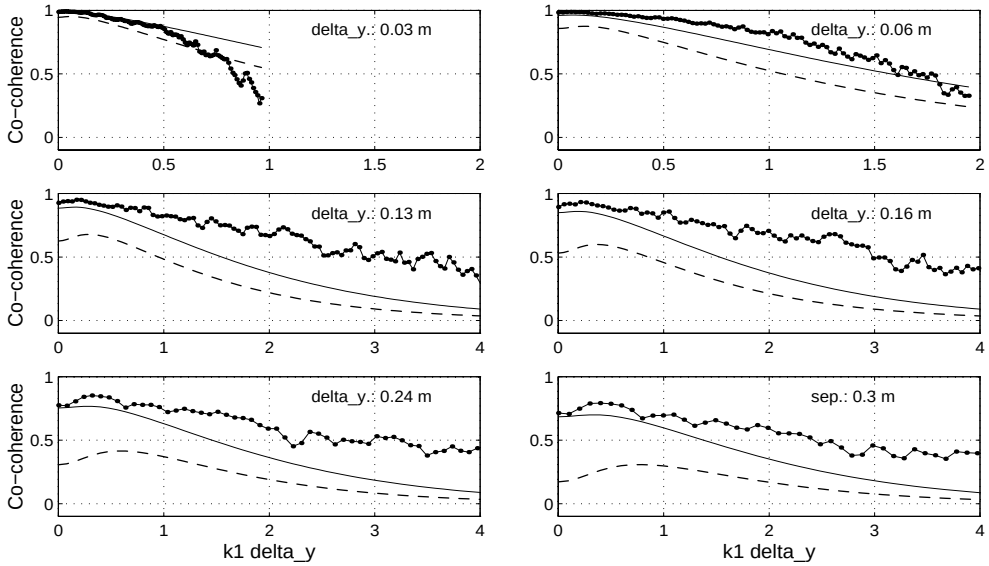

Figure 29: Co-coherence as a function of $k_1\Delta y$ for the lift forces (dotted line) for B/D **= 10** and for the wind for the **large spires exposure**. Solid line: v with L_{coh}= 0.44 and $\mathcal{L}$=0.32 m; dashed line: w with L_{coh}= 0.33 and $\mathcal{L}$=0.24 m.

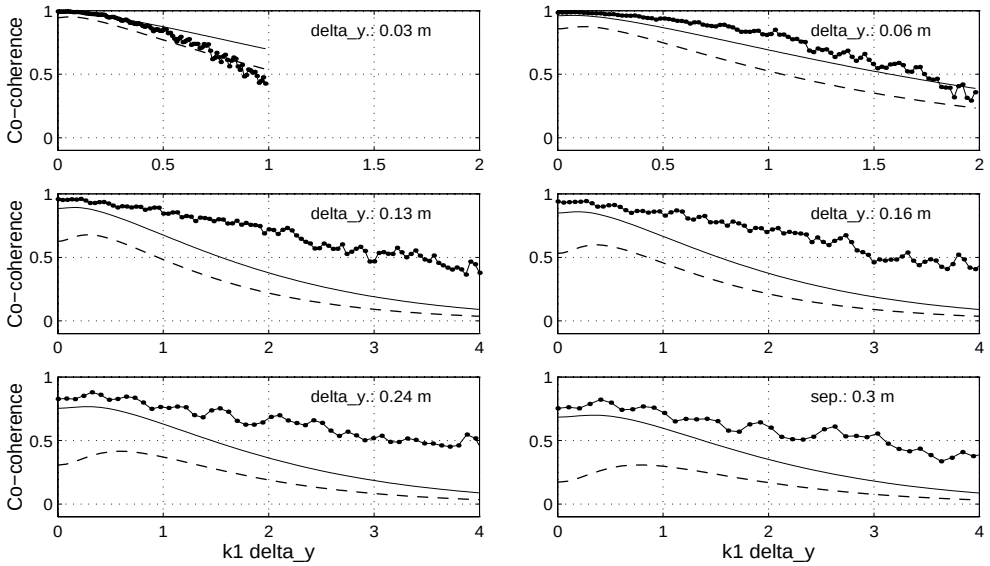

Figure 30: Co-coherence as a function of $k_1\Delta y$ for the lift forces (dotted line) for B/D **= 12.67** and for the wind for the **large spires exposure**. Solid line: v with L_{coh}= 0.44 and $\mathcal{L}$=0.32 m; dashed line: w with L_{coh}= 0.33 and $\mathcal{L}$=0.24 m.

4.2.3 Influence of the $\mathcal{L}_w/B$ ratio

To characterize the influence of the $\mathcal{L}_w/B$ ratio on the co-coherence of the forces, a series of comparisons are presented in Figs. 31 to 36. In theory, test conditions with similar $\mathcal{L}_w/B$ ratios should show similar co-coherence curves. This is verified qualitatively in Fig. 31. For all separations, the co-coherence of the lift for the B/D=10 and the medium spire exposure is equivalent to the B/D=12.67 case with the large spire exposure.

For a more rigorous analysis, in addition to the geometric similarity represented by $\mathcal{L}_w/B$, the comparisons should be based on the normalized separation $\Delta y/B$ and the wave-length to the deck-width ratio k_1B. For similar $\mathcal{L}_w/B$ the comparisons between different deck widths B_1 and B_2 should verify the following expression:

$$cocoh_{FF}(k_1B_1, \Delta y/B_1) = cocoh_{FF}(k_1B_2, \Delta y/B_2) \tag{21}$$

Fig. 32 presents a comparison for the same test conditions as Fig. 31 but using the extended geometric similarity described above. The agreement between these two cases is excellent.

When the test conditions of Fig. 31 are reversed, one would expect that the combination of the larger deck width and the medium spires will have smaller co-coherence than the combination of smaller deck width with the larger spires. Surprisingly, this

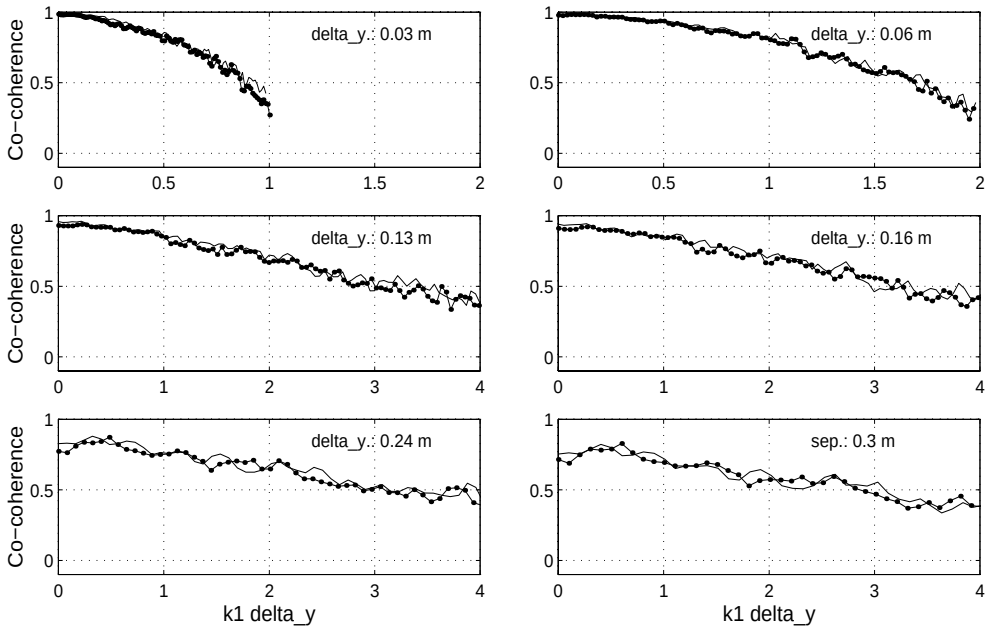

Figure 31: Comparisons of the co-coherence of the lift forces for two test conditions: $B/D = 10$ (dotted line) with the medium spire exposure, $\mathcal{L}_w/B$ =0.73, and B/D = 12:67 (solid line) with the large spire exposure, $\mathcal{L}_w/B$ =0.63.

was verified only for very small k_1B (smaller than 1.0) as presented in Fig. 33. For larger k_1B, the two curves collapsed indicating that the test case with the larger deck width showed more co-coherence than anticipated.

Fig. 34 reports two cases where $\mathcal{L}_w/B \approx 0.58$. The case with the larger deck width showed considerably larger co-coherence than the case with the narrower deck in grid turbulence. This confirms the trend of the latter case and suggests that the span-wise co-coherence of the forces is influenced not only by the $\mathcal{L}_w/B$ ratio but also directly by the deck width itself. Note that for this case the exposures have similar turbulence intensity but the grid turbulence has a much larger content of small scale turbulence that might play a role in the process.

A comparison where one of the cases would clearly not satisfy the condition of the strip assumption, stating that the scale of turbulence should be bigger than the characterisitic length of the body is presented in Fig. 35. It is for B/D= 12.67 and the grid exposure so that $\mathcal{L}_w/B = 0.23$ which is compared to a $\mathcal{L}_w/B = 1.5$ case. As expected, the $\mathcal{L}_w/B = 1.5$ case showed co-coherence curves larger than the $\mathcal{L}_w/B = 0.23$ case up to k_1B values of 2.0. For larger k_1B the $\mathcal{L}_w/B = 0.23$ case showed larger co-coherence. It is likely that the secondary span-wise flows are important for the $\mathcal{L}_w/B = 0.23$ case, increasing the co-coherence drastically. It is

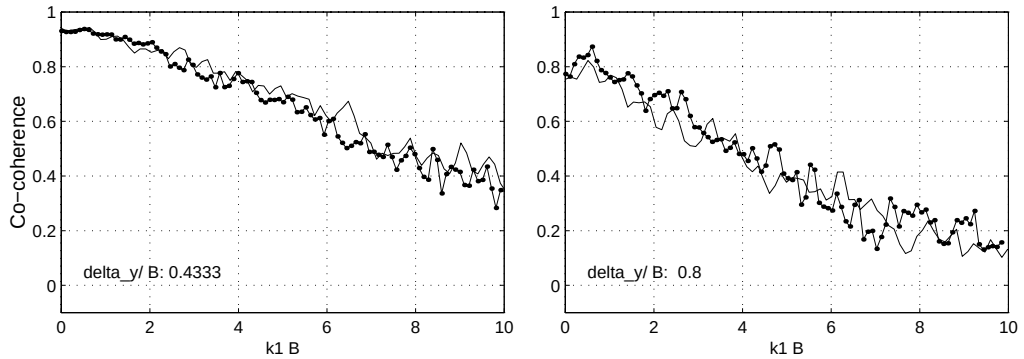

Figure 32: Same test conditions as Fig. 31 but the comparison is made as a function of normalized separations $\Delta y/B$ and the wave-length to the deck-width ratio k_1B. $B/D = 10$ and $\mathcal{L}_w/B$ =0.73: dotted line; $B/D = 12{:}67$ and $\mathcal{L}_w/B$ =0.63: solid line.

believed that very early, as the approaching vortices are passing the bridge deck, they are getting reorganized by the deck itself in a more coherent manner, even though the deck remains stationary.

Finally, Fig. 36 compares two cases where $\mathcal{L}_w/B \approx 0.7 - 0.6$. The test conditions with the larger deck width has larger co-coherence for all normalized separations and all values of k_1B.

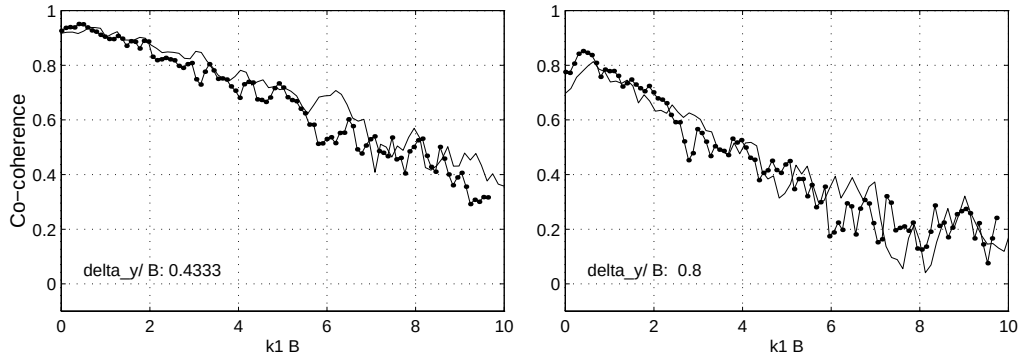

Figure 33: Comparisons of the co-coherence of the lift forces for two test conditions: $B/D = 10$ (dotted line) with the large spire exposure, $\mathcal{L}_w/B$ =0.80, and $B/D =$ 12:67 (solid line) with the medium spire exposure, $\mathcal{L}_w/B$ =0.58.

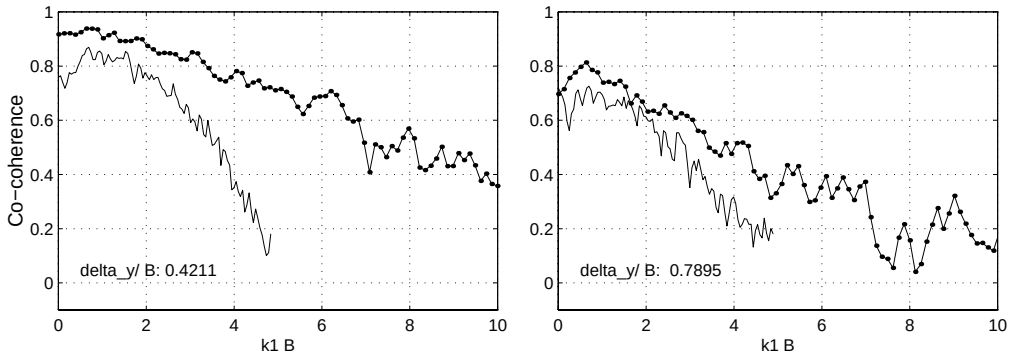

Figure 34: Comparisons of the co-coherence of the lift forces for two test conditions: $B/D = 12{:}67$ (dotted line) with the medium spire exposure, $\mathcal{L}_w/B$ =0.58, and B/D = 5 (solid line) with the grid exposure, $\mathcal{L}_w/B$ =0.57.

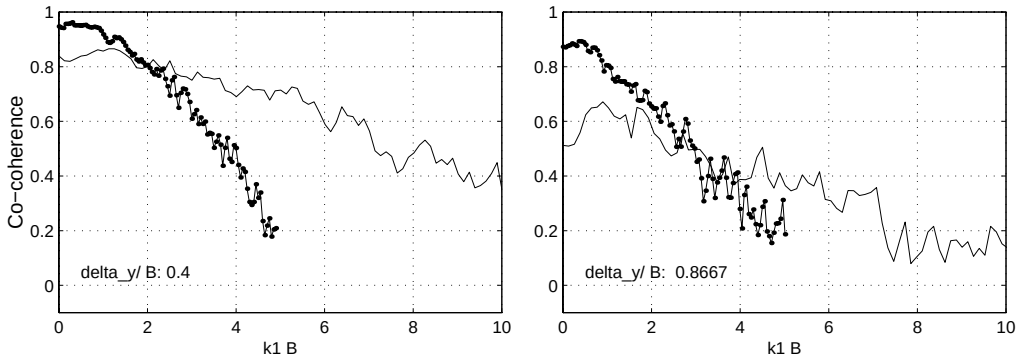

Figure 35: Comparisons of the co-coherence of the lift forces for two test conditions: B/D = 5 (dotted line) with the medium spire exposure, $\mathcal{L}_w/B$ =1.5, and B/D = 12:67 (solid line) with the grid exposure, $\mathcal{L}_w/B$ =0.23.

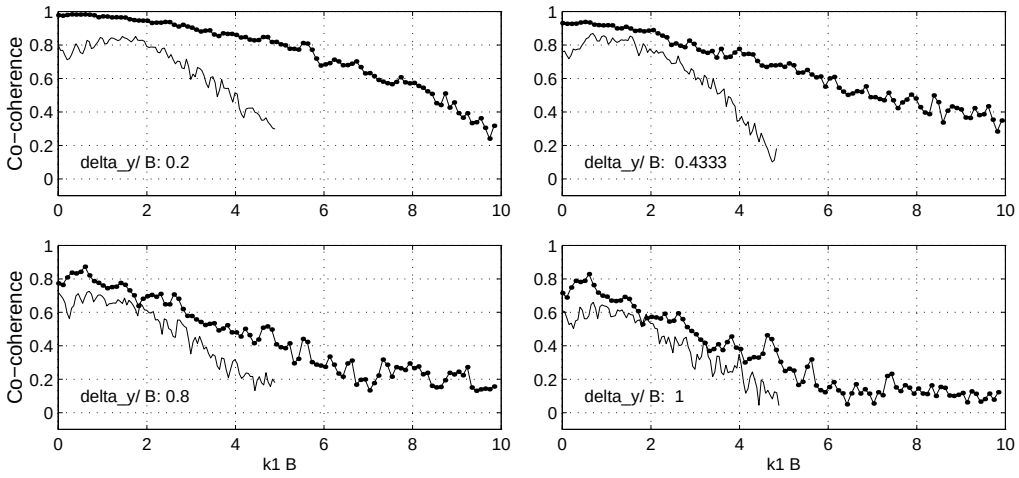

Figure 36: Comparisons of the co-coherence of the lift forces for two test conditions: $B/D = 10$ (dotted line) with the medium spire exposure, $\mathcal{L}_w/B = 0.73$, and $B/D = 5$ (solid line) with the grid exposure, $\mathcal{L}_w/B = 0.57$.

4.2.4 Influence of the railings

Experience has shown that conventional road equipment such as crash barriers, median dividers and wind breaks can change significantly the aerodynamics of a bridge deck. To study this aspect, the presence or lack of railings on the deck was kept as a test parameters throughout this study. All the results reported previously referred to the without railing configuration.

Railings made of thin brass rods, $\approx 60\%$ porous with an overall height equal to 30% of the deck depth, were mounted at the leading and trailing edges of the top surface of the section models. The railings represented a crash barrier with a relatively large porosity commonly used on bridge decks in Europe.

Based on observations made during this study, the influence of the railings on the dynamic characteristics of the buffeting wind loads can be summarised as follows:

1. Generally, an increase of span-wise coherence of the forces was observed when railings were fitted to the section models.

2. The increase of co-coherence for lift and overturning moment was compensated for by a reduction of the cross-sectional forces on a given strip fitted with railings.

3. The larger the deck width the lesser the influence of the railings.

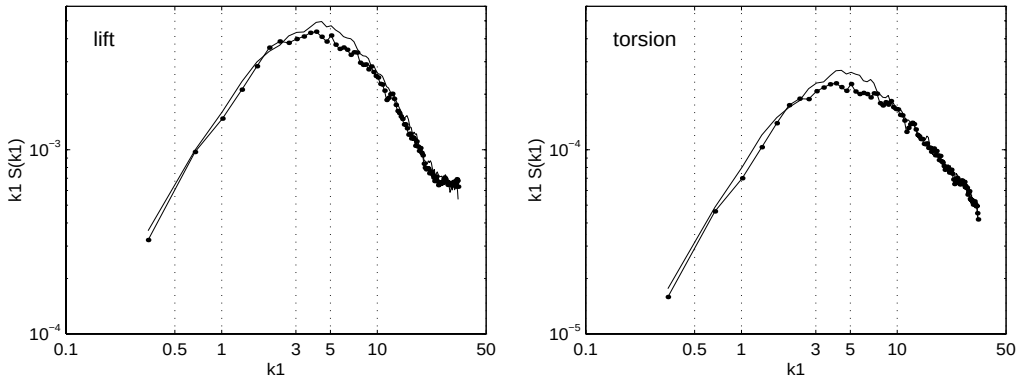

Figure 37: Power spectral density of $C_{z,m}$ versus k_1 for the medium spire exposure and $B/D = 5$, with railings (dotted line) and without railings (solid line)

4. The smaller the scales of turbulence the larger the increase of co-coherence for the with railing case, especially for smaller separations.

The observations of point 1 and 2 are illustrated by Fig. 37 and Fig. 38 for the medium spire exposure and B/D= 5. For the larger aspect ratio, B/D= 12.67, the influence of the railings appeared negligible. Fig. 39 illustrates points 3 and 4. For small separations and smaller length scales, the span-wise coherence was found to be larger with the railings in place.

By inspection of the unsteady pressure distribution (see Figs. 40 and 41), it was observed that the separation bubble was longer when the railings were fitted to the section model. However, the large suction peaks observed on the top surface of the deck near the leading edge were reduced by the presence of the railings. This could explain the observed reduction of the cross-sectional forces on a strip (Fig. 37). The elongation of the separation bubble due to the railings likely facilitates the generation of secondary cross flows that would increase the span-wise co-coherence and cross-correlation. This process is less important for the larger deck widths since secondary cross flows are probably already active and the span-wise co-coherence is already large.

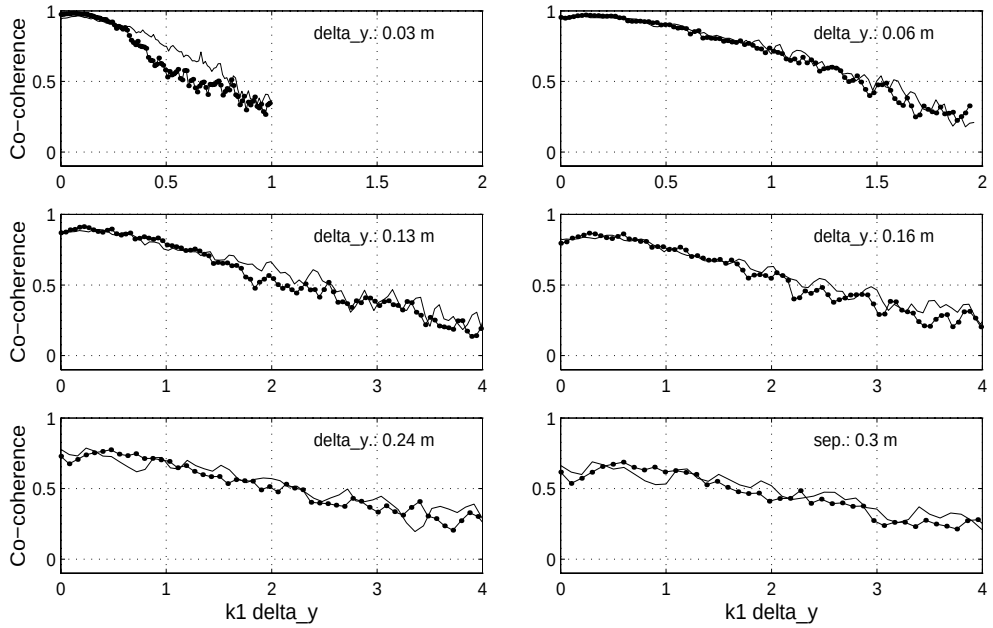

Figure 38: Co-coherence of the lift forces for the with railings (dotted line) and without railings (solid line) configurations, $B/D = 5$, medium spire exposure.

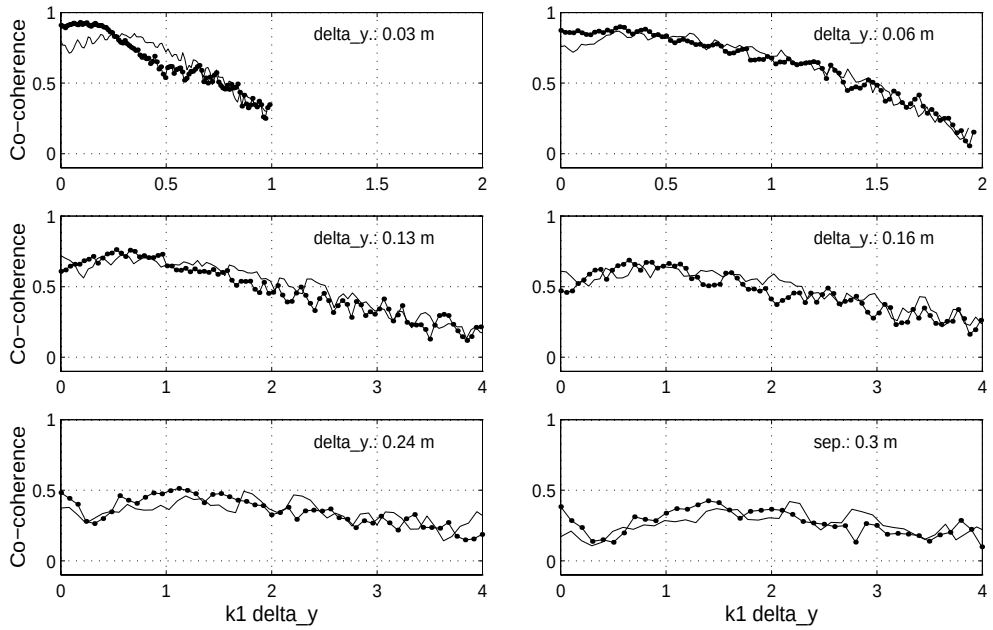

Figure 39: Co-coherence of the lift forces for the with railings (dotted line) and without railings (solid line) configurations, $B/D = 5$, grid exposure.

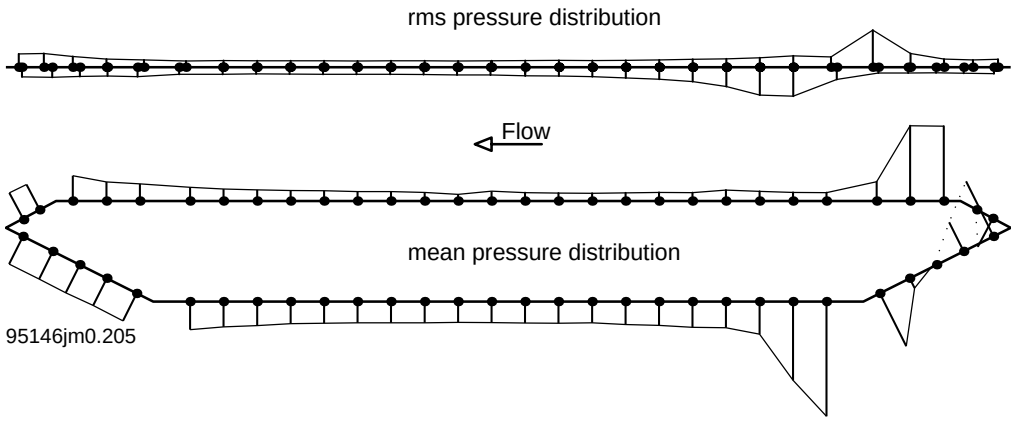

Figure 40: Surface pressure distribution on B/D= 10, smooth flow, without railings, 9 ms^{-1}. Scaling: depth of deck= mean C_p of 1 and rms C_p of 0.5. Polarity: negative away from the surface. The rms distribution is given for the projected tributary area.

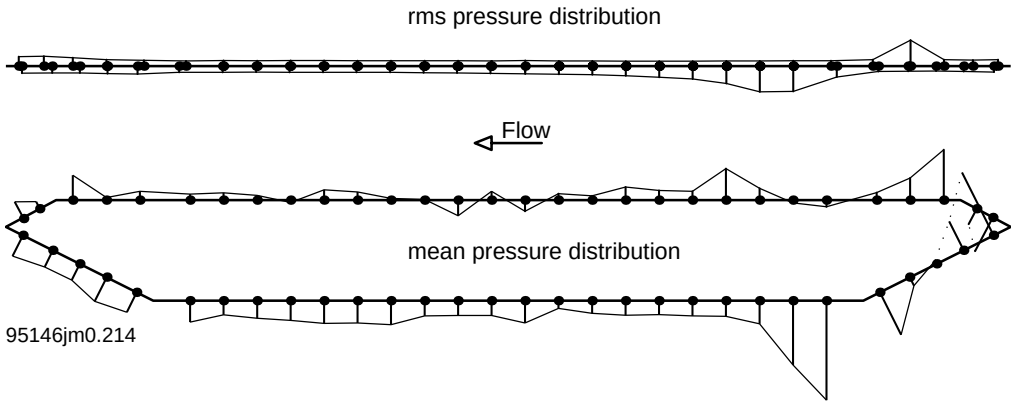

Figure 41: Surface pressure distribution on B/D= 10, smooth flow, with railings, 9 ms^{-1}. Scaling: depth of deck= mean C_p of 1 and rms C_p of 0.5. Polarity: negative away from the surface.

4.2.5 Influence of the angle of wind incidence

The angle of wind incidence was also chosen as a test parameter. The tests were performed by systematically changing the angle of attack of the motionless section models for the medium spire exposure. The range of angle covered was limited between -2° and +2° (positive nose up).

In general, the positive angles of wind incidence gave rise to larger span-wise co-coherence, the separation bubble behing elongated on the top surface. As observed earlier the larger co-coherence was compensated for by smaller aerodynamic forces on a cross-sectional strip. However, in opposition to the observations made during the study of the influence of the railings, a larger influence was found for the larger deck widths. In fact, for the B/D=5 case, no real difference were observed in the co-coherence curves for the angles tested.

Fig. 42 to Fig. 44 summarise the influence of the angle of wind incidence.

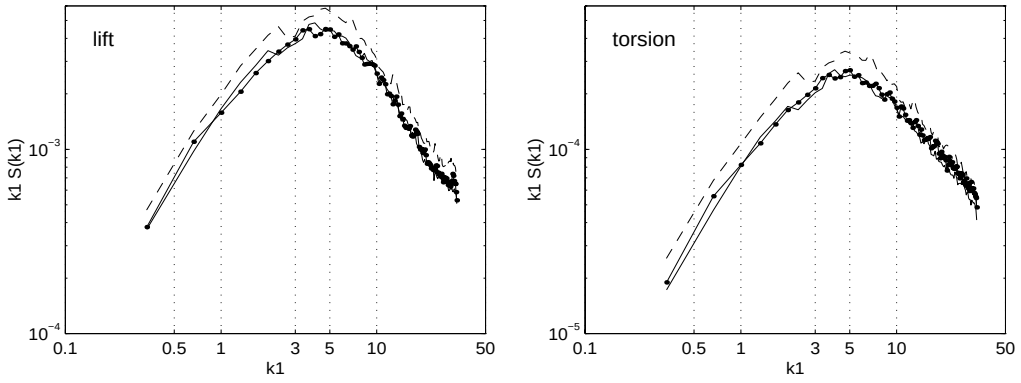

Figure 42: Power spectral density of $C_{z,m}$ versus k_1 for the medium spire exposure and B/D = 12.67, for three angles of wind incidence. Solid line: 0°; dotted line: +2°; dashed line: -2°.

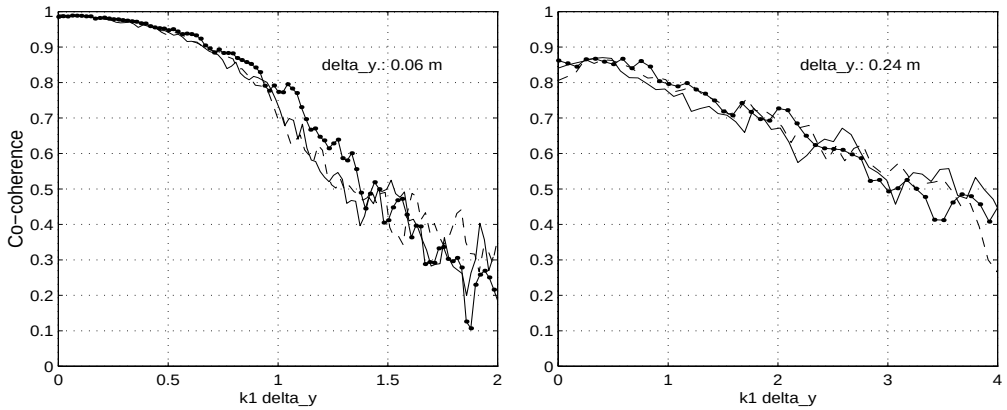

Figure 43: Comparisons of the co-coherence of the lift forces for three angles of wind incidence, for $B/D = 12.67$ with railings, medium spire exposure. Solid line: 0°; dotted line: +2°; dashed line: -2°.

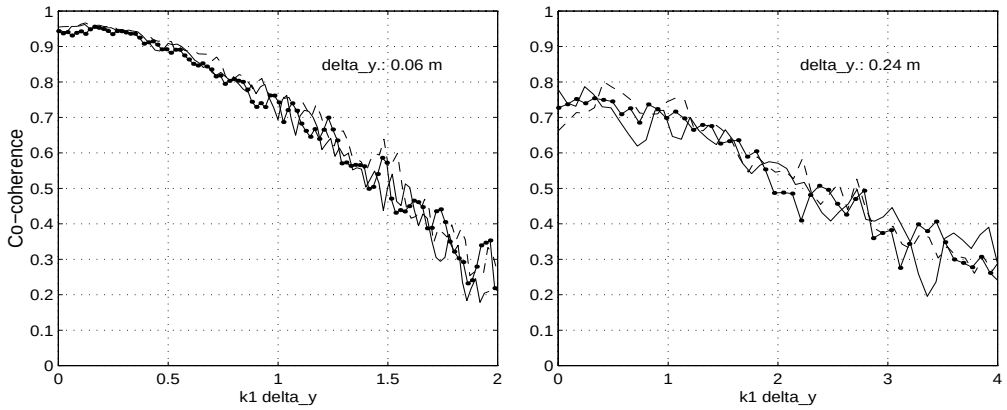

Figure 44: Comparisons of the co-coherence of the lift forces for three angles of wind incidence, for $B/D = 5$ with railings, medium spire exposure. Solid line: 0°; dotted line: +2°; dashed line: -2°.

5 Concluding remarks

A clear link between the aerodynamic admittance and the span-wise co-coherence of the forces was observed. For example, an observed deficit of lift for a given chord-wise strip expressed by a low cross-sectional admittance was compensated for by an increase in span-wise co-coherence of the forces between the neighbouring strips. Probably the parts of the waves of incident flow that do not affect a given strip will however affect the unsteady character of the forces next to that strip span-wise. It appeared that this process was strongly influenced by the $\mathcal{L}_w/B$ and by the deck width itself, the wider the deck, the larger the co-coherence due to an increased rate of formation of secondary cross-flow.

The application of the strip assumption for the deck cross-sections studied has therefore some limitations, even though the simulated $\mathcal{L}_w/B$ ratio was representative of full-scale conditions. The three-dimensionality of the flow, and of the buffeting wind loading, thus plays an important role. A 3-D empirical model describing the spatial distribution of the gust loading on bridge decks is then necessary. This is the object of Part II-B of this research.

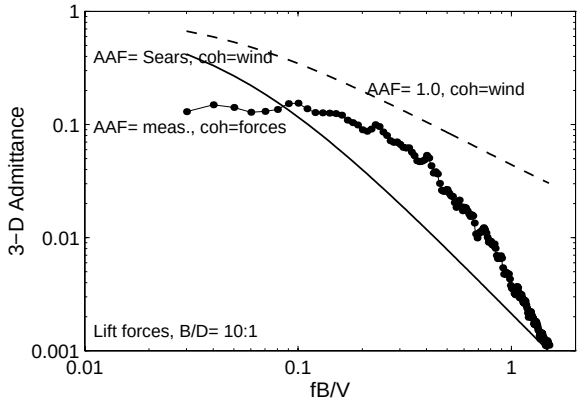

fB/V	Error margin of 3−D AAF (calc.−meas.)/meas.	
	AAF=Sears	AAF=1
0.04	+122 %	+300 %
0.08	+15 %	+200 %
0.1	−25 %	+124 %
0.2	−55 %	+120 %
0.3	−70 %	+105 %
0.4	−78 %	+97 %
0.8	−65 %	+500 %

Figure 45: Comparisons between theory (solid and dashed lines) and direct measurements (dotted line) of the aerodynamic admittance of a span (3-D admittance: AAF x JAF) for a bridge deck with a uniform mode shape.

Error margin related to the strip assumption Fig. 45 compares analytical predictions based on the strip assumption to direct measurements of the lift forces for $B/D = 10$. The quantity compared is the product of the cross-sectional admittance (AAF) and the results of integration across the span of the co-coherence of the wind velocity or the lift forces. This product defines the aerodynamic admittance

of a span (or a 3-D admittance).

Calculations of the 3-D admittance were made for three cases: i) where quasi-steady aerodynamics is assumed ($AAF = 1.0$); ii) where AAF is represented by Sears function; and, iii) where direct measurements of AAF and co-coherence of the lift forces are used. Cases i) and ii) are based on the strip assumption. Fig. 45 reports the error margin of the calculations. The error margin is not negligible, and for the range of fB/V of interest the strip assumption can lead to underestimation of the wind loading.

Acknowledgements

The financial support of the COWIfoundation for the experimental part of this research is gratefully acknowledged.

References

[1] Larose G.L.,"The span-wise coherence of wind forces on streamlined bridge decks", in *Proc. of 3rd Int'l Colloquium on Bluff Body Aerodynamics and Applications*, Blacksburg, Virginia, USA, July 1996.

[2] Davenport, A.G., King, J.P.C, and Larose, G.L. "Taut strip model tests", in *Proc. of Int'l Symposium on Aerodynamics of Large Bridges*, Copenhagen, Feb. 1992, 113-124.

[3] Larose G.L.,*The Response of a Suspension Bridge Deck to Turbulent Wind: The Taut Strip Model approach*, M. E. Sc. Thesis, University of Western Ontario, Canada, March 1992.

[4] Roberts J.B. and Surry D., "Coherence of grid generated Turbulence", *J. Engineering Mechanics*, ASCE, **99**, No. EM6, Dec. 1973, 1227-1245.

[5] Mann J., "The spatial structure of neutral atmospheric surface-layer turbulence",*J. Fluid Mech.* (1994), **273**, 141-168.

[6] Mann J., Kristensen L. and Courtney M.S., *The Great Belt Coherence Experiment - A study of atmospheric turbulence over water*, Risø Report No. R-596, 1991, 51 p.

[7] Dennis J.E. and Woods D.J. *New Computing Environments: Microcomputers in Large-Scale Computing*, A. Wouk (editor), SIAM, 1987, 116-122.

[8] Irwin H.P.A.H., *Wind Tunnel and Analytical Investigations of the Response of Lions' Gate Bridge To Turbulent Wind*, National Research Council of Canada, NAE LTR-LA-210, June 1977, 62 p.

[9] Engineering Sciences Data Unit, *Characteristics of Atmospheric Turbulence Near The Ground, Part III: variations in space and time for strong winds*, Data Item 86010, October 1986.

[10] Fichtl G.H. and McVehil G.E., "Longitudinal and lateral spectra of turbulence in the atmospheric boundary layer at the Kennedy Space Center", *J. Applied Meteorology* (1970), **9**, 51-63.

[11] Fung Y.C., *An Introduction to the Theory of Aeroelasticity*, Dover Publications Inc., N.Y., 1969.

Appendix A Photographs of the experimental set-up

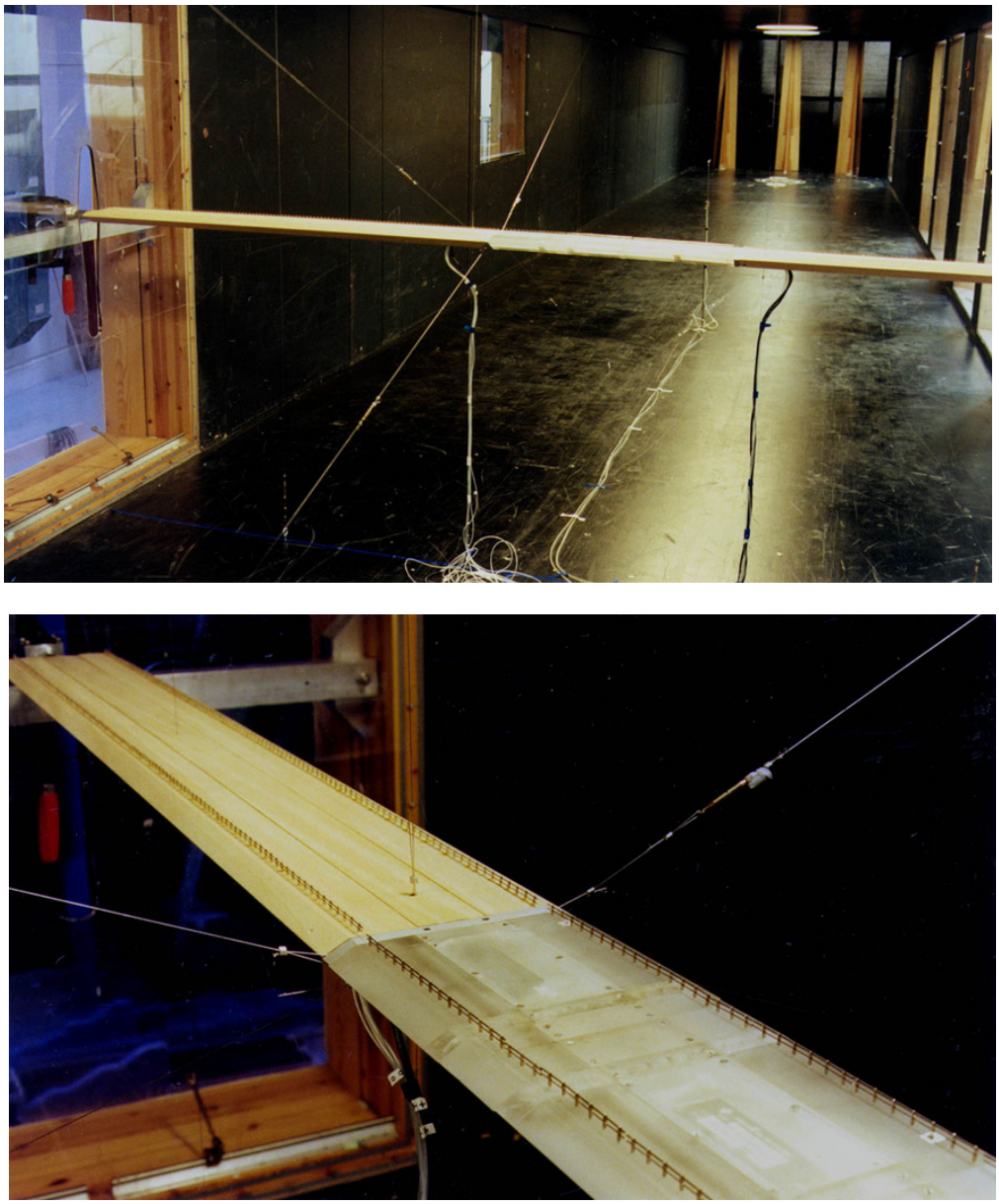

Figure 48: Views of the B/D=5 section model in DMI's Wind Tunnel II.

.

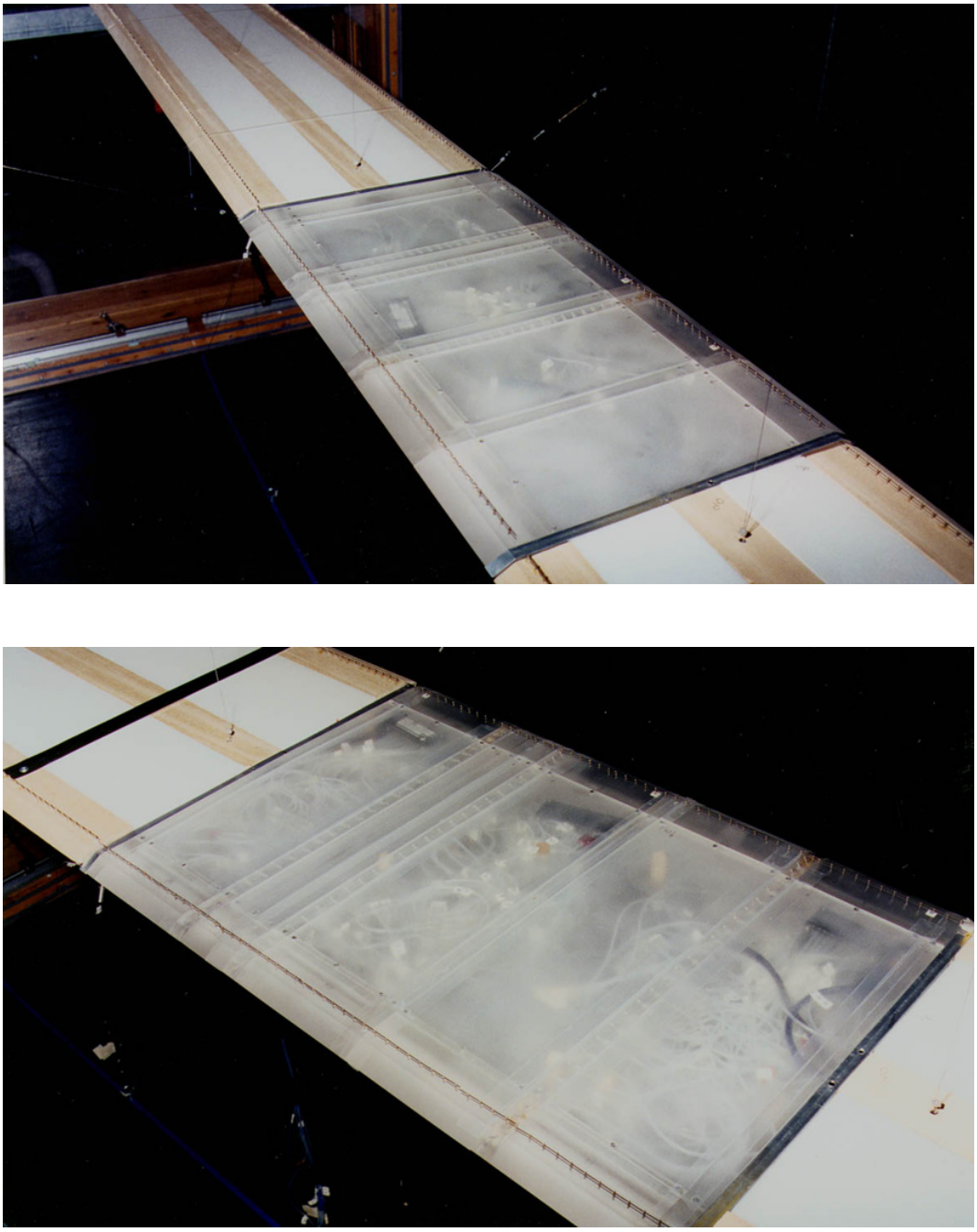

Figure 49: Views of the B/D=10 (top) and B/D=12.67 section models.

.

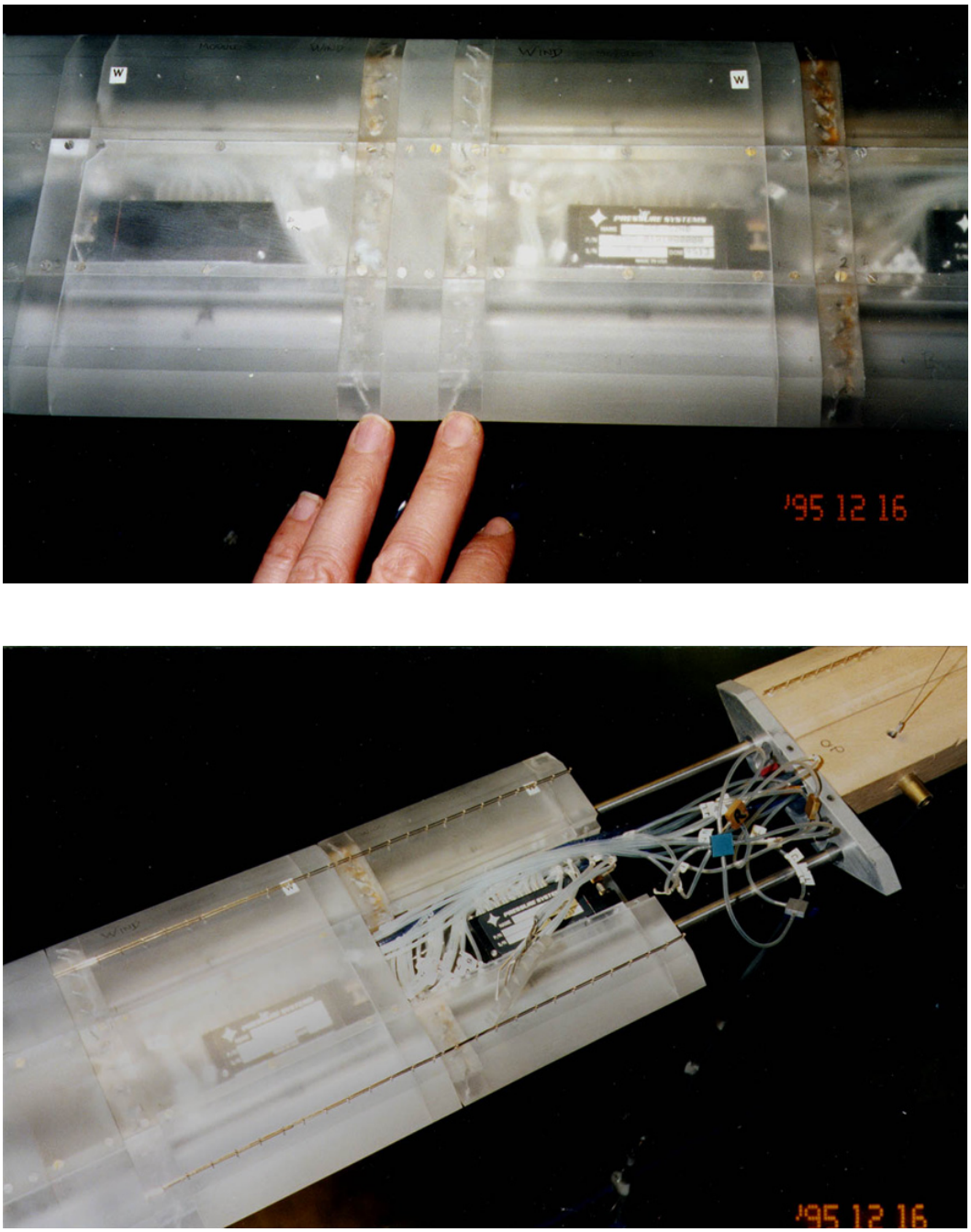

Figure 50: Details of the centre portion of the B/D=5 section model.

.

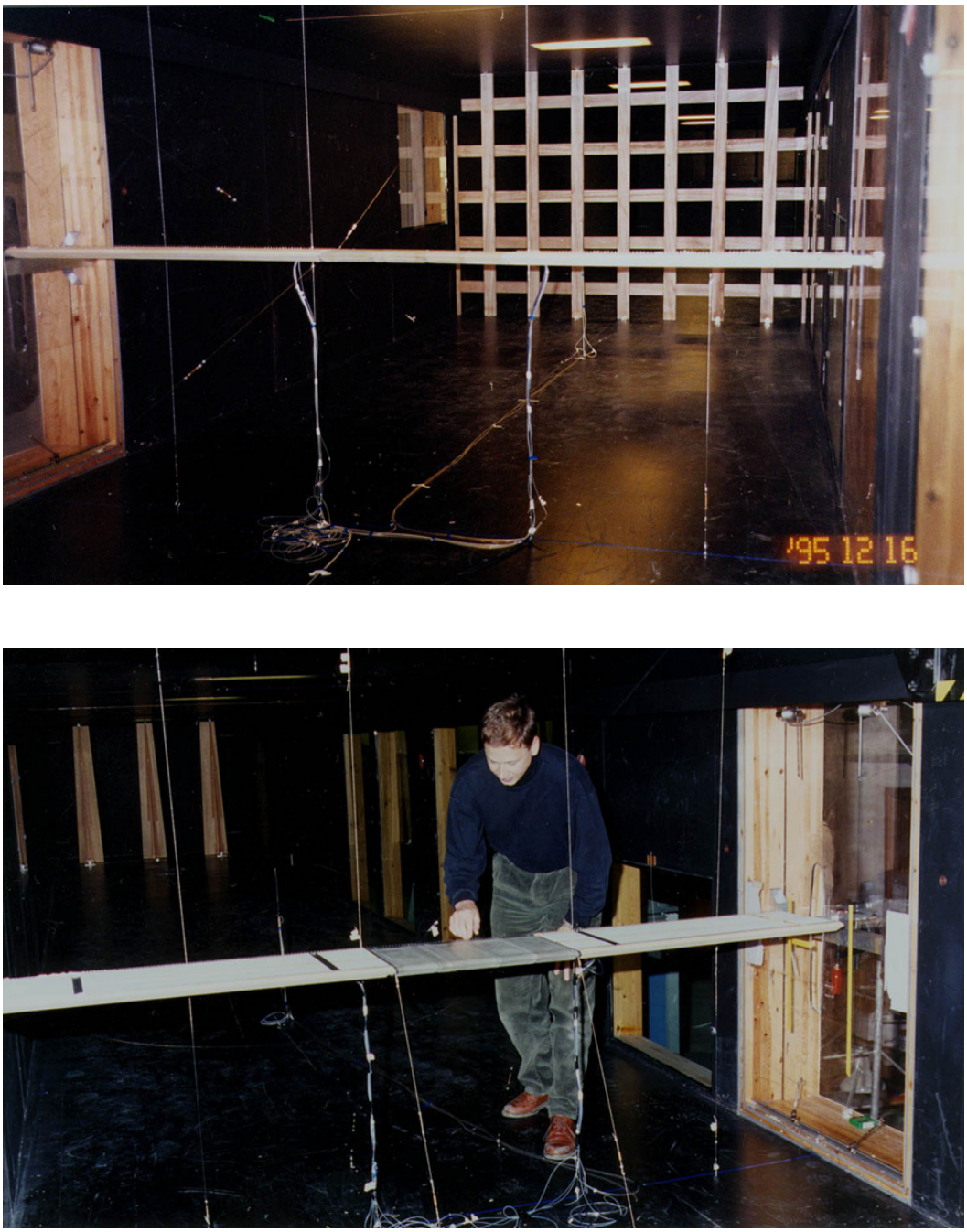

Figure 51: View of the grid exposure (top) and the large spire exposure.

.

Part II
Experiments and Analysis

Part II-B
Gust loading on streamlined bridge decks

GUY L. LAROSE[a,b] and JAKOB MANN[c]

[a] *Department of Structural Engineering and Materials, Technical University of Denmark, 2800 Lyngby, Denmark*
[b] *Danish Maritime Institute, Hjortekærsvej 99, 2800 Lyngby, Denmark*
[c] *Risoe National Laboratory, 4000 Roskilde, Denmark*

(Published in *J. of Fluids and Structures* 1998 **12**, 511-536)

Abstract

The current analytical description of the buffeting action of wind on long-span bridges is based on the strip assumption. However, recent experiments on closed box girder bridge decks have shown that this assumption is not valid and is the source of an important part of the error margin of the analytical prediction methods. In this paper, an analytical model that departs from the strip assumption is used to describe the gust loading on a thin airfoil. A parallel is drawn between the analytical model and direct measurements of gust loading on motionless closed box girder bridge decks. Empirical models of aerodynamic admittance and span-wise coherence of the aerodynamic forces are proposed for a family of deck cross-sections.

1 Introduction

In the theory of buffeting of slender line-like structures, Davenport clearly stated the assumptions made as well as the limitations of the theory. One assumption concerns the size of the structure in relation to the size of the gusts [1]:

...that the structures (or structural members) are sufficiently slender for the secondary span-wise flow and redistribution of pressures to be neglected, such that the pressures on any section of the span are only due to the wind incident on that section; ...

This referred to the strip assumption which was also used by Liepmann as a solution to the buffeting problem of aircraft wings [2]. Davenport commented that this assumption seemed reasonable for a thin cable or an open lattice truss but was not likely to be valid for structure with larger aspect ratio such as buildings [1].

Experience has shown that this assumption appeared to be valid for the case of buffeting drag forces on slender structures where the characteristic length of the body could be more than 100 times smaller than the scales of the longitudinal components of the turbulence ($\approx$ 100 - 200 m) [3]. However for the buffeting lift forces, where the characteristic length of the structure can be the width of a closed-box girder bridge deck, $\approx$ 20-35 m, and the length scales of the vertical gusts could be of the order of $\approx$ 30-50 m, the assumption failed as originally expected by Davenport.

The non-validity of the strip assumption for the lift and torsion buffeting analysis has been shown experimentally in many occasions, firstly by Nettleton on an airfoil in grid turbulence [4], than by Melbourne in full scale and model scale on the West Gate Bridge [5] and more recently by Larose [6, 7], Sankaran et al. [8], Kimura et al. [9], and Bugonovic Jakobsen [10]. Larose et al. [11] (see also Part II-A) evaluated the error margin of the variance of the buffeting response associated with the use of the strip assumption. For lift, it varied between a 70 % underestimation for a reduced velocity of 2 to a 100% overestimation for a reduced velocity of 20.

The strip assumption is nevertheless at the base of the current buffeting theory of line-like structures, both for the frequency domain and time domain approaches.

The objective is this paper is to propose the use of a model of the buffeting wind loads on closed-box girder bridge decks that departs from the strip assumption and reduces the error margin of the analytical prediction methods.

2 Theory: lift force induced by turbulence

In this section the simplest analytical model of the lift forces induced by the gustiness of the wind acting on a motionless bridge deck is discussed. Only the vertical gusts (w component of the wind fluctuations) are considered and it is assumed that the deck cross-section is slender enough to have aerodynamic characteristics similar to a thin airfoil (flat plate).

The two main assumptions that were put forward to bring an approximate solution to the problem are: i) quasi-steady aerodynamics and ii) the strip assumption. The quasi-steady assumption implies that the lift force at a position y at the time

t on a bridge deck is equal to the force that would have been if the instantaneous velocity $w(t, y)$ persisted for an infinitely long time everywhere on the deck.

Under the strip assumption the lift force (per unit length) on a strip at a position y along the bridge deck is equal to the lift force per unit length that would have been if the wind fluctuations had been fully correlated along the deck. The forces on a strip are thus assumed to be induced by the gust acting on that strip only without considering the gusts on the neighbouring strips.

For an airfoil, the applicability of Sears' analysis of the unsteady lift forces induced by a transversally fully coherent sinusoidal gust [7] is based on the strip assumption.

2.1 Quasi-steady aerodynamics

For a flat plate with a lift slope C_z' of 2π, the quasi-steady assumption implies

$$F_z(x, y) = 2\pi w(x, y), \tag{1}$$

where the lift F_z has been normalized suitably and instead of t the coordinate in the flow direction, $x = \bar{V}t$ is used ($\bar{V}$ is the mean wind speed, see Fig. 1). The covariance function of the lift force is defined, assuming $\langle F_z \rangle = 0$, as

$$R_L(x, y) = \langle F_z(x', y') F_z(x' + x, y' + y) \rangle, \tag{2}$$

where $\langle\ \rangle$ denotes ensemble averaging. The one- and two-dimensional spectra of the lift force are defined as

$$S_L(k_1) = \frac{1}{2\pi} \int_{-\infty}^{\infty} R_L(x, 0) \exp(-\mathrm{i}k_1 x)\, \mathrm{d}x \tag{3}$$

and

$$S_L(k_1, k_2) = \frac{1}{(2\pi)^2} \int_{-\infty}^{\infty} \int_{-\infty}^{\infty} R_L(x, y) \exp(-\mathrm{i}(k_1 x + k_2 y))\, \mathrm{d}x\, \mathrm{d}y, \tag{4}$$

and similarly for the vertical wind speed w.

Fourier transforming the covariance function of both sides of (1) in the x- and y-directions, the two-dimensional lift force spectrum is obtained:

$$S_L(k_1, k_2) = 4\pi^2 S_w(k_1, k_2). \tag{5}$$

Equation (5) can be reduced to a one-dimensional force spectrum by:

$$S_L(k_1) = \int_{-\infty}^{\infty} S_L(k_1, k_2)\, \mathrm{d}k_2 \tag{6}$$

$$= 4\pi^2 S_w(k_1). \tag{7}$$

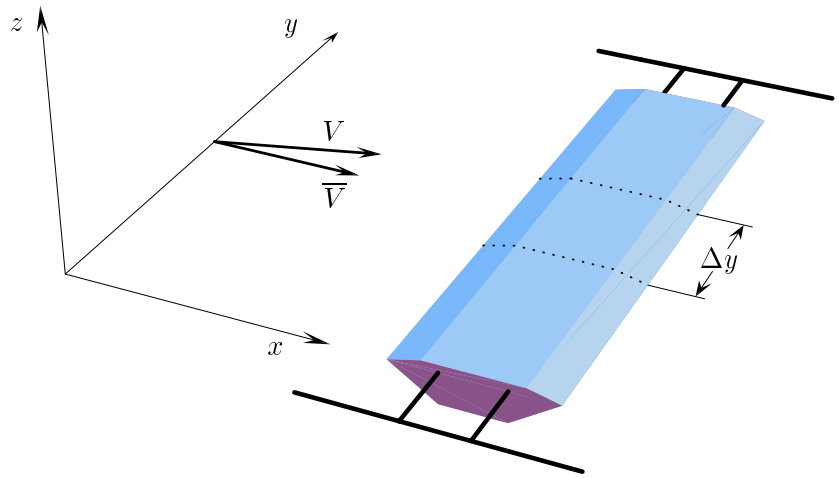

Figure 1: The coordinate system has the x-axis in the direction of the mean wind $\overline{V}$, y along the bridge deck, and z perpendicular to the two other axes. V is an instantaneous wind velocity deviating randomly from $\overline{V}$ and Δy is the separation between strips equipped with pressure transducers.

The cross-spectrum of the lift forces between strips at point 1 and point 2 separated by Δy, $S_{L_1L_2}(k_1, \Delta y)$ [1] can also be derived from the two-dimensional spectrum:

$$S_{L_1L_2}(k_1, \Delta y) = \int_{-\infty}^{\infty} S_L(k_1, k_2) \mathrm{e}^{\mathrm{i}k_2 \Delta y} \mathrm{d}k_2 \tag{8}$$

The span-wise root coherence of the lift forces, $\mathrm{coh}_L^{1/2}$, is obtained by dividing

[1] Note that the symbol S_L has several different meanings: $S_L(k_1)$ is the force spectrum measured on one strip of the infinitely long airfoil, $S_{L_1L_2}(k_1, \Delta y)$ is the cross-spectrum calculated from measurement at two strips separated by Δy, and $S_L(k_1, k_2)$ is the two-dimensional force spectrum. This could, in principle, be evaluated by measuring forces at any point along the foil and in time, and Fourier transforming both in t and y.

the cross-spectrum by the one-dimensional force spectrum:

$$\mathrm{coh}_L^{1/2}(k_1, \Delta y) \equiv \frac{S_{L_1 L_2}(k_1, \Delta y)}{S_L(k_1)}. \tag{9}$$

2.2 Introducing unsteadiness

Faced with the problem of the unsteady nature of the lift forces due to wind gusts, Sears investigated the forces on an airfoil due to a special vertical velocity spectrum (in [7]):

$$S_w(k_1, k_2) = S_w(k_1)\delta(k_2) \tag{10}$$

where δ is Dirac's delta function, that is, gusts with sinusoidal variations of w only in the direction of the mean flow (x) and no variations in the y direction or or fully correlated gusts.

Sears found from the linearized equations of fluid motion and the Kutta-Joukowski condition (no singularities at the rear end of the airfoil) that:

$$S_L(k_1) = 4\pi^2 |\phi(\tilde{k}_1)|^2 S_w(k_1) \tag{11}$$

where $\tilde{k}_1 = k_1\, B/2$, B is the deck width (or the chord of the airfoil) and,

$$|\phi(\tilde{k}_1)|^2 = \left| \frac{J_0(\tilde{k}_1)\, K_1(i\tilde{k}_1) + i J_1(\tilde{k}_1) K_0(i\tilde{k}_1)}{K_1(i\tilde{k}_1) + K_0(i\tilde{k}_1)} \right|^2 \qquad \text{(Sears' function)}. \tag{12}$$

J_0, J_1 are Bessel functions and K_0, K_1 are modified Bessel functions of the second kind.

An approximation to Sears' function was proposed by Liepmann and is of the form:

$$|\phi(\tilde{k}_1)|^2 \approx \frac{1}{1 + 2\pi\tilde{k}_1} \qquad \text{(Liepmann's approximation)}. \tag{13}$$

With (11) and (13), it is clear that the lift forces reduce as k_1 increases. The unsteady forces are also smaller that one would expect if quasi-steady conditions were applicable. Sears demonstrated that for any variation of the wavenumber above 0, (i.e. for any flow fluctuation with a finite wavelength) the fluctuating lift will be less than the quasi-steady value.

This reduction of lift with wavenumber is generally represented by the aerodynamic admittance. It can be seen as a measure of the effectivness of a body in extracting energy from the various frequency components of the turbulence.

The aerodynamic admittance can be defined as:

$$A(k_1) = \frac{S_L(k_1)}{C_z'^2 S_w(k_1)}. \tag{14}$$

Based on this definition and on (7), $A(k_1) = 1.0$ for the quasi-steady case. For a thin airfoil in a fully correlated gust (which is equivalent to the strip assumption):

$$A(k_1) = |\phi(\tilde{k}_1)|^2. \tag{15}$$

Applying the strip assumption it is also possible to calculate the span-wise coherence of the forces:

$$\mathrm{coh}_L^{1/2}(k_1, \Delta y) = \mathrm{coh}_w^{1/2}(k_1, \Delta y). \tag{16}$$

Sears' function (or Liepmann's approximation to Sears' function) is often used in bridge aerodynamics to represent the aerodynamic admittance. It tends to 1.0 for $f \to 0$. Experiments in turbulent flow on section models of streamlined bridge decks have shown that the admittance tends to be lower than (12) for low frequencies and, if the bridge deck is bluff, higher at high frequencies [6]. Furthermore, the span-wise coherence of the lift forces was found to be much higher than for w in clear contrast to (16) [7, 9, 10].

2.3 Lifting the strip assumption

The natural extension to Sears' analysis is due to Graham [13] from an original suggestion by Ribner [14]. Ribner proposed in 1957, as an alternative approach to the strip assumption method, to calculate the unsteady lift for an incident flow field represented by a superposition of plane sinusoidal wave motions of all orientations and wavelengths (equivalent to $S_w(k_1, k_2)$). This required a two-wavenumber aerodynamic admittance.

Graham [13] numerically computed the exact two-wavenumber aerodynamic admittance using lifting-surface theory for an airfoil of infinite span length due to gusts with arbitrary horizontal wavevectors (k_1, k_2). In his derivation, Graham used the same linear assumption as in Sears' analysis but worked with yawed sinusoidal gusts that could vary in y as well as in x. That is to say that a chord-wise strip could be partially immersed in a gust oncoming from a certain horizontal direction but also be influenced by a gust from a different direction. This is departing from the strip assumption and it is a better representation of the physics of incident gusts being distorted and diverted as they approach the body. An experimental validation of Graham's approach is presented by Jackson *et al.* [14].

The two-wavenumber spectrum of the lift forces becomes:

$$S_L(k_1, k_2) = 4\pi^2 |\phi(\tilde{k}_1, \tilde{k}_2)|^2 S_w(k_1, k_2) \tag{17}$$

where

$$|\phi(\tilde{k}_1, \tilde{k}_2)|^2 \approx \frac{1}{1 + 2\pi\tilde{k}_1} \left[\frac{\tilde{k}_1^2 + 2/\pi^2}{\tilde{k}_1^2 + \tilde{k}_2^2 + 2/\pi^2} \right] \quad \text{(Mugridge)}. \tag{18}$$

Equation (18) is an approximate closed-form expression due to Mugridge [15] of the aerodynamic admittance. It is presented as a correction factor to the Sears' function. It reduces to (13) for fully coherent gusts (when $\tilde{k}_2 = 0$).

Other approximate closed-form expressions of Graham's exact solution exist, namely by Filotas and by Blake [16], however, Mugridge's approximation is most valid for the lower wavenumber range ($k_1 < 2$) which is the range of interest for bridge aerodynamics.

Application of the two-wavenumber model: Using (17) it can be shown that $A(k_1)$ do not tend to 1.0 as $k_1 \to 0$ [14]. This is in agreement, at least qualitatively with results of experiments on thin airfoils and bridge decks.

The span-wise coherence is linked to the cross-sectional admittance through equations (8) and (9). Mann [17] has calculated the cross-spectrum and the span-wise coherence of the lift forces on a thin airfoil in isotropic turbulence based on (8), (17) and Mugridge's approximation. It resulted that $\mathrm{coh}_L^{1/2} \neq \mathrm{coh}_w^{1/2}$ ($\mathrm{coh}_L^{1/2}$ was found larger) confirming several experimental observations of the non-validity of the strip assumption. Section 3.2 presents similar calculations.

3 Experimental validations

All the quantities of section 2.3 can be measured directly or evaluate indirectly in controlled experiments on section models in a wind tunnel. The validation of the two-wavenumber model (referred to later on as the 3-D model) of the lift force is thus possible.

The ideal case would have been to conduct a series of experiments in isotropic turbulence on a thin airfoil with a lift slope approaching 2π. However, the ultimate objective of this research being the application of the 3-D model to bridge aerodynamics, the experiments were conducted on section models with cross-sectional dimensions and proportions typical of modern closed-box girder bridge decks.

3.1 The experiments

Direct measurements of the buffeting forces on motionless section models in turbulent flow were conducted in the DMI's Boundary Layer Wind Tunnel-II. The dynamic force measurements were based on simultaneous measurements of unsteady surface pressures on three chord-wise strips of the section models, the span-wise separations of the strips being adjustable. The cross-section studied were typical closed-box girder bridge decks as seen on Fig. 2.

The parameters of the experiments were: the width-to-depth ratios B/D of the section models, the length scales of turbulence, the presence or lack of railings and

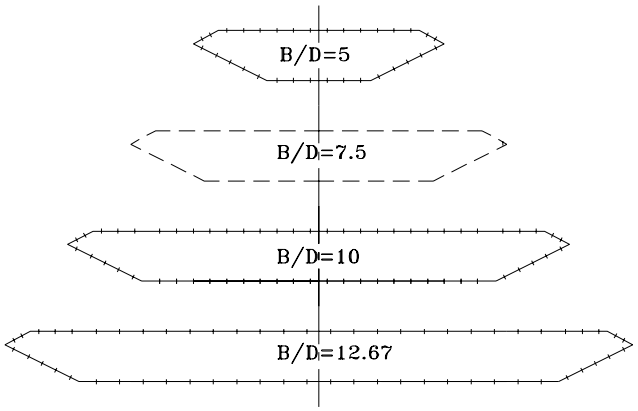

Figure 2: Cross-sectional shape of the models investigated. The $B/D = 7.5$ cross-section was studied in another occasion and the results are reported elsewhere [6].

the influence of the angle of wind incidence. A detailed account of the experiments is given in [11].

For each case, power spectral densities of the lift and torque coefficients were calculated as well as the span-wise coherence of the buffeting forces.

3.1.1 Description of the incident turbulent flow field

Three turbulent wind fields were used in the parametric investigations of the buffeting forces, two generated by spires placed 15 m upstream of the model and one by a coarse grid placed 4.6 m upstream. The two spire sets gave similar length scales of turbulence but different turbulence intensities while the position of the grid was selected to match the turbulence intensity of one of the spire sets but giving much smaller length scales. The spires also gave a slight anisotropy to the flow.

The grid had an isotropic mesh of 0.34 m with a bar size of 0.085 m. The medium spires, in a set of three, were 0.32 m wide at the base, 0.20 m at the top and 1.8 m high, while the large spires were 0.36 m at the base, 0.23 m at the top and 1.72 m high. The tests in the wind tunnel were typically conducted at a mean wind speed of 15 ms^{-1}.

For each wind field the u, v and w components of the wind were fitted with the isotropic turbulence model based on the von Kármán spectrum described by Mann in [18]. The spectral tensor fitted particularly well the span-wise root coherence (or co-coherence) measurements made by hot-wire anemometry.

The one-point spectrum of the w-component was fitted with:

Table 8: Characteristics of flow conditions for the three exposures in relation to the width of the models based on the least square fit of the von Kármán spectrum.

Exposure	w-component				$\mathcal{L}_w/B$		
	I_w (%)	L (m)	$\alpha\epsilon^{\frac{2}{3}}$ $(\frac{m^{\frac{4}{3}}}{s^2})$	$\mathcal{L}_w$ (m)	$B/D = 5$	$B/D = 10$	$B/D = 12.67$
Large spires	8.8	0.43	3.4	0.24	-	0.80	0.63
Medium spires	7.2	0.39	2.1	0.22	1.50	0.73	0.58
Grid	7.6	0.15	5.1	0.09	0.57	0.29	0.23

$$S_w(k_1) = \frac{3}{110}\alpha\epsilon^{\frac{2}{3}}\frac{3L^{-2} + 8k_1^2}{\left(L^{-2} + k_1^2\right)^{\frac{11}{6}}}, \tag{19}$$

where L is a length scale and $\alpha\epsilon^{\frac{2}{3}}$ represents the rate of dissipation of turbulent kinetic energy. Both quantity were obtained by least square fit of the measured spectra. L was converted to $\mathcal{L}$, the wavelength associated with the peak of the spectrum in its $k_1 S_w(k_1)$ representation, using:

$$\mathcal{L}_w \quad = \quad \frac{2}{(6 + 3\sqrt{5})^{\frac{1}{2}}} L \approx 0.561L. \tag{20}$$

$\mathcal{L}$ was prefered to the conventional integral length scale since it represents the wavelength of the gusts that carry most of the energy of the turbulence.

Examples of fits using (19) are shown on Fig. 3. The resulting ratios between the length scales and the deck widths studied, $\mathcal{L}_w/B$, are given in Table 8.

3.1.2 Measured aerodynamic admittance functions

The aerodynamic admittances were calculated based on the experimental determination of the spectrum of the lift coefficient $S_{C_z}(f)$, the lift slope and the spectra of the u and w component of the oncoming wind fluctuations. The following expression was used:

$$|A_z(f)|^2 = \frac{\bar{V}^2\, S_{C_z}(f)}{4\, C_z^2\, S_u(f) + C_z'^2\, S_w(f)} \tag{21}$$

The contribution of the u-component can be considered negligible for the cross-sections studied here, as can be evaluated based on the static coefficients of Table 9.

Selected results of the direct measurements of the aerodynamic admittance are presented in Figs. 4 to 7. Fig. 4 shows the variations of the admittance for a fixed L_w and varying B. On Fig. 5, the admittance curves are given for a constant B while the exposures are varied. It can be observed that the larger the chord-to-depth ratio or the smaller the gusts, the closer are the curves to the linear theory

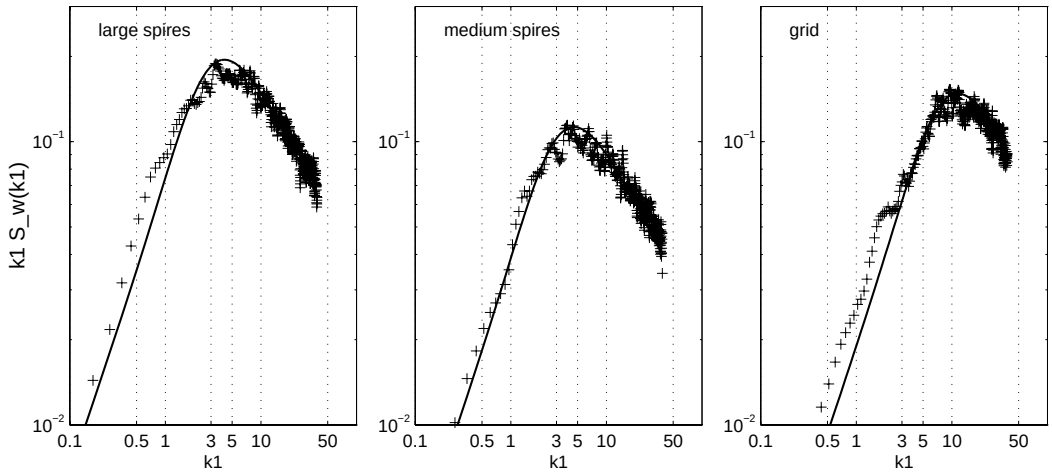

Figure 3: Spectra of the vertical wind fluctuations for the three exposures of this study. Solid line: fit of von Kármán spectrum using (19).

for a thin airfoil (dashed lines on the graphs). This was expected since the linear theory is for a fully attached flow and since the larger the chrod-to-depth ratio, the smaller the separation region in relation to the deck width, approaching fully attached conditions. Also, the smaller the gusts, the smaller the length of the separation bubble which favors re-attachment of the flow.

Fig. 6 shows the variations of the lift aerodynamic admittance for a selection of $\mathcal{L}_w/B$ ratios. The same test cases are presented in Fig. 7 but the ordinate has been multiplied by the square of the lift slope to facilitate the interpretation of the results. All curves were found below the linear theory and an important deficit of lift was found in the low reduced frequency range. Even though the deck cross-section studied had poorer lift characteristics than a thin airfoil, they could generate has much lift than the linear theory predicted at higher reduced frequencies for the same input wind spectrum. The body-induced turbulence is probably the source of the observed larger than anticipated lift.

Table 9: Time averaged aerodynamic force coefficients (based on B) for the medium spire exposure, deck without railings.

B/D	C_z	C_m	C_z'	C_m'
5	-0.154	0.026	4.04	1.03
10	-0.118	0.010	4.62	1.18
12.67	-0.128	-0.004	4.75	1.14

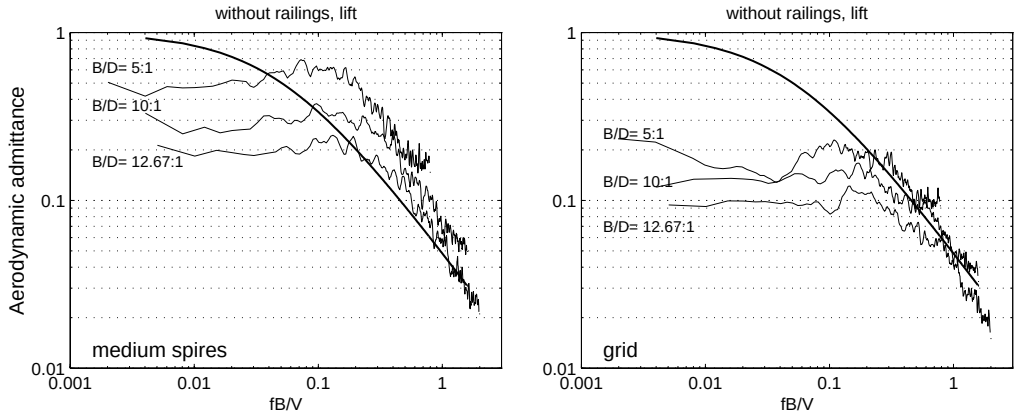

Figure 4: Variations of the aerodynamic admittance with reduced frequency for the medium spire and the grid exposures for three B/D ratios. The thick line is Liepmann's approximation (13) to Sears' function.

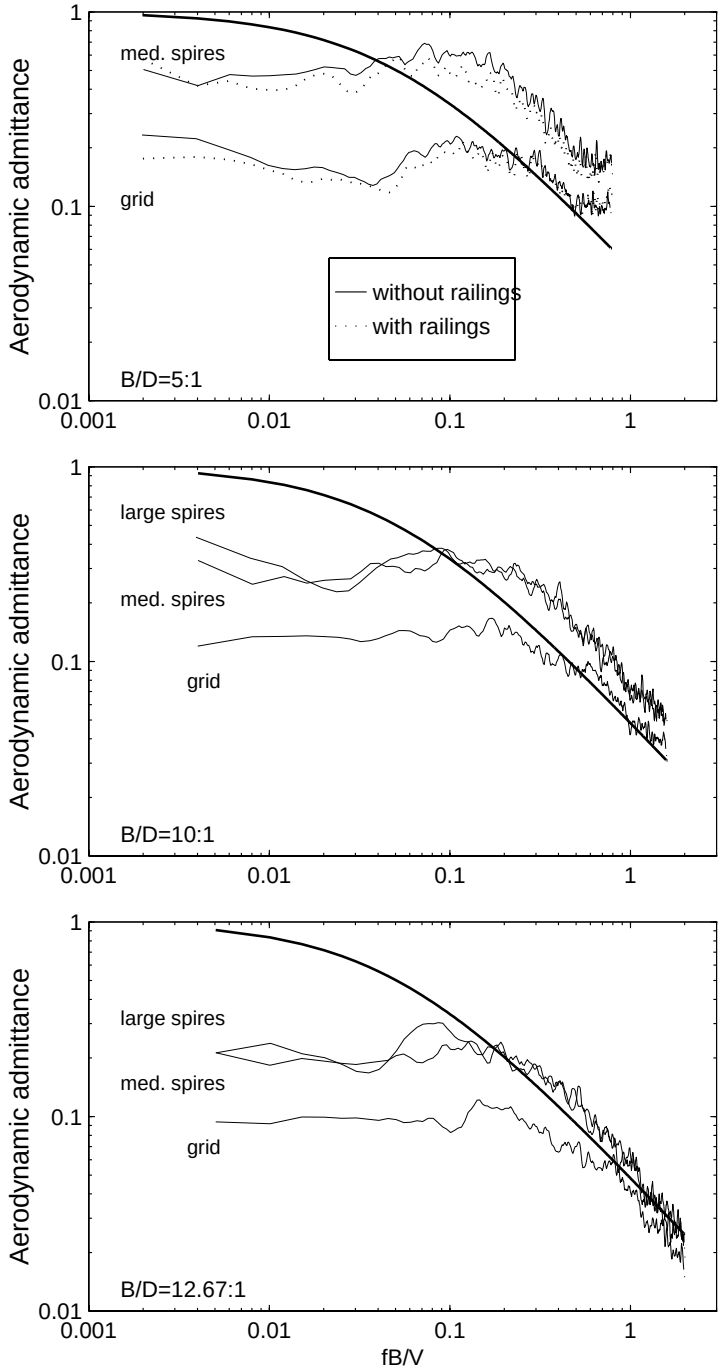

Figure 5: Variations of the lift aerodynamic admittance with reduced frequency for all exposures and all B/D.

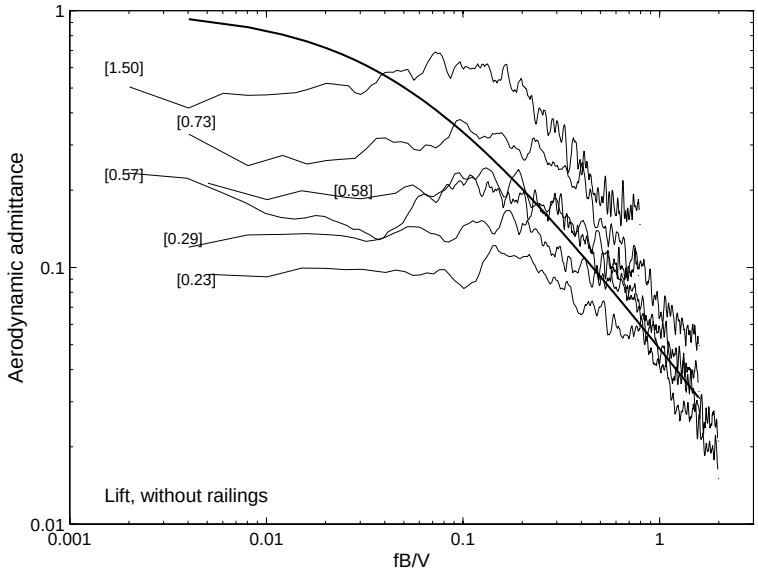

Figure 6: Variations of the vertical aerodynamic admittance with reduced frequency. The numbers in [ ] refer to the $\mathcal{L}_w/B$ ratio.

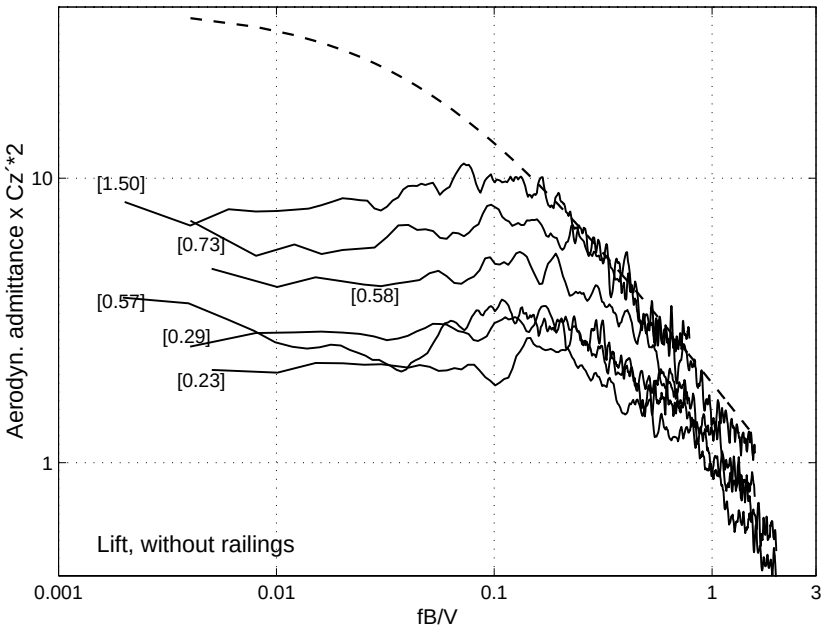

Figure 7: Lift aerodynamic admittance functions for six different $\mathcal{L}_w/B$ ratio. The admittance has been multiplied by $C_z'^2$ to be compared with Liepmann's approximation to Sears' function for a flat plate with a lift slope of 2π (dash line).

3.1.3 Measured span-wise co-coherence of the forces

The experimentally determined span-wise distribution of the lift forces are presented here under the form of co-coherence function or normalized co-spectrum. Co-coherence is the real part of the cross-spectrum of the forces between two strips normalized by the one-point spectrum. The advantage of the co-coherence presentation over the root coherence is that it can show if the forces become negatively correlated for higher frequencies or large separations.

The span-wise co-coherence of the lift forces are presented on Figs. 8 and 9. The test conditions selected are for the medium spire exposure and the $B/D = 5$ and 10 ratios respectively. Also shown on the plots are the variations of the co-coherence of the w component of the wind for the medium spire exposure. The curves shown (solid line) are based on a fit of the measured co-coherence data with the von Kármán spectral tensor for isotropic turbulence described in [18]. The co-coherence of the forces was found larger the the co-coherence of the incident wind.

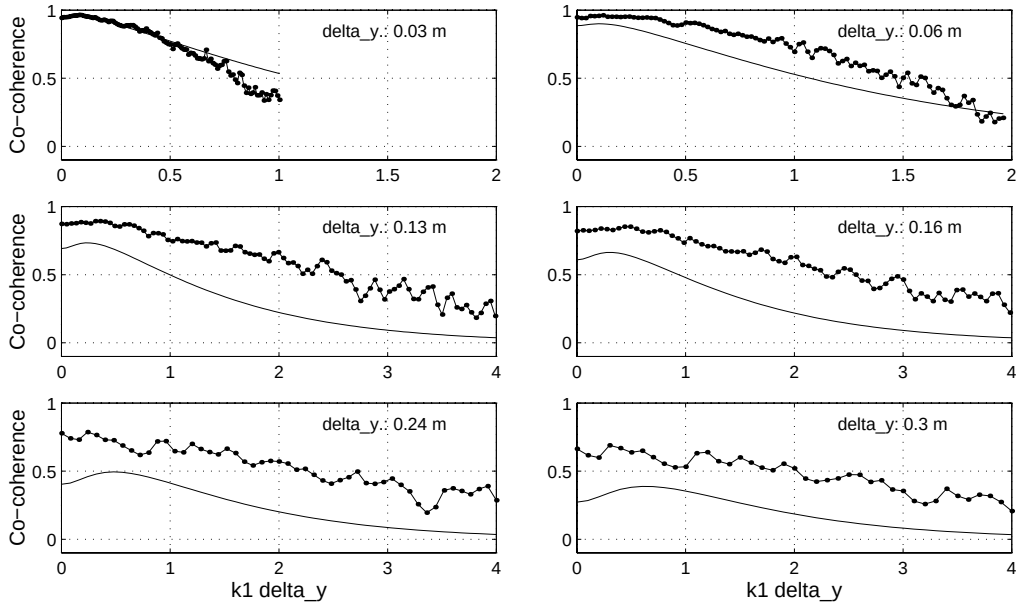

Figure 8: Variations of span-wise co-coherence as a function of $k_1\Delta y$ for the lift forces (dotted line) for $\mathcal{L}_w/B = 1.5$ compared to the wind fluctuations (solid line: w with L= 0.39).

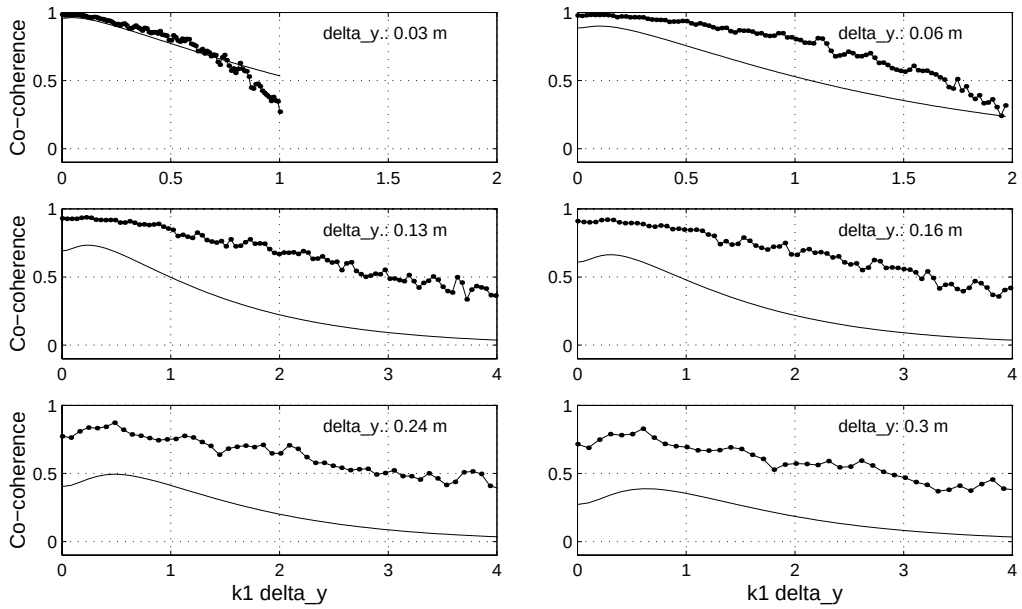

Figure 9: Variations of span-wise co-coherence as a function of $k_1\Delta y$ for the lift forces (dotted line) for $\mathcal{L}_w/B = 0.73$ compared to the wind fluctuations (solid line: w with L= 0.39).

3.2 Applications of the 3-D analytical model

The two-wavenumber spectra $S_w(k_1, k_2)$ modelling the flow fields of the experiments was calculated using the von Kármán isotropic turbulence tensor [18] and the fitted length scales given in Table 8.

Calculations of $\mid A(k_1) \mid$ and $\mathrm{coh}_L^{1/2}(k_1, \Delta y)$ using the 3-D model of Section 2.3 and Mugridge's approximation (18) were made for a series of $\mathcal{L}_w/B$ ratio corresponding to the experimental conditions. The results of the analytical calculations are presented on Figs. 10 and 11.

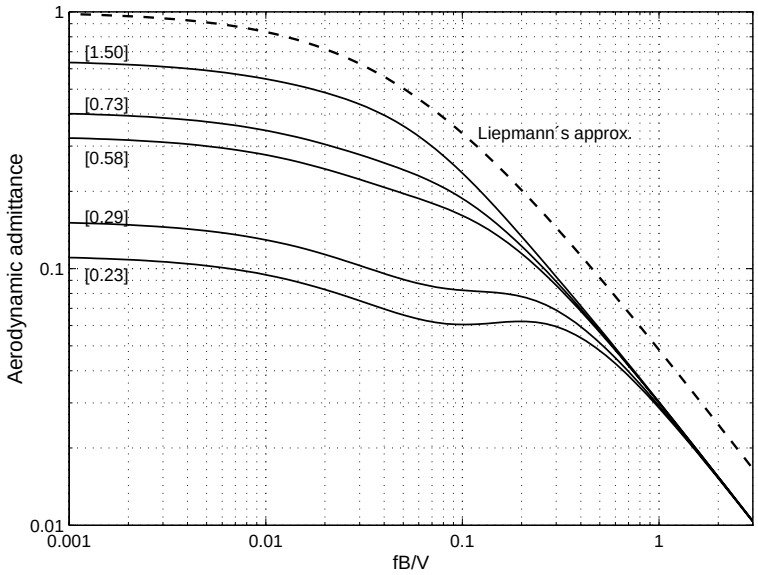

Figure 10: Analytical calculation of the aerodynamic admittance for a thin airfoil using (17) and Mugridge's approximation, for isotropic turbulence with length scale $\mathcal{L}_w$ for different values of B. The numbers in [ ] refer to the $\mathcal{L}_w/B$ ratio.

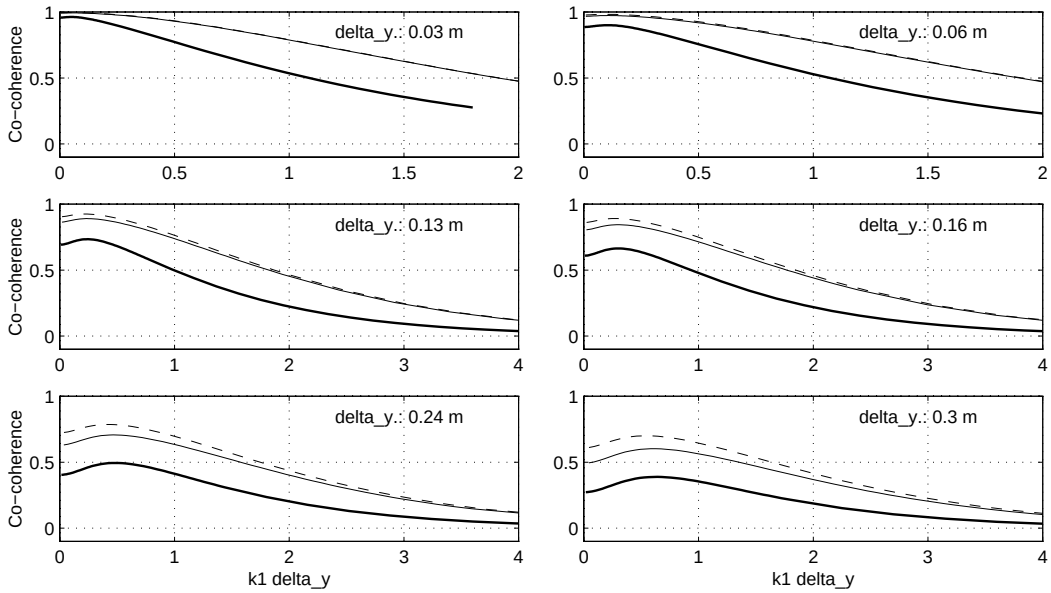

Figure 11: Analytical calculations of span-wise co-coherence of lift forces based on the 3-D model and Mugridge's approximation. Thin line: $\mathcal{L}_w/B = 1.5$; dashed line: $\mathcal{L}_w/B = 0.73$ and thick solid line: w-component of the wind fluctuations using the von Kármán spectral tensor with L=0.39.

3.3 Discussions

A qualitative agreement was observed between the measured admittance and the analytically calculated admittance using the 3-D model. The agreement improves as the width-to-depth ratio increases or as the aerodynamics of the cross-sections approach the aerodynamics of a flat plate. As observed earlier [6], the bluffer the body, the larger the admittance at higher frequency compared to the prediction for a thin airfoil.

Another important qualitative agreement refers to an admittance value different from 1.0 for low reduced frequency. For the larger $\mathcal{L}_w/B$ ratios, the analytical calculations did not give an admittance value larger than 0.62, even at low reduced velocity. Also, calculated and measured admittance curves for low $\mathcal{L}_w/B$ ratio have similar shapes. Going from low frequency to higher frequency the curves have a trough corresponding to the largest value of S_w, then a peak corresponding to the largest value of S_L and finally have a sudden drop with more or less the same slope. This apparent point of inflection in the admittance curves can be observed for cases where the incident vortices are small in comparison to the deck width, resulting in a frequency shift between the peak of the wind spectrum and the peak of lift force spectrum.

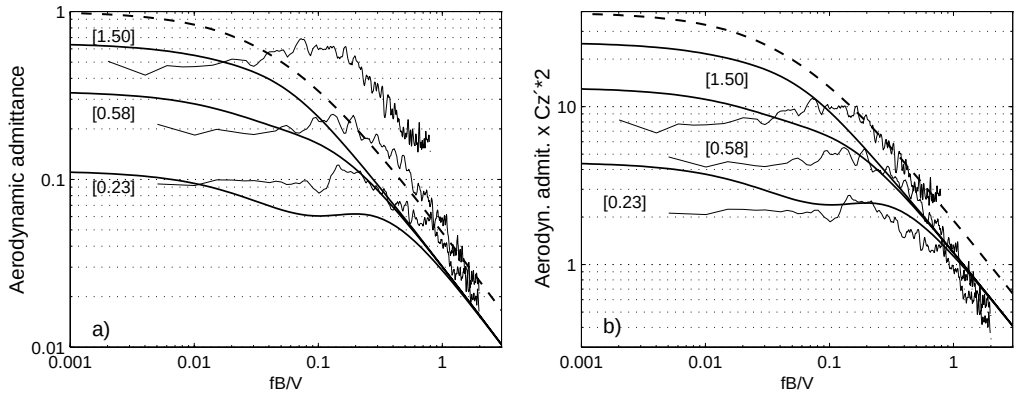

Figure 12: Comparisons between analytical calculations of lift aerodynamic admittance using the 3-D model for a thin airfoil and direct measurements on bridge decks for three $\mathcal{L}_w/B$ ratios. The dashed line is Liepmann's approximation to Sears' function. On **b)** the ordinate has been multiplied by the square of the lift slope.

Figs. 12 and 13 show quantitative comparisons of the analytical calculations and direct measurements of admittance for selected $\mathcal{L}_w/B$ ratios. On Fig. 12 **a)** it can be seen that the analytical calculation approaches the measured admittances at very

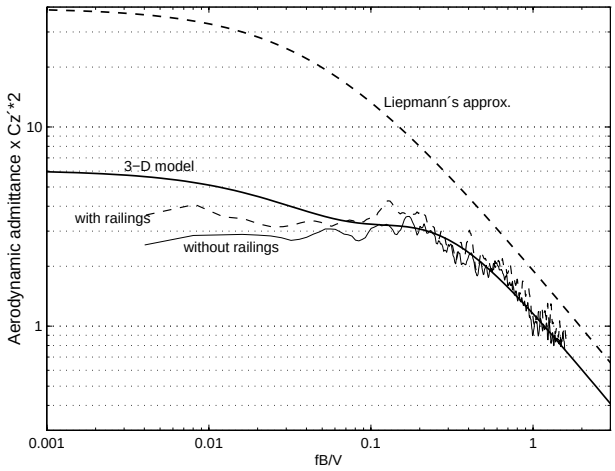

Figure 13: Comparisons between analytical calculation (thick solid line) of lift aerodynamic admittance using the 3-D model for a thin airfoil and direct measurement on a bridge deck with B/D=10 for $\mathcal{L}_w/B = 0.29$. The ordinate has been multiplied by the square of the lift slope.

low reduced frequency. This aspect is positive since it indicates that for quasi-steady conditions, the linear 3-D theory and the experiments are in agreement. It also validates some previously publised measurements of the aerodynamic admittance of bluff bodies that have been disregarded since they did not tend to 1.0 for very low reduced frequency. For higher fB/V, the bridge decks produce body-induced turbulence that increases their admittance characteristics in comparisons with the theory.

Fig. 12 **b)** compares the product of $A_z(f)$ and $C_z'^2$ for the theory and the experiments. It indicates that if the test case approach fully re-attached flow conditions, the bridge deck could generate similar lift than a thin arifoil. This aspect is also illustrated on Fig. 13 where the case with railings, which has shown a smaller separation bubble, has lift characteristics closer to the 3-D theory than the case without railings.

Span-wise co-coherence: Qualitative agreement was also observed between analytical calculations with the 3-D model and direct measurements of the span-wise co-coherence of the forces. Most importantly $coh_L^{1/2}$ was found larger than $coh_w^{1/2}$ confirming earlier observations. The calculations also reinforced the observation reported in [11] that the lower the aerodynamic admittance the larger the span-wise co-coherence confirming the link between the two quantities.

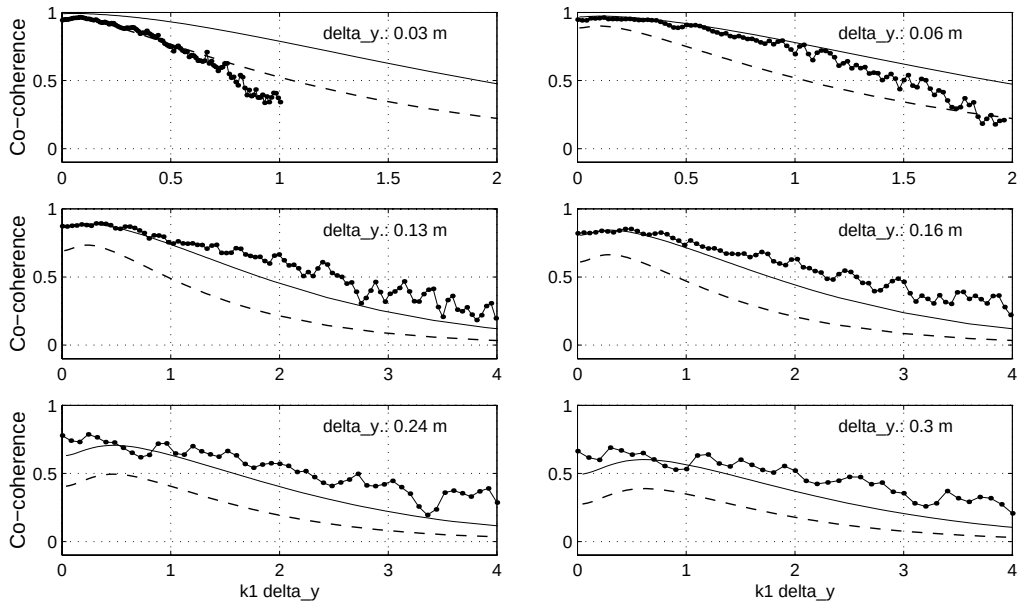

Figure 14: Comparisons between calculations (solid line) and direct measurements (dotted line) of the span-wise co-coherence of the lift forces as a function of $k_1\Delta y$ for $\mathcal{L}_w/B = 1.5$. The dashed line represents the variations of $cocoh_w^{1/2}$ of the incident wind (L=0.39 m).

Direct comparisons between calculations with the 3-D model and experiments are shown on Figs. 14 and 15. The agreement is excellent for the smaller separations in the lower wave number range. For the smallest separation, 0.03 m, the calculation overestimated the co-coherence for all $k_1\Delta y$. In fact, for this case, $cocoh_L \approx cocoh_w$. This observation, for very small separation in comparison to the deck width, was also reported in other studies [6, 9] and can not really be explained by the theory presented here.

It can be observed also by comparing Fig. 14 to Fig. 15, that as $\mathcal{L}_w/B$ reduces or as the influence of the small scale turbulence increases, the 3-D model underestimated the large co-coherence measured at higher wave numbers during the experiments. The flow mechanisms involved in the re-attaching shear layer (as described in Part 1-A) which has shown a tendency to spread span-wise the vortices at high frequencies can explained the difference, since the theory does not take this effect into account. This underestimation however is compensated by a higher aerodynamic admittance obtained from the calculations when compared to the theory.

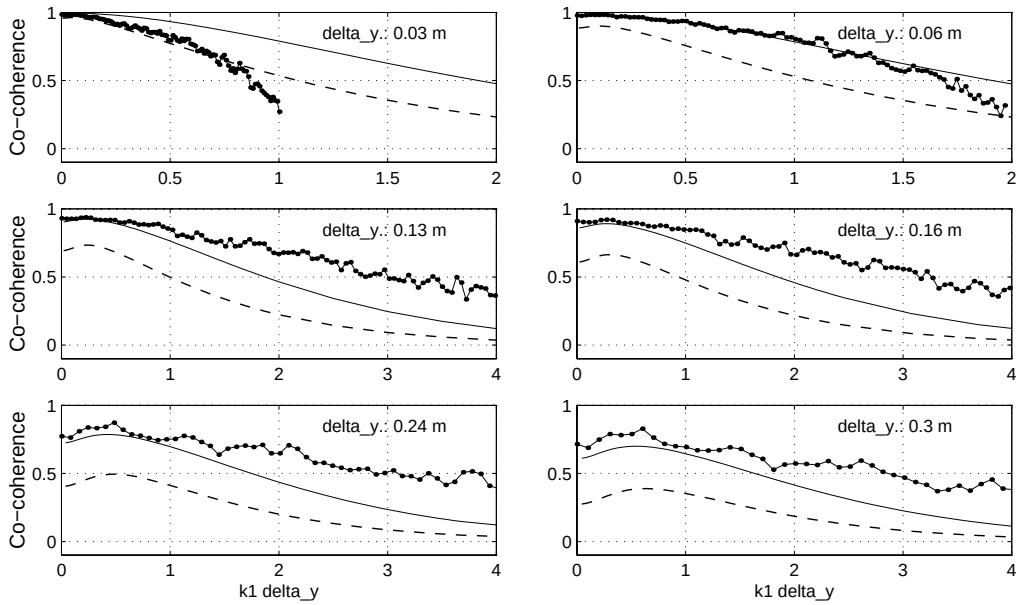

Figure 15: Comparisons between calculations (solid line) and direct measurements (dotted line) of the span-wise co-coherence of the lift forces as a function of $k_1\Delta y$ for $\mathcal{L}_w/B = 0.73$. The dashed line represents the variations of $cocoh_w^{1/2}$ of the incident wind (L=0.39 m).

Pressure distribution: The earlier remark concerning the measurement of larger $A_z(k_1)$ than calculations for the higher frequencies for the bluffer bridge deck can partly be explained by inspection of the unsteady pressure distribution.

Figs. 16 and 17 present mean and rms pressure distribution for the medium spire exposure for $B/D = 5$ and $B/D = 10$ cases respectively. The pressure fluctuations for the 10:1 case are concentrated near the leading edge while the fluctuations for the 5:1 case are extended more downstream, almost up to mid-chord. The latter represent probably a shedding zone of vortices at or just after the reattachment point. These vortices will later on mix with the wake and influence the formation of lift. It is the zone of formation of what has been called the *signature turbulence* or the body-induced turbulence. For the 10:1 case, body-induced turbulence is also present but it is believed that it does not mix in the same manner with the wake since the convection length and the velocity is greater. The vortices are likely to be distorted by the mean velocity field enveloping the body following the rapid distortion theory. The rms pressure distribution for the 10:1 and 12.67:1 models approaches the pressure distribution for the thin airfoil case.

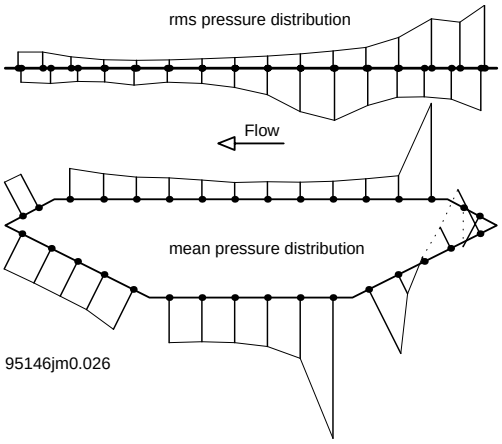

Figure 16: Surface pressure distribution on B/D= 5, medium spire case, without railings, 15 ms^{-1}. Scaling: depth of deck= mean C_p of 1 and rms C_p of 0.5. Polarity: negative away from the surface. The rms distribution is given for the projected tributary area.

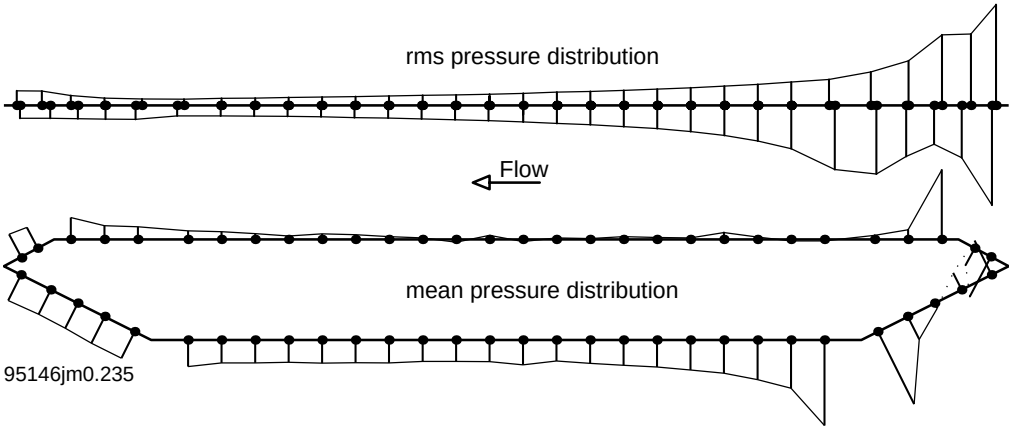

Figure 17: Surface pressure distribution on B/D= 10, large spire exposure, without railings, 15 ms^{-1}. Scaling: depth of deck= mean C_p of 1 and rms C_p of 0.5.

The suggestion that the body-induced turbulence is the cause of the higher lift admittance for bridge decks than the theory predicts for a thin airfoil also applies to the torsional admittance. In fact for torsion, this effect should be even greater since the zones that are affected on the deck (at the trailing edge) have an important contribution to the torsional forces. This is confirmed on Fig. 18 where the measured aerodynamic admittance in torsion [2] is compared to Liepmann's approximation for the lift admittance.

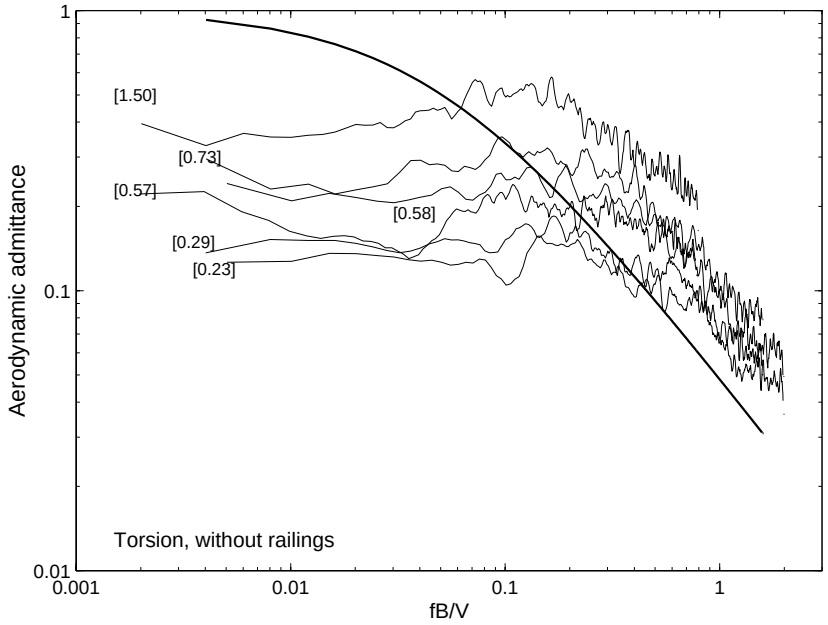

Figure 18: Variations of the torsional aerodynamic admittance with reduced frequency. The numbers in [ ] refer to the $\mathcal{L}_w/B$ ratio. The thick line shows the Liepmann's approximation to the lift admittance.

[2]The experimental determination of the torsional admittance is similar to the lift admittance. The subscript z in equation (21) is replaced by subscript m.

4 Empirical model of the spatial distribution of the buffeting forces on closed-box girder bridge decks

The 3-D analytical model of the gust loading on a thin airfoil has shown qualitative agreement with the experimental description of the spatial distribution of the wind forces on bridge decks. It has helped to understand the generation of lift on a chord-wise strip and has explained the observed larger span-wise coherence of the aerodynamic forces.

Quantitatively however, it has failed to reproduce closely the aerodynamic admittance of the bluffer closed-box girder bridge decks in the 0.03 to 1 reduced frequency range that is of interest for long-span bridge aerodynamics. For the more slender bridge decks, e.g. $B/D > 10$, it is believed that it could be used as an alternative to the Sears' function.

In the following, an empirical model of the spatial distribution of the wind forces due to turbulence on closed-box girder bridge decks is presented. The model is inspired by the 3-D analytical model and is based on direct measurements of the gust loading.

4.1 Cross-sectional aerodynamic admittance as a function of $\mathcal{L}_w/B$

By inspection of the aerodynamic admittance curves, either obtained from analytical calculations or direct measurements, a quasi-linear dependence on the $\mathcal{L}_w/B$ ratio was depicted. To quantify this dependence, attempts to collapse the admittance curves on one line were made. The best collapses are shown in Fig. 19 both for the analytical calculations and the experiments. The similarities between the sets of curves are remarkable. The best collapse was obtained when the ordinate was normalized by $\mathcal{L}_w/B$ to some power and when fB/V was further reduced also by $\mathcal{L}_w/B$ to some power.

Based on this collapse, an empirical expression that could describe the aerodynamic admittance as a function of $\mathcal{L}_w/B$ and $f_r = fB/V$ was sought. The best fit of the measured aerodynamic admittance curves was obtained with the following expression:

$$\left|A_{z,m}(f_r, \frac{\mathcal{L}_w}{B})\right|^2 = \frac{a\,(1+\sqrt{f_r})}{1+b\,f_r^2}, \tag{22}$$

where

$$a = 0.34\,\left[\frac{\mathcal{L}_w}{B}\right]^{0.95} \quad \text{and} \quad b = 9.10\,\left[\frac{\mathcal{L}_w}{B}\right]^{2/3} \quad \text{for lift; and,} \tag{23}$$

$$a = 0.30\,\left[\frac{\mathcal{L}_w}{B}\right]^{0.70} \quad \text{and} \quad b = 4.30\,\left[\frac{\mathcal{L}_w}{B}\right]^{1/2} \quad \text{for moment.} \tag{24}$$

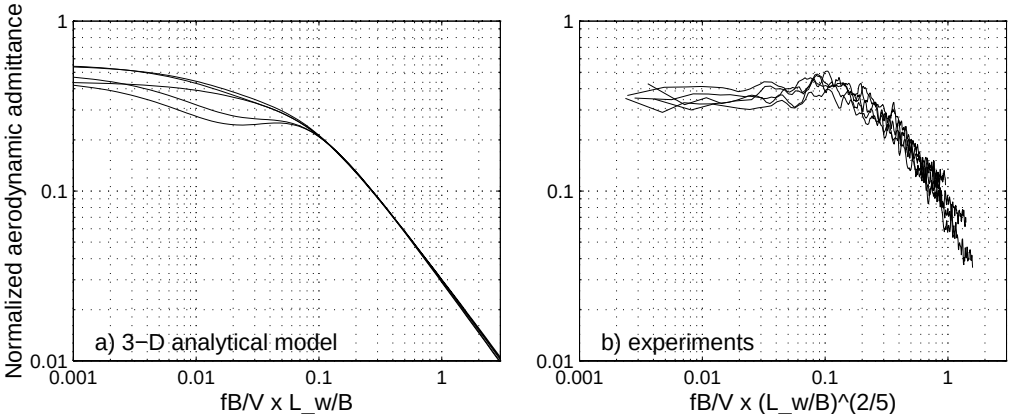

Figure 19: Collapse of lift aerodynamic admittance functions for five $\mathcal{L}_w/B$ ratios, varying from 1.5 to 0.23. In **a)** the admittances calculated using the 3-D model have been normalized by $(\mathcal{L}_w/B)^{0.95}$ and are plotted versus $(fB/V) \cdot (\mathcal{L}_w/B)$. In **b)** the measured admittances have been normalized by $(\mathcal{L}_w/B)^{0.90}$ and are plotted versus $(fB/V) \cdot (\mathcal{L}_w/B)^{2/5}$.

The limits of validity of the empirical expression above, related to the family of closed-box girder bridge decks studied here, are:

$$5 < B/D < 15 \qquad \text{and} \qquad 0.2 < \mathcal{L}_w/B < 2. \tag{25}$$

Examples of the fit of equations (22) to the experimental data are given in Figs. 20 and 21.

4.2 Model of the span-wise co-coherence of the aerodynamic forces

Integral length scales: The width of the correlation has been represented in Part I-B by the integral length scales:

$$L^y = \int_0^\infty R_{12}(\Delta y)\mathrm{d}(\Delta y) \tag{26}$$

where R_{12} is the correlation coefficient. The correlation width can be calculated from the measured correlation coeffient of the input, the w component, and directly compared to the correlation width of the output, the aerodynamic forces. On the basis of the strip assumption, for very large gusts compared to the size of the structure, $L^y_{L,M}$ should tend to L^y_w for a motionless structure.

The correlation width of the aerodynamic forces is compared in Fig. 22 to the correlation width of the w component for all the test cases of this study. Also included in the graphs are results obtained by other researchers (see Part I-B) for similar streamlined bodies but for different experimental conditions.

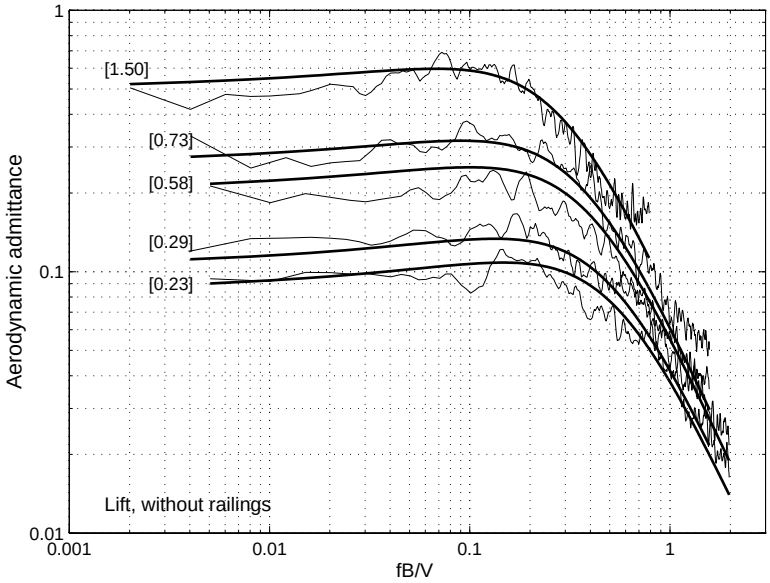

Figure 20: Variations of lift aerodynamic admittance functions for five $\mathcal{L}_w/B$ ratios (numbers in [ ]). The smooth solid lines show a fit of the measured data using equation (22).

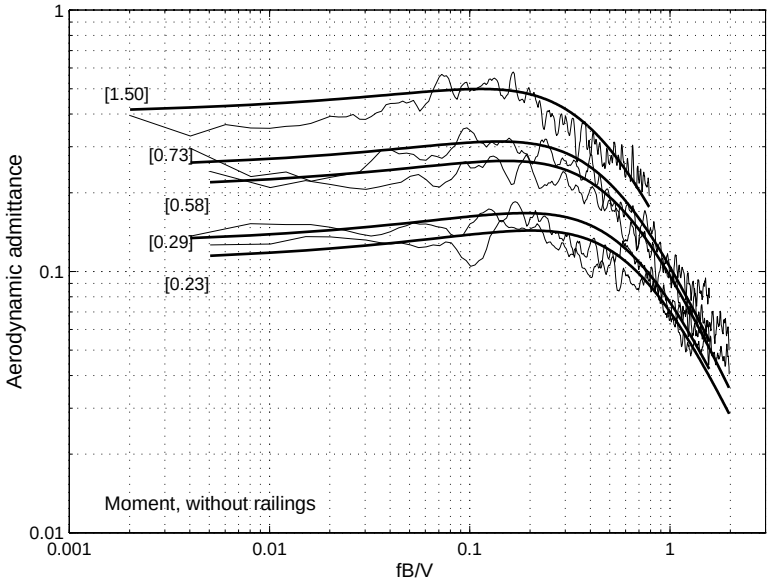

Figure 21: Variations of moment aerodynamic admittance functions for five $\mathcal{L}_w/B$ ratios (numbers in [ ]). The smooth solid lines show a fit of the measured data using equation (22).

The data points appeard to fall well on one line when plotted as a function of $\mathcal{L}_w/B$ and tends toward unity as $\mathcal{L}_w/B$ increases as assumed by the strip theory. From Fig. 22, the width of influence of the gusts can be determined for a given $\mathcal{L}_w/B$ ratio. For conditions representative of full-scale conditions for closed-box girder bridge decks ($1 < \mathcal{L}_w/B < 2$), the width of the influence of the vertical gusts on the lift forces was found to be at least 2 times the integral length scale of the gusts themselves.

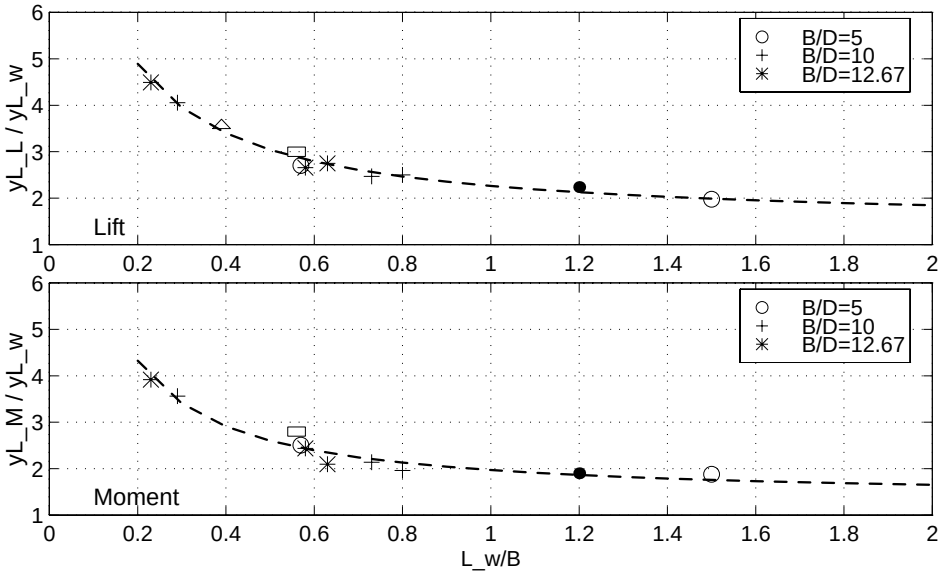

Figure 22: Variations of the ratio of the integral length scales of the forces to the integral length scales of w, $L^y_{L,M}/L^y_w$, as a function of the $\mathcal{L}_w/B$ ratio. All data points are from the present research, with the exception of: △: Nettleton [4]; •: Larose [6]; and □: Bogunovic Jakobsen [10].

Force co-coherence: By inspection of the variations of the co-coherence of the lift forces with $k_1\Delta y$ it was observed that:

1. the shape and magnitude of the curves have more affinity with the co-coherence of v than w. This affinity is though to be only coincidental;

2. the decay of the force co-coherence is slower than the incident wind co-coherence and appears to be a function of the span-wise separation.

In search for an adequate empirical model of the force co-coherence curves, attempts where made to fit the data with the analytical expressions of the co-coherence

of the wind derived from the von Kármán spectrum in Mann *et al.* [19]. The expressions for the v and w components are reproduced here:

$$cocoh_v(\Delta y, k_1) = \frac{2}{\Gamma\left(\frac{5}{6}\right)}\left(\frac{\gamma}{2}\right)^{\frac{5}{6}}\left[K_{5/6}(\gamma) + \frac{3(\Delta y k_1)^2}{3\gamma^2 + 5(\Delta y k_1)^2}\gamma K_{1/6}(\gamma)\right] \quad (27)$$

$$cocoh_w(\Delta y, k_1) = \frac{2}{\Gamma\left(\frac{5}{6}\right)}\left(\frac{\gamma}{2}\right)^{\frac{5}{6}}\left[K_{5/6}(\gamma) - \frac{3\left(\frac{\Delta y}{k_1}\right)^2}{3\gamma^2 + 5(\Delta y k_1)^2}\gamma K_{1/6}(\gamma)\right] \quad (28)$$

where $K_{1/6,5/6}$ are modified Bessel functions of the second kind and,

$$\gamma = \left(\Delta y^2 k_1^2 + \frac{\Delta y^2}{L^2}\right)^{\frac{1}{2}} = k_1 \Delta y \sqrt{1 + \frac{1}{k_1^2 L^2}} \quad (29)$$

is the von Kármán collapsing parameter.

A similar analysis was made by Kimura et al. [9] for flat cylinders. At first the calculated co-coherence using the 3-D model and Mugridge's approximation where fitted with equations (27) and (28). The expression for w did not fit particularly well the lift co-coherence when compared to the fit obtained with the expression for v (as observed in point 1 above). To improve further the fit, the wave number k_1 in equation (27) was raised to an exponent **a** as suggested by point 2 and as proposed by Kimura et al. The exponent **a** and the length scale L were kept as floating parameters for the least square fits. An example of the fit is given in Fig. 23 and the results for three $\mathcal{L}_w/B$ ratios are shown in Fig. 24.

The best fit was obtained when **a**= 0.95 and when L_L, the length scale related to the lift forces, was varied as a function of Δy as seen on Fig. 24. It was also observed that if L_L was normalized by L, the von Kármán length scale describing the input wind field, and plotted versus normalized separation $\Delta y/B$, the results fitted well on one line and tend to a value slightly lower than 1 (see right-hand-side graph of Fig. 24).

In a similar fashion, all measured co-coherence of the aerodynamic forces of this study were fitted with equation (27) with $k_1^{\mathbf{a}}$, keeping the exponent **a** and the length scale L_L as a floating parameter for the least square fits. An example of the fit is given in Fig. 25 and the results for all $\mathcal{L}_w/B$ ratios are shown in Fig. 26. It can be observed from Fig. 26 that the normalized lift length scale L_L/L also tends to a value near 1.0 for larger $\Delta y/B$ and that the curves are grouped by chord-to-thickness B/D. For example, the $\mathcal{L}_w/B$ =1.5 and 0.57 are from B/D=5 in two different exposures, and showed exactly the same L_L/L and **a** for both cases.

For separations smaller than half the deck width it is clear that the larger the deck width, the larger the lift length scales. It indicates that the longer the incident large-eddies are being distorted over the deck, the larger the possibility of forming secondary cross-flow, the larger the span-wise coherence.

The exponents **a** also appeared to be grouped by B/D ratios; the larger the deck width, the smaller the exponent up to a certain plateau. This exponent gives an indication of the rate of decay of the co-coherence with frequency. As described in Part I-B, bluff bodies have a tendency to spread the separated flow vortices (body-induced turbulence) span-wise as they are convected over the body. Since the larger the after-body the larger this effect, it could explain the observed relatively larger influence of the higher frequency gusts for the wider decks, represented by smaller exponents **a**.

The value of **a** for $B/D = 10$ and 12.67 appeared to tend toward 0.75 for larger $\Delta y/B$. This is in agreement with results by Kimura et al. [9] who obtained **a**=0.74 for flat cylinders with $B/D = 8.7$.

It was observed that, at high frequencies, the measured co-coherences were in most cases larger than predicted by the analytical model (see Fig. 14). The failure of the 3-D analytical model (chain-dotted line in Fig. 26 and solid lines on Fig. 14) has probably to do with separated flow vortices, which may have strong span-wise co-coherence. Separated flow is out of reach of the analytical model.

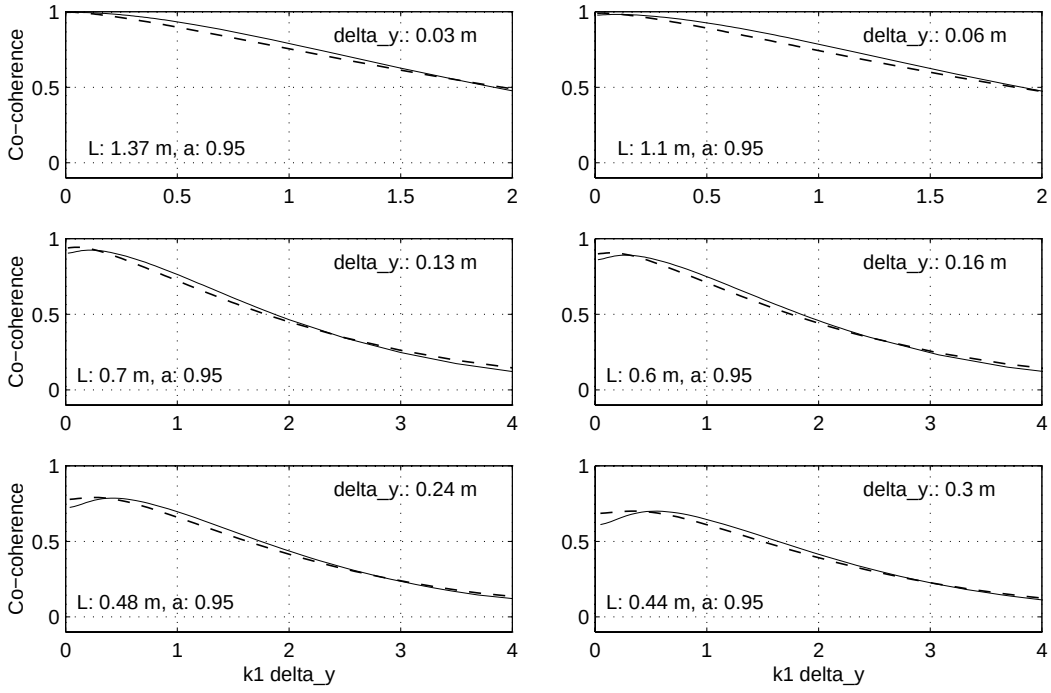

Figure 23: Example of the least square fit of the force co-coherence, calculated using the 3-D model and Mugridge's approximation and fitted with equation (27) with $k_1^{\mathbf{a}}$ for $\mathcal{L}_w/B$= 0.73.

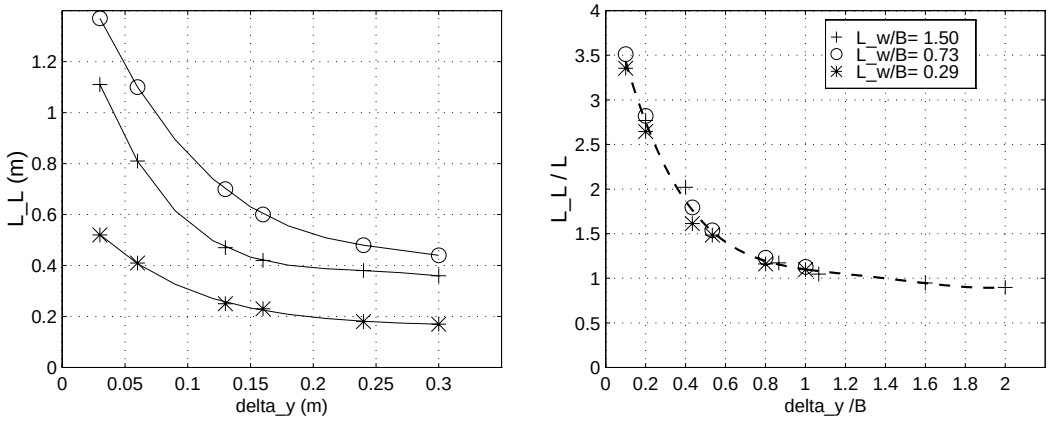

Figure 24: Results of the fit of the co-coherence of the lift forces calculated using the 3-D model and Mugridge's approximation and fitted with equation (27) with $k_1^{\mathbf{a}}$.

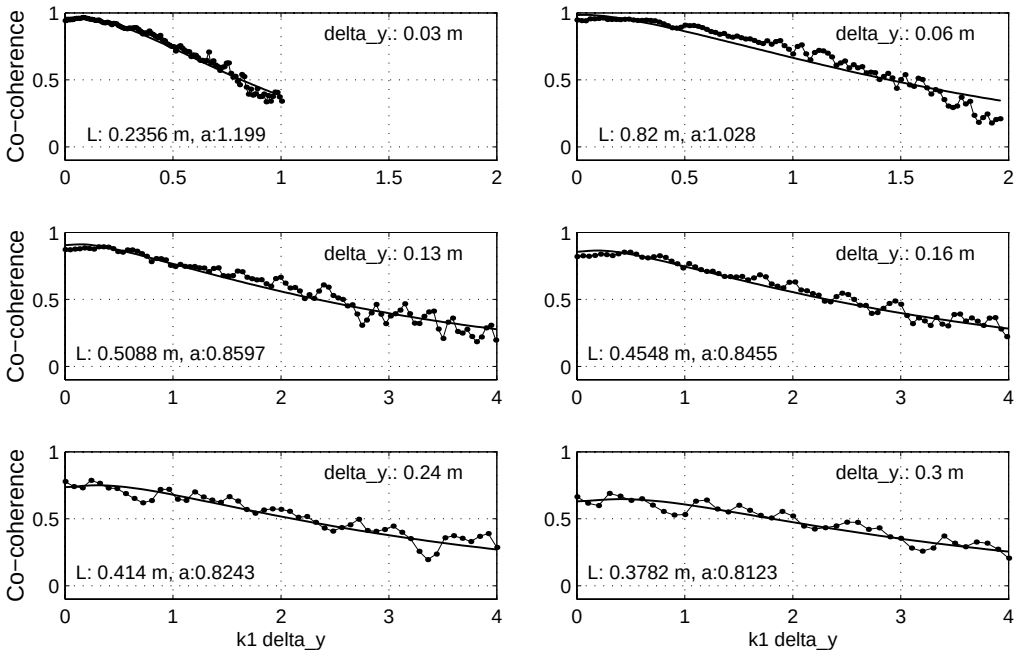

Figure 25: Example of the least square fit of the measured co-coherence of the lift force with equation (27) with $k_1^{\mathbf{a}}$ for $\mathcal{L}_w/B = 1.50$.

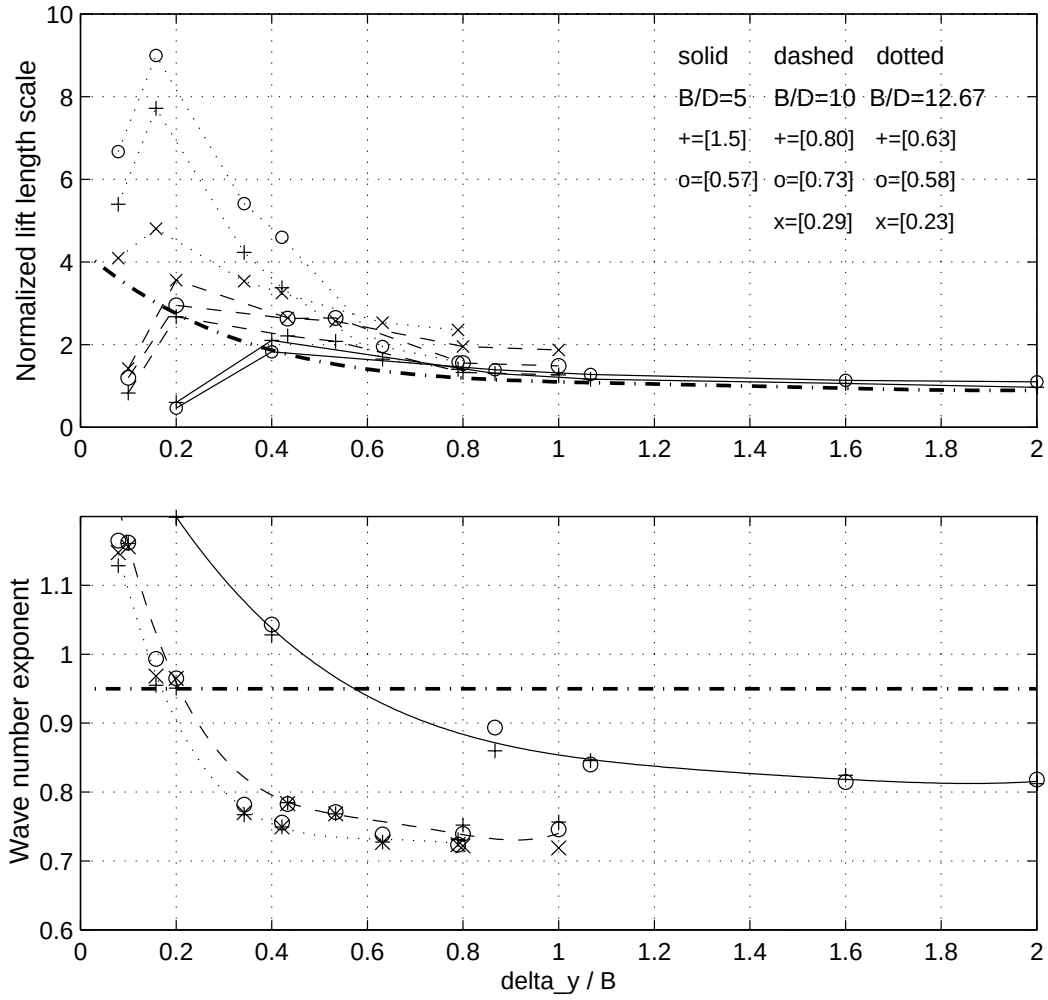

Figure 26: Results of the fit of the measured co-coherence of the lift forces as a function of $\Delta y/B$. The ordinate of the top graph is the lift length scale L_L obtained from the fit of equation (27) and normalized by the length scale L of the incident flow. The chain-dotted line refers to the theoretical calculations with the 3-D model. The wave number exponent refers to $\mathbf{a}$ in $k_1^{\mathbf{a}}$.

Empirical formulations

Relationships between L_L, $\mathbf{a}$ and $\Delta y/B$ were extracted from the results presented above. In combination with the analytical description of the incident wind field, they form the basis of an empirical model of the spatial distribution of the aerodynamic forces on closed box girder bridge decks of the cross-section family studied here.

The span-wise co-coherence of the lift forces can be expressed as a function of $\Delta y, k_1, \frac{\mathcal{L}_w}{B}, \frac{B}{D}$ by:

$$cocoh_L(\eta) = \frac{2}{\Gamma\left(\frac{5}{6}\right)}\left(\frac{\eta}{2}\right)^{\frac{5}{6}}\left[K_{5/6}(\eta) + \frac{3(\Delta y k_1^{\mathbf{a}})^2}{3\eta^2 + 5(\Delta y k_1^{\mathbf{a}})^2}\eta K_{1/6}(\eta)\right] \quad (30)$$

where: (31)

$$\eta = k_1^{\mathbf{a}}\Delta y\sqrt{1 + \frac{1}{(k_1^{\mathbf{a}}L_L)^2}} \quad (32)$$

$$\mathbf{a} = \left(\frac{B}{D}\right)^4 \frac{(p + \frac{\Delta y}{B})^2}{(q + r\,\frac{\Delta y}{B})^2}; \quad p = 0.16,\ q = 0.088,\ r = 0.935 \quad (33)$$

$$L_L = L\,\frac{(p + \frac{\Delta y}{B})^2}{(q + r\,\frac{\Delta y}{B})^2}; \qquad p = 1.0,\ q = 0.46,\ r = 1.42 \quad (34)$$

A graph showing the variations of L_L and $\mathbf{a}$ as a function of $\Delta y/B$ for the lift forces is given in Fig. 27. For the sake of simplicity, the variations of L_L/L with Δy extracted from the calculations of co-coherence with the 3-D model were used to represent L_L in equation (34). The effect of this simplification was found to be negligible and is illustrated in the following.

Fig. 28 shows 3 graphs of the co-coherence as a function of η for all $\mathcal{L}_w/B$ ratios of this study, for all separations. The co-coherence data collapsed very well. In a) the measured co-coherence is plotted versus η calculated directly using the results of the fitting of L_L and $\mathbf{a}$ as reported in Fig. 26. The dark solid line represents the best fit of the collapsed data with:

$$cocoh_L(k_1, \Delta y, \frac{\mathcal{L}_w}{B}, \frac{B}{D}) = \exp[-c_1(\eta)^{c_2}]\cos(c_3\eta) \quad (35)$$

where c_1, c_2 and c_3 are given in Fig. 28. This expression was used in Part II-A to model the co-coherence of the incident wind field.

In b), the measured co-coherences are also plotted versus η but with L_L and $\mathbf{a}$ calculated using equations (34) and (33). The resulting curve is practically identical to a) confirming that the simplification for L_L is adequate. In c) the co-coherence calculated using the empirical model, equations (30) to (34), is plotted as a function of η. The resulting c_1, c_2 and c_3 describe the same function as in a) and b) of Fig. 28.

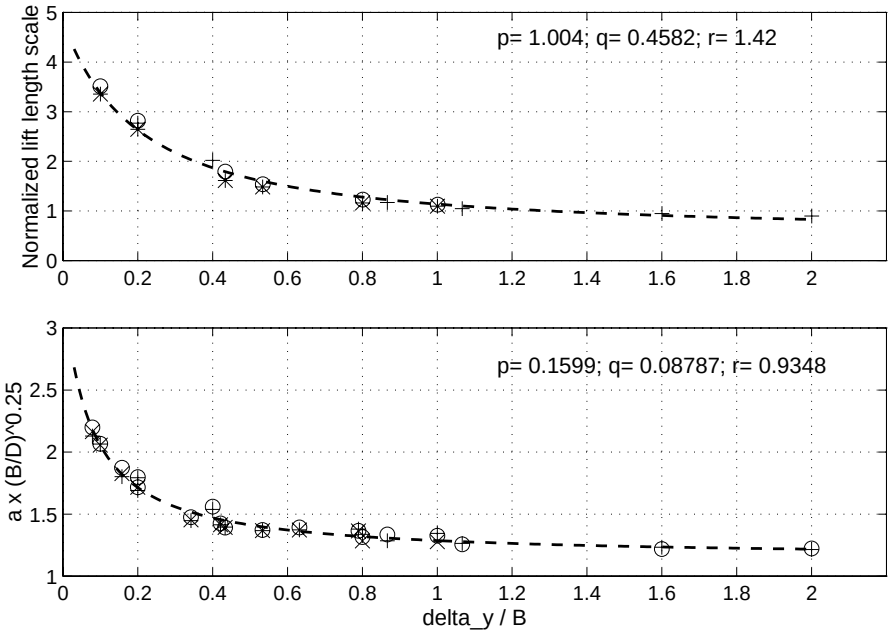

Figure 27: Collapse of L_L and $\mathbf{a}$ based on the fit of the co-coherence of the lift forces with equation (27) with $k_1^{\mathbf{a}}$ for all cases.

The co-coherence calculated with the 3-D analytical model were also plotted as a function of η. The collapsed data fit well equation (35) with: c_1= 0.356, c_2= 1.33 and c_3=0.22.

Joint acceptance function: The evaluation of the spatial distribution of the aerodynamic forces is at the hearth of the calculation the joint acceptance function, JAF. As defined in Part I-B, this quantity is a measure of the correlation between the vibration mode and the wind loading across the span.

To assess the adequacy of the empirical model described above, the joint acceptance function was calculated for a uniform mode shape, $\mu(x)$= 1, over a 2.55 m span (section model span), for B/D= 10, L=0.39 m. The calculations are reported in Fig. 29 as a function of reduced frequency for 4 conditions:

1. on the basis of the strip assumption, $cocoh_L \approx cocoh_w$;
2. using the fit of the calculated co-coherence of the forces for a thin airfoil with the 3-D model and Mugridge's approximation;
3. using the directly measured co-coherence of the lift forces;
4. and using the empirical model described above (30) with the fitted L_L and $\mathbf{a}$.

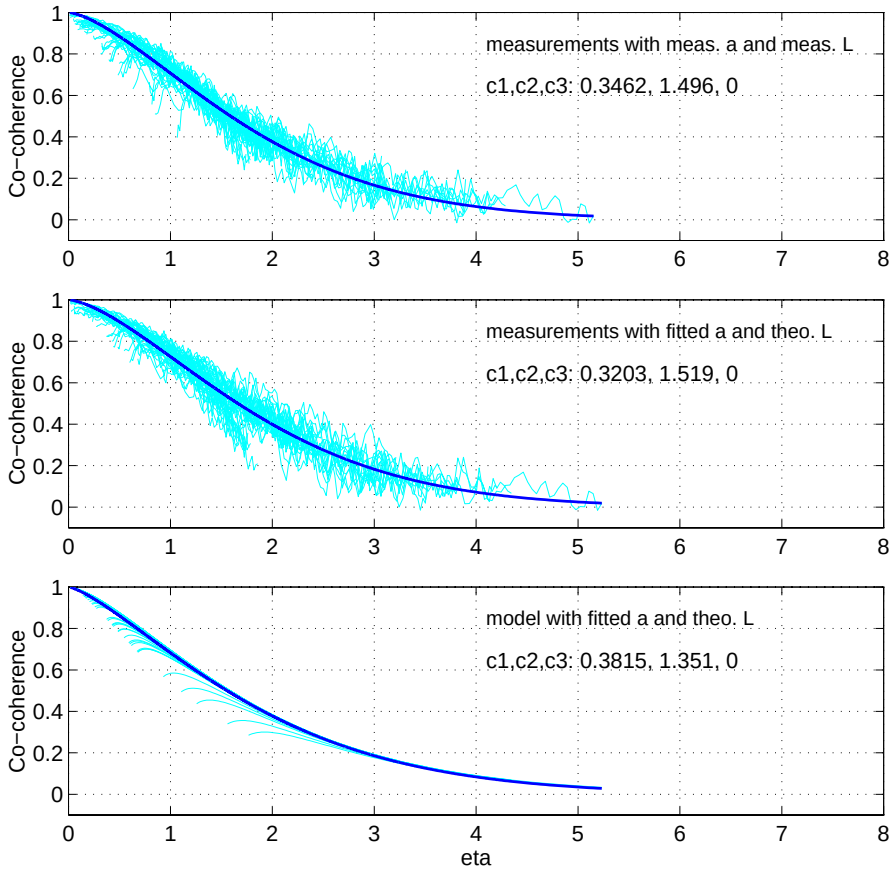

Figure 28: Variations of the measured co-coherence of the lift forces as a function of η for all separations and all $\mathcal{L}_w/B$ of this study. The solid line is the best fit of the collapsed data with equation (35) where the constants c_1, c_2 and c_3 are given in the graphs.

The calculations on the basis of the strip assumption clearly underestimated the joint acceptance function while the empirical model closely matched the JAF based on the directly measured co-coherence of the lift. Calculations with the 3-D model (case 2) gave a good approximation to the JAF in the lower fB/V range but failed to follow the mode shape of the JAF in the higher range ($.1 < fB/V < 1$). Case 2 has a constant wave number exponent ($\mathbf{a}$=0.95) for all span-wise separations, therefore does not decay in the same manner as the measured co-coherence for a closed box girder bridge deck. The shape of the JAF for cases 3 and 4 are consistent with the results reported earlier in [6] and summarised in Part I-B.

A similar shape of the JAF was obtained by Hoi [20] from measurements on a section model of the Bronx-Whitestone Bridge. Hoi made one of the rare direct

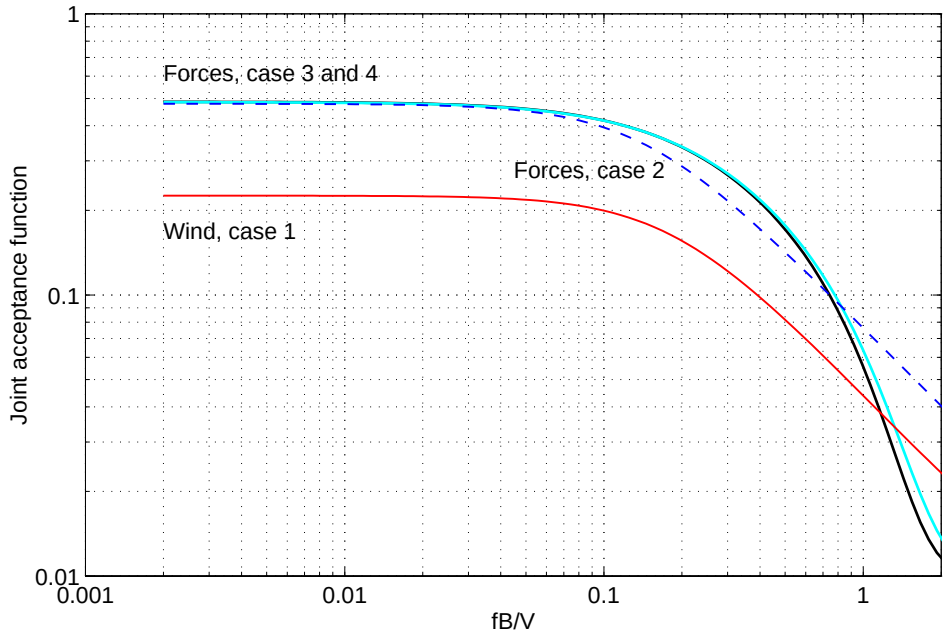

Figure 29: Variations of the joint acceptance function with reduced frequency for four cases.

measurements of the joint acceptance function by simultaneously measuring the total lift forces at the extremities of a section model in motion and the lift forces on a floating segment at the center of the model. Dividing the first quantity by the second gave a JAF curve in excellent agreement with the curve obtained here, even though Hoi's experiments was for a truss girder bridge.

Co-coherence of the overturning moment: The analysis described above was repeated for the aerodynamic overturning moment of the bridge deck and the results are summarised in Figs. 30 to 32. Similar variations of the L_M/L and $\mathbf{a}$ with $\Delta y/B$ were obtained when compared with the lift force results. The scatter of L_M/L for $\Delta y/B < 0.50$ was lower than observed for the lift forces and coincidently followed the variations of L_L extracted from the 3-D analytical model (chain-dotted line in Fig. 30). The exponent $\mathbf{a}$ was found to be slightly higher than for the lift indicating slightly more rapid decay of the moment co-coherence. The best fit of the exponent $\mathbf{a}$ was obtained with:

$$\mathbf{a} \;=\; \left(\frac{B}{D}\right)^{1/.15} \frac{(p+\frac{\Delta y}{B})^2}{(q+r\,\frac{\Delta y}{B})^2}; \quad p=0.098,\; q=0.059,\; r=0.970 \qquad (36)$$

as shown in Fig. 31.

The moment co-coherence was plotted as a function of η (32), with **a** defined by (36) and L_M/L defined by (34). The results are shown in Fig. 32 for the same cases as Fig. 28. The collapse of the moment co-coherence was found to be even better than for the lift co-coherence and was well described by the empirical model.

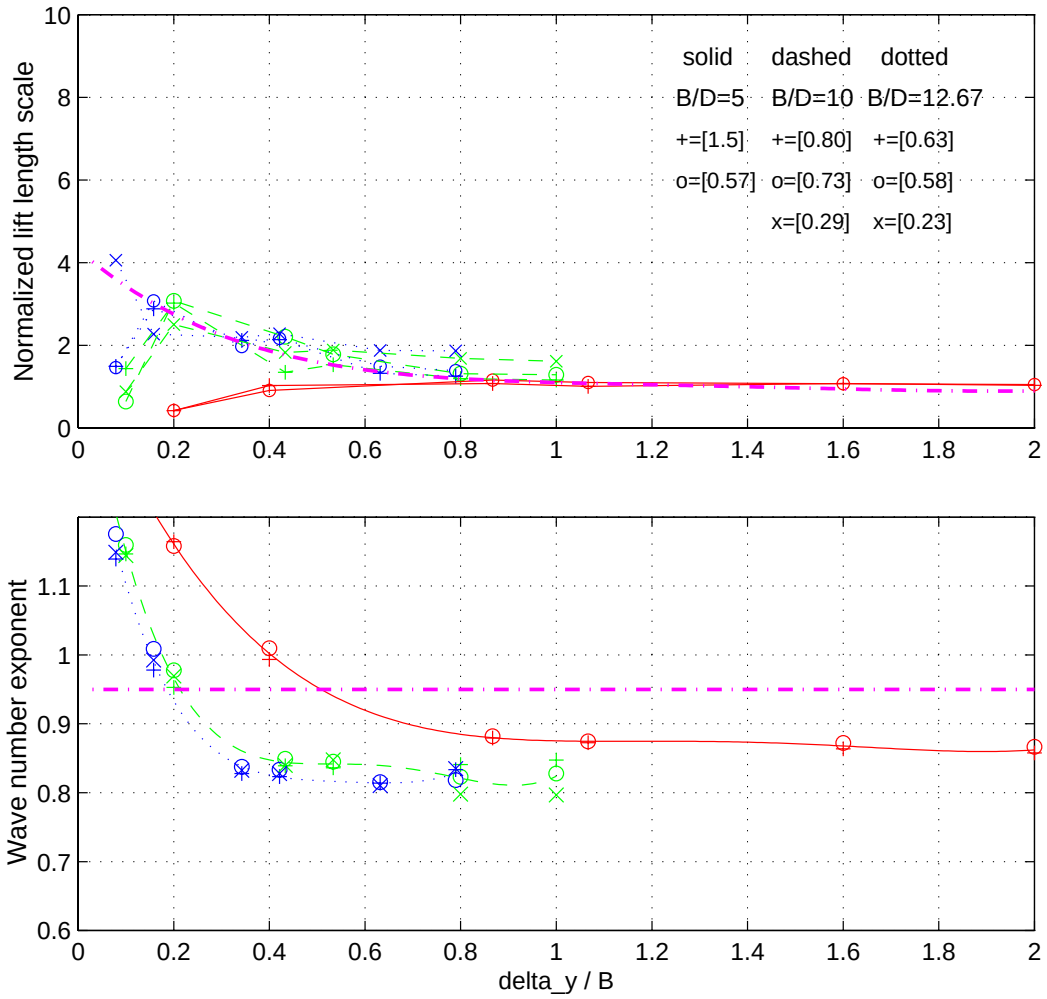

Figure 30: Results of the fit of the measured co-coherence of the torsional forces as a function of $\Delta y/B$. The chain-dotted line refers to the theoretical calculations with the 3-D model. The wave number exponent refers to **a**.

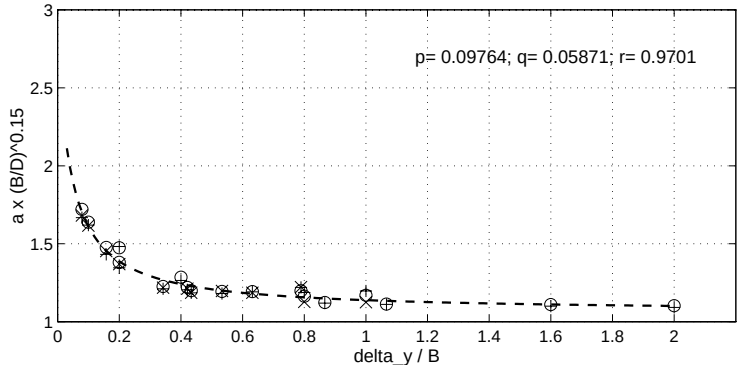

Figure 31: Collapse of **a** based on the fit of the co-coherence of the torsional forces with equation (27) with $k_1^{\mathbf{a}}$ for all cases.

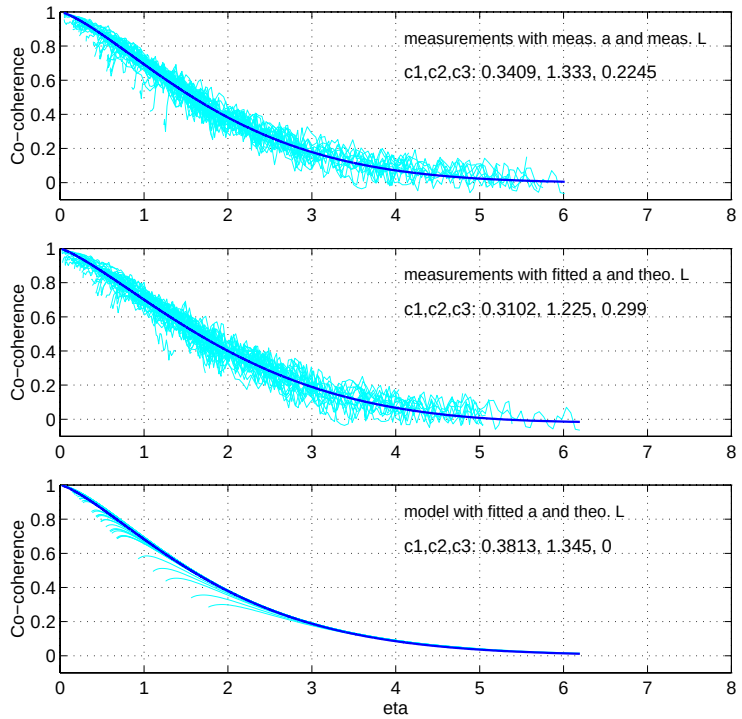

Figure 32: Variations of the measured co-coherence of the overturning moment as a function of η for all separations and all $\mathcal{L}_w/B$ of this study. The solid line is the best fit of the collapsed data with equation (35) where the constants c_1, c_2 and c_3 are given in the graphs.

5 Conclusions

An analytical model that departs from the strip assumption was presented to describe the gust loading on a thin airfoil in isotropic turbulence. The 3-D model is based on a two horizontal wavevector analysis as opposed to the fully correlated sinusoidal gust analysis due to Sears.

The 3-D model has shown qualitative agreement with the experimental description of the aerodynamic admittance and the spatial distribution of the gust loading on bridge decks. It has helped understand the generation of lift on a chord-wise strip and has explained the observed larger span-wise co-coherence of the forces when compared to the co-coherence of the incident wind.

Quantitatively however, the 3-D analytical model did not reproduce adequately some aspects of the gust loading on the bluffer closed box girder bridge decks. An empirical model was thus derived to describe the gust loading on the family of closed box girder bridge decks of this study. The empirical model departs from the strip assumption and was inspired by the analytical description of the incident wind field as well as the 3-D model of the spatial distribution of the aerodynamic forces.

It is likely that the empirical model could be extended to the cross-sections of other closed box girder bridge decks provided that the aerodynamic characteristics approached the flat plate characteristics. For relatively open truss girder bridge decks the strip assumption would certainly provide a fair approximation at low frequencies but the body-induced turbulence will dominate at high frequencies. In this situation, the recommendation is to rely on ad hoc wind tunnel tests to determine the gust loading.

Acknowledgements: The financial support of the COWIfoundation for the experimental part of this research is gratefully acknowledged as well as the research scholarship provided by the Danish Research Academy.

References

[1] Davenport A.G., "The response of slender, line-like structures to a gusty wind", in *Proc. of Institution of Civil Engineers*, **23**, Nov. 1962, 389-408.

[2] Liepmann H.W.,"On the application of statistical concepts to the buffeting problem", *J. Aero. Science*, **19**, no 12, Dec. 1952, 793s.

[3] Vickery B.J., "Fluctuating lift and drag of a long cylinder of square cross-section in a smooth and turbulent stream", *J. Fluid Mech.* (1966) **25**, 481-494.

[4] Ektin B., *Dynamics of Atmospheric Flight*, John Wiley and Sons, 1971, pp. 547-548.

[5] Melbourne W. H., "Comparison of model and full-scale tests of a bridge and chimney stack", in *Proc. of Int'l Workshop on Wind Tunnel Modelling*, Maryland, USA, 1982, 637-653.

[6] Larose G.L., *The Response of a Suspension Bridge Deck to Turbulent Wind: The Taut Strip Model approach*, M.E.Sc. Thesis, University of Western Ontario, Canada, March 1992.

[7] Larose G.L., Davenport A.G., and King J.P.C., "On the unsteady aerodynamics forces acting on a bridge deck in turbulent flow", in *Proc. of the 7th US Nat. Conf. on Wind Engineering*, UCLA, Los Angeles, USA, June 1993.

[8] Sankaran R. and Jancauskas E.D., "Measurements of cross-correlation in separated flows around bluff cylinders", *J. Wind Eng. Ind. Aerodyn.*, **49** (1993), 279-288.

[9] Kimura K., Fujino Y., Nakato S. and Tamura H., "Characteristics of the buffeting forces on flat cylinders", in *Proc. of 3rd Int'l Colloquium on Bluff Body Aerodynamics and Applications*, Blacksburg, Virginia, USA, July 1996.

[10] Bogunovic Jakobsen J., *Fluctuating wind load and response of a line-like engineering structure with emphasis on motion-induced wind forces*, Ph.D. Thesis, The Norwegian Institute of Technology, Trondheim, Norway, 1995.

[11] Larose G.L., Tanaka H., Gimsing N.J. and Dyrbye C., "Direct measurements of buffeting wind forces on bridge decks", accepted for publication in *Proc. of 2nd European African Conf. on Wind Eng.*, Genova, Italy, June 1997.

[12] Fung Y.C., *An Introduction to the Theory of Aeroelasticity*, Dover Publications Inc., N.Y., 1969.

[13] Graham J.M.R., "Lifting-surface theory for the problem of an arbitrary yawed sinusoidal gust incident on a thin aerofoil in incompressible flow", *Aeronautical Quaterly*, **21**, May 1970, 182-198.

[14] Jackson R., Graham J.M.R. and Maull D.J., "The lift on a wing in a turbulent flow", *Aeronautical Quaterly*, **24**, part 3, Aug. 1973, 155-166.

[15] Mugridge B.D., "Gust loading on a thin aerofoil", *Aeronautical Quaterly*, **22**, Aug. 1971, 301-310.

[16] Blake W.K., *Mechanics of flow-induced sound and vibration*, Volume 1, Academic Press Inc., Orlando, Florida, 1986, p. 743.

[17] Mann J., "The strip assumption in bridge aerodynamics", unpublished Technical Note, Danish Maritime Institute, Oct. 1995.

[18] Mann J., "The spatial structure of neutral atmospheric surface-layer turbulence", *J. Fluid Mech.* (1994) **273**, 141-168.

[19] Mann J., Kristensen L. and Courtney M.S., *The Great Belt Coherence Experiment - A study of atmospheric turbulence over water*, Risø Report No. R-596, 1991, 51 p.

[20] Hoi C.L., *Measurements of the aerodynamic derivatives of a section model*, M. Eng. Thesis, University of Western Ontario, Canada, 1982, 130 p.

Part III
Applications

Part III-A
Experimental determination of the aerodynamic admittance of a bridge deck segment

GUY L. LAROSE[a,b]

[a] *Danish Maritime Institute, Hjortekærsvej 99, 2800 Lyngby, Denmark*
[b] *Department of Structural Engineering and Materials, Technical University of Denmark, 2800 Lyngby, Denmark*

(Published in *Journal of Fluids and Structures* 1999, **13**, 1029-1040)

Abstract

The gust loading on bridge decks is described by the dynamic forces on a chord-wise strip and by the spatial distribution of these forces across the span. An experimental method to evaluate the aerodynamic admittance of a segment of a bridge deck that includes a combination of the cross-sectional admittance and the spatial distribution of the forces is presented in this paper. The method is based on wind tunnel tests in turbulent flow on a motionless section model of the deck. The approach has been validated experimentally on a closed-box girder bridge deck but can be applied to bridge decks of any cross-section.

1 Introduction

The spectrum of the modal lift forces due to the buffeting action of the wind on a bridge deck has been expressed (Davenport 1962) by

$$S_{F_z}(f_j^*) = \left(\frac{\rho \bar{V} B}{2}\right)^2 \left(4C_z^2 S_u(f^*) + C_z'^2 S_w(f^*)\right) \; |A_z(f^*)|^2 \; | \; J_z(f_j^*) \; |^2, \qquad (1)$$

where f_j^* is a reduced frequency $= f_j B/\bar{V}$ associated with the j^{th} vibration mode; $|A_z(f^*)|^2$ is a lift cross-sectional admittance linked to the longitudianl, u, and vertical, w, components of the turbulence; $\mid J_z(f_j^*) \mid$ is the joint acceptance function of mode j; ρ, B, $\bar{V}$, C_z and C_z' are respectively the air density, the deck width, the mean wind velocity at deck level, the lift coefficient and the variations of the lift coefficient with angle of wind incidence; and S_{u,w,F_z} denotes power spectral density of the wind components u or w or of the lift force F_z. Equation (1) can be written for the lateral and torsional degrees of freedom by replacing subscript z by x and m respectively.

The cross-sectional aerodynamic admittance can either be approximated as in Liepmann (1952), Davenport (1962), Irwin (1977) using for example analytical expressions derived for a thin airfoil (Fung 1969), or measured as in Lamson (1957), Holmes (1975), Walshe & Wyatt (1983), Jancauskas (1983), Jancauskas & Melbourne (1986), Kawatani & Kim (1992), Sankaran & Jancauskas (1992), Larose (1992), Sato *et al.* (1994), and Bogunovic Jacobsen (1995) or evaluated indirectly (Grillaud *et al.* 1991). Liepmann's approximation to Sears' function is the most commonly used form of the lift aerodynamic admittance of a thin airfoil in fully correlated gusts with sinusoidal fluctuations (Liepmann 1952):

$$\mid \phi_z(f^*) \mid^2 = \frac{1}{1 + 2\pi^2 f^*}. \tag{2}$$

The joint acceptance function is of the form:

$$|J_z(f_j^*)|^2 = \int_0^l \int_0^l \frac{S_{L_1L_2}(\Delta y, f^*)}{S_L(f^*)} \; \mu_j(y_1)\, \mu_j(y_2)\, \mathrm{d}y_1 \mathrm{d}y_2, \tag{3}$$

where μ_j is the j^{th} mode shape and $S_{L_1L_2}/S_L$ is the normalized cross-spectrum of the lift force between strips 1 and 2 separated by a span-wise distance Δy.

It has been shown (Larose 1992; Bogunovic Jacobsen 1995 and in Part I and II of this thesis) that the evaluation of the joint acceptance function is problematic given the difficulty in defining the spatial distribution of the aerodynamic forces that appeared to be better correlated than the wind fluctuations of the incident flow. In Part II-B an analytical model of the span-wise lift force coherence has been proposed and compared to direct measurements of the gust loading (Larose *et al.* 1997) for a family of streamlined bridge decks. The applicability of this analytical model and of an ad hoc empirical model is limited until now to deck cross-sections that have a relatively long, fully re-attached flow region, i.e. bridge decks with aerodynamic characteristics approaching the characteristics of a thin airfoil.

This paper presents an experimental method to evaluate, for bridge decks of any cross-section, an aerodynamic admittance that includes a combination of the cross-sectional admittance and the span-wise distribution of the forces. This quantity will be referred to as segmental admittance of a motionless bridge deck. Even though it

is obtained from an intrinsically two-dimensional approach (a 2-D section model), it has a three-dimensional (3-D) character when compared to the cross-sectional admittance of a strip that is purely two dimensional (2-D). The main advantage of the proposed approach is that it eliminates the difficult task of measuring the span-wise cohrence of the aerodynamic forces to obtain a clear picture of the spatial distribution of the gust loading.

By itself the proposed technique to measure the aerodynamic admittance is not new. It has been used by several researchers, e.g. Walshe & Wyatt (1983), Sato *et al.* (1994), and Bogunovic Jacobsen (1995). However, the definition of what one really measures is original and has been verified experimentally. The verification was made possible with the help of the analytical and empirical models presented in Part II-B of this thesis and published in Larose & Mann (1998).

2 Description of the approach

The experimental technique consists of measuring the vertical, torsional and lateral forces at the extremities of a section model of a bridge deck, in turbulent flow, the model being restrained from any wind-induced motion. For the experiments to be valid, four main criteria have to be respected:

(i) the section model has to be as rigid and as light as possible so that its lowest eigen frequency corresponds to a region of the wind spectrum where only a fraction of the wind energy of the largest gusts is present (above 20 Hz);

(ii) the length-to-width ratio of the model should be larger than 6:1 to ensure an adequate representation of the gust loading;

(iii) the geometric scale of the model should be selected in relation to the length scale of the incident turbulent flow field, and the span-wise coherence of the flow field should be representative of full-scale conditions; for lift and pitching moment it is essential to respect in model scale the ratio of the length scales of the vertical component of the turbulence to the deck width, while a definite mismatch between the full-scale and model-scale length scales of the longitudinal component would be acceptable; for drag, a mismatch of 2 to 3 in u-component length scales is acceptable since the characteristic dimensions, the deck depth (typically 3-4 m), is often much smaller than the u-component length scales (typically 150-200 m).;

(iv) and, the model should not undergo any visible motions during the wind tunnel tests (high frequency vibrations with amplitude less than 0.3 mm).

These four criteria can generally be met in today's wind tunnel operations. However, since it is difficult to alter the span-wise coherence of the incident flow field in

the wind tunnel to match the flow conditions of the natural wind at a given site, that aspect of criterion (iii) can be limited to a documentation of the span-wise coherence of the flow. Generally, the root coherence in the wind tunnel should approach the root coherence of the natural wind, and if anything, it would be slightly larger in model scale. The influence of the variations of the root coherence of the flow on the spatial distribution of the wind loading in model scale is a field of research that awaits development.

Also related to criterion (iii), a series of experiments conducted by the author and reported in Larose (1992) and in Part II-A have shown that the lift and pitching moment cross-sectional aerodynamic admittances were directly proportional to the ratio of the w-component length scales to the deck width, $\mathcal{L}_w/B$. These experiments were conducted for closed-box girder bridge decks. It was observed however that the lift and pitching moment admittances were insensitive to the u-component length scales. It is believed that the generation of lift and pitching moment on a bridge deck is only slightly influenced by the energy distribution of the u-component spectrum. This influence is mostly associated with the energy content of the small scale turbulence which wind tunnels have generally no problem producing.

The measured time histories of the aerodynamic forces are converted to power spectral densities of the body-force coefficients, $S_{C_{z,x,m}}(f)$. The spectra of the force coefficients will in most cases show a resonant peak at the eigen frequency of the force balance and model ensemble. If the model meets criterion (i), the resonant peak can be filtered out by fitting a single degree-of-freedom mechanical admittance function to the peak and subsequently removing its contribution without affecting the lower frequency part of the spectra that contains the information required.

The resulting lift force spectrum corresponds in all points to the spectrum defined by equation (1) but in a dimensionless form

$$S_{C_z}(f_j^*) = \frac{S_{F_z}(f_j^*)}{\left(\frac{\rho \bar{V}^2 B}{2}\right)^2}. \tag{4}$$

Rearranging (1), the lift aerodynamic admittance can be obtained by a quotient of a combination of spectral functions:

$$\mid A_z(f^*) \mid^2 = \frac{\bar{V}^2 S_{C_z}(f^*)}{\left(4C_z^2 S_u(f^*) + {C'_z}^2 S_w(f^*)\right) \mid J_z(f^*) \mid^2}. \tag{5}$$

The subscript j has vanished from equation (5) since no motion of the model should be present (criterion (iv)).

Similarily, the aerodynamic admittance of the pitching moment can be expressed by

$$\mid A_m(f^*) \mid^2 = \frac{\bar{V}^2 S_{C_m}(f^*)}{\left(4C_m^2 S_u(f^*) + {C'_m}^2 S_w(f^*)\right) \mid J_m(f^*) \mid^2}, \tag{6}$$

where

$$S_{C_m}(f_j^*) = \frac{S_M(f_j^*)}{\left(\frac{\rho \bar{V}^2 B^2}{2}\right)^2}, \tag{7}$$

and M is the pitching moment about the bridge longitudinal axis.

All quantities of the right-hand-side of equations (5) and (6) can be determined experimentally, with the exception of the joint acceptance function. The one-point spectrum and the span-wise coherence of the wind have to be determined without the model in place and the static coefficients and their linearized slope have to be obtained from tests in turbulent flow for wind conditions (wind speed and turbulence intensity) identical to the test conditions that prevailed during the force measurements.

Equations (5) and (6) can define two quantities depending on how the joint acceptance function is evaluated. If $\mid J_{z,m}(f^*) \mid^2$ is evaluated using the span-wise co-coherence of the aerodynamic forces obtained from experiments or from the empirical model of Part II-B, equations (5) and (6) would define a cross-sectional admittance, $\mid A_{z,m}(f^*) \mid_{2-\mathrm{D}}$, roughly comparable to Sears' function [3].

If $\mid J_{z,m}(f^*) \mid^2$ is evaluated on the basis of the strip assumption using the span-wise co-coherence of the incindent w fluctuations, equations (5) and (6) would define a segmental admittance, $\mid A_{z,m}(f^*) \mid_{\mathrm{seg.}}$, that includes in its definition the three-dimensionality of the wind loading, implying a larger span-wise co-coherence of the aerodynamic forces.

As mentioned above, the evaluation of $\mid A_z(f^*) \mid_{\mathrm{seg.}}$ has a major advantage over the evaluation for the cross-sectional admittance since it does not require an evaluation of the span-wise coherence of the forces. It can thus be used for any cross-sectional shape that could be modelled by a 2-D section model. Its disadvantage is that it can not really be compared to any other benchmark quantity unless an evaluation of the spatial distribution of the forces is made (or is available) for the cross-section studied.

3 Experimental verification

The technique described above was used to determine the cross-section admittance and the segmental admittance of a closed-box girder bridge deck. The results were compared with the cross-sectional admittance measured directly on a chord-wise strip of a section model, as described in Part II-A and Larose *et al.* (1997), for a similar ratio of the turbulence length scale to the deck width and similar turbulence intensity.

[3] Note that Sears' function represents the lift admittance of a thin airfoil in a fully correlated sinusoidal gusts while $\mid A_z(f^*) \mid_{2-\mathrm{D}}$ is the lift admittance of a bluff body in turbulent flow with random fluctuations in u, v and w.

3.1 Force measurements

A section model of the Höga Kusten Bridge in its construction stage configuration (60% porous railings, no median divider) was mounted rigidly in the force balance rig of DMI's (Danish Maritime Institute) 2.6 m wide, 1.8 m high and 21 m long Boundary Layer Wind Tunnel 2. The model length was l=2.55 m and was built at a geometric scale of 1:60 (deck width, B=0.367 m). A sketch of the deck cross-section is given in Figure 1. The deck width to deck depth ratio for this bridge is B/D=5.5.

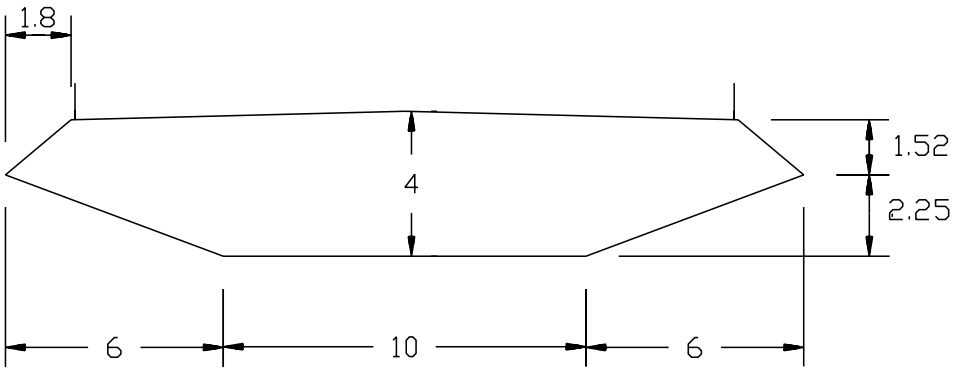

Figure 1: Sketch of the deck cross-section of the Höga Kusten Bridge (dimensions in meters).

The wind tunnel tests were conducted at a mean wind speed of 8.0 m/s in turbulent flow. Large spires mounted at the inlet of the wind tunnel, 15 m upstream of the model were used to generate the turbulent flow field. The vertical turbulence intensity at deck level, I_w was 7.3 % and the vertical turbulence macroscale, $\mathcal{L}_w$ (inverse of the wave number corresponding to the peak of the wind spectrum in its $fS_w(f)$ representation [4]) was 0.22 m. The ratio $\mathcal{L}_w/B$ was 0.60. In itself the ratio of 0.60 does not meet criterion (iii) for this bridge deck. A ratio of $\mathcal{L}_w/B$ between 1 and 1.5 would be a better modelling of the full-scale conditions. However, the point of this experimental verification is to compare the present method with a more involved method where direct measurements of the spatial distribution of the wind loading have been made for many $\mathcal{L}_w/B$ ratios, including 0.60, 0.75 and 1.5 for bridge decks of similar cross-section to the deck studied here (see Part II). In the latter, the cross-sectional admittance was found to be proportional to $\mathcal{L}_w/B$ to the 7/6 power.

The auto-spectra of the u and w components of the wind are given in Figure 2.

[4]For the von Kármán spectrum, $\mathcal{L}_{u,w}$ is related to the integral length scales $L^x_{u,w}$ through the following: $L^x_u \approx 0.92\mathcal{L}_u$ and $L^x_w \approx 0.67\mathcal{L}_w$.

The mean force coefficients and their variations with angle of wind incidence were measured for the same exposure and are reported in Table 1.

Table 10: Static coefficients for the Höga Kusten Bridge (construction stage) in turbulent flow. The coefficients are normalized by the deck width B.

$C_z(0°)$	$C'_z(0°)$	$C_m(0°)$	$C'_m(0°)$
-0.36	4.2	0.013	1.07

Time histories of the drag and lift forces and the pitching moment were measured at the extremities of the model and were recorded at a sampling frequency of 200 Hz, for 180 sec. Figures 3 and 4 show the power spectral densities (1024-point fast Fourier transforms) of the lift and torsional aerodynamic coefficients. Also shown on the graphs is a fit of a single degree-of-freedom mechanical admittance function of the measured spectral estimates and the resulting filtered spectra where the resonant peak has been removed.

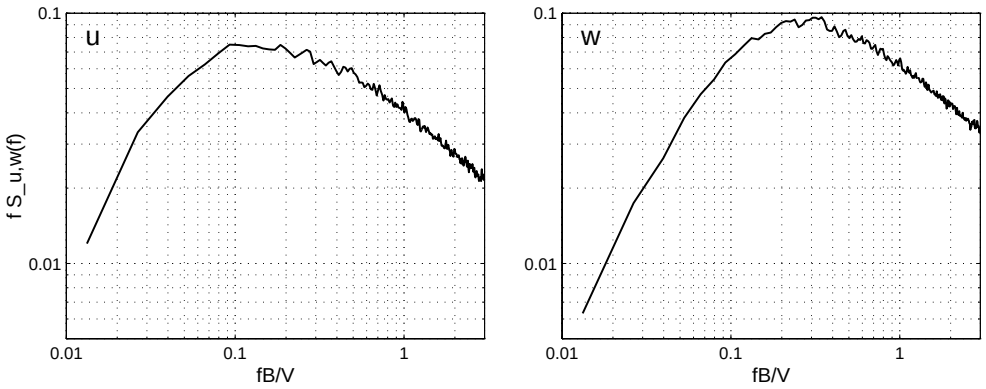

Figure 2: Spectra of the u and w components of the incident turbulent flow as a function of reduced frequency.

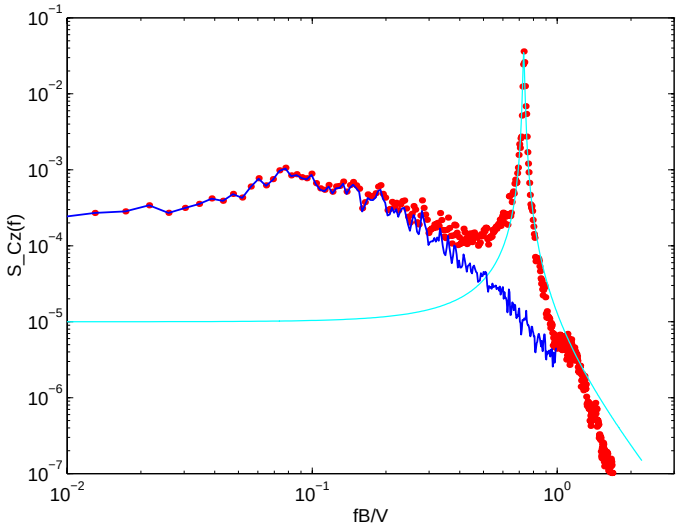

Figure 3: Spectra of the lift coefficient as a function of reduced frequency. Dots: measured spectral estimates; light solid line: fit of a mechanical admittance function; solid line: filtered spectra.

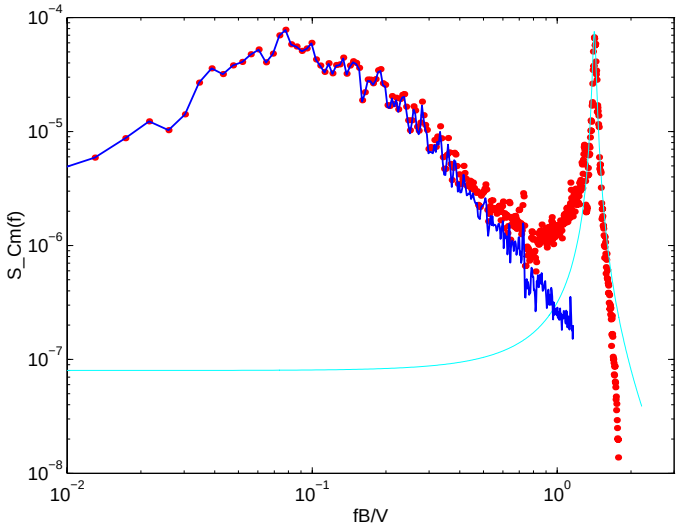

Figure 4: Spectra of the pitching moment coefficient as a function of reduced frequency. Dots: measured spectral estimates; light solid line: fit of a mechanical admittance function; solid line: filtered spectra.

3.2 Evaluation of the joint acceptance function

Since the section model was motionless during the force measurements, i.e. $\mu(y) = 1.0$ in (3), the joint acceptance function can be simplified to a double integration across the model span of the co-coherence of the aerodynamic forces or of the wind fluctuations.

The span-wise normalized co-spectrum of the wind fluctuations for the turbulent flow field of this investigation was described in Part II-A by

$$\mathrm{cocoh}_w(\gamma) = \exp\left[-c_1\gamma^{c_2}\right]\cos(c_3\gamma), \tag{8}$$

where

$$\gamma = k_1\Delta y\sqrt{1+\frac{1}{(k_1L)^2}}, \tag{9}$$

with $k_1 = 2\pi f/\bar{V}$ (wave number), L_{coh}=0.27 m (a length scale fitted to the experiments), c_1= 0.73, c_2=1.03, and c_3=0.27. γ is the von Kármán collapsing parameter.

An empirical formulation of span-wise co-coherence of the lift and torsional forces for a family of closed-box girders similar to the deck of the Höga Kusten Bridge was given in Part II-B and is of the form:

$$\mathrm{cocoh}_{L,M}(\eta) = \exp\left[-c_1\eta^{c_2}\right]\cos(c_3\eta) \tag{10}$$

where, for lift,

$$\eta = k_1^a\Delta y\sqrt{1+\frac{1}{(k_1^aL_F)^2}}; \tag{11}$$

$$L_F = L\,\frac{(p+\frac{\Delta y}{B})^2}{(q+r\,\frac{\Delta y}{B})^2} \qquad p=1.0,\ q=0.46,\ r=1.42,\ L=0.39\mathrm{m}; \tag{12}$$

$$a = \left(\frac{B}{D}\right)^4\frac{(p+\frac{\Delta y}{B})^2}{(q+r\,\frac{\Delta y}{B})^2} \quad p=0.160,\ q=0.088,\ r=0.935; \tag{13}$$

and c_1= 0.346, c_2=1.50, and c_3=0.

For the pitching moment:

$$a = \left(\frac{B}{D}\right)^{1/0.15}\frac{(p+\frac{\Delta y}{B})^2}{(q+r\,\frac{\Delta y}{B})^2} \quad p=0.098,\ q=0.059,\ r=0.970, \tag{14}$$

and c_1= 0.341, c_2=1.33, and c_3=0.22.

The joint acceptance function was calculated for the three cases given above and the results are shown in Figure 5. The difference between the curves for the forces and the curve for the wind is due to the three-dimensionality of the wind loading, the span-wise co-coherence of the forces being larger than the co-coherence of the incident flow.

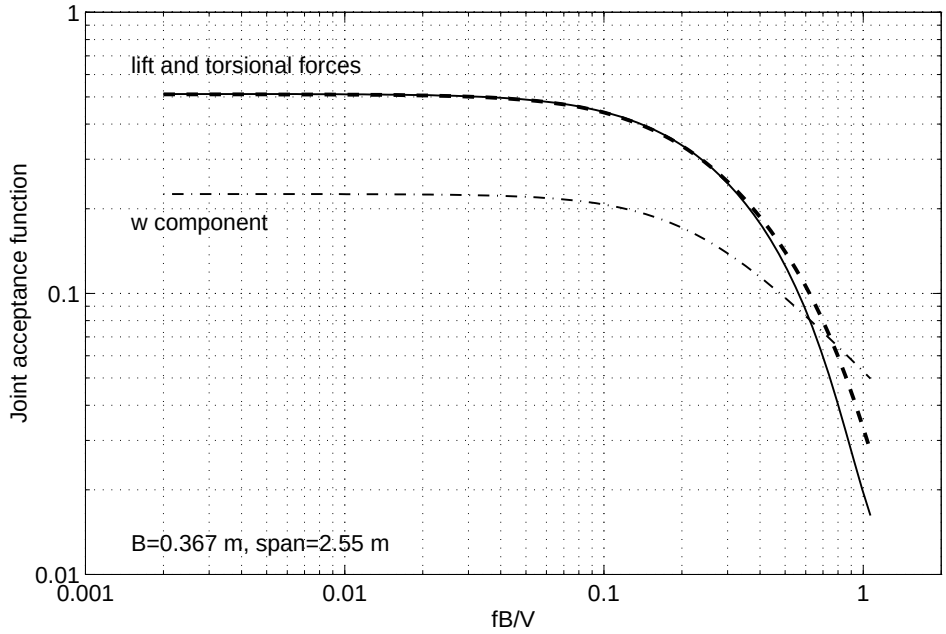

Figure 5: Variations of the joint acceptance function with reduced velocity for a 2.55 m long section model, with uniform mode shape, B=0.367 m and B/D=5.5.

3.3 The aerodynamic admittances

The cross-sectional admittance and the segmental admittance were calculated using equations (5) and (6) for both lift and pitching moment and the results are shown in Figures 6 and 7. The cross-sectional admittance obtained with this technique agreed very well with the cross-sectional admittance measured directly on a chordwise strip (dotted line on the graphs) for $\mathcal{L}_w/B$= 0.58 on a similar cross-section. The segmental admittance showed larger values than the cross-sectional admittance since it included the contribution of the secondary cross-flow over the 2.55 m span that increased the force co-coherence.

Also shown in Figures 6 and 7 is a comparison of the cross-sectional admittance obtained from the technique described here, compared to the Liepmann's approximation to Sears' function and to the empirical model of the 2-D aerodynamic admittance given in Part II-B. The Sears' function considerably overestimated the 2-D admittance for fB/V smaller than 0.1 while the empirical model gave satisfactory results for both lift and pitching moment admittances for this $\mathcal{L}_w/B$ ratio.

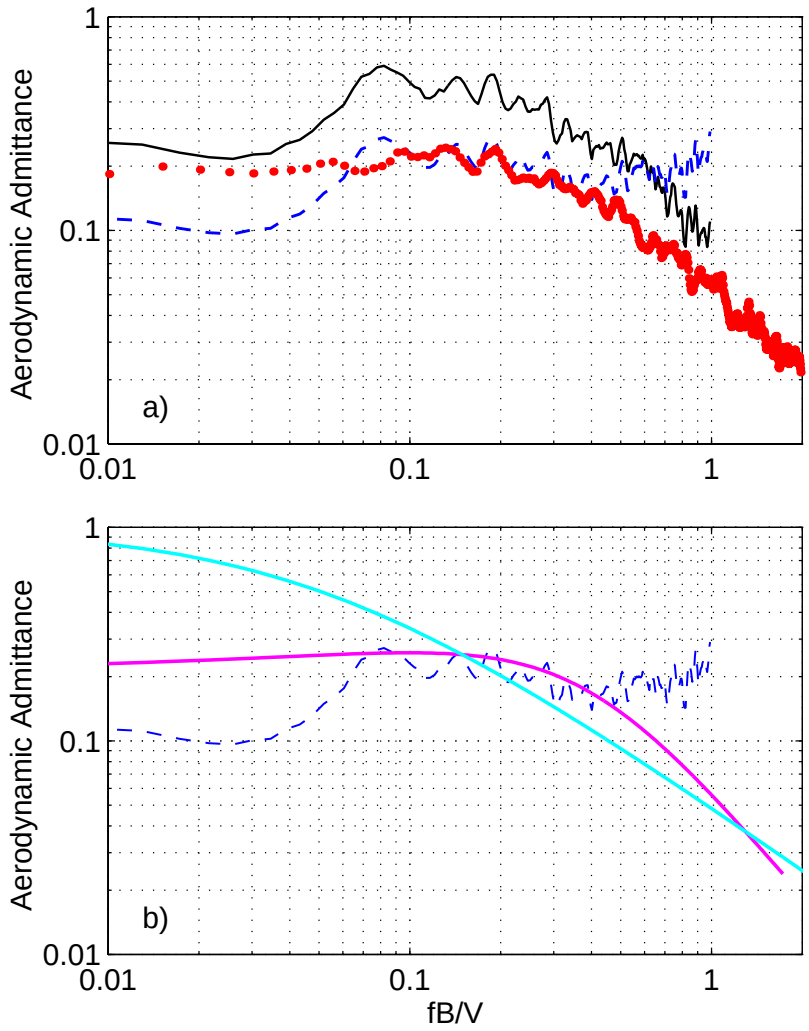

Figure 6: Variations of the lift aerodynamic admittance as a function of fB/V. On **a)**, dots: admittance directly measured from a chord-wise strip as reported in Larose *et al.* (1997), for $\mathcal{L}_w/B$=0.58; solid line: segmental admittance; dashed line: cross-sectional admittance determined with the present method. On **b)**, light solid line: Sears' function; dark solid line: empirical model of 2-D aerodynamic admittance of Larose & Mann (1998) for $\mathcal{L}_w/B$=0.60; dashed line: cross-sectional admittance determined with the present method.

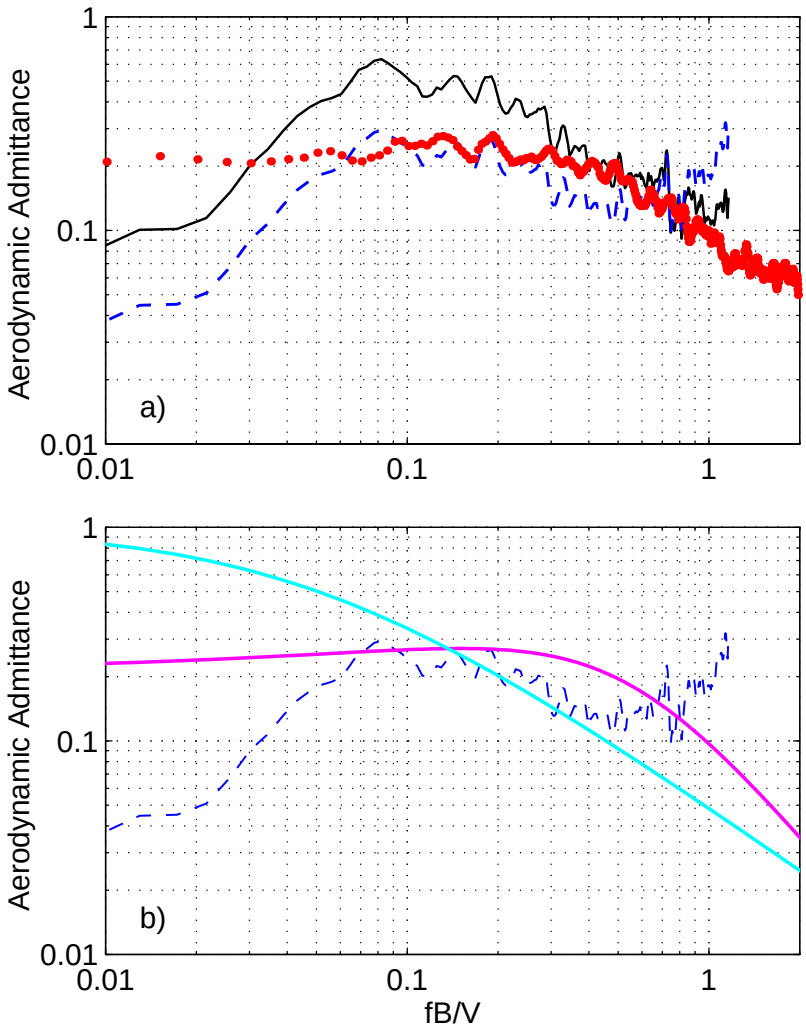

Figure 7: Variations of the pitching moment aerodynamic admittance as a function of fB/V. On **a)**, dots: admittance directly measured from a chord-wise strip as reported in Larose *et al.* (1997), for $\mathcal{L}_w/B$=0.58; solid line: segmental admittance; dashed line: cross-sectional admittance determined with the present method. On **b)**, light solid line: Sears' function; dark solid line: empirical model of 2-D aerodynamic admittance of Larose & Mann (1998) for $\mathcal{L}_w/B$=0.60; dashed line: cross-sectional admittance determined with the present method.

4 Truss girder decks and other bluff cross-sections

The present method can as well be applied to bridge decks with more complex cross-sections such as truss girder decks or composite decks made of a concrete slab supported by longitudinal edge beams and transversal floor beams. The main difficulty of the technique resides in building a section model with a very large flexural and torsional rigidity to reduce the influence of the resonant amplification of the aerodynamic forces. This technique has recently been applied for a truss girder bridge deck with fairly large structural members and the results are presented in Figure 8. The static aerodynamic force coefficients of the deck in question are given in Table 2 (based on the deck width).

The drag admittance was calculated by replacing subscript z by subscript x in equation (5). The results are compared in Figure 8 to the empirical expression of the drag admittance of flat plates normal to a turbulent flow as proposed by Vickery (1965).

Table 11: Static aerodynamic force coefficient for a truss girder bridge deck in turbulent flow (normalized by the deck width)

$C_z(0°)$	$C'_z(0°)$	$C_m(0°)$	$C'_m(0°)$	$C_x(0°)$	$C'_x(0°)$
-0.05	3.4	0.10	0.03	0.43	-0.34

The measured admittance of Figure 8 agreed well with similar measurements made for the truss girder of the Akashi-Kaikyo Bridge reported by Sato *et al.* (1994).

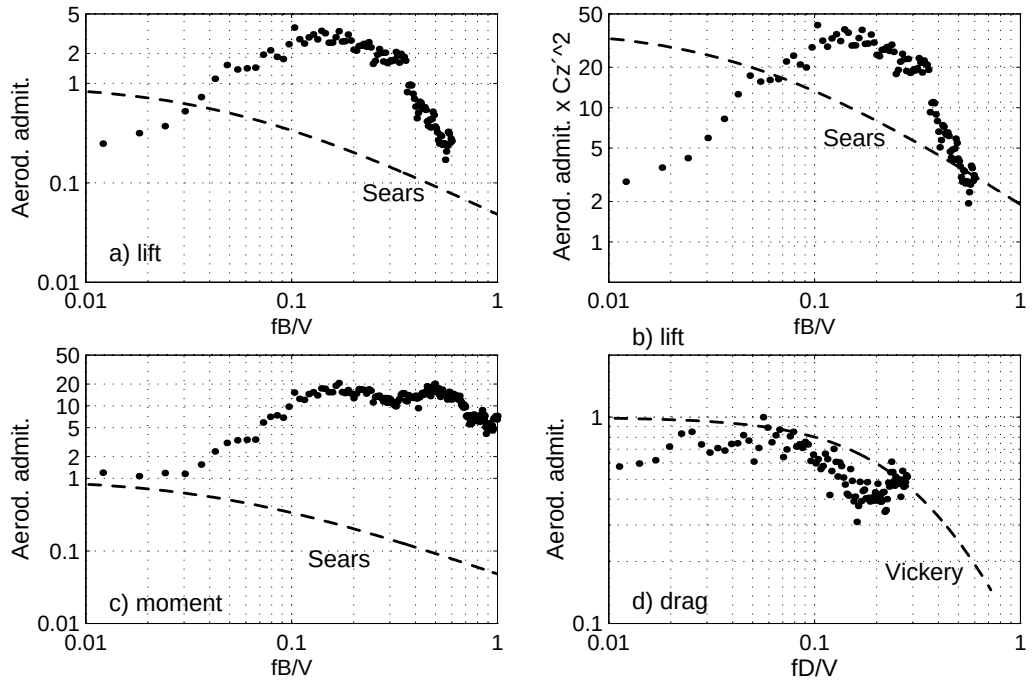

Figure 8: Segmental aerodynamic admittance for a truss girder bridge deck measured with the present technique. On **b)** the ordinate has been multiplied by the lift slope squared. On **d)** the dashed line refers to the drag admittance proposed by Vickery (1965): $[1/(1+(2fD/V)^{(4/3)}]^2$ where D is the deck depth.

5 Conclusion

An experimental approach to evaluate the aerodynamic admittance of a segment of a bridge deck was presented. The aerodynamic characteristic obtained with this technique has a three-dimensional character since it includes the influence of the span-wise distribution of the aerodynamic forces. The approach can be used for bridge deck of any cross-section.

REFERENCES

BOGUNOVIC JAKOBSEN, J. **1995** Fluctuating wind load and response of a line-like engineering structure with emphasis on motion-induced wind forces. Ph.D. Thesis, The Norwegian Institute of Technology, Trondheim, Norway.

DAVENPORT, A.G. **1962** The response of slender, line-like structures to a gusty wind. In *Proceedings of Institution of Civil Engineers* **23**, 389-408.

FUNG, Y.C. **1969** *An Introduction to the Theory of Aeroelasticity.* New York: Dover Publications.

GRILLAUD G., FLAMMAND O. & BARRÉ C. **1991** Comportement au vent du Pont de Normandie: Etude en soufflerie atmosphérique sur maquette aéroélastique à échelle du 1/200ème. Centre Scientifique et Technique du Bâtiment, Nantes, France, EN-AS 91.5 C, 22 p.

HOLMES J.D. **1975** Prediction of the response of a cable-stayed bridge to turbulence. In *Proceedings of 4th International Conference on Buildings and Structures* London, England. Cambridge: Cambridge University Press.

IRWIN H.P.A.H. **1977** Wind Tunnel and Analytical Investigations of the Response of Lions' Gate Bridge To Turbulent Wind. National Research Council of Canada, NAE LTR-LA-210, 62 p.

JANCAUSKAS E.D. **1983** The cross-wind excitation of bluff structures and the incident turbulence mechanism. Ph.D. Thesis, Monash University, Melbourne, Australia.

JANCAUSKAS E.D. & MELBOURNE W.H. **1986** The aerodynamic admittance of two-dimensional rectangular cylinders in smooth flow. *Journal of Wind Engineering and Industrial Aerodynamics* **23**, 395-408.

KAWATANI M. & KIM H. **1992** Evaluation of aerodynamic admittance for buffeting analysis. *Journal of Wind Engineering and Industrial Aerodynamics* **41-44**, 613-624.

LAMSON P. **1957** Measurements of lift fluctuations due to turbulence. NACA TN-3880.

LAROSE, G.L. **1992** The response of a suspension bridge deck to turbulent wind: the taut strip model approach. M.E.Sc. Thesis, University of Western Ontario, London, Ontario, Canada.

LAROSE, G.L., TANAKA H., GIMSING N.J. & DYRBYE C. **1997** Direct measurements of buffeting wind forces on streamlined bridge decks. *Journal of Wind Engineering and Industrial Aerodynamics* **74-76**, 809-818.

LAROSE G.L. & MANN J. **1998** Gust loading on streamlined bridge decks. *Journal of Fluids and Structures* **12**, 511-536.

LIEPMANN, H.W. **1952** On the application of statistical concepts to the buffeting problem. *Journal of Aeronautical Science* **19**, 793-810.

Sankaran, R. & Jancauskas, E.D. **1992** Direct measurement of the aerodynamic admittance of two-dimensional rectangular cylinders in smooth and turbulent flows. *Journal of Wind Engineering and Industrial Aerodynamics* **41-44**, 601-611.

Sato H., Matsuno Y. & Kitagawa M. **1994** Evaluation of the aerodynamic admittance for the stiffening girder of the Akashi Kaikyo Bridge. In *Proceedings of the 13th. Japan National Symposium on Wind Engineering*, paper **23**, 131-136 (in japanese).

Vickery, B.J. **1965** On the flow behind a coarse grid and its use as a model of atmospheric turbulence in studies related to wind loads on buildings. National Physical Laboratory, Aero Report 1143.

Walshe D.E. & Wyatt T.A. **1983** Measurements and application of the aerodynamic admittance function for a box-girder bridge. *Journal of Wind Engineering and Industrial Aerodynamics* **14**, 211-222.

Part III
Applications

Part III-B
Performance of streamlined bridge decks in relation to the aerodynamics of a flat plate

GUY L. LAROSE[a,b] AND FLORA M. LIVESEY[a]

[a] *Danish Maritime Institute, Hjortekærsvej 99, 2800 Lyngby, Denmark*
[b] *Department of Structural Engineering and Materials, Technical University of Denmark, 2800 Lyngby, Denmark*

(Published in *J. of Wind Engineering and Industrial Aerodynamics* **69-71** (1997), 851-860)

Abstract

The aerodynamics of three modern bridge decks are compared to the aerodynamics of a 16:1 flat plate. The comparisons are made on the basis of the analytical evaluation of the performance of each cross-section to the buffeting action of the wind. In general the closed-box girders studied in this paper showed buffeting responses similar to a flat plate with the exception of the multi-box girder which performed much better aerodynamically.

1 Introduction

The objective of this paper is to compare the aerodynamic performance of selected streamlined bridge decks to the performance of a flat plate in turbulent flow. The comparisons are based on the main aerodynamic properties of the deck cross-section, that is: static force coefficients, aerodynamic derivatives and aerodynamic admittances. Most of the properties were obtained from wind tunnel tests on section models carried out at the Danish Maritime Institute.

The deck cross sections studied here, all closed steel box girders that have been designed with the emphasis on aerodynamics (therefore the appellation *streamlined*),

belong to the following structures: the proposed suspension bridge across the Straits of Messina, Italy; the Pont de Normandie, recently completed in France; and the Höga Kusten Bridge under construction in Sweden.

Fig. 1 shows the cross-sections of the three above-mentioned bridge decks. The proposed Messina Straits Bridge would have a $3300m$ long mainspan, a deck width of $60m$ and a width-to-depth ratio, B/D, of 13. The Pont de Normandie, an $856m$ mainspan cable-stayed bridge, has a $B/D = 7.5$ (a $23m$ wide deck, once the nosings were in place, with a depth of $3m$). The Höga Kusten Bridge, a $1210m$ mainspan suspension bridge, has a deck width of $22m$ and a maximum depth of $4m$ yielding $B/D = 5.5$. The reference flat plate is very slender with a $B/D = 16$. Note that both the Pont de Normandie and the Höga Kusten Bridge were tested in their construction stage configuration with temporary railings.

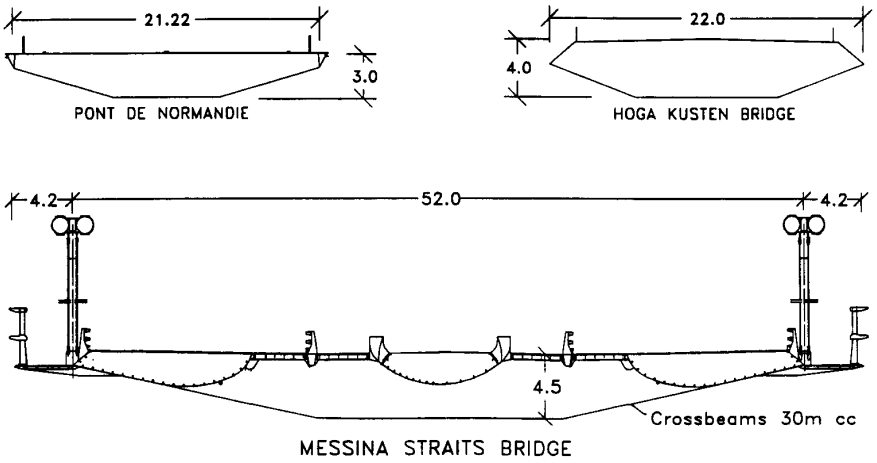

Figure 1: Deck cross-sections of the Messina Straits Bridge, Pont de Normandie and the Höga Kusten Bridge (dimensions in meters).

The evaluation of the performance of each of the decks in comparison to a flat plate is based on the analytical prediction of the buffeting response. Similar studies can be found in the literature [1, 2] but in most of the cases the comparisons are based on the aeroelastic behaviour and the stability limit, except in [3] where the experimentally determined responses of various bridge decks (from the Tacoma Narrows to the Pont de Normandie) are compared to the response of a flat plate.

2 Comparison of static force coefficients

Section model tests were conducted for all three bridge decks in DMI's $2.6m$-wide boundary layer wind tunnel or in the $1.0m$-wide closed circuit wind tunnel, to mea-

sure time averaged drag, lift and moment coefficients versus angle of wind incidence. The tests were typically conducted in turbulent flow with a vertical turbulence intensity of 6% generated by large spires $20m$ upstream of the model, with the exception of the Messina Bridge which was tested in smooth flow. The coefficients for the flat plate in turbulent flow were obtained from [4].

The coefficients presented in Fig. 2 were normalized by B and were converted to force coefficients C_x, C_z and C_m, with reference to a coordinate system fixed to the body, where the subscripts x, z, m denote respectively the lateral, vertical and torsional degrees of freedom of the deck. The table in Fig. 2 summarises the results for 0° wind incidence; C'_z and C'_m denote the rate of change of the coefficients with angle of attack around 0°.

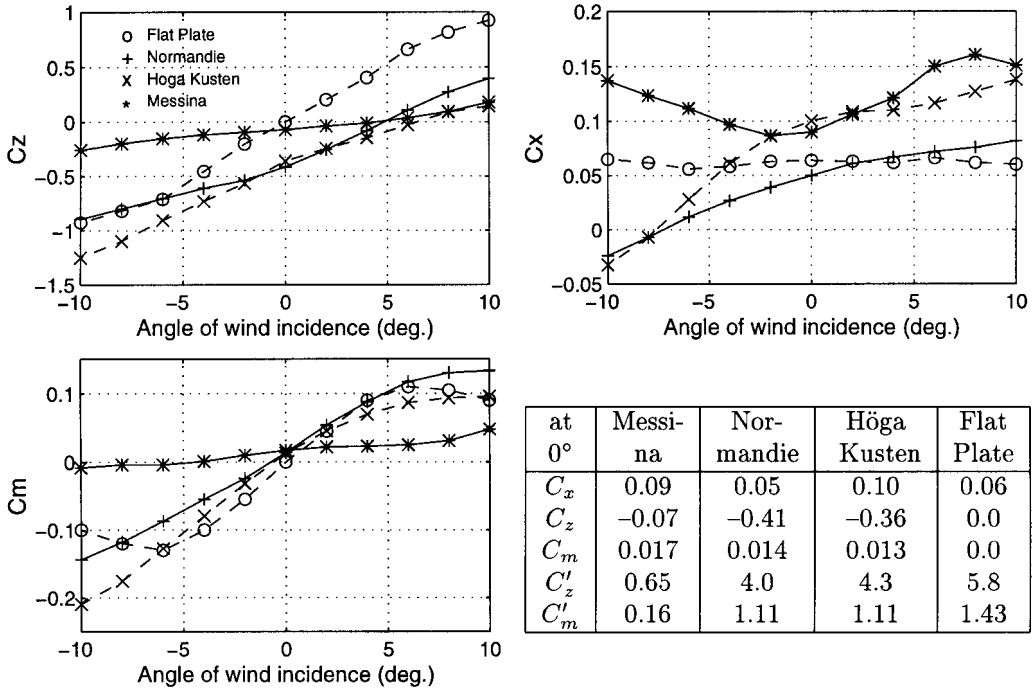

at 0°	Messina	Normandie	Höga Kusten	Flat Plate
C_x	0.09	0.05	0.10	0.06
C_z	–0.07	–0.41	–0.36	0.0
C_m	0.017	0.014	0.013	0.0
C'_z	0.65	4.0	4.3	5.8
C'_m	0.16	1.11	1.11	1.43

Figure 2: Variations of C_x, C_z and C_m with angle of wind incidence for 4 cross-sections.

Assuming that the instantaneous forces on the bridge deck are equal to the steady forces induced by a steady wind of the same relative velocity and direction as the instantaneous wind (i.e. quasi-steady aerodynamics), Davenport [5] showed that:

1. the forces due to turbulence are proportional to the product of the mean

wind velocity, the longitudinal velocity fluctuations and $C_{x,z,m}$, added to the product of the vertical velocity fluctuations and $C'_{x,z,m}$;

2. C_x and C'_z, contribute respectively to the lateral and vertical aerodynamic damping by an amount proportional to the mean wind velocity;

3. C'_m contributes to the torsional stiffness of the system; if positive, the torsional stiffness will decrease in proportion to the square of the wind velocity.

Thus, Fig. 2 reveals a good deal about the aerodynamic performance of the decks studied. First both C'_z and C'_m are positive for all cross-sections which means favorable aerodynamic damping. In general the decks have C'_m values that follow the flat plate value and a C'_z that is relatively smaller than that for the flat plate. Also, they have a negative C_z at 0° which indicates that the deck is pushed downward as the wind speed increases. This negative lift is generally compensated for by the upward force produced by the wind on the cable system.

The multi-box girder of the Messina Straits Bridge, however, has very favorable static coefficients that put it in a class of its own. This deck has both C'_z and C'_m equal to a quarter of the corresponding values of the other cross-sections and $C_{z,m}$ are almost zero at 0°. Good performance with regards to buffeting is anticipated as well as a high stability limit.

3 Aerodynamic derivatives and admittances

The motional aerodynamic derivatives and the aerodynamic admittances have been measured directly or indirectly for these deck cross-sections. The main characteristics are presented here with the emphasis put on the relationships between these quantities and the static coefficients.

The aerodynamic admittance is a measure of the effectiveness of a body in extracting energy from the oncoming turbulence. It was introduced by Davenport, firstly to express that the wind loading is not necessarily quasi-steady and may vary with frequency, and secondly to represent the spatial variations in the flow over the region influencing the forces on a cross-section. This second aspect is now being studied in more details by the authors [6].

Fig. 3 presents direct measurements (dashed lines) of aerodynamic admittances as a function of reduced frequency ($f^* = fB/V$). The solid line represents the Liepmann's approximation to the Sears function analytically derived for a flat plate (thin airfoil) with a lift slope of 2π in a fully correlated sinusoidal gust [7]:

$$|\phi(f^*)|^2 = \frac{1}{(1 + 2\pi^2 f^*)} \quad \text{(Liepmann)} \tag{1}$$

The admittance measurements were done either by integration of the surface pressures on a cross-sectional strip of a section model (as in Part II-A) or by measuring

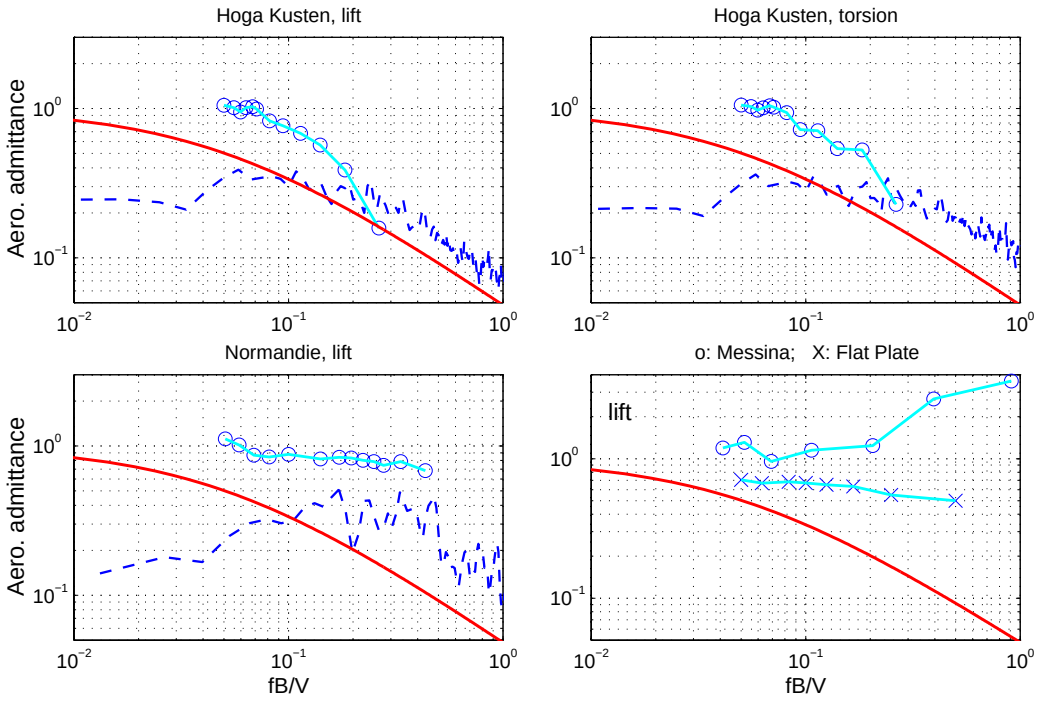

Figure 3: Variations of aerodynamic admittances with reduced frequency. **Solid line**: Liepmann's approximation, equation (1); **dashed lines**: direct measurements of admittance on section models; and **light lines with o and x**: indicator of unsteadiness i.e. ratio of the unsteady lift slopes $C'_z(f^*)$ to the steady case $C'_z(0)$.

the lift forces at the extremity of a very rigid $2.55m$ long section model and dividing by the incoming flow characteristics (auto-spectra and span-wise coherence). The procedures behind the measurements are reported elsewhere [3, 8] (see also Part II-A and III-A).

Also shown on Fig. 3 (o and x) is an attempt to relate the aerodynamic admittance to the ratio $C'_z(f^*)/C'_z(f=0)$, that is, the unsteady lift slope to the steady case. Intuitively this ratio should be related to the first definition of the aerodynamic admittance. The unsteady lift slope can be directly obtained from the relationships between the force coefficients and the aerodynamic derivatives H_1^* and A_1^* [9] as per equations (2) and (3) obtained assuming quasi-steady aerodynamics:

$$H_1^* = \frac{-C'_z}{2K} \; ; \quad A_1^* = \frac{C'_m}{2K} \; ; \quad H_3^* \approx \frac{-C'_z}{2K^2} \; ; \quad A_3^* \approx \frac{C'_m}{2K^2} \tag{2}$$

$$H_2^* \approx \frac{C'_z}{2K} n_\theta \; ; \quad A_2^* \approx \frac{-C'_m}{2K} n_\theta \; ; \quad n_z(K) = \frac{A_1^*}{H_1^*} \; ; \quad n_\theta(K) = \frac{A_3^*}{H_3^*} \tag{3}$$

where $K = \frac{2\pi fB}{V}$, B is the deck width, V the mean wind speed and $n_{z,\theta}$ are the points of application of the aerodynamic forces expressed as a fraction of B.

For the flat plate, the unsteady lift slope can be obtained analytically via the relationship between the Theodorsen function [9], the aerodynamic derivatives and equations (2). The Sears function can also be related to the aerodynamic derivatives through the Theodorsen function [7].

The ratio $C_z'(f^*)/C_z'(0)$ can be seen as an indicator of unsteadiness. If it drops with increasing f^*, it is believed that the aerodynamic admittance will do the same. This trend can be observed, at least qualitatively, on Fig. 3 for the Höga Kusten Bridge and the Pont de Normandie.

Based on this, it is expected that the aerodynamic admittance for the Messina Bridge would not drop with reduced frequency but increase to values above unity. This would correspond to the effect of the self-induced turbulence created by the upwind box girder and affecting the wind loading on the downstream components of the deck at higher reduced frequencies.

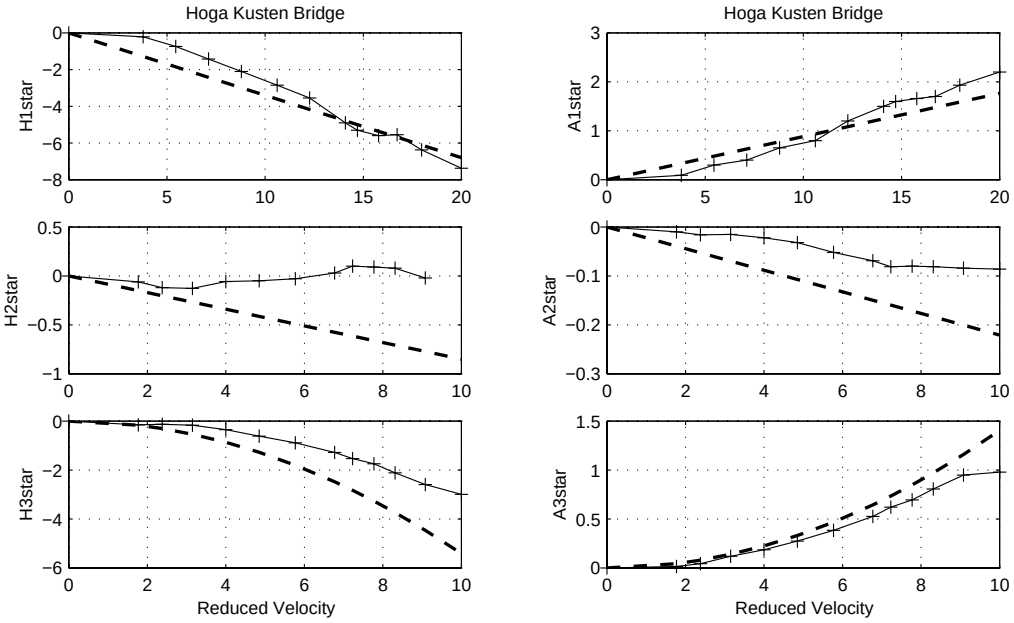

Figure 4: Variations of $H^*_{1,2,3}$ and $A^*_{1,2,3}$ with reduced velocity for the Höga Kusten Bridge. The dashed lines are predictions derived from quasi-steady aerodynamics using the coefficients of Fig. 2 and $n = 0.25$.

Fig. 4 to 6 shows some of the measured motional aerodynamic derivatives in Scanlan's notation [9], using the inital displacement method, as a function of reduced velocity, and compares them to approximations using equations (2) and (3). The agreement is surprisingly clear except for H_2^* and A_2^* where quasi-steady aerodynamics would predict erroneous values. This could lead to miscalculation of the torsional aerodynamic damping if quasi-steady aerodynamic assumptions were maintained. The relationship between H_2^*, A_2^* and the lift and torsion slopes is questionable and the reader is referred to [10] for a detailed discussion on the matter.

4 Prediction of the buffeting response

The spectral approach described in [11] was used here to predict the buffeting response of the cross sections. In the calculations, equation (4) was used along with the following functions: aerodynamic admittance, $|A_z(f^*)|^2$ as measured (except for Messina and the flat plate where the Liepmann's approximation to the Sears function, equation (1), was used), aerodynamic damping extracted from the aerodynamic derivatives (5), Kaimal wind spectra $fS_w(f)/\sigma_w^2$, a typical first symmetric mode shape, a structural damping (ζ_s) of 0.5% of critical and a ratio of the mass of

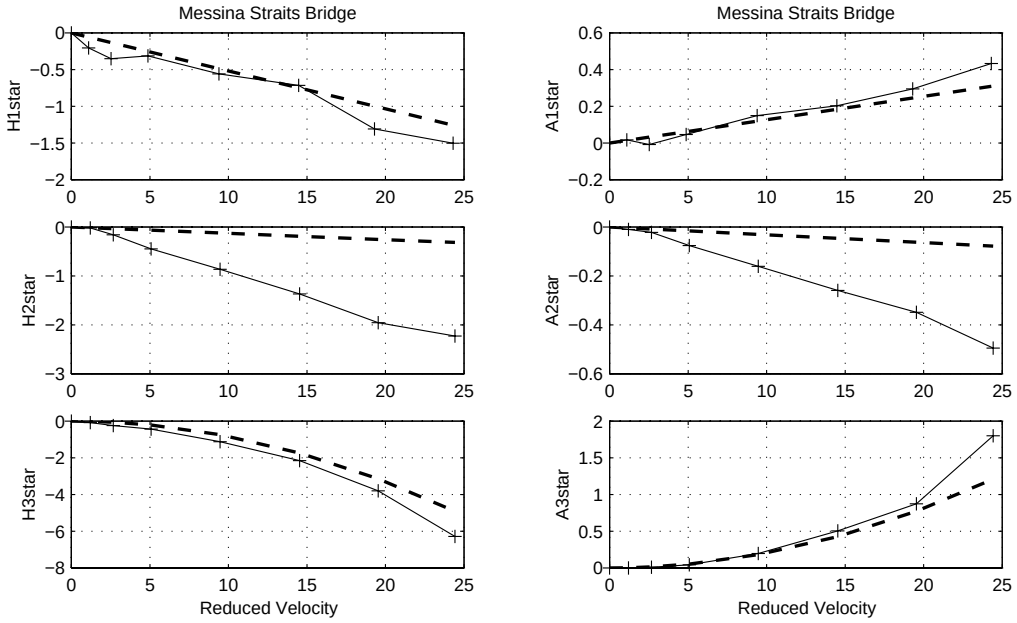

Figure 5: Variations of $H_{1,2,3}^*$ and $A_{1,2,3}^*$ with reduced velocity for the Messina Straits Bridge. The dashed lines are predictions derived from quasi-steady aerodynamics using the coefficients of Fig. 2 and $n = 0.25$.

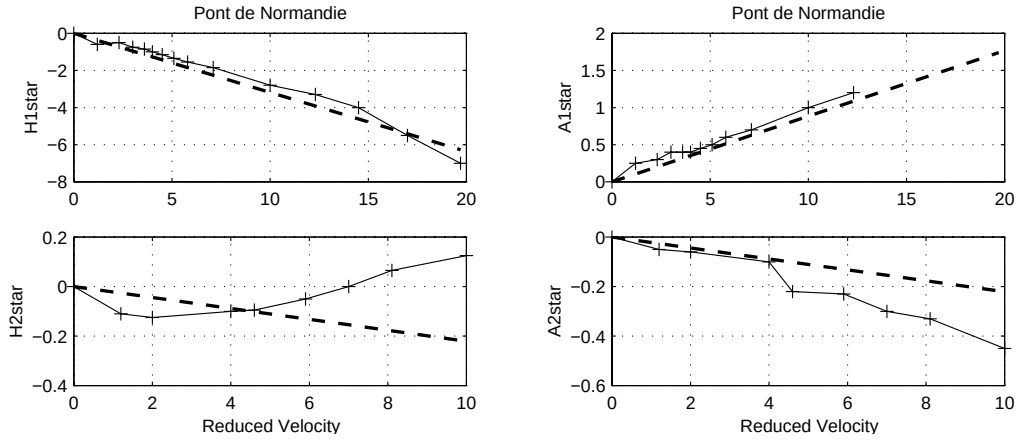

Figure 6: Variations of $H^*_{1,2}$ and $A^*_{1,2}$ with reduced velocity for the Pont de Normandie. The dashed lines are predictions derived from quasi-steady aerodynamics using the coefficients of Fig. 2 and $n = 0.25$.

the displaced air to the mass of the deck, $\rho B^2/m$, corresponding to the characteristics of each of the deck. This ratio was in fact the same for Pont de Normandie, Höga Kusten and the flat plate.

The normalized modal root-mean-square response (acceleration), for the vertical modes of the deck can be expressed by:

$$\frac{\tilde{r_{j,z}}}{I_w B \omega_j^2} \approx \frac{C_z'}{8\pi^2} \left[\frac{V}{f_j B}\right]^2 \frac{\rho B^2}{m} \sqrt{\frac{f\,S_w(f)}{\sigma_w^2}\ |A_z(f^*)|^2\ |J_{z,j}(f^*)|^2\ \frac{\pi/4}{\zeta_s + \zeta_{a,z}(f^*)}} \qquad (4)$$

where the subscript j denotes the j^{th} mode of vibration and $|J_{z,j}(f^*)|^2$ is the joint acceptance function which was calculated on the basis of the strip assumption. A similar expression can be written for the torsional response by replacing subscript z by m and $\rho B^2/m$ by $\rho B^4/I_\theta$, I_θ being the mass moment of inertia per unit length of the deck.

The aerodynamic damping was defined as:

$$\zeta_{a,z}(f^*) \approx -H_1^*(f^*)\frac{\rho B^2}{2m}; \qquad \zeta_{a,\theta}(f^*) \approx -A_2^*(f^*)\frac{\rho B^4}{2I_\theta} \qquad (5)$$

Fig. 7 presents the results of the predictions along with the aerodynamic derivatives used to define the aerodynamic damping. The rms modal resonant response (acceleration), $\tilde{r_j}$, was normalized by the vertical turbulence intensity I_w, the angular frequency of mode j, ω_j^2, and B as in [3, 11]. The vertical responses collapse well on one line for the Pont de Normandie and Höga Kusten and were found to perform

slightly better than the flat plate at high reduced velocities. This difference can mostly be attributed to the differences in the low reduced frequency range between the Sears function and the directly measured aerodynamic admittances. The deck of Messina showed a much better performance.

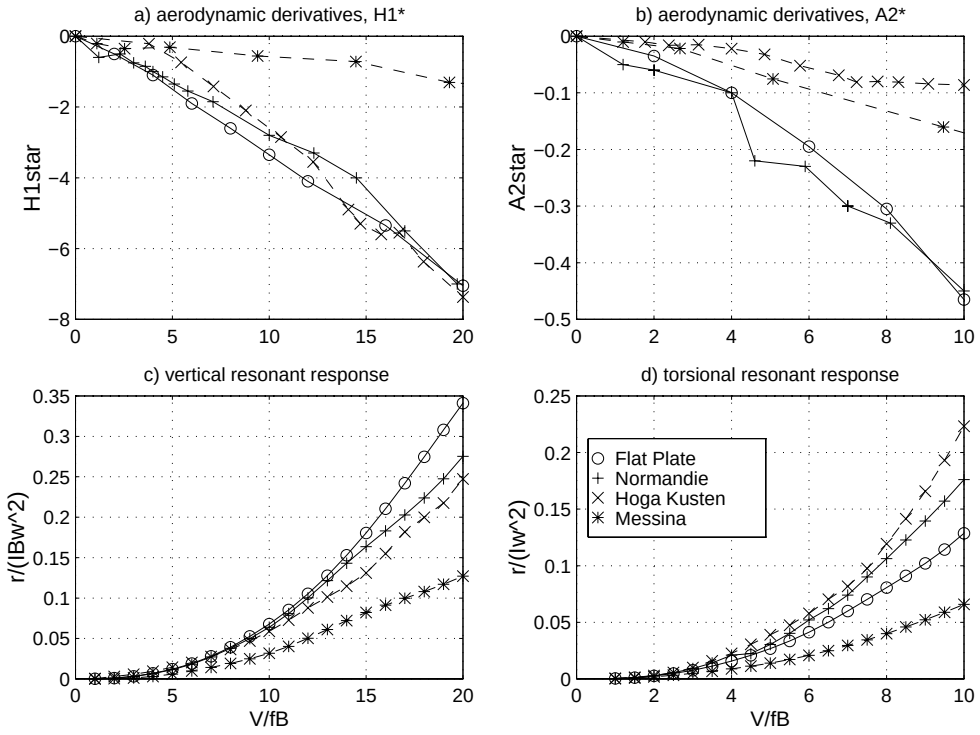

Figure 7: Variations of the aerodynamic derivatives a) H_1^*, b) A_2^*, and the normalized resonant modal responses, $\tilde{r_j}/I_w B\omega_j^2$, c) vertical, d) torsional with reduced velocity $V/f_j B$ for three deck cross-sections compared to a 16:1 flat plate

For the torsional response, the aerodynamic damping (which is a function of A_2^* and B) appears to dominate, since the performance seemed to be inversely proportional to the width-to-depth ratio. For example, the Höga Kusten Bridge has considerably lower A_2^* values than the Pont de Normandie and the flat plate, directly resulting in a larger torsional response. Also, it should be noted that the low torsional response of the Messina Bridge is largely due to strong aerodynamic damping provided by optimized wind screens that act as dampers and its very large deck width.

5 Conclusions

Examining the aerodynamic properties and the buffeting response of the Messina Straits Bridge leads to the conclusion that bridge designs can be optimized to perform aerodynamically much better than a flat plate, both in lift and torsional responses. However, the Pont de Normandie and the Höga Kusten Bridge, which are more typical deck designs, gave similar responses to a flat plate according to the buffeting response predictions. The lower torsional aerodynamic damping for the Höga Kusten Bridge, partly due to its lower width-to-depth ratio, leads to the larger torsional response predicted by the buffeting theory.

Acknowledgements: The valuable contribution of Dr Hiroshi Tanaka to this paper, through discussions and supervision, is kindly acknowledged as well as the financial support of the first author by the Danish Research Academy.

References

[1] Selberg, A. and Hjorth-Hansen, E., "The Fate of Flat Plate Aerodynamics in the World of Bridge Decks", in *Proc. of The Theodorsen Colloquium 1976*, Oslo, Norway.

[2] Sarkar P.P., Jones N.P., and Scanlan R.H., "A comparative study of the aeroelastic behavior of three flexible bridges and a thin airfoil", in *Proc. of the 7th US Nat. Conf. on Wind Engineering*, UCLA, Los Angeles, USA, June 1993, 595-604.

[3] Davenport, A.G., King, J.P.C, and Larose, G.L. "Taut Strip Model Tests", in *Proc. of Int'l Symposium on Aerodynamics of Large Bridges*, Copenhagen, Feb. 1992, 113-124.

[4] Kirkwood, K., *Aspects of Aerodynamics of Cable-stayed Bridges During Construction*, M.E.Sc. Thesis, University of Western Ontario, Canada, 1991.

[5] Davenport, A.G., "The Action of Wind on Suspension Bridges", in *Proc. of Int'l Symposium on Suspension Bridges*, L.N.E.C., Lisbon, 1966, 79-100.

[6] Larose G.L.,"The span-wise coherence of wind forces on streamlined bridge decks", in *Proc. of 3rd Int'l Colloquium on Bluff Body Aerodynamics and Applications*, Blacksburg, Virginia, USA, July 1996.

[7] Fung Y.C., *An Introduction to the Theory of Aeroelasticity*, Dover Publications Inc., N.Y., 1969.

[8] Larose G.L.,*The Response of a Suspension Bridge Deck to Turbulent Wind: The Taut Strip Model Approach*, M. E. Sc. Thesis, University of Western Ontario, Canada, March 1992.

[9] Simiu E. and Scanlan R.H. *Wind Effects on Structures*, Wyley Intersciences Pub., N.Y., 1986.

[10] Jensen A.G.,"Fluid Dynamic Derivatives, Marine and Wind Engineering Approaches", in *Proc. of 3rd Int'l Colloquium on Bluff Body Aerodynamics and Applications*, Blacksburg, Virginia, USA, July 1996.

[11] Larose G.L., Davenport A.G. and King J.P.C. "Wind effects on long-span bridges: consistency of wind tunnel results", *J. Wind Eng. and Ind. Aerodyn.* **41-44**, (1992), 1191-1202.

.